Investigating the Role of Apoptosis-stimulating of P53 Protein 2 (ASPP2) in Development of the Central Nervous System



Jie Yin

St Anne's College

University of Oxford

A thesis submitted for the degree of

Doctor of Philosophy

Michaelmas 2020

Declaration

This thesis is submitted to the University of Oxford for the degree of Doctor of Philosophy in Clinical Medicine. All of the work presented in this thesis is the result of my own work unless indicated here and in the corresponding sections. High-Resolution Episcopic Microscopy (HREM) imaging of WT and ASPP2 knock out embryos was carried out by Dr. Jaroslav Zak. *Aspp2-KO* and reconstituted cells were generated by Dr. James Hokfung Chan. Mass spectrometry-based phosphoproteomic analysis was performed by Dr. James Hokfung Chan and Dr. Kundan Sharma. The work described herein has not been accepted or submitted for any degree, diploma, or other qualification at the University of Oxford or any other institution.

Acknowledgements

I received a huge amount of help from many people during this long but fulfilling journey. The research presented in this thesis would not have been completed without their support. First of all, I would like to thank my supervisors Prof. Xin Lu and Prof. Francis Szele for their dedicated guidance and support. They were always willing to assist in any way they could and continuously provided encouragement during the running of the research project. They were mentors who respected my ideas, given me the freedom to pursue an independent line of research, and taught me to articulate those ideas into the strongest arguments possible with the available data. I have learned so much from them.

From the bottom of my heart, I would like to say thank you to all my colleagues, the lab support team of the Ludwig Institute for Cancer Research, and staffs work in the animal facility at the Wellcome Trust Centre for Human Genetics for their help through my project, especially to Abeer Al-Shammari and Sun Bin for sharing their expertise in neurosphere culture and electroporation technique, Mark Shipman and Richard Lisle for assistance with microscopy and image analysis, Indrika Ratnayaka for preparing histological samples, Jade Harris and Douglas Passos for setting up and monitoring timed pregnant mice, and James Hokfung Chan for analysing the phosphoproteomic data. Without their help, this project would not have been the same. I would also like to thank Jo Wainwright and Alexandra Ward for their day-to-day help with all the paperwork. Special thanks go to all my friends inside and outside of the lab, particularly Bin Sun, Yichen Li and Xiaoyue Han for the joyful time we spent together and their immense encouragement and support during hard times. They are heartfelt friends who made this journey more colourful.

I must also take this opportunity to express my sincere gratitude to the China Scholarship Council-University of Oxford joint scholarship and the Nuffield Department of Clinical Medicine. I won’t be able to complete my study at the University of Oxford without the financial support they provided.

Abstract

Development of the structurally complicated central nervous system (CNS) involves a set of highly organized events including neurogenesis and neuronal migration. ASPP2 has been reported to be important for CNS development in both humans and mice. ASPP2 plays an important role in inhibiting excessive proliferation of neural stem cells (NSCs) and maintaining the polarity of the neuroepithelium in the developing mouse brain. However, the function of ASPP2 in neuronal migration and potential brain malformations caused by ASPP2 deficiency at postnatal stages remain uncharacterized.

This study found that *Aspp2-KO* mice show diminished olfactory bulbs, whose development relies on chain migration of neuroblasts in the rostral migratory stream (RMS). Subsequent in vivo and in vitro migration assays demonstrated that ASPP2 deficiency resulted in the impaired formation of the chain-like structure and neuroblasts migrating in the RMS. ASPP2 deficiency also impaired radial neuronal migration in the neocortex leading to periventricular nodular heterotopia (PNH), which was characterized by periventricular clusters of neurons that failed to migrate into the neocortex.

Dynamic regulation of the actin cytoskeleton, mediated by Rho GTPases and their downstream kinases, plays an essential role in developmental neuron migration disorders. A phosphoproteomic analysis using wild-type and *ASPP2-KO* U2OS cells indicates that ASPP2 may regulate the cytoskeleton through Rho-ROCK signalling. Indeed, my study demonstrated that ASPP2 physically interacted with ROCK2 and potentiated its phospho-kinase activity towards MYPT1 and MLC2, thus positively regulating RhoA-mediated actomyosin stress fibre formation and cell migration. This work revealed novel functions of ASPP2 in regulating Rho-ROCK signalling, actin cytoskeleton, and neuronal migration.

Table of Contents

Declaration ..... *i*

Acknowledgements ..... *ii*

Abstract ..... *iii*

Table of Contents ..... *iv*

List of Tables ..... *vii*

List of Figures ..... *viii*

Chapter 1: Introduction and Background *1*

1.1 A Brief Summary of CNS Development. **1**

1.2 Neurogenesis in the Developing Neocortex. **4**

1.2.1 Neurogenic Phases and Progenitor Subtypes. 5

1.2.2 Symmetric Versus Asymmetric Divisions. 8

1.3 Neuronal migration during brain development. **12**

1.4 Grey matter heterotopia **16**

1.4.1 Periventricular nodular heterotopia (PNH). 17

1.4.2 Subcortical band heterotopia (SBH). 20

1.5 Apoptosis Stimulating Protein of p53 2 (ASPP2) **25**

1.5.1 Pro-apoptotic function of ASPP2 26

1.5.2 ASPP2 is a haploinsufficient tumour suppressor 28

1.5.3 ASPP2 as a targeting subunit of protein phosphatase 1 (PP1) 29

1.5.4 ASPP2 as a regulator of cell polarity 31

1.5.5 ASPP2 in central nervous system (CNS) development 32

1.6 Aim of this study **34**

Chapter 2: Materials and Methods *35*

2.1 Materials **35**

2.1.1 Reagents 35

2.1.2 Home-made buffers 37

2.1.3 Primers 42

2.1.4 Antibodies 43

2.1.5 Cell lines 44

2.1.6 Mice 46

2.2 Methods **47**

2.2.1 Animal work 47

2.2.1.1 Mice maintenance 47

2.2.1.2 Mouse genotyping 47

2.2.1.3 BrdU labelling for studying neuroblast migration *in vivo* 48

2.2.1.4 Quantification of RGC spindle orientation 49

2.2.1.5 Cardiac perfusion fixation 50
2.2.2 Histology techniques 51
2.2.2.1 Brain tissue processing and sectioning. 51
2.2.2.2 Haematoxylin and Eosin (H&E) staining 51
2.2.2.3 Immunohistochemistry (IHC) staining 52
2.2.2.4 Immunofluorescence staining 53
2.2.3 Tissue culture and cell-based assays 54
2.2.3.1 *In vitro* neuroblast migration assay using RMS explants 54
2.2.3.2 *Ex utero* electroporation and brain slice culture 55
2.2.3.3 Moue embryonic neural stem cells culture 56
2.2.3.4 BrdU NSCs proliferation assay 58
2.2.3.5 Neurosphere growth assay 59
2.2.3.6 Maintenance of cell lines 59
2.2.3.7 Real-time cell migration assay 59
2.2.3 DNA and RNA techniques 60
2.2.3.1 Transforming competent cells and plasmid DNA extraction 60
2.2.3.2 RNA extraction, reverse transcription, and real-time quantitative PCR 61
2.2.4 Biochemistry 64
2.2.4.1 RhoA activity assay 64
2.2.4.2 ROCK activity assay 65
2.2.4.3 Co-Immunoprecipitation (Co-IP) 67
2.2.4.4 Protein analysis by western blot 68
2.2.5 Statistical analysis 70

Chapter 3: ASPP2 deficiency impairs chain migration of neuroblasts leading to diminished olfactory bulbs. 72

3.1 *Aspp2-KO* mice have smaller olfactory bulbs. 73

3.2 ASPP2 deficiency impairs the migration of neuroblasts from the SVZ to the olfactory bulb. 76

3.3 ASPP2 is necessary for neuroblasts to form chains in the SVZ and the RMS. 80

3.4 ASPP2 deficiency impairs chain formation and migration of neuroblasts *in vitro*. 82

3.5 Summary 84

Chapter 4: ASPP2 deficiency impairs radial migration leading to periventricular nodular heterotopia (PNH). 86

4.1 *Aspp2-KO* mice developed periventricular nodular heterotopia (PNH). 87

4.2 ASPP2 deficiency leads to impaired radial migration. 92

4.3 ASPP2 does not affect the VZ lining and RGC scaffold. 96

4.4 The influence of ASPP2 on the proliferation of neural stem cells. 98
4.4.1 ASPP2 does not influence Notch signalling in neural stem cells *in vitro*. 99
4.4.2 ASPP2 does not influence NSC proliferation and neurosphere growth *in vitro*. 101
4.4.3 ASPP2 deficiency leads to the randomization of the spindle orientation of RGCs *in vivo*. 104

4.5 Summary 108

Chapter 5: ASPP2 regulates actin cytoskeleton and cell migration through Rho-ROCK signalling. 110

5.1 Phosphoproteomic analysis reveals ASPP2 may regulate cytoskeleton through Rho-ROCK signalling. 112

5.2 ASPP2 deficiency impairs actomyosin stress fibre formation. 119

5.3 ASPP2 deficiency impairs cell migration. 121

5.4 ASPP2 deficiency impaired phosphorylation of downstream effectors of Rho-ROCK signalling. 123

5.5 ASPP2 does not regulate RhoA-ROCK signalling by interacting with RhoA. 126

5.6 ASPP2 interacts with ROCK2 and enhance its activity. 128

5.7 ASPP2 may influence ROCK activity in a PP1-dependent manner....130

5.8 ASPP2 does not interact with Filamin A.....134

5.9 Summary 137

Chapter 6: Discussion 139

6.1 ASPP2 in regulating Rho-ROCK signalling and the actin cytoskeleton.....139

6.2 ASPP2 in neuronal migration.....146

6.3 ASPP2 in developing periventricular nodular heterotopia (PNH). 149

6.4 Drawbacks and Future directions 156

6.4.1 The CNS phenotypes caused by loss of ASPP2 were not comprehensively characterized. 156

6.4.2 The role of ASPP2 in regulating migratory behaviors of neurons needs further investigation. 158

6.4.3 There is a gap between molecular mechanism identified in U2OS cells and the mouse phenotypes. 160

Reference....162

List of Tables

Table 2. 1 List of Chemicals, Reagents, and Kits 35
Table 2. 2 List of primers for RT-PCR 42
Table 2. 3 List of primers for genotyping 43
Table 2. 4 List of primary antibodies 43
Table 2. 5 List of secondary antibodies 44
Table 2. 6 Components of genotyping PCR reaction 48
Table 2. 7 PCR program for genotyping 48
Table 2. 8 Components of the reverse transcription reaction 63
Table 2. 9 Components of RT-PCR reaction 63
Table 2. 10 Programme for RT-PCR 64
Table 2. 11 Reaction setup for ROCK activity assay 66
Table 2. 12 Recipes for stacking and resolving gels 69

List of Figures

Figure 1. 1 Formation of the neural tube from the neural plate. 2
Figure 1. 2 Schematic representation of interkinetic nuclear migration (INM). 3
Figure 1. 3 Architecture of the early central nervous system. 4
Figure 1. 4 Neocortex development in mice and humans. 7
Figure 1. 5 Model of spindle orientation in the symmetric and asymmetric division. 9
Figure 1. 6 Model of the spindle orientation machinery. 10
Figure 1. 7 Asymmetric segregation of fate determinates during RGC divisions. 11
Figure 1. 8 Three modes of neuronal migration. 13
Figure 1. 9 The saltatory movement of migrating neuroblasts. 14
Figure 1. 10 Domain organization of the ASPP proteins. 26

Figure 3. 1 *Aspp2-KO* mice showed diminished olfactory bulbs. 75
Figure 3. 2 *Aspp2-KO* mice showed more DCX+ cells in the SVZ but fewer in the OB. 78
Figure 3. 3 Newborn neuroblasts failed to reach the olfactory bulb effectively in *Aspp2-KO* mice. 79
Figure 3. 4 ASPP2 deficiency leads to the failure of neuroblasts chain formation in the SVZ and the RMS. 81
Figure 3. 5 ASPP2 deficiency impairs chain formation and migration of neuroblasts in vitro. 84

Figure 4. 1 *Aspp2-KO* mice develop PNH largely comprised of mature neurons. 90
Figure 4. 2 *Aspp2-KO* embryos at E14.5 show abnormalities representing PNH. 91
Figure 4. 3 pCAG-CRE-GFP plasmids successfully knockout ASPP2 in NSCs in Trp53bp2 loxP/loxP mice. 93
Figure 4. 4 ASPP2 deficiency leads to impaired radial migration. 95
Figure 4. 5 ASPP2 doesn't affect VZ lining and RGC scaffold. 97
Figure 4. 6 mRNA levels of Notch target genes in WT and *Aspp2-KO* NSCs/NPCs with or without Dll4 treatment. 100

Figure 4. 7 ASPP2 does not influence NSCs proliferation and neurospheres growth in vitro. 102
Figure 4. 8 ASPP2 deficiency leads to the randomization of spindle orientation in dividing RGCs in E14.5 neocortex. 107
Figrue 4. 9 *Aspp2-KO* neocortex exhibited fewer Pax+ RGCs and more Tbr2+ IPCs. 108

Figure 5. 1 Overview of the mass spectrometry-based phosphoproteomic analysis using WT and *ASPP2-KO U2OS* cells. 114
Figure 5. 2 Pathway enrichment analysis reveals ASPP2 is involved in Rho signalling- mediated cytoskeleton regulation. 116
Figure 5. 3 Phosphorylation motif analysis identifies prominent ASPP2 regulating phosphoproteins as ROCK substrates. 118
Figure 5. 4 ASPP2 deficiency impaired Rho activator induced actomyosin stress fibre formation. 120
Figure 5. 5 ASPP2 deficiency impaired U2OS cell migration 122
Figure 5. 6 ASPP2 deficiency impaired the phosphorylation of downstream effectors of Rho-ROCK signalling. 125
Figure 5. 7 ASPP2 does not regulate RhoA-ROCK signalling through RhoA 127
Figure 5. 8 ASPP2 interacts with ROCK2 and enhances its activity. 129
Figure 5. 9 ASPP2 may influence ROCK activity in a PP1-dependent manner. 133
Figure 5. 10 ASPP2 does not interact with Filamin A. 136

Figure 6. 1 Proposed model of how *Aspp2-KO* mice develop PNH. 153

Chapter 1: Introduction and Background

1.1 A Brief Summary of CNS Development.

Central nervous system (CNS) development starts with the formation of the neural tube during early embryonic development. The notochord secretes growth factors to induce differentiation of the overlying segment of the ectoderm, which leads to the formation of a thickened structure called the neural plate. The invagination of a furrow along the dorsal midline of the neural plate produces the neural groove, which merges at the dorsal apex to form the neural tube (**Figure 1.1**).

The neural tube wall constitutes a pseudostratified columnar epithelium, which is made up of highly polarized cells called neuroepithelial cells (NECs). NECs have bipolar processes that span the entire thickness of the neural tube(Kielar et al., 2014; Lui et al., 2011; Paridaen & Huttner, 2014). They extend their apical process to attach the surface of the neuronal tube canal, where their endfeet form adherens junctions and tight junctions. NECs also elongate their basal process to contact the laminal side. NECs divide symmetrically to self-renew and drive the expansion of the neural tube. In order to maintain the pseudostratified cytoarchitecture while accommodating extensive proliferation, NECs undergo a unique form of cell division known as interkinetic nuclear migration (INM), which is a cell cycle-related periodic movement of the cell nucleus. As depicted in **Figure 1.2**, cell nuclei are located at the basal end of the cell during S phase, move from the basal side towards the apical side during G2 phase, undergo M phase close to the ventricular surface, and then migrate to the basal side during G1phase (Kosodo et al., 2011; Taverna & Huttner, 2010).

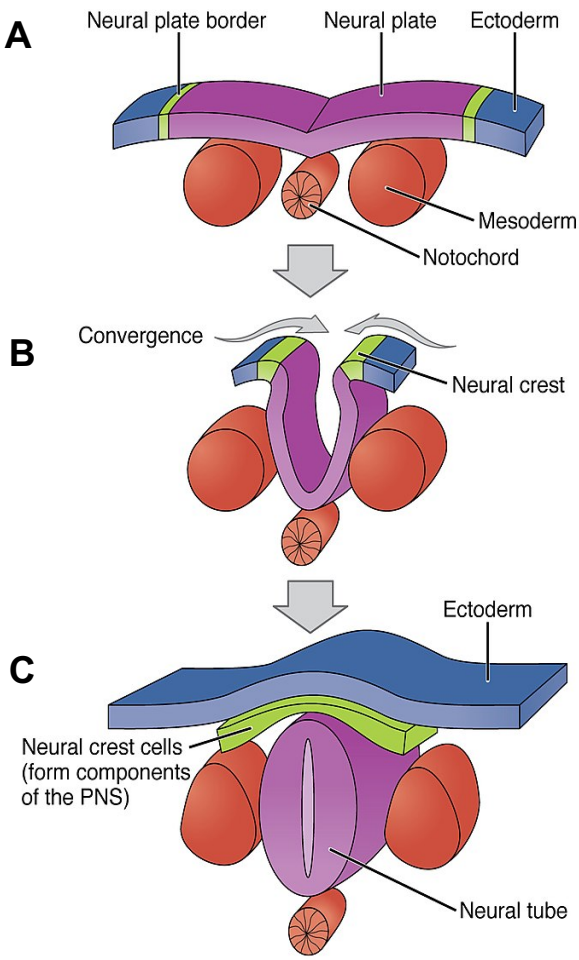


Figure 1. 1 Formation of the neural tube from the neural plate.

(A) Neuroectoderal tissues differentiate from the ectoderm and thicken into the neural plate. The neural plate border separates the ectoderm from the neural plate. (B) The neural plate bends dorsally, with the two ends eventually joining at the neural plate borders, which forms the neural crest. (C) The closure of the neural tube disconnects the neural crest from the epidermis. Neural crest cells differentiate to form most of the peripheral nervous system. Adapted from Anatomy & Physiology. http://cnx.org/content/col11496/1.6/

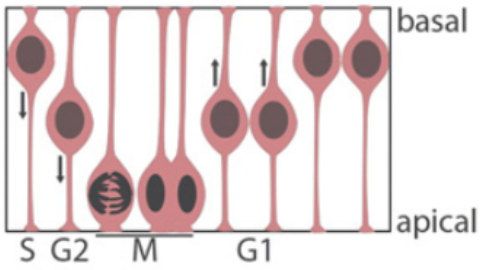


Figure 1. 2 Schematic representation of interkinetic nuclear migration (INM).

Nuclear movement in progenitor cells of the ventricular zone (VZ) is coordinated with the cell cycle phases: Cell nuclei are located at the basal end of the cell during S phase, move from the basal side towards the apical side during G2 phase, undergo M phase close to the ventricular surface, and then migrate to the basal side during G1phase. Adapted from Xiangning Jiang, 2016.

As the neural tube expands, swellings appear at the cranial end to form more mature structures. The morphological changes represent the onset of rostral-caudal regionalization within the CNS. As shown in **Figure 1.3**, three primitive vesicles appear first: prosencephalon, mesencephalon, and rhombencephalon. These structures subsequently develop into five secondary vesicles, which then each generate one of the main regions of the brain: 1) prosencephalon becomes the telencephalon (cortex) and diencephalon (thalamus, hypothalamus, and retina); 2) mesencephalon becomes the midbrain; 3) the rhombencephalon becomes the metencephalon (pons and cerebellum) and the myelencephalon (medulla). The caudal neural tube develops into the spinal cord.

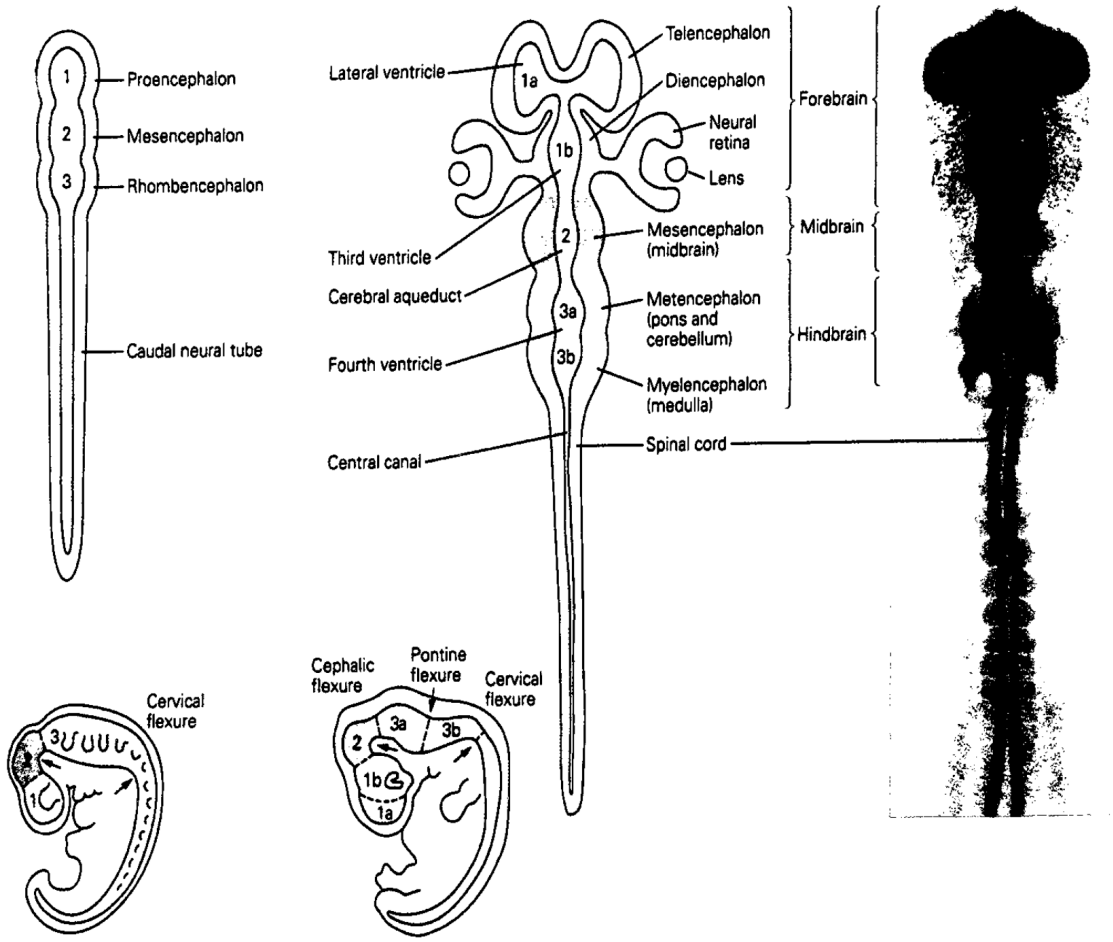


Figure 1. 3 Architecture of the early central nervous system.

Adapted from Kandel, Schwarz, and Jessell. Principles of Neural Science.

1.2 Neurogenesis in the Developing Neocortex.

The cerebral cortex is the visible surface layer of the hemispheres, which includes more ancient allocortex and more recently evolved neocortex. The neocortex comprises the vast majority of the cerebral cortex and is responsible for higher-order cognitive functions. It has six horizontal layers segregated principally by cell type and neuronal connections, from superficial to deep, I to VI. It is the most functionally and structurally complicated component of the central nervous system (CNS). Building up this highly organized

cytoarchitecture involves the production of a wide variety of cell types at the proper location, in the correct number, and within the right timing.

1.2.1 Neurogenic Phases and Progenitor Subtypes.

During the initial proliferative phase (E ≤ 11–12 in mice), NECs undergo self-renewing symmetric divisions to expand the stem cell pool and thicken the neuroepithelium (Rakic, 1995), which has a significant impact on the surface area and thickness of the neocortex (Paridaen & Huttner, 2014; Sun & Hevner, 2014; Dehay et al., 2015). At the onset of neurogenesis (E11-12 in mice), NECs change their identity, including reduced Golgi-derived apical trafficking and loss of tight junctions, and they turn into radial glial cells (RGCs). RGCs maintain some features of NECs including adherens junctions at the ventricular surface and elongated process that span the entire thickness of the cortex. RGCs are characterized by their high expression of the transcription factors Pax6, Sox2, and by the high expression of glial markers GLAST and BLBP (Hartfuss et al., 2001).

In the first phase of neurogenesis, an RGC can either undergo symmetric division to generate two RGCs or undergo asymmetric division to produce one RGC and one neuron (Noctor, 2008). As corticogenesis proceeds, RGCs stop to generate neurons directly from the asymmetric division. Instead, an RGC divides asymmetrically to produce one RGC and one intermediate progenitor cell (IPC). IPCs are transiently amplifying progenitors with high expression of the transcription factor Tbr2. IPCs lose the apical contact with the ventricular zone and achieve a multipolar morphology. They delaminate from the VZ to settle in the subventricular zone (SVZ) and then divide symmetrically to produce neurons. Some IPCs are capable of several rounds of self-renewal to expand the progenitor cell pool

before turning into neurons (Noctor et al., 2004). Neuronal generation is significantly increased through this type of indirect neurogenesis. It has been shown that each RGC can give rise to 8–9 neurons distributed throughout the different layers in mouse brain development (Gao et al., 2014). Neurons generated in the SVZ migrate through the intermediate zone (IZ), which is made up of white matter, to form the cortical plate (CP), which will give rise to cortical layers II to VI. The cortical plate separates the preplate into two parts. The Cajal-Retzius cells are above the cortical plate and form the marginal zone (cortex layer I), while the subplate is below the six cortical layers. At the end stage of neurogenesis, RGCs undergo asymmetric self-consuming division to generate two neurons (Noctor et al., 2004). They can also go through apoptosis or give rise to astrocytes or oligodendrocytes.

To summarize, the total amount of neurons generated is influenced by the initial stem cell pool (NECs), by the gradual switch from RGC mediated direct neurogenesis to IPC mediated indirect neurogenesis, and by the duration of the neurogenic phase. Interestingly, a major difference has been identified between lissencephalic species like rodents and gyrencephalic species such as primates in terms of the size of the progenitor pool and the length of the neurogenic phase. The SVZ in primates is separated by the inner fibre layer (IFL) into two layers: the inner SVZ (iSVZ) contains only IPCs, equivalent to the SVZ in rodents, and the outer SVZ (oSVZ) which contains an extra type of progenitor called basal RGCs (bRGCs). bRGCs are rare in mice and they don’t form a distinct OSVZ (X. Wang et al., 2011). bRGCs are produced by symmetric divisions of apical RGCs (Hansen et al., 2010; Lui et al., 2011; Shitamukai & Matsuzaki, 2012). Unlike multipolar IPCs, bRGCs have an apical or a basal process or both processes (Betizeau et al., 2013; Lamonica et al.,

2013). They subsequentially generate more bRGCs and IPCs to significantly expand the pool of progenitor cells. In addition, IPCs in the SVZ undergo at most two rounds of divisions in the mouse (Noctor et al., 2004), while there are more rounds of IPC division in humans and other primates (Betizeau et al., 2013; Fietz et al., 2012; Martínez-Cerdeño et al., 2012).

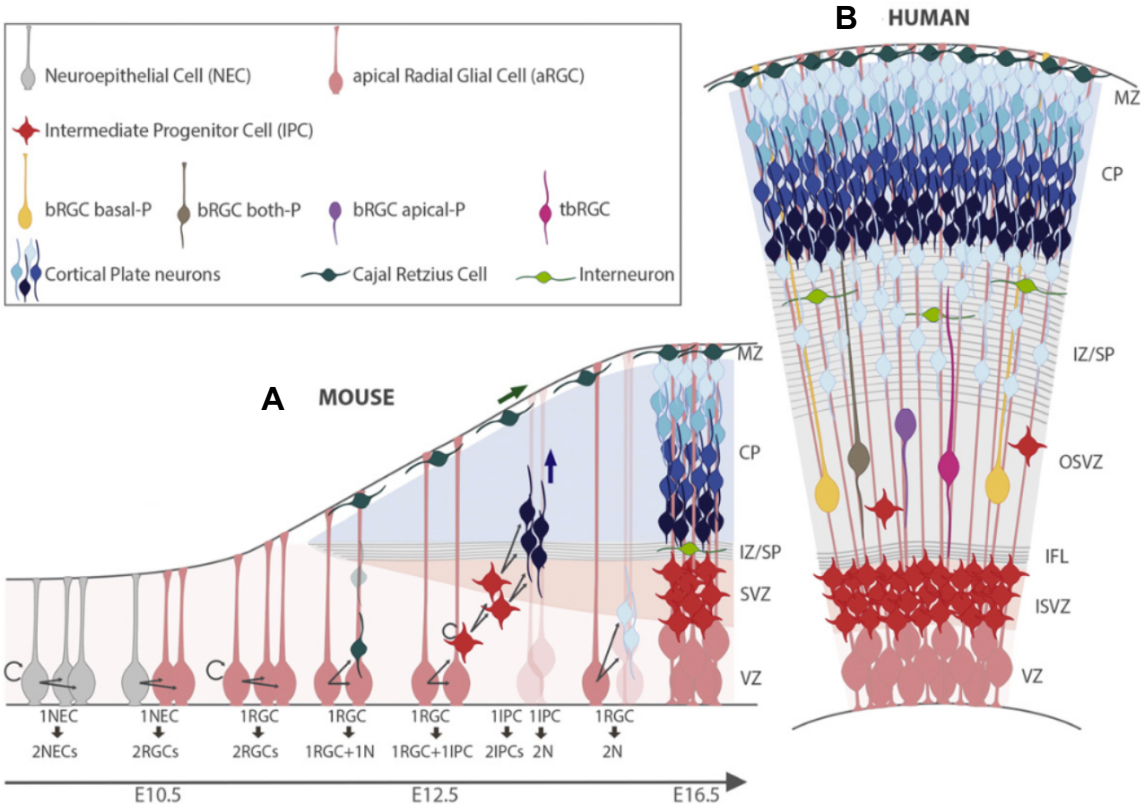


Figure 1. 4 Neocortex development in mice and humans.

(A) Neurogenesis in mice: NECs self-renew by dividing symmetrically, then turn into RGCs. RGCs divide either symmetrically to self-renew, or asymmetrically to produce primary neurons which migrate to the cortical surface to form the marginal zone (MZ), and to IPCs which populate the sub-ventricular zone (SVZ) and subsequently turn into neurons. New-born neurons migrate along the basal process of RGCs towards their destined layers. At later stages, RGCs can undergo final symmetric divisions generating two neurons. (B) Human foetal cortex at a developmental stage around 15 PCW. The major differences with the mouse embryonic developing cortex are 1) the SVZ is split into inner (iSVZ) and outer (oSVZ) regions by the inner fibre layer (IFL); 2) the remarkable expansion of the IZ/SP.

The oSVZ comprises IPCs and further progenitor subtypes named basal RGCs (bRGCs): b-RGC basal-P with a basal process, b-RGC apical-P with an apical process, b-RGC both-P with an apical process and a basal process; tbRGC, a transient bRGC with short apical and basal processes. Adapted from (X. Jiang & Nardelli, 2016).

1.2.2 Symmetric Versus Asymmetric Divisions.

As mentioned in section 1.2.1, dynamic switches between asymmetric and symmetric cell division modes of radial glial cells (RGCs) are critical for brain development. The percentage of asymmetric division increases from the onset of neurogenesis and peaks at E14, when neurogenesis is most active. After that, the percentage of asymmetric division decreases gradually (Paridaen & Huttner, 2014). Cellular mechanisms determining division types of NPCs can be classified into 1) regulating mitotic spindle orientation and 2) inheritance of cell fate determinants.

Spindle orientation seems to be a critical initial factor in determining the outcome of RGC divisions. When RGCs divide symmetrically to self-renew, they have planar spindle orientation (Figure 1.5). However, the RGC dividing asymmetrically to produce one RGC and one neuron or one IPC has oblique spindle orientation (Figure 1.5). Disruption of planar orientations by inducing oblique/vertical orientations or randomization of orientations results in depletion of the progenitor pool (Yingling et al., 2008). Disruption of oblique orientations causes reduced production of neurons (Postiglione et al., 2011).

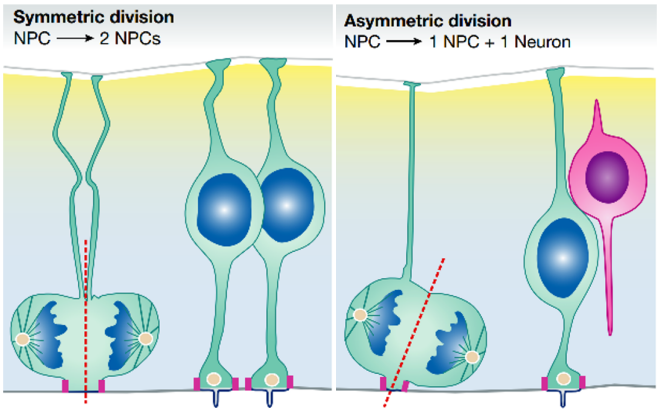


Figure 1. 5 Model of spindle orientation in the symmetric and asymmetric division. Symmetric division yields two NPCs, whereas asymmetric NPC division yields one NPC daughter and one differentiating daughter cell. Adapted from (Paridaen & Huttner, 2014).

The spindle orientation machinery involves the growth of spindle microtubules from the centrosome, anchoring astral microtubule to the subcortical actin cytoskeleton and positioning spindle poles through cortical F-actin flow. Astral microtubule anchoring is mediated by dynein-dynactin and the LGN/Gα/NuMA complex. As shown in **Figure 1.6**, in planar divisions, the LGN complex localizes at the two lateral sides and associates with both spindle poles (Peyre et al., 2011). This localization pattern seems to be achieved by the exclusion of the LGN complex from the apical domain mediated by the Par complex (Hao et al., 2010). In oblique divisions, LGN only associates with the spindle pore oriented at the apical domain of the dividing cell (El-Hashash & Warburton, 2011). On the other side of the dividing cell, mLnsc may displace NuMA from the LGN complex thus disrupt microtubule anchoring (Žigman et al., 2005).

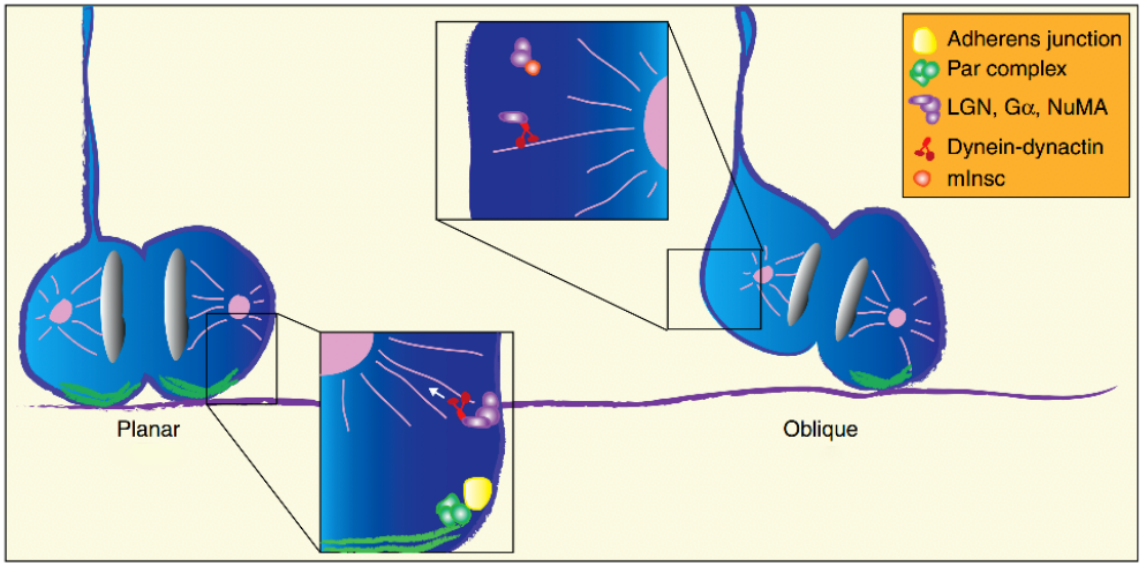


Figure 1. 6 Model of the spindle orientation machinery.

During planar divisions (left), LGN associates with NuMA and Gα to direct the spindle pole away from the apical domain along the planar axis. NuMA acts as the bridge between LGN at the lateral poles and dynein/dynactin, which drive spindle pole positioning through directed microtubule transport. During oblique divisions (right), mInsc may compete for binding with LGN and displace NuMA from the LGN complex thereby uncoupling spindle pole positioning and lateral cortex anchoring relative to the apical domain. Adapted from (Lancaster & Knoblich, 2012).

Spindle orientation is not the sole determining factor of division outcomes. Asymmetric segregation of cell fate determinants also plays important roles (Figure 1.7). Notch signalling components such as Delta-like 1, Mindbomb, and Numb are asymmetrically inherited by the two daughter cells. Delta-like 1 is a Notch ligand while Numb is a Notch antagonist. Mindbomb is a regulator of the internalization of Notch ligand. Differentially distributed Notch components lead to high Notch signalling in one daughter cell which will remain as RGC while low notch signalling in the other daughter cell which undergoes the differentiation process. The apical Par complex also localizes asymmetrically in dividing RGCs. Par3 can interact with Numb and promote Notch activity. The daughter cell

inheriting a higher level of Par3 has enhanced Notch activity and thus retains RGC's fate (Bultje et al., 2009). More importantly, the Par complex is essential for maintaining or reestablishing the apical domain at the ventricular surface, which is important for RGCs maintenance. The daughter cell lacking the apical domain will delaminate from the VZ and undergo a differentiation process. Besides polarity proteins, other cytoplasmic proteins also show asymmetric inheritance during RGC divisions. Staufen can bind a set of mRNAs that induce cell cycle exit and differentiation. The protein mRNAs complex is then segregated into differentiating daughter cells (Kusek et al., 2012; Vessey et al., 2012).

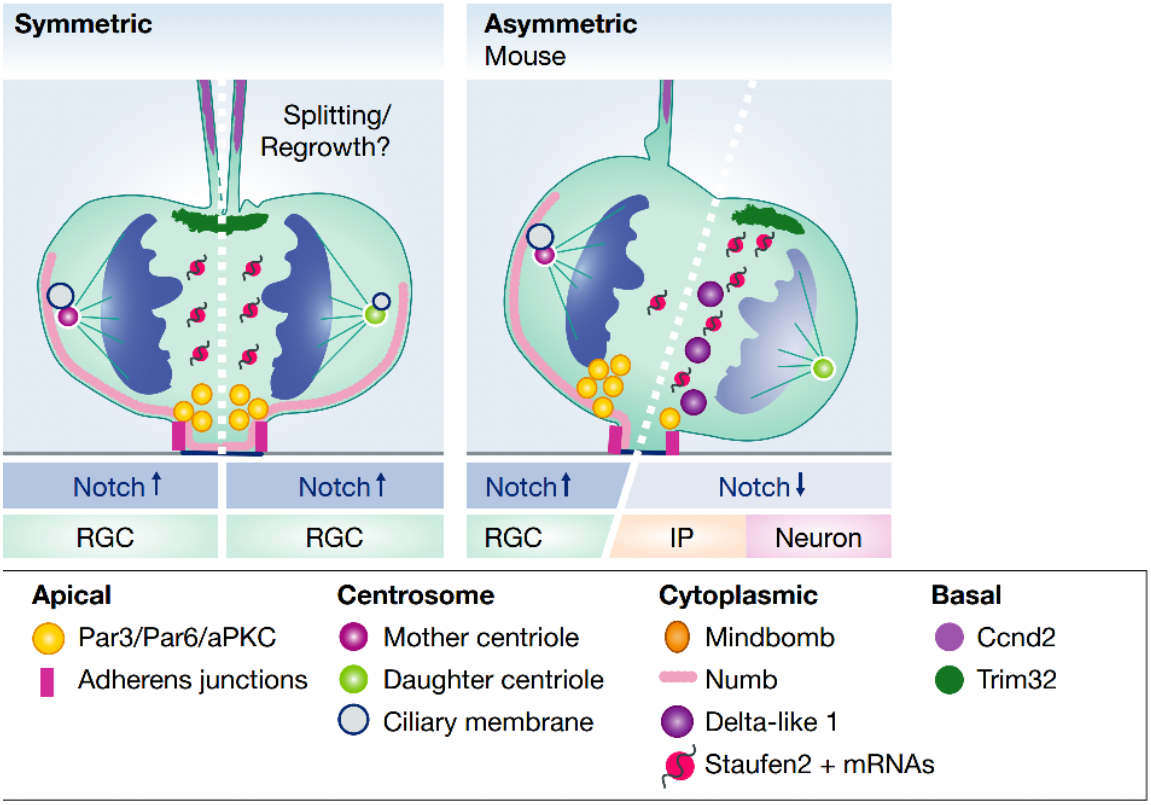


Figure 1. 7 Asymmetric segregation of fate determinates during RGC divisions.

Cell fate determinants are equally (symmetric division, left) or unequally (right) distributed between daughter cells. Adapted from (Paridaen & Huttner, 2014).

1.3 Neuronal migration during brain development.

The newly generated neurons need to travel from their birthplaces to their destinations in order to form highly laminated cortical structures and coordinated neuronal circuits of the central nervous system (CNS). During brain development, there are mainly three modes of migration: radial migration, tangential migration, and chain migration (**Figure 1.8**). Firstly, in the developing neocortex, excitatory projection neurons are born in the ventricular zone (VZ) and subventricular zone (SVZ). New-born neurons migrate as multipolar cells independent of the radial scaffold in the SVZ and lower IZ (Tabata & Nakajima, 2003). They become bipolar as they leave the IZ and switch their migration mode to saltatory locomotion along with the radial processes of RGCs into the cortical plate (Nadarajah et al., 2001). Secondly, inhibitory GABAergic interneurons born in the medial ganglionic eminence migrate tangentially in streams into the cerebral cortex (Ang et al., 2003). They then switch to radial migration to integrate into the various cortical layers (Anderson, 1997; Wonders & Anderson, 2006). Thirdly, the neuroblasts born in the late embryonic, postnatal and adult SVZ form elongated chain-like aggregates that migrate through the rostral migratory stream (RMS) to the olfactory bulb (OB) (Lois et al., 1996; Lois & Alvarez-Buylla, 1994). In the OB, neuroblasts detach from the chains and migrate radially to the outer layers where they differentiate into interneurons.

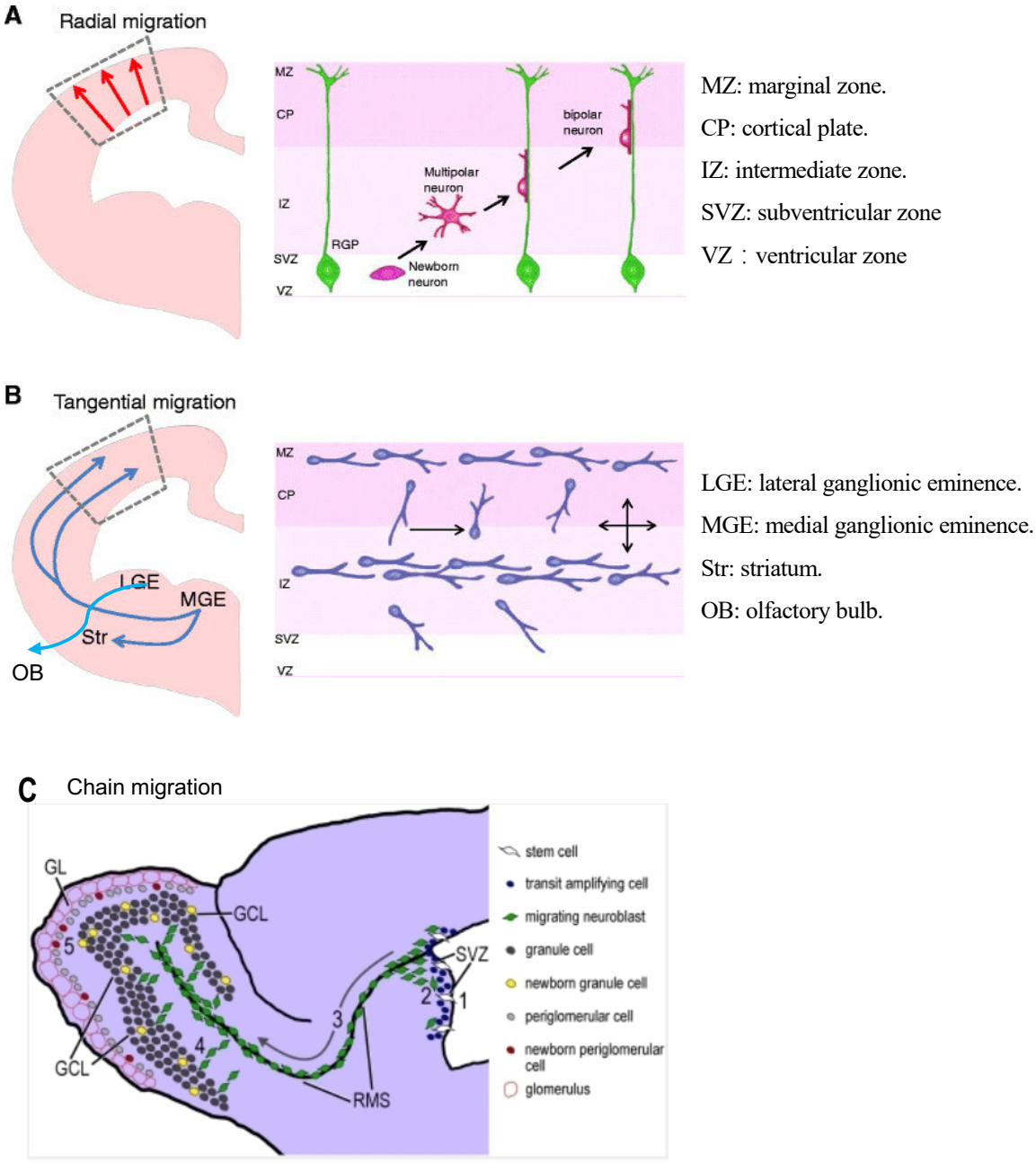


Figure 1. 8 Three modes of neuronal migration.

(A) Neurons born in the VZ/SVZ migrate radially into the neocortex. (B) Neurons born in the medial ganglionic eminence migrate tangentially into the neocortex. (C) Chain migration of neuroblasts in the rostral migratory stream (RMS). Modified from (Moffat et al., 2015; Sui et al., 2012).

Despite differences in migratory routes and types, the bipolar migrating neurons/neuroblasts are characterized by a saltatory movement encompassing cyclical steps: extension of the leading process, swelling formation and centrosome migration, nuclear movement, and somal translocation (Schaar & McConnell, 2005) (Figure 1.9). These saltatory movements are achieved by the dynamic rearrangement of the cytoskeleton in response to extracellular cues (Ridley, 2003; Walsh, 2000).

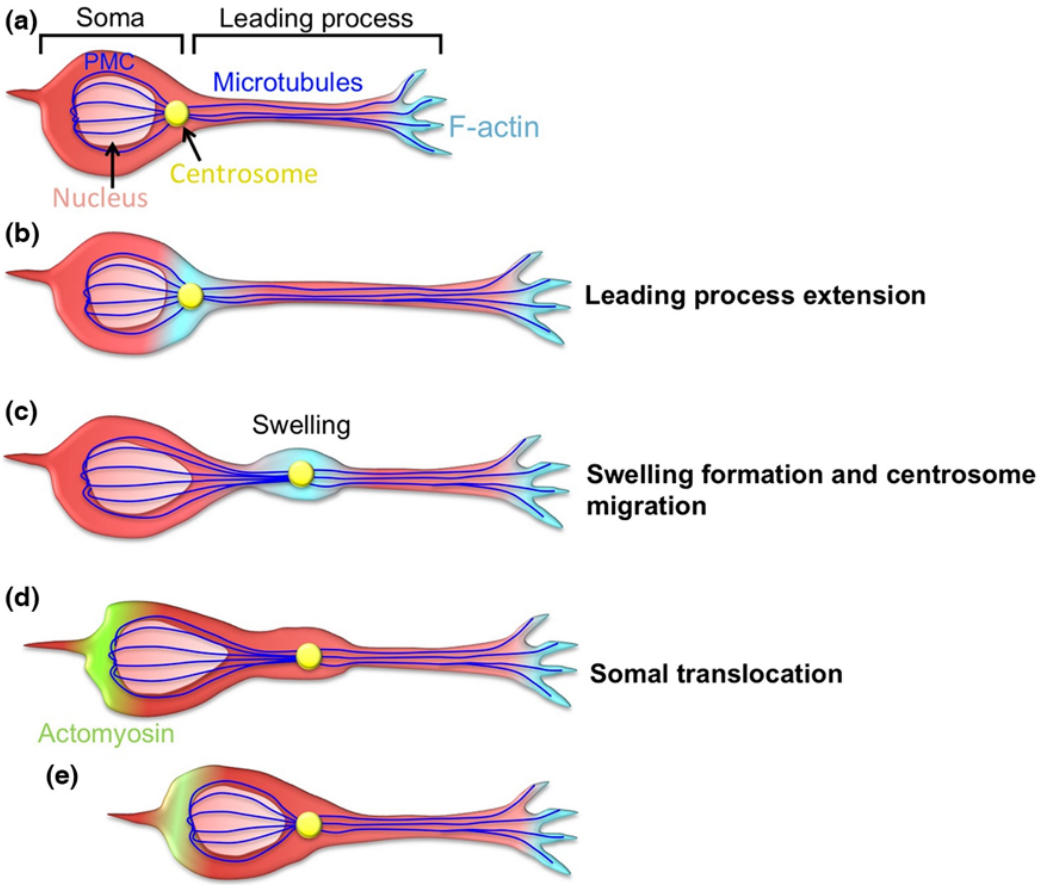


Figure 1. 9 The saltatory movement of migrating neuroblasts.

(a)The typical morphology of a migrating neuroblast. PMC: perinuclear microtubule cage. (b) extension of the leading process. (c) swelling formation and centrosome migration. (d-e) somal translocation. Adapted from (Kaneko et al., 2017).

Extension of the leading process helps to determine the direction of migration (Valiente & Martini, 2009). The growth cone-like structure at the tip of the leading process actively extends lamellipodia and filopodia, which is driven by Rac1 and CDC42 mediated actin reorganization (Guan et al., 2007; Whitford et al., 2002). Actomyosin or so-called stress fibre is enriched in the leading process (Rivas & Hatten, 1995; Solecki et al., 2009; Trivedi et al., 2017). Regulation of actin polymerization by various factors, such as Vav3 which can activate Rac1, Drebrin and Fascin which are actin-binding proteins, is necessary for the formation and extension of the leading process (Khodosevich et al., 2009; Sonego et al., 2013, 2015). Besides actin cytoskeleton, microtubules are also important for the extension of the leading process. Inhibiting the stability of microtubules by nocodazole suppresses the extension of the leading process (Schaar & McConnell, 2005). Deficiency in cyclin-dependent kinase 5 or doublecortin, which are regulators of microtubule organization, leads to abnormal highly branched and shorter leading processes (Hirota et al., 2007; Koizumi, Higginbotham, et al., 2006).

After the formation of the leading process, the centrosome migrates into the leading process, and a cytosolic dilation forms around the centrosome (Schaar & McConnell, 2005). The centrosome functions as an organizing centre for microtubules in the leading process and enwrapping the nucleus (Tsai et al., 2007). Local RhoA activation at the swelling is important for the swelling formation and centrosome migration (Ota et al., 2014; Shinohara et al., 2012).

While the centrosome migrates into the leading process, the nucleus is captured by the perinuclear microtubule cage and pulled forward by centrosome movement. Myosin II

activity and F-actin are enriched at the swelling and the rear of the cell during somal translocation (Schaar & McConnell, 2005; Shinohara et al., 2012). F-actin flow along the leading process driven by actomyosin activity is necessary for generating traction force for nucleus movement and soma translocation (He et al., 2010; Solecki et al., 2009; Trivedi et al., 2017; Umeshima et al., 2019). Actomyosin contractility also functions at the rear of the nucleus to push the cell body forward during retraction of the trailing tail (Bellion, 2005; Martini & Valdeolmillos, 2010; Schaar & McConnell, 2005). Inhibiting myosin II or ROCK, a regulator of actomyosin formation, suppresses somal translocation (Schaar & McConnell, 2005; Shinohara et al., 2012). Deficiency in mDia, a regulator of actin polymerization, also causes impaired somal translocation (Shinohara et al., 2012).

1.4 Grey matter heterotopia

Malformations of cortical development (MCDs) are a group of disorders resulting from disruptions of developmental processes of the cerebral cortex including the proliferation of neural progenitor cells, neuronal migration, and layer organization. Based on the disrupted processes, MCDs can be classified into different groups. Microcephaly or megalencephaly characterized by size-reduced or enlarged brains is caused by reduced or enhanced proliferation respectively. Defects in neuronal migration lead to grey matter heterotopia, which is characterized by the ectopic accumulation of neuron clusters along the ventricular walls (periventricular nodular heterotopia, PNH) or ribbons of grey matter beneath the cortex (subcortical band heterotopia, SBH). Alterations on post-migrational processes are causes of polymicrogyria, characterized by a cortex with multiple small gyri.

MCDs are important causes of childhood epilepsy. MCDs are responsible for up to 40% of cases of medication-resistant childhood epilepsies (Barkovich et al., 2012; Guerrini & Dobyns, 2014). Around 75% of the patients with MCDs have epilepsy (Leventer et al., 1999). Associated with seizures, the patients also show other symptoms including developmental delay and intellectual disability. Cognitive deficits are more frequent and severe when epilepsy begins early in life (Berg et al., 2017).

1.4.1 Periventricular nodular heterotopia (PNH).

Periventricular nodular heterotopia is the most common type of malformation of cortical development (MCD). It is characterized by nodular masses of grey matter that locate at the surface of ventricular walls and protrude into the lumen. PNH can be unilateral or bilateral. The heterotopic tissue can appear as a single nodule or as many contiguous or numerical nodules. These ectopic nodules contain both neurons and glial cells, and sometimes have rudimentary lamination (Tassi et al., 2005).

The most commonly mutated gene found in patients with PNH is the X-linked *FLNA* gene. In a study of 120 patients with PNH, mutations of *FLNA* were found in all 10 families with X-linked inheritance and 49% of patients irrespective of familial or sporadic occurrence (Parrini et al., 2006). In another study, *FLNA* mutations were found in 26% of sporadic patients with PNH (Fox et al., 1998). *FLNA* mutations in the male may lead to prenatal lethality, so only a few living male patients with PNH caused by *FLNA* mutations have been reported (V L Sheen, 2001). The sex ratio was skewed with 93% of *FLNA* mutations in female patients and 7% in male patients. The FLNA gene encodes Filamin A, which is an actin-binding phosphoprotein. Filamin A crosslinks actin filaments into orthogonal

networks (Nakamura et al., 2007) and regulates reorganization of the actin cytoskeleton leading to changes in cell shape and migration (Stossel et al., 2001). Consistent with its importance in neurodevelopment, Filamin A is highly expressed in prenatal and neonatal brains, and its expression level declines during adolescence (Stossel et al., 2001). *Flna* knockout mice showed a high rate of early embryonic lethality with severe cardiovascular defects. The few surviving mice had smaller brains without any neuronal heterotopia (Feng et al., 2006). However, *in utero* knockdown of *Flna* in the developing neocortex of rat has reproduced a PNH phenotype similar to the one observed in human patients, and juvenile *FlnA*-knockdown rats are highly susceptible to seizures (Carabalona et al., 2012). In *FlnA*-knockdown rats, PNH resulted from disruption of the apical process of radial glial cells in the ventricular zone and impaired migration of neurons into the cortical plate. Inhibition of the function of Filamin A by overexpressing a mutant Filamin A prevents neurons from maintaining consistent polarity toward a specific direction and decreases motility in the subventricular and intermediate zones (Nagano et al., 2004). In contrast, inhibiting Filamin A degradation by silencing Filamin A-interacting protein promotes the development and maintenance of a bipolar shape of migrating neurons in the subventricular and intermediate zones (Nagano et al., 2004). Interestingly, another study showed that wild-type Filamin A over-expression inhibited neuronal migration (Sarkisian et al., 2006). These results suggest that Filamin A is involved in maintaining the apical process of radial glial cells and the integrity of ventricular lining, and in regulating neuronal migration through cell shape and migratory polarity.

It has been demonstrated that mice mutant for MEKK4, a MAP kinase that regulates the CSBP2 and JNK-MAPK pathways, developed PNH associated with breaches in the

neuroependymal lining which were largely comprised of neurons that failed to reach the cortical plate (Sarkisian et al., 2006). Interestingly, the expression of Filamin A was elevated near sites of failed neuronal migration. Phosphorylation of FLNA at serine 2152 depends on MEKK4 signalling and phosphorylation of this residue influences Filamin A localization at the cell membrane. These results suggest that MEKK4 deficiency causes PNH through regulating functions of Filamin A in the mouse. Up to now, mutations in *MEKK4* have not been characterized in human PNH patients.

Mutations in the *ARFGEF2* gene have been reported to cause an autosomal recessive condition of microcephaly and periventricular neuronal heterotopia in two families (Volney L. Sheen et al., 2004). *ARFGEF2* encodes the brefeldin A (BFA)-inhibited guanine nucleotide-exchange factor-2 (GEF2) (BIG2), which regulates vesicle trafficking and transport of membrane molecules from the trans-Golgi network (TGN) (Shin et al., 2005). Inhibition of BIG2 disturbed the localization of such E-cadherin and β-catenin at the cell surface by preventing their transport from the Golgi apparatus (Volney L. Sheen et al., 2004).

It has been reported that mutations in genes encoding the receptor-ligand cadherin pair *DCHS1* and *FAT4* lead to a recessive syndrome that includes periventricular neuronal heterotopia (Cappello et al., 2013). FAT4 is a member of the protocadherin superfamily and DCHS1 is a ligand of FAT4. These two proteins constitute an apically located heterophilic adhesive complex that is biochemically and spatially distinct from adherens junctions (Ishiuchi et al., 2009). *Dchs1* and *Fat4* knockout mice were neonatal lethal and showed no morphological or histological evidence of MCDs at embryonic stages.

Knocking down *Dchs1* and *Fat4* in mouse developing neocortex by in utero electroporation resulted in increased proliferation and abnormal distribution of neural progenitor cells and arrest of neuronal migration in the subventricular zone and intermediate zone (Cappello et al., 2013).

Periventricular neuronal heterotopia has also been observed in patients with chromosomal rearrangements in 5q14.3 (Cardoso et al., 2008), 5q15 (V L Sheen et al., 2003), 6q25 (Cellini et al., 2012), 6q27 (V. Conti et al., 2013) and 7q11 (Ferland et al., 2006). *C6orf70* has been identified as a putative causal gene for the 6q27-related form while the aetiology remains unknown for the other forms. *C6orf70* encodes the endoplasmic reticulum membrane-associated RNA degradation protein (ERMARD). The silencing of *C6orf70* in the developing rat neocortex resulted in the migration arrest of neurons in the ventricular zone (VZ) and intermediate zone (IZ), which can be rescued by concomitant expression of wild-type human C6orf70 protein.

1.4.2 Subcortical band heterotopia (SBH).

Unlike PNH in which the abnormal accumulation of neurons is found at the ependymal lining of the ventricle, subcortical band heterotopia (SBH), also known as double cortex syndrome, is characterized by band-like clusters of tissue located beneath the cerebral cortex. In most cases, the heterotopic bands are bilateral. The overall cortical thickness is increased due to the heterotopic cortex. However, the normal overlying cerebral cortex is thinner and may have shallow sulcation and a simplified gyration pattern.

The most commonly mutated gene found in patients with SBH is the X-linked *DCX* gene. While heterozygous females develop SBH, the majority of hemizygous males develop lissencephaly, which is characterized by a smooth brain without the development of folds and grooves at the surface of the cortex. Only a few male SBH patients associated with *DCX* mutations have been reported (D'Agostino, 2002; Dobyns, 2010; Quélin et al., 2012). This may be explained by that these patients have mild mutations that allow the residual function of DCX. *DCX* mutations are found in up to 88% of sporadic SBH cases and 100% of familial SBH cases. DCX (Doublecortin) is a microtubule-associated protein (MAP). The doublecortin domain at the N terminal binds to tubulin and enhances microtubule polymerization and stabilizes microtubules (Horesh et al., 1999; Moores et al., 2004; Sapir, 2000). DCX is highly expressed in new-born neuronal precursor cells. The expression level remains high during the process of migration from VZ/SVZ to destinations in the cortical plate. Downregulation of DCX occurs when neuronal precursors become mature neurons in the cortical plate (Brown et al., 2003).

In utero shRNA mediated knockdown of *Dcx* in the rat developing neocortex leads to the arrest of multipolar neurons in the intermediate zone to form subcortical band heterotopia within the white matter (Bai et al., 2003). A small amount of *Dcx* knockout neurons exhibit bipolar morphology but fail to reach their correct layers in the cortical plate, which suggests that Dcx is important not only for multipolar-to-bipolar transition but also for the subsequent radial migration process. The same strategy of *Dcx* knockdown in mouse only leads to laminar displacement of the neocortex caused by impaired radial migration but no formation of SBH (Ramos et al., 2005). Strikingly, *Dcx* knockout mice show normal neocortical neurogenesis and neuronal migration but only mildly disrupted lamination of

the CA3 area of the hippocampus (Corbo et al., 2002). Defects in neuronal migration arise from an acute knockdown strategy rather than a knockout strategy, which suggests that there are some compensatory mechanisms in *Dcx* knockout mice. *Dclk1* encodes doublecortin like kinase 1 (DCLK1), which is also a microtubule-associated protein and has microtubule-polymerizing activity. Similar to *Dcx*, *Dclk1* knockout does not cause neuronal migration defects while *Dclk1* knockdown does (Koizumi, Tanaka, et al., 2006). In support of the compensation hypothesis, double *Dcx/Dclk1* knockout mice show defects of neuronal migration whereas single *Dcx* or *Dclk1* knockout mice do not (Corbo et al., 2002; Koizumi, Higginbotham, et al., 2006).

LIS1 mutations account for a small proportion of sporadic SBH cases (Mineyko et al., 2009; Sicca et al., 2003). *LIS1*, also known as *PAFAH1B1,* encodes platelet-activating factor acetylhydrolase 1b regulatory subunit 1, which is an important binding partner and regulator of the microtubule minus end-directed motor dynein. LIS1 can target dynein to the microtubule plus end and enhance dynein-mediated microtubule sliding. LIS1/dynein complex is involved in coupling the nucleus to the centrosome, which is required for nuclear movement during neuronal migration (Tanaka et al., 2004). Interestingly, LIS1 also binds to microtubule-associated proteins including DCX (Caspi et al., 2000). Functional genetic interaction of *Lis1* and *Dcx* in neuronal migration in the mouse neocortex has been reported (Pramparo et al., 2010). *Lis1* knockdown mediated by shRNA in rat caused accumulation of multipolar cells in the VZ/SVZ due to the failure of multipolar to bipolar transition. Those few bipolar cells that reached the intermediate zone also exhibited defects in somal translocation (Tsai et al., 2005). Lis1 knockout mice showed defects in neocortical

and hippocampal neurogenesis and migration (Gambello et al., 2003; Hirotsune et al., 1998).

In addition to *DCX* and *LIS1*, genes encoding microtubule subunits (*TUBA1, TUBG1*) and microtubule-dependent motor protein (*KIF2A*) have been reported to be associated with SBH in rare cases. *TUBA1* mutations are common in patients with lissencephaly. A mutation in *TUBA1* was reported in a patient with SBH (Poirier et al., 2007). Mouse Tuba1 mutation in the GTP binding pocket affects tubulin heterodimer formation and leads to disrupted lamination of the neocortex and hippocampus accompanied by impaired neuronal migration (Keays et al., 2007). A mutation in *TUBG1* was identified in a patient with laminar heterotopia associated with posterior pachygyria and a dysmorphic corpus callosum (Poirier et al., 2013). Tubg1 knockout mice exhibited the arrest of neuronal migration in the SVZ and IZ (Poirier et al., 2013). A mutation in *KIF2A,* which encodes a microtubule-dependent motor protein that drives depolymerization of microtubules, was identified in a patient with frontal band heterotopia and microcephaly (Poirier et al., 2013). *Kif2a* knockout mice showed abnormal lamination of the neocortex and hippocampus accompanied by defects in neuronal migration (Homma et al., 2003). Interestingly, mutations in these genes are missense heterozygous mutations suggests that SBH associated with these genes is caused by a dominant-negative effect rather than haploinsufficiency.

Eml1, which encodes a microtubule-associated protein that modulates the assembly and organization of the microtubule cytoskeleton, has been identified as the mutated gene in the spontaneously arisen HeCo mice that display SBH phenotype (Croquelois et al., 2008;

Kielar et al., 2014). Furthermore, *EML1* was found to be mutated in human patients with PNH and SBH accompanied by polymicrogyria and agenesis of the corpus callosum (Kielar et al., 2014). Interestingly, the authors found that Eml1 did not affect neuronal migration. Instead, misspaced apical progenitors caused by disrupted spindle orientation contributed to heterotopia formation in HeCo mice.

The genes mentioned above including *DCX, LIS1, TUBA1, TUBG1, KIF2A,* and *EML1* are either microtubule subunits or important regulators of the microtubule cytoskeleton, which highlights the essential role of microtubule dynamics in the development of SBH. In addition to these genes classically involved in tubulinopathies, deficiency in other genes including *RhoA*, *Rapgef2,* and *Pard3* have been shown to cause the SBH phenotype in the mouse. However, mutations or deletions in these genes have not been identified in human patients with SBH. RhoA is a member of the Rho family of small GTPases, which is mainly associated with cytoskeleton organization to regulate cell shape, attachment, and motility. RhoA deletion in the developing cerebral cortex leads to SBH in the middle of the cortical wall (Cappello et al., 2012). RhoA deficient radial glia cells lose their apical anchoring and exhibit increased proliferation in ectopic places throughout the cortical wall. Alterations in the radial glia scaffold are caused by the destabilization of both the actin and the microtubule cytoskeleton. Surprisingly, RhoA deficient neurons migrated normally when transplanted into wild-type cerebral cortex, which suggests that defects in radial glial cells alone can sufficiently cause SBH. Pard3 encodes the cell polarity protein Par3, which plays a central role in the formation of the epithelial tight junction. The conditional *Pard3* knockout mice share similarities with the *RhoA* knockout mice. Par3 deletion resulted in the overproduction of RGCs located outside the VZ. These RGCs subsequently undergo

accelerated and excessive neurogenesis, leading to the formation of massive subcortical band heterotopia (SBH) underneath an apparently layered but thinner cortex. The excessive proliferation was caused by increased YAP/TAZ activity in the Par3 deficient neural progenitor cells (W. A. Liu et al., 2018). The *Pard3* knockout mouse model also highlights the essential role of radial glial cells in developing SBH. Rapgef2 is a guanine nucleotide exchange factor specific for the small GTPases Rap1 and Rap2 (Pham et al., 2000), which are involved in neurite outgrowth and neuronal polarization through regulation of the cytoskeletal network (Hisata et al., 2007; Schwamborn & Püschel, 2004). *Rapgef2* conditional knockout in the developing neocortex results in an ectopic cortical mass underlying a relatively normal cortex (Terashima et al., 2009). The altered cellular process causing SBH in the *Rapgef2* conditional knockout mice remains unclear.

In conclusion, genes associated with human patients and genetic animal models suggest that grey matter heterotopia may be caused by a combination of the altered cellular process including the proliferation of neural progenitor cells, integrity of radial scaffold, and neuronal migration. Dysregulation of actin and microtubule cytoskeleton dynamics may represent the common mechanism of developing grey matter heterotopia.

1.5 Apoptosis Stimulating Protein of p53 2 (ASPP2)

Apoptosis stimulating protein of p53 2 (ASPP2) is one of the ASPP family of proteins including ASPP1, ASPP2, and inhibitory ASPP (iASPP2). As indicated by the name, the ASPPs protein family plays an essential role in regulating apoptosis. ASPP1 and ASPP2 activate the p53-mediated apoptotic response while iASPP inhibits it. This family of proteins has a highly conserved common C-terminal sequence containing ankyrin repeats,

an SH3 domain and a proline-rich region. ASPP1 and ASPP2 have a β-grasp ubiquitin-like fold (UBL) followed by a predicted α-helical domain at the N-terminal. Two ASPP2 variants were discovered as p53 binding protein (53BP3) and Bcl-2 binding proteins (Bbp).

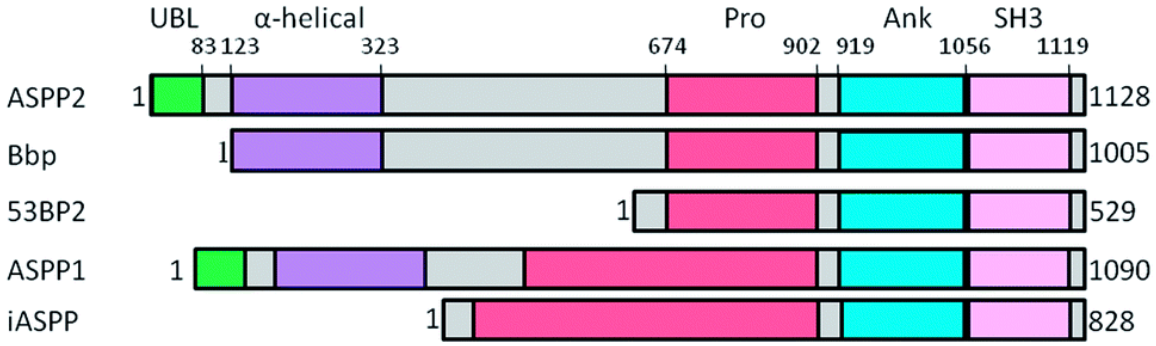


Figure 1. 10 Domain organization of the ASPP proteins.

Adapted from Iosub-Amir A, 2014.

1.5.1 Pro-apoptotic function of ASPP2

P53 is a transcription factor that induces cell cycle arrest at the G1/S phase for DNA repairing and activates DNA repair proteins to fix DNA damage and initiates apoptosis if DNA damage is irreparable. In response to DNA damage, the ASPP2 SH3 domain binds to the p53 core domain. More specifically, the n-Src loop and the RT loop of the ASPP2 SH3 domain bind the L3 loop of p53 while the fourth Ank repeat of ASPP2 binds the L2 loop of p53 (Gorina & Pavletich, 1996). ASPP2-p53 interaction facilitates the binding of p53 to its target DNA and selectively induces the transcription of pro-apoptotic genes (Samuels-Lev et al., 2001). P53 target genes including PIG3, PUMA, and Fas/CD95 are upregulated by ASPP2 while Mdm2 and cyclin G are not affected. The influence of ASPP2 on p53 targets p21 and Bax remains controversial. ASPP2 does not influence the cell cycle

arrest activity of p53 (Bergamaschi et al., 2004). The precise mechanism underlying the specificity of ASPP2 on p53 target genes is not fully understood yet. It has been proposed that binding of ASPP2 to p53 induces conformational changes of p53 that conferring its target specificity (Gorina & Pavletich, 1996). The p53 family members p63 and p73 are also transcription factors regulating cell cycle arrest and apoptosis. But they are more important for cell development and have a minor role in tumour suppression. ASPP2 can interact with p63 and p73 and induce transcription of pro-apoptotic genes in a very similar way to ASPP2-p53 interaction (Bergamaschi et al., 2004; Canning et al., 2012).

The Bac-2 family proteins are another group of important regulators of apoptosis. The Bac-2 family contains both pro-apoptotic (e.g., Bax and Bak) and anti-apoptotic (e.g., Bcl-2, Bcl-X, Bcl-W) members, which form homo-/heterodimers. The Bcl-2 family controls a key step in the intrinsic pathway of apoptosis: the mitochondrial outer membrane permeability. Bbp is partly localized at the mitochondria and is involved in the intrinsic pathway of apoptosis (Kobayashi et al., 2005). Bbp mediated cell death is inhibited by expression of Bcl2 and Bcl-X (Takahashi et al., 2005), suggesting ASPP2 can regulate apoptosis through Bcl-2 family proteins. A combination of peptide arrays, biophysical and computational methods revealed that the Ank-SH3 domain of ASPP2 binds two homologous sites in three anti-apoptotic proteins (Bcl-2, Bcl-x, and Bcl-w): the conserved BH4 motif, which is important for the anti-apoptotic function and a binding site for the pro-apoptotic family members (Katz et al., 2008). This suggests that ASPP2 induces apoptosis through binding and inhibiting the functional sites of anti-apoptotic Bcl-2 proteins, promoting the release of pro-apoptotic proteins.

1.5.2 ASPP2 is a haploinsufficient tumour suppressor

Clinical studies have revealed that ASPP2 expression is frequently downregulated in a wide variety of human cancers such as breast cancer, acute lymphoblastic leukaemia, and hepatitis B virus-positive hepatocellular carcinoma, and low ASPP2 expression correlates with poor clinical outcome. (Agirre et al., 2006; Cobleigh et al., 2005; Hedenfalk et al., 2001; Lossos et al., 2002; Samuels-Lev et al., 2001; Zhao et al., 2009). Interestingly, the downregulation of ASPP2 expression is found more frequently in tumours harbouring wild-type p53 than those with p53 mutations (Samuels-Lev et al., 2001). The regulation of ASPP2 expression remains largely unknown. E2F, a known activator of the p53 apoptotic activity, has been shown to bind the ASPP2 promotor and to increase ASPP2 expression (Fogal et al., 2005). Although the mechanism behind the downregulation of ASPP2 in human cancers remains unclear, methylation of the ASPP2 promoter causing epigenetic silencing may be involved (Z.-J. Liu et al., 2005).

Hyoungseok and colleagues found that single nucleotide polymorphisms (SNPs) at the *TP53BP2* locus are associated with gastric cancer susceptibility (Ju et al., 2005). Considering ASPP2's function in regulating p53 activity, it is reasonable to speculate that ASPP2 may mediate tumour suppression through p53. In line with this idea, residues in p53 that are important for ASPP2-p53 interaction are frequently mutated in human cancers (Gorina & Pavletich, 1996). Such clinical observations suggest that ASPP2 is a tumour suppressor.

The idea of ASPP2 being a tumour suppressor has been tested by two *Aspp2-KO* mouse models. Vives and colleagues found that ASPP2$^{+/-}$ mice (targeting exon3 of *Trp53bp2*) had an increased incidence of developing spontaneous and γ-irradiation-induced tumours

including lymphoma, sarcoma, and very rarely carcinoma. (Vives, 2006). In this *Aspp2-KO* mouse model, ASPP2$^{+/-}$-p53$^{+/-}$ mice developed spontaneous lymphoma earlier and at an overall higher frequency compared to ASPP2$^{+/+}$-p53$^{+/-}$ mice. This suggests that ASPP2 may cooperate with p53 in tumorigenesis. However, accelerated sarcoma development was not observed in ASPP2$^{+/-}$-p53$^{+/-}$ mice. Another *Aspp2-KO* mouse model (targeting exons 10-17) developed by Kampa and colleagues revealed that ASPP2$^{+/-}$ mice showed accelerated development of spontaneous tumours and γ-irradiation-induced high-grade thymic lymphomas (Kampa et al., 2009). However, they failed to observe accelerated tumorigenesis in ASPP2$^{+/-}$-p53$^{+/-}$ mice compared to ASPP2$^{+/+}$-p53$^{+/-}$ mice.

ASPP2$^{+/-}$ primary thymocytes showed attenuated apoptotic response after γ-irradiation (Kampa et al., 2009). This suggested that accelerated thymic lymphomagenesis in ASPP2$^{+/-}$ may be caused by reduced apoptosis, which resulted in the persistence of thymocytes harbouring tumorigenic mutations.

1.5.3 ASPP2 as a targeting subunit of protein phosphatase 1 (PP1)

About one-third of all eukaryotic proteins are regulated by reversible phosphorylation. There are a large number of serine/threonine kinases (over 500) but a limited number of serine/threonine phosphatase catalytic subunits (around 40) (Virshup & Shenolikar, 2009). Protein phosphatases 1 and 2A (PP1 and PP2A) are the most ubiquitous and abundant serine/threonine phosphatases. There are four PP1 catalytic subunits encoded by three genes: the ubiquitously expressed PP1α, PP1β and PP1γ1, and the testis-specific PP1γ2. They achieve substrate specificity by cooperating with a large collection of targeting subunits, which recruit specific substrates to the phosphatase catalytic subunit. Most of the PP1 interacting proteins contain the RVXF motif that can bind a hydrophobic groove in the

PP1 catalytic subunit (Wakula et al., 2003). ASPP2 is one of the RVXF motif-containing PP1 targeting subunits. The crystal structure of the human ASPP2/PP1 complex revealed that apart from using the canonical RVXF motif that binds the PP1 catalytic domain, ASPP2 also engages the PP1 C-terminal tail with its SH3 domain (Bertran et al., 2019). The ASPP2 SH3 domain can discriminate between PP1 isoforms: ASPP2 showed a significant preference for PP1α with an affinity of 13.6 nM which is 13- and 14-fold higher than that for PP1β and PP1γ1, respectively (Bertran et al., 2019).

By far, only a limited number of ASPP2/PP1 targets have been identified. First, ASPP2 recruit PP1 to dephosphorylate transcriptional coactivators of the Hippo pathway TAZ and YAP at Ser89/Ser311 and S127, respectively, facilitating their nuclear translocation and transcriptional activities (C.-Y. Liu et al., 2011; Royer et al., 2014). Second, ASPP1/ASPP2 recruit PP1 to dephosphorylate the kinetochore component Hec1 at Ser165 (P. Zhang et al., 2015). Phospho-Hec1 (Ser165) needs to be removed to allow timely anaphase entry and failure to remove phosphor-Hec1 (Ser165) leads to massive segregation errors (Wei et al., 2011). ASPP1/2 co-depleted cells showed unaligned chromosomes and disrupted chromosome segregation (P. Zhang et al., 2015). The same group also found that ASPP1/ASPP2 recruit PP1 to dephosphorylate and the centrosome linker protein C-Nap1 at Ser2417/2421 and ASPP1/ASPP2 double deletion inhibited re-association of C-Nap1 with centrosome at the end of mitosis (P. Zhang et al., 2015). However, the authors did not investigate whether ASPP1 or ASPP2 single deletion would generate a similar phenotype.

1.5.4 ASPP2 as a regulator of cell polarity

Cell polarity refers to the asymmetric organization of cell membrane proteins, cytoskeleton, and organelles, which is a fundamental property that enables them to acquire optimized shapes for various functions. For example, epithelial cells exhibit polarized cell morphology characterized by distinct apical, lateral, and basal plasma membrane domains. It has been proposed that the sharp distinction between apical and basolateral domains is achieved by the segregation of apical and basolateral polarity determinants by mutual antagonism. For instance, the apical PAR complex, consisting of PAR3, PAR6, and atypical PKC (aPKC), function as an apical determinant. aPKC phosphorylates the basolateral determinants PAR1 and Lgl at residues important for membrane binding to exclude them from the apical domain (Betschinger et al., 2003; Atsushi Suzuki et al., 2004; Yamanaka et al., 2003). PAR1 phosphorylates PAR3 and excludes it from the lateral membrane domain (Benton & Johnston, 2003). Lgl inhibits the activity of aPKC in the lateral domain. (Yamanaka et al., 2003).

PAR3 localizes to primordial cell-cell contacts prior to PAR6 and aPKC (A Suzuki, 2002). In the presence of active CDC-42, a small amount of PAR3 is necessary and sufficient to recruit PAR6/ aPKC and form the PAR complex. ASPP2 can bind PAR3 through its N-terminal (residues 1-353) at the primordial cell-cell contacts before PAR6/ aPKC is recruited (Cong et al., 2010; Sottocornola et al., 2010a). The junctional localization of ASPP2 and PAR3 is interdependent: ASPP2 and PAR-3 do not localize in this area unless they are in a complex (Cong et al., 2010; Sottocornola et al., 2010a). Deletion of ASPP2 or disruption of the ASPP2/PAR3 interaction causes defects in cell polarity (Cong et al., 2010). PAR3 has been shown to interact with PP1α (Traweger et al., 2008). Recent work further

reveals that ASPP2/PP1 dephosphorylates PAR3 at Ser852 to facilitates its rapid localization to tight junctions. Ser85 or Ser889 unphosphorylatable PAR3 mutants ectopically localize to the lateral membrane and form protein clusters (Yamashita et al., 2020). These data together demonstrate that ASPP2-PAR3 interaction is required for proper localization of PAR3 at primordial cell-cell contacts and development of the apical domain. The importance of ASPP2's function in regulating the PAR complex has also been revealed during H. *pylori* infection. Cytotoxin-associated gene A (CagA) injected by H. *pylori* interacts with ASPP2 and promotes remodelling of the PAR complex which leads to loss of cell polarity (Buti et al., 2020).

The interaction between ASPP2 and PAR3 is not affected by the PAR complex inhibitor Lgl (Cong et al., 2010). However, other factors have been reported to influence the ASPP2-PAR3 complex: FIH-1 hydroxylates ASPP2 at Asn986 and FIH-1 knockdown impairs ASPP2-PAR3 interaction and relocates them to the cytoplasm (Janke et al., 2013). Besides, under hypoxic conditions, the ubiquitin ligase Siah interacts with ASPP2 resulting in its proteasomal degradation and impaired the activity of ASPP2 in regulating tight junction integrity and cell polarity in 3D organotypic culture (H. Kim et al., 2014).

1.5.5 ASPP2 in central nervous system (CNS) development

ASPP2 has been shown to be important for the central nervous system (CNS) development both in human and in mice. 1q41q42 microdeletion syndrome is caused by deletions in the chromosomal 1q41−q44 region. The patients show various symptoms including developmental delay, typical facial dysmorphic features, brain abnormalities, and intellectual disability. By analyzing the smallest region of overlap (SRO) of deletions and

comparing the brain stricture between *TP53BP2* deleted and non-deleted patients, *TP53BP2* has been identified to be responsible for brain abnormalities including neural tube defects (NTDs), hydrocephalus, agenesis of the corpus callosum, and microcephaly (Zak et al., 2016). Consistent with this finding, *TP53BP2* is most highly expressed in the ventricular and subventricular zones in the human embryonic brain throughout gestation (Zak et al., 2016). In mice, *Trp53bp2* starts to be expressed at E9.5 in the brain, spinal cord, and optic cup (Sottocornola et al., 2010a). *Aspp2-KO* caused 100% neonatal lethality in mice with C57BL/6 background; 30% of the *Aspp2-KO* mice in mixed C57BL/6-129/Sv background survived birth, but all died before weaning; The majority of *Aspp2-KO* mice survived after weaning under Balb/c background (Zak et al., 2016). Lethality may be caused by the developmental problems in the central nervous system (CNS) and the heart, including NTDs, hydrocephalus, abnormal twisted heart, and ventricular septal defect. Similar to the lethality rate, the severity of developmental problems was dependent on the mouse genetic background: NTDs were detected in 46% of embryos with C57BL/6 background, 15% of embryos with mixed C57BL/6-129/S background, and 8% of embryos with Balb/c background (Zak et al., 2016). 67−100% of C57/BL6 and 33−56% of Balb/c *Aspp2-KO* embryos had abnormal heart position and 67% C57/BL6 and 33% Balb/c of *Aspp2-KO* embryos had ventricular septal defects. Mechanistically, ASPP2 colocalizes with ZO1 and PAR3 at the neuroepithelium and the choroid plexus in the embryonic brain and ASPP2 deficiency leads to impaired integrity of tight/adherens junctions in the choroid plexus, loss of neuroepithelium polarity at the ganglionic eminence, as well as increased proliferation and expanded neural progenitor pool (Sottocornola et al., 2010a). However, whether the increased proliferation of neural progenitors is directly caused by the loss of integrity of the neuroepithelium is not fully understood.

1.6 Aim of this study

This project aims to further investigate the function of ASPP2 in the development of the central nervous system in mice by addressing the following questions:

1. Whether loss of ASPP2 will lead to any brain malformation at postnatal stages in Balb/C mice?

2. Is ASPP2 involved in other cellular processes such as neuronal migration apart from regulating proliferation?

3. What are the underlying molecular mechanism?

Chapter 2: Materials and Methods

This chapter will describe the materials, methods, and protocols utilized in experiments through the course of this thesis. They are presented here so that the technical details will not be described again in chapters 3,4 and 5.

2.1 Materials

2.1.1 Reagents

Table 2. 1 List of Chemicals, Reagents, and Kits

Product name	Manufacturer	Cat. number
Rho activator II	Cytoskeleton, Inc	CN-03
Proteinase K	Sigma-Aldrich	3115828001
BrdU	Abcam	ab142567
Doxycycline	Takara Bio Europe	631311
Recombinant Mouse DLL4	Bio-Techne	1389-D4-050
Poly-D-Lysine	MP Biomedicals UK	0210269450
Protease Inhibitor Cocktail	Roche	11697498001
Phosphatase inhibitor	Roche	4906845001
Fast green	Sigma-Aldrich	F7252
Fluoromount	Cambridge Bioscience	0100-01
Tamoxifen	MP Biomedicals UK	0215673883
Donkey Serum	Sigma-Aldrich	D9663

Product name	Manufacturer	Cat. number
Phalloidin, CF(R)568	Cambridge Bioscience	00044-T-BT
Matrigel, Phenol red free	VWR International	734-0272
Millicell Cell Culture Insert	Millipore UK	PI8P01250
Mini-Protein TGX gels	Bio-Rad	4561095
B-27 Plus Neuronal Culture System	Life Technologies	A3653401
Neurobasal Medium	Life Technologies	21103049
B-27 Plus Supplement (50X)	Life Technologies	A3582801
Accutase Cell Dissociation Reagent	Life Technologies	A1110501
Nuclease-Free Water	Life Technologies	AM9938
Pierce IP lysis buffer	Fisher Scientific UK	11820084
Western Blot stripping buffer	Insight Biotechnology	sc-281698
Dynabeads Protein G	Life Technologies	10003D
ROCK kinase activity assay Kit	Sigma-Aldrich	CSA001
RhoA G-LISA Activation Assay Kit	Cytoskeleton, Inc	BK124
EndoFree Plasmid Maxi Kit	QIAGEN	12362
Cells-to-CT 1-Step Power SYBR Green Kit	Life Technologies	A25601
DNA-free DNA Removal Kit	Life Technologies	AM1906

2.1.2 Home-made buffers

RIPA buffer:

10 mM Tris-Cl (pH 8.0)

1 mM EDTA

0.5 mM EGTA

1% Triton X-100

0.1% sodium deoxycholate

0.1% SDS

140 mM NaCl

Adjust pH to 7.4. Store at -20°C.

Urea Buffer:

8 M urea

1 M thiourea

0.5% (w/v) CHAPS

50 mM DTT

24 mM spermine

Aliquoted into 1.5 mL Eppendorf tubes. Store at -20°C.

0.5% NP-40 IP buffer:

20 mM Tris HCl pH 8

137 mM NaCl

10% glycerol

1% Nonidet P-40 (NP-40)

2 mM EDTA

Filtered and Store at 4°C.

6x Laemmli buffer:

1.2 g SDS

0.93 g DTT

6 mg bromophenol blue

4.7 ml glycerol

1.2 ml Tris 0.5 M (pH 6.8)

Aliquoted into 1.5 mL Eppendorf tubes. Store at -20°C.

Blocking buffer for IHC and IF:

10% normal goat serum (IHC) or 10% normal donkey serum (IF)

1% BSA

0.3% Triton X100

in PBS

Aliquoted into 1.5 mL Eppendorf tubes. Store at -20°C.

0.1M PB:

NaH_2PO_4 3.864 g

Na_2HPO_4 10.22 g

ddH_2O Up to 1000 mL

Adjust pH to 7.4. Store at room temperature.

Cryoprotectant:

Sucrose 300 g

Polyvinyl-pyrrolidone (PVP-40) 10 g

0.1M PB 500 ml

Ethylene glycol 300 ml

ddH_2O Up to 1000 mL

Store at -20°C.

GNT buffer:

50 mm KCl

1.5 mm MgCl2

10 mm Tris-HCl (pH 8.5)

0.01% (w/v) Gelatin

0.45% (v/v) NP-40

0.45% (v/v) Tween-20

Autoclaved and keep at 4 ◦C.

4% PFA:

Paraformaldehyde (PFA) 20 g

0.1M PBS (pH 7.4) Up to 1000 ml

Heat to 70°C in fume hood on a magnetic stirrer until PFA dissolved. Filtered and aliquoted into 50 mL falcon tubes and 1.5 mL Eppendorf tubes. Store at -20°C.

Sodium citrate antigen retrieval buffer:

2.94 g Sodium citrate

ddH_2O to 1000 mL

Adjust pH to 6.0. Store at room temperature.

EDTA antigen retrieval buffer:

0.37 g EDTA

ddH_2O to 1000 mL

Adjust pH to 8.0. Store at room temperature.

10x PBS:

17.8 g $Na_2HPO_4 \cdot 2H_2O$

2.4 g KH_2PO_4

80 g NaCl

2 g KCl

ddH_2O to 1000 mL

Store at room temperature.

10x TBS:

24g Tris Base

88g NaCl

ddH_2O to 1000 mL

Adjust pH to 7.6. Store at room temperature. To make 1xTBST, dilute 10XTBS and add 0.1% Tween 20 detergent.

50x TAE Buffer:

242 g Tris base

57.1 ml Glacial Acetic Acid

100 ml 0.5 M EDTA (pH 8.0)

ddH_2O to 1000 mL

Adjust pH to 8.5. Store at room temperature.

10x SDS-PAGE Running buffer:

30 g Tris base

144 g glycine

10 g SDS

ddH_2O to 1000 mL

Store at room temperature.

10x SDS-PAGE transfer buffer:

725 g glycine

145 g Tris

ddH_2O to 5000 mL

Store at room temperature. Add 20% Ethanol when making 1x buffer.

2.1.3 Primers

Table 2. 2 List of primers for RT-PCR

Target gene	Primers (5'-3')
trp53bp2 (exon3)	Forward: TGCAGGCCACACAGAAATTG
	Reverse: ACAATGCAATGGCGTCCATC
hey1	Forward: CTGAAAATGCTGCACACTGC
	Reverse: ATGCTCAGATAACGGGCAAC
hey2	Forward: TTGAAGATGCTCCAGGCTACAG
	Reverse: TCTGTCAAGCACTCTCGGAATC
hes1	Forward: ACACCGGACAAACCAAAGAC
	Reverse: TATTCTTGCCCTTCGCCTCTTC
hes5	Forward: AGTCCCAAGGAGAAAAACCGA
	Reverse: GCTGTGTTTCAGGTAGCTGAC
nrarp	Forward: TGACCCTGCGTGCAAAAATG
	Reverse: AAAAGCGCAGAAGACCGAAG
otx2	Forward: TCCAATGCGGCTGTAAGTTC
	Reverse: TTGTTTGGAGGCGCAAAGTC
gli2	Forward: ACAAAGCCTTCTCCAATGCC
	Reverse: ACAGTCTTCACATGCTTGCG
pax6	Forward: TGCCCTTCCATCTTTGCTTG
	Reverse: TCTGTTGCTTTTCGCTAGCC
ecmes	Forward: TGTACAACAGCGCTTGCAAG
	Reverse: AATAAGCCCCCATGCCTTTG

Table 2. 3 List of primers for genotyping

Target gene	Primers (5'-3')	Expected bands
Trp53bp2	F4: CGGTTTGGAAGTCAAAGGAA B3: TCAATGTGTCCAGCACCCTA PGK2: TACCCGCTTCCATTGCTCAG	WT: 597 bp Knockout: 800 bp
Trp53bp2 ^{loxP}	SDL1: TGGACAGGCTGAGCTGTTAG SDL2: ACACTTTCACCAACCCTAGGTC	WT: <200 bp Mutant: >200 bp

2.1.4 Antibodies

Table 2. 4 List of primary antibodies

Antigen	Host	Supplier	Catalog No.	Application
mouse ASPP2	Rabbit mAb	Homemade	-	WB (1:750)
human ASPP2	Mouse mAb	Santa Cruz	sc-135818	WB (1:1000)
				IP (1:125)
MLC2	Rabbit mAb	CST	8505S	WB (1:1000)
P-MLC2(Ser19)	Rabbit pAb	CST	3671S	WB (1:1000)
				IF (1:100)
MYPT1	Rabbit mAb	CST	8574S	WB (1:1000)
P-MYPT1 (Thr 853)	Rabbit pAb	CST	4563S	WB (1:1000)
ROCK1	Rabbit mAb	CST	4035S	WB (1:1000)
ROCK2	Rabbit mAb	CST	9029S	WB (1:1000)
				IP (1:50)
P-ROCK2 (Ser1366)	Rabbit pAb	Abcam	Ab228008	WB (1:1000)
RhoA	Rabbit pAb	Abcam	Ab86297	WB (1:1000)
PP1- α	Goat pAb	Santa Cruz	sc-6105	WB (1:2000)
PP1- β	Mouse mAb	Santa Cruz	sc-373782	WB (1:1000)
PP1- γ	Mouse mAb	Santa Cruz	sc-515943	WB (1:1000)
GFP	Chicken pAb	aveslabs	GFP-1010	IF (1:4000)

β -actin HRP	Mouse mAb	Santa Cruz	sc-47778	WB (1:1000)
DCX	Goat pAb	Santa Cruz	Sc-8066	IF (1:400)
	Rabbit pAb	CST	4604S	IF (1:500)
BrdU	Rat mAb	Abcam	Ab6326	IF (1:250)
NeuN	Rabbit mAb	Abcam	ab177487	IF (1:500)
β -Catenin	Mouse mAb	BD	610153	IF (1:200)

Table 2. 5 List of secondary antibodies

	Host	**Supplier**	**catalogue No.**	**Application**
Alexa Fluor®488 Anti-Rabbit IgG (H+L)	Donkey	Invitrogen	A-21206	IF (1:300)
Alexa Fluor®488 Anti-Mouse IgG (H+L)	Donkey	Invitrogen	R37114	IF (1:300)
Alexa Fluor®488 Anti-Chicken IgY (H+L)	Goat	Invitrogen	A-11039	IF (1:300)
Alexa Fluor®488 Anti-Rat IgG (H+L)	Donkey	Invitrogen	A-21208	IF (1:300)
Alexa Fluor®546 Anti-Rabbit IgG (H+L)	Donkey	Invitrogen	A-10040	IF (1:300)
Anti-Goat Immunoglobulins/HRP	Rabbit	Dako	P0449	WB (1:2000)
Anti-Rabbit Immunoglobulins/HRP	Swine	Dako	F0205	WB (1:2000)
Anti-Mouse Immunoglobulins/HRP	Goat	Dako	P0447	WB (1:2000)

2.1.5 Cell lines

ASPP2-KO U2OS cell line was generated by James Hokfung Chan, a former PhD student in our lab. *ASPP2-KO U2OS* cells were created using WT U2OS cells following the protocol in Zhang et al. (Ran F, 2013). The single-guide-RNA (sgRNA) target ASPP2 exon 6 (5'- GAG CAC TTA AAG GCC ACG -3') was cloned into the CRISPR-Cas9 plasmid carrying the Cas9 nuclease (PX459) using BbsI restriction enzyme sites. The plasmid was then sequenced using hU6-F primer to confirm the incorporation of the sgRNA. WT U2OS

cells were then either co-transfected with PX459 and a GFP expression-only plasmid (pCMV-GFP), or transfected with pCMV-GFP plasmid alone. 36 hours post-transfection, GFP-positive cells were FACS-sorted and plated at low density on 15cm dish. Cell culture medium was supplemented with 8 μg/mL of puromycin to select resistant single cell clones. Single cell clones were then picked and expanded and ASPP2 expression analyzed by western blot. The CRISPR-Cas9 plasmid, pSpCas9(BB)-2A-Puro (PX459) V2.0, was a gift from Feng Zhang (Addgene plasmid ID: 62988). The GFP-expression plasmid, pCMV-GFP, was a gift from Connie Cepko (Addgene plasmid ID: 11153).

Stable *ASPP2-KO U2OS* cells re-expressing doxycycline-inducible WT or RVxF mutant ASPP2 were generated by inserting pTet-On-Tp53bp2 and pCAG-rtTA (reverse tetracycline transactivator) using the PiggyBac transposon system. *Aspp2-KO* cells were co-transfected with the piggyBac transposon vector carrying ASPP2 cDNA downstream of the Tet-ON promoter, the piggyBac transposase vector (Transposagen) and the piggyBac vector expressing reverse tetracycline transactivator (rtTA) from a CAG constitutive promoter and neomycin resistance gene. The transfection was performed using Lipofectamine LTX with PLUS Reagent (Thermo Fisher Scientific). 24 hours after transfection, the cells were selected with neomycin (Gibco) at a concentration of 700 μg/ml for one week and the cells that survived were single-cell sorted into 96-well plates. Single cell clones were then expanded and splitted in a 1:2:2 ratio with 20% seeded on a normal 96-well plate and 80% seeded on two separate NuncTM MicroWellTM 96-Well Optical-Bottom Plates with Polymer Base (Thermo Fisher Scientific) for immunofluorescence screening. The two optical-bottom 96-well plates were treated with or without doxycyline hydrochloride solution (Sigma) at 50 ng/mL for 16 hours. Immunofluorescence was then performed using anti-FLAG antibody (Sigma) as the primary antibody. The 96-well

Optical-Bottom Plates were then screened using under a confocal microscope system (LSM 710; Carl Zeiss). Clones that showed positive FLAG-tag staining were selected for validation by western blot analysis. The original piggyBac vectors were from Dr. Kazuhiro Murakami (RIKEN, Kobe, Japan) and were kindly provided by Dr. Pakavarin Louphrasitthiphol from the Goding lab (Ludwig Institute, Oxford).

2.1.6 Mice

ASPP2 germline knockout (KO) mice were generated as previously described (Vives, V, 2006). In brief, *Trp53bp2*, encoding mouse ASPP2, in IT2 embryonic stem (ES) cells were inactivated by a targeting vector in which exon 3 of *Trp53bp2* and 2kb of its upstream sequence was replaced by a neomycin-resistance gene cassette, which resulted in disruption of the open reading frame of *Trp53bp2*. Correctly targeted ES cells were microinjected into C57BL/6 blastocysts to generate germline transmitting chimeric mice that were crossed onto the C57BL/6 background. Deletion of ASPP2 protein in null embryos was validated by western blot using two different antibodies raised against the N-terminal of ASPP2 (residues 59–383) or the middle part of ASPP2 (residues 500–600). *Trp53bp2*-heterozygous mice in the C57BL/6 background developed normally while most *Trp53bp2*-homozygous mice died before birth. To study the brain malformations caused by ASPP2 deletion at postnatal stages, *Aspp2-KO* mice on the Balb/c background were generated by backcrossing. *Aspp2-KO* Balb/c mice were born according to Mendelian segregation, and the majority survived after weaning.

2.2 Methods

2.2.1 Animal work

2.2.1.1 Mice maintenance

Mice were housed in the animal facility at the Wellcome Trust Centre for Human Genetics in Oxford on a standard 12 h light/dark schedule with unlimited access to chow and water. All animal research was conducted in accordance with the Animals (Scientific Procedures) Act of 1986 (UK) with protocols approved by Oxford University Research Ethics Committee and licensed by the UK Home Office (PIL: I8A33FB88; PPL: 30/3451).

2.2.1.2 Mouse genotyping

For mouse embryos and neonatal pups, tail tips were obtained from dead embryos or pups for genotyping. For older mice suitable for ear clips, ear biopsies were collected with an ear punch and were used for genotyping. Tail tissues or ear tissues were incubated in 100ul of GNT lysis buffer containing 100 ug/mL proteinase K (QIAGEN) at 55℃ in a water bath overnight. Then samples were incubated at 95℃ for 10 minutes to inactivate the proteinase K. Samples were vortexed and spun down. 1 µl of the supernatant was used as the DNA template for a standard polymerase chain reaction (PCR).

GoTaq® Green Master Mix (Promega) was used for genotyping PCR reactions. Components of PCR reaction mixture for genotyping were listed in the following table:

Table 2. 6 Components of genotyping PCR reaction

Template DNA	1µl
2x GoTaq® Green Master Mix	10µl
Primer 1 (10µM)	1µl
Primer 2 (10µM)	1µl
ddH_2O	To 20µl

The PCR program for genotyping was as follows:

Table 2. 7 PCR program for genotyping

Step	Temperature	Duration
1	95℃	5 minutes
2	95℃	40 seconds
3	60℃	40 seconds
4	72℃	40 seconds
Repeat steps 2 to 4 30 times		
5	72℃	3 minutes
6	4℃	Keep

PCR products were submitted to agarose gel electrophoresis. DNA samples were loaded into 2% agarose gel (2% agarose powder in TAE buffer) containing 20µg/ml EtBr and electrophoresed in TAE buffer at 90V for approximately 30 minutes. DNA bands were visualized by using the BioDoc benchtop trans-illuminator (UVP).

2.2.1.3 BrdU labelling for studying neuroblast migration *in vivo*

I used three pairs of WT and *Aspp2-KO* mice aged around P30, each pair came from the same litter, received a single intraperitoneal injection of BrdU (concentration at 10mg/ml)

at a dosage of 50mg/kg. Four days after injection, mice had perfusion fixation, and brains were harvested and processed as described in "Brain tissue processing and sectioning". To obtain a panoramic view of the distribution of BrdU positive cells in the SVZ, the RMS, and the olfactory bulb, brains were cut into 30 μm-thick sagittal sections. For quantification of the BrdU positive cell numbers in the SVZ and the olfactory bulb, brains were cut into 30 μm-thick coronal sections. Sections were stained for BrdU as described in "Immunofluorescence staining", except that sections were treated with cold 1M HCl for 10 minutes on ice to denature DNA so that anti-BrdU antibody can access the BrdU within the DNA. For each mouse, six sections, with an interval of 90 μm in between, containing the RMS were used for quantification. Z-stack images across 10 μm were acquired using confocal microscopy. The surface area of the RMS in the sections and the number of BrdU positive cells within this area were measured using ImageJ. The intensity of BrdU positive cells was presented as the number of BrdU positive cells per mm^2. Quantification of the number of BrdU positive cells in the SVZ was performed in the same way.

2.2.1.4 Quantification of RGC spindle orientation

Paraffin-embedded coronal brain sections (5μm-thick) form three pairs of WT and *Aspp2-KO* embryos at E14.5, each pair were from the same litter, were used for analysis. For each embryo, 7 sections containing the neocortex with an interval of 20μm in between, were used. All the RGCs in anaphase, characterized by parallel sister chromatids, located at the ventricular surface of the neocortex were found under confocal microscopy and imaged. For each embryo, 100- 150 RGCs in anaphase were imaged. Then the angle of the cleavage plane relative to the ventricular surface was measured using image-processing software

ZEN (Zeiss). RGCs with the angle of cleavage plane lower than 60º were classified as asymmetric division and the rest of them were classified as symmetric division.

2.2.1.5 Cardiac perfusion fixation

Perfusion fixation through the heart was applied to mice before harvesting brains for the following two purposes. First, perfusion fixation can clear blood from the mouse brain tissue, which can significantly reduce the background staining in the subsequent immunofluorescent staining or immunohistochemistry staining. Second, perfusion fixation helps to obtain a more uniform fixation of the mouse brain compared to the immersion of the brain into the fixative solution. Third, perfusion fixation helps to harden the brain tissue therefore making it much easier to dissect out the brain without any damage.

Sodium pentobarbital solution was diluted to 9.1mg/ml in 0.9% NaCl solution. Mice received an intraperitoneal injection of sodium pentobarbital at a dosage of 90 mg/kg. Enough depth of anaesthesia was determined by the pinch-response method. The heart was exposed by surgically opening up the thoracic cavity. A needle was inserted directly into the protrusion of the left ventricle of the heart. A cut was made in the atrium with sharp scissors. A steady flow of 0.9% saline solution was delivered into the heart by a perfusion pump to wash away the blood. After the blood had been cleared, cold 4% paraformaldehyde (PFA) in PBS was delivered until proper fixation was achieved. Then, brains were dissected out and immersed in 4% PFA for 3 hours for post-fixation.

2.2.2 Histology techniques

2.2.2.1 Brain tissue processing and sectioning.

For adult mice, perfusion fixation was applied before harvesting brains, and brains were further fixed in 4% PFA for 3 hours. For mouse embryos and neonatal pups, brains were dissected out directly and immersed in 4% PFA overnight at 4 °C. Fixed brains underwent different processes depends on whether the brain was used for paraffin-embedded sections or frozen sections. For paraffin-embedded sections, fixed brains were processed automatically by an Excelsior tissue processor (Thermo Fisher) using the routine overnight program in which brains were dehydrated in a series of ethanol, cleared in histoclear (National diagnostics) then immersed in paraffin wax. Processed brain tissues were embedded in paraffin blocks and cut into 4 μm-thick sections by microtome (Leica). For frozen sections, fixed brains were transferred into 15% sucrose in PBS at 4°C until tissue sinks, then transferred into 30% sucrose in PBS at 4°C until tissue sinks. Dehydrated brain tissues were embedded in OCT in cryomolds. Cryomolds were placed in a solution of dry ice and ethanol for snap-freezing. Frozen brains embedded in OCT were cut into 30 μm-thick sections by cryostat microtome (Leica) and free-floating sections were stored in cryoprotectant buffer at -20°C. If frozen OCT blocks cannot be sectioned immediately, OCT embedded blocks were wrapped in aluminium foil and stored at -80°C.

2.2.2.2 Haematoxylin and Eosin (H&E) staining

Paraffin-embedded sections were placed at 60°C for 15 minutes to melt paraffin wax then immediately transferred into histoclear. Sections were deparaffinized in histoclear two times, 10 minutes each, and rehydrated in 100% ethanol for 5 minutes, 90% ethanol for 2

minutes, and 70% ethanol for 2 minutes. After washing briefly in distilled water, sections were stained in Harris hematoxylin solution for 5 minutes, differentiated in 1% acid alcohol for 5 seconds, incubated in Scott's water for 30 seconds for bluing, then counterstained in eosin solution for 2 minutes, with the washing in running tap water for 5 minutes after each step. Sections were dehydrated in 70% ethanol for 2 minutes, 90% ethanol for 2 minutes, and 100% ethanol for 2 minutes. Sections were then incubated in histoclear 2 times, 5 minutes each. Finally, sections were mounted with a non-aqueous VectaMount mounting medium (Vector Labs).

2.2.2.3 Immunohistochemistry (IHC) staining

Paraffin-embedded sections were deparaffinized by incubation at 60°C for 15 minutes followed by two changes of histoclear, 10 minutes each. Sections were then rehydrated in 100% ethanol for 5 minutes, 90% ethanol for 2 minutes, and 70% ethanol for 2 minutes. After washing in PBS 3 times, 5 minutes each, sections were treated with 3% H_2O_2 in methanol for 10 min at room temperature to inactivate endogenous peroxidase. After washing in PBS 3 times, 5 minutes each, sections were immersed in boiling EDTA antigen retrieval buffer for 15 minutes in a microvalve to expose antigenic epitopes. Sections were left in EDTA antigen retrieval buffer until the temperature dropped down to room temperature. After a brief wash in PBS, sections were incubated in blocking buffer (10% normal goat serum, 1% BSA, 0.3% tritonX100 in PBS) for 1 hour at room temperature to reduce unspecific antibody binding. After aspirating blocking buffer, sections were incubated with primary antibody diluted in blocking buffer overnight at 4°C in a humidified chamber, then incubated with biotinylated secondary antibodies diluted in blocking buffer for 1 hour at room temperature in a humidified chamber followed by incubation in Avidin-

Biotin Complexes for 30 minutes at room temperature, with washing in PBS for 15 minutes, after each step. HRP substrate solution was applied to sections until a satisfactory brown colour was visualized. Sections were counterstained with hematoxylin for 5 minutes, dehydrated in 70% ethanol for 2 minutes, 90% ethanol for 2 minutes, and 100% ethanol for 2 minutes. Sections were then incubated in histoclear for 2 times, 5 minutes each, then mounted with non-aqueous VectaMount mounting medium (Vector Labs).

2.2.2.4 Immunofluorescence staining

For paraffin-embedded sections, deparaffinization, rehydration, and antigen retrieval were applied to sections as described in the method of immunohistochemistry (IHC) staining before the blocking step. For free-floating frozen sections, brain sections were transferred from the cryoprotectant buffer to PBS buffer and washed for 3 times, 5 minutes each. Paraffin-embedded sections or free-floating frozen sections were incubated in blocking buffer (10% normal donkey serum, 1% BSA, 0.3% tritonX100 in PBS) for 1 hour at room temperature to reduce unspecific antibody binding. After blocking, sections were incubated with primary antibody diluted in blocking buffer overnight at 4°C in a humidified chamber, washed with PBS 3 times, then incubated with Alexa Fluor conjugated secondary antibodies diluted in blocking buffer for 1 hour at room temperature in a humidified chamber. Nucellus was stained with 1ug/ml DAPI in PBS for 20 minutes at room temperature. Sections were washed in PBS for 20 minutes with gentle shaking, then mounted with aqueous anti-fade mounting medium.

2.2.3 Tissue culture and cell-based assays

2.2.3.1 *In vitro* neuroblast migration assay using RMS explants

The RMS tissue was dissected and cultured as previously described (Dixon, K J, 2017). WT and ASPP2 knock littermates at postnatal day 1 or day 2 were decapitated and their brains were carefully dissected on ice without any damage to the olfactory bulb. Brains were embedded in 4% low-melting-point agarose and then cut into 200 μm-thick coronal slices by using a vibratome (Leica VT1200S). The frequency and the travel speed of the razor blade were set to level 10 and level 6, respectively. Brain slices were transferred into cold HBSS on ice. Only the two slices containing the largest RMS area were used. To clearly identify the border of the RMS within these slices, the angle of the light source was adjusted onto the centre of the slice so that the RMS can be distinguished from the surrounding tissue. The RMS tissue was dissected out by making cuts on the inside of the RMS border using two insulin syringe needles. Then the RMS tissue was cut into many small pieces approximately 200 μm wide by using insulin syringe needles. Each RMS piece was subsequently embedded in the mixture of 30 μl Matrigel (Corning) and 10 μl complete neurobasal medium (neurobasal medium containing B27, 4mM glutamine, 1mg/ml bFGF, 1ng/ml EGF, and penicillin/streptomycin) and placed in a well of 96-well plates. Plates were put in a 37°C incubator for 15 minutes for the Matrigel to polymerize. After polymerization, 50 μl complete neurobasal medium was added to cover Matrigel in each well. RMS explants were cultured for 48 hours in an incubator at 37°C with 5% CO_2. RMS explants were imaged by bright field light microscopy. The area of the RMS explant body and the edge of the migrating cells were determined by using ImageJ. Migration capacity was indicated by the ratio of the area of migrating cells to the area of the RMS explant.

Two independent experiments were performed. In total there were 12 RMS explants from 2 WT mice and 14 RMS explants from 3 *Aspp2-KO mice*.

2.2.3.2 *Ex utero* electroporation and brain slice culture

Protocols of *Ex Utero* electroporation and brain slices culturing were modified from previously described methods (Nelson, B. R. 2013; Anda, F. C. 2013). *Trp53bp2*$^{loxp/loxp}$ male mice and *Trp53bp2*$^{loxp/loxp}$ female mice were paired for timed mating. Timed-pregnant mice were sacrificed at E14.5 (the day of the vaginal plug was considered E0.5) and embryos were collected in an ice-cold HBSS filled dish. The torso of the embryo was embedded in low-melting-point agarose gel on ice to prevent the head from moving around. 1 µl DNA solution containing pCAG-EYFP or pCAG-CRE-EYFP plasmids (1.5µg/µl) and 0.2mg/ml fast green in sterile PBS was injected into the lateral ventricle by a mouth-controlled micropipette. The successful injection was indicated by the shape of the lateral ventricle can be visualized by green colour. Electrodes tweezer (BTX The Electroporation Experts, 45-0487) was placed over the head in a manner to target current into the dorsal neocortex. Plasmids were electroporated by 4 square pulses of 40 mV for 50 ms with 500 ms inter-pulse intervals discharged by the electroporator (ECM 830 Square Wave Electroporation System). Heads of the embryo were cut off and embedded in 4% low-melting-point agarose and then cut into 200 µm-thick coronal slices by using a vibratome (Leica VT1200S). The frequency and the travel speed of the razor blades set to level 10 and level 4, respectively.

Brain slices attached to the agarose were cultured on membranes with 0.4 µm pore size (Millipore, PICM0RG50) in slice culture medium (Neurobasal supplemented with 2% B27, 1% N2, 0.5 mM Glutamine, 1% penicillin/streptomycin, and 5% horse serum) in an

incubator maintained at 37 °C with 60% humidity and 5% CO2 for 72 hours. During culturing, medium volume was adjusted twice per day to make sure brain slices were covered with only a thin film of the medium at the upper surface. Cultured brain slices were fixed with ice-cold 4% PFA for 20 minutes and embedded in OCT for frozen sectioning to generate 30 μm-thick free-floating sections. Sections were stained with an anti-GFP antibody to visualize the distribution of GFP positive cells.

Based on the density of DAPI staining, the neocortex was divided into different layers including cortical plate (CP), subplate (SP), intermediate zone (IZ), and ventricular zone/ subventricular zone (VZ/SVZ). The number of GFP positive cells in different layers of the neocortex was counted by ImageJ. The ratio of the number of GFP positive cells in a specific layer to the total number of GFP positive cells in the neocortex was calculated. 6 brain slices from 3 embryos electroporated with pCAG-EYFP plasmids (WT group), and 6 brain slices from 3 embryos electroporated with pCAG-CRE-EYFP plasmids (*Aspp2-KO* group) were included for quantification and comparison.

2.2.3.3 Moue embryonic neural stem cells culture

The neurosphere culture system has been widely used as an in vitro model system for studying the proliferation and differentiation of neural stem cells. Neural stem cells isolated from neurogenic niches such as the neocortex and the ganglionic eminence can form free-floating spheres in an environment lacking adherent substrates. ASPP2$^{+/-}$ male mice and ASPP2 $^{+/-}$ female mice were paired for timed mating. Timed-pregnant mice were sacrificed at E12.5 (the day of the vaginal plug was considered E0.5) and embryos were collected in an ice-cold HBSS filled dish. Tail tips of embryos were collected and used for genotyping.

Brains were dissected out under the microscope in a dish filled with cold HBSS. The neocortex tissue was carefully cut off by fine scissors and collected in Neural basal medium (Gibco) on ice. Collected neocortex tissues were briefly centrifuged to spin down the tissues, the supernatant was removed. Tissues were incubated in 1 ml accutase solution (Sigma) for 10 minutes at 37°C and dissociated into single cells by gentle pipetting up and down until a milky like the suspension was achieved. Then, the suspension was allowed to settle for 1 minute so as the non-dissociated clumps precipitate. The dissociated single-cell suspension was transferred to a tube containing 1 ml Neural basal medium to dilute the accutase. Cells were spun down and washed with 2 ml Neural basal medium. Washed cell pellet was resuspended in 1 ml complete NSCs culture medium (Neurobasal medium supplemented with 2% B27, 0.5 mM Glutamine, 20ng/ml bFGF, 20ng/ml EGF, and 1% penicillin/streptomycin). Cell density was counted. Cells were seeded at the density of $2x10^5$ cells/ mL in complete NSCs culture medium into a well of extra-low-attachment 6-well plates. Cells were cultured at 37° C in a humidified incubator with 5% CO_2. Neurospheres were formed in 3-4 days.

When neurospheres were ready for a subculture (approximately 150 μm in diameter), the medium with suspended neurospheres was collected and centrifuged at 110g for 3 minutes at room temperature. The supernatant was removed, and the cell pellet was resuspended in 1 mL accutase solution (Sigma) for 10 minutes at 37°C with gentle agitation. Then neurospheres were dissociated by pressing the 1mL pipette tip to the bottom of the tube and pipetting the suspension up and down until a milky like the suspension was achieved. The unbroken spheres were discarded. The single-cell suspension was centrifuged at 120g for

5 minutes, and the cell pellet was resuspended in a complete NSCs culture medium. Cells were seeded at a concentration of $5x10^4$ cells/ mL into ultra-low-attachment 6-well plates.

2.2.3.4 BrdU NSCs proliferation assay

Primary neurospheres were disassociated into single cells as described above. Single cells were seeded on round cover glasses pre-coated with poly-lysine so that NSCs can attach to the cover glasses. 48 hours after seeding, cells were treated with 10 μM BrdU for 2 hours. Cells were fixed with ice-cold 4% PFA solution in PBS on ice for 10 minutes. After washing with PBS 3 times, 5 minutes each, fixed cells were incubated with cold 1M HCl for 10 minutes on ice to denature DNA so that anti-BrdU antibody can access the BrdU within the DNA. After washing, cells were incubated in blocking buffer (10% normal donkey serum, 1% BSA, 0.3% tritonX100 in PBS) for 1 hour at room temperature to reduce unspecific antibody binding. After blocking, cells were incubated with anti-BrdU antibody diluted in blocking buffer overnight at 4°C, washed with PBS 3 times, then incubated with Alexa Fluor conjugated secondary antibodies diluted in blocking buffer for 1 hour at room temperature. Nuclei were stained with 1ug/ml DAPI in PBS for 10 minutes at room temperature. Cover glasses were washed in PBS for 20 minutes with gentle shaking, then mounted on slides with aqueous anti-fade mounting medium.

Three NSCs lines cultured form 3 WT embryos and three lines from 3 *Aspp2-KO* embryos were used for this assay. Cells from each line had been seeded on three cover glasses as technical triplicates. For each cover glass, three images were taken by confocal microscopy. For each image, the total cell number and the number of BrdU positive cells were counted

by ImageJ, and the percentage of BrdU positive cells was calculated. Therefore, 9 images of WT NSCs and 9 images of *Aspp2-KO* NSCs were compared.

2.2.3.5 Neurosphere growth assay

Secondary and tertiary neurospheres were disassociated into single cells and seeded into ultra-low-attachment 6-well plates at a density of 30,000 cells per well. Four days later, neurospheres were imaged by bright field light microscopy. The diameters of each neurosphere were measured by using ImageJ. Both WT group and *Aspp2-KO* group had three NSCs lines cultured from three embryos.

2.2.3.6 Maintenance of cell lines

U2OS cell lines were cultured in DMEM supplemented with penicillin/streptomycin (100 U/ml), L-glutamine (2 mM), and 10% (v/v) FBS in T-75 flasks (Falcon). Cell cultures were maintained in a Heraeus incubator at 37°C with 5% CO2. Once reaching confluence, cells were washed with PBS and incubated with 0.05% Trypsin-EDTA for serval minutes at 37°C until cells started to detach. Trypsinisation was terminated by adding an appropriate volume of DMEM with FBS. The cell suspension was collected in a 15 ml Falcon tube and centrifuged at 300g for 3 minutes. The cell pellet was resuspended in DMEM. Cells were seeded in fresh flasks at the desired density.

2.2.3.7 Real-time cell migration assay

Cell migration assay was carried out by using the xCELLigence Real-Time Cell Analyzer Dual Plate (RTCA-DP) instrument according to the manufacturer's recommendations

(ACEA Biosciences). 160 µl of DMEM medium containing 10% FBS or DMEM medium alone (served as negative control) was added to each well of the bottom chamber of the 16-well xCELLigence CIM-plate (ACEA Biosciences). After assembling the upper chamber with the bottom chamber, 50 µl of DMEM medium containing vehicle or ROCK inhibitor Y27632, a known inhibitor of cell migration, was added to each well of the top chamber. The assembled CIM-plate was placed in an incubator at 37°C for 30 min for pre-equilibrium. Meanwhile, WT and *ASPP2-KO U2OS* Cells that had been serum-starved for 12 hours were dissociated into single cells by 0.05% Trypsin-EDTA solution, counted, and resuspended in DMEM medium without FBS. Cells were seeded into the upper chamber of the 16-well CIM plate at a density of 50,000 cells per well. The loaded CIM-plate was placed in the incubator for 20 minutes to allow cells to settle on the microporous PET membrane between the upper chamber and the lower chamber. Then the CIM-plate was installed in the xCELLigence RTCA-DP machine (ACEA Biosciences). The electrical impedance changes caused by cells adhere to microelectrode sensors beneath the microporous PET membrane were monitored every 15 minutes for 25 hours. Cell index values, which were directly proportional to the area covered by cells, were calculated and plotted using the RTCA software (ACEA Biosciences). Two independent experiments were performed each carried out in triplicates.

2.2.3 DNA and RNA techniques

2.2.3.1 Transforming competent cells and plasmid DNA extraction

pCAG-EYFP and pCAG-CRE-EYFP plasmids used for electroporation were kindly given by Dr. Bin Sun from Professor Francis Szele's lab. Plasmids were expanded by

transforming commercially available chemically competent bacteria, bacteria culture, and plasmids DNA extraction. Competent cells were thawed on ice. 0.1 µl of DNA plasmids were added into competent cells and properly mixed by gently flicking the bottom of the Eppendorf tube. The mixture was incubated on ice for 30 minutes, placed in a 42 ℃ water bath for 30 seconds, then placed back on the ice for 3 minutes. 500 µl of SOC media was added and the transformed cells were incubated at 37°C for 30 minutes on an orbital shaker at 200 rpm. 30 µl of cell transformed cell suspension was added onto an LB agar plate with selection antibiotic and spread evenly by a sterile spreader. The agar plate was incubated at 37°C overnight. The next morning, individual colonies were picked up by a sterile pipette tip and immersed in a culture tube containing 3 mL of LB media supplemented with Ampicillin. Culture tubes were incubated at 37°C for 2 hours on an orbital shaker at 250 rpm. Then, 1 ml of bacteria culture was transferred into a flask (1L) containing 150 mL of LB media plus ampicillin. The flask was incubated at 37°C overnight on an orbital shaker at 250 rpm. On the next day, bacteria culture was centrifuged at 3,000 rpm for 30 minutes to precipitate the bacteria. The supernatant was removed, and the bacteria pellet was used for maximum preparation of DNA plasmids by using the EndoFree Plasmid Maxi Kit (Qiagen) according to the manufacturer's protocol. Extracted plasmid DNA was dissolved in ddH_20. The DNA concentration was measured by micro-volume spectrophotometer NanoDrop. The plasmid DNA solution was aliquoted and stored at -80°C.

2.2.3.2 RNA extraction, reverse transcription, and real-time quantitative PCR

Brain tissue samples or neurosphere samples were homogenized in TRIZOL reagent by a homogenizer. For NSCs grown in monolayer, cells were washed with ice-cold PBS once and then lysed directly by adding the proper amount of TRIZOL reagent (1mL per 3.5cm

diameter dish) and pipetting the lysate up and down. The cell lysate was vortexed thoroughly. The homogenized sample was incubated at room temperature for 5 minutes to permit the complete dissociation of nucleoprotein complexes. Samples were centrifuged, and the supernatant was transferred to a fresh tube. 0.2 mL chloroform was added to 1ml TRIZOL reagent. The mixture was vortexed vigorously for 30 seconds, incubated at room temperature for 3 minutes, and centrifuged at 12,000g for 15 minutes at 4°C. The colourless upper phase was transferred into a fresh tube without disturbing the interphase. An equal amount of isopropyl alcohol was added to the aqueous upper phase. The mixture was incubated at room temperature for 10 minutes and then centrifuged at 12,000 for 15 minutes to precipitate the RNA pellet. The supernatant was removed completely. The RNA pellet was washed with 75% ethanol in RNase-free water once. Leftover ethanol was removed completely to let the pellet dry for 2 minutes. RNA was dissolved in RNase-free water. The concentration of the RNA solution was measured by micro-volume spectrophotometer NanoDrop.

Reverse transcription was performed using the SuperScript™ IV First-Strand Synthesis System (Thermo Fisher). The reverse transcription reaction mix was listed as below:

Table 2. 8 Components of the reverse transcription reaction

50μM Oligo d(T)18 primer	1μl
10mM dNTP mix (10mM each)	1μl
Template RNA	500ng or 1μg
RNase-free water	To 13μl
Incubate at 65°C for 5 minutes Incubate on ice for 2 minutes	
100mM DTT	1μl
Ribonuclease Inhibitor	1μl
5x SSIV Buffer	4μl
Reverse transcriptase (200U/μl)	1μl
Incubate at 55°C for 30 minutes Incubate at 80°C for 10 minutes	

20μl of cDNA was diluted by adding 80μl RNase-free water. 1μl of cDNA was used in each reaction of the subsequent RT-PCR. Components of the RT-PCR reaction mix was listed as below:

Table 2. 9 Components of RT-PCR reaction

Template cDNA	1μl
2x SYBR Green Master Mix	10μl
Forward Primer (10μM)	1μl
Reverse Primer (10μM)	1μl
Nuclease-free water	To 20μl

Quantitative PCR was performed on the StepOnePlus Real-Time PCR machine. The program used was as follows:

Table 2. 10 Programme for RT-PCR

Temperature	Duration	Cycle
95℃	10 minutes	1
95℃	15 seconds	
55℃	30 seconds	40
72℃	20 seconds	
	Melting curve	

Data were collected at the elongation phase of each cycle. The relative expression level of each target gene was analyzed based on the ΔΔCt method with Actin and GAPDH as reference genes.

2.2.4 Biochemistry

2.2.4.1 RhoA activity assay

RhoA activity was determined using G-LISA® RhoA Activation Assay Biochem Kit™ (Cat. BK#124, Cytoskeleton). Confluent cells in 6-well plates were serum-starved for 12 hours before treatment with Rho activator for indicated time periods. Cells were washed with ice-cold PBS once and harvested in 80 µl G-LISA lysis buffer. Protein concentration was measured, and samples were adjusted to the same protein concentration as described in "Protein analysis by western blot". 25 µl cell lysate, or 25 µl lysis buffer (Blank control), or 25 µl RhoA-GTP protein (positive control) was mixed with 25 µl binding buffer. The mixture was added into a well pre-coated with Rhotekin-RBD protein, which selectively binds to Rho-GTP, and incubated on a cold orbital microplate shaker at 400 rpm for 30 minutes at 4 °C. Wells then washed twice with 200 µl wash buffer at room temperature. Wash buffer was completely removed by vigorously flicking the plate to avoid high

background readings. Wells were incubated with 200 µl of antigen-presenting buffer for 2 minutes at room temperature. After washing, 50 µl of diluted anti-RhoA primary antibody was added into each well and incubated on an orbital shaker at 200 rpm at room temperature for 45 minutes. Meanwhile, secondary HRP labelled antibodies were diluted in antibody dilution buffer at a ratio of 1/62.5. Wells were washed three times with 200 µl of wash buffer. 50 µl of diluted secondary antibody was added to each well and incubated on an orbital shaker at 200 rpm at room temperature for 45 minutes. Wells were washed three times with 200 µl of wash buffer. HRP detection reagents A and B were mixed and 50 µl of the mixed HRP reagent was added into each well and incubated at 37 °C for 15 minutes. 50 µl of stop buffer was added to each well. Absorbance at 490 nm was read by a microplate spectrophotometer.

2.2.4.2 ROCK activity assay

ROCK activity was measured using the ROCK Activity Assay Kit (Cat. CSA001, Millipore). Confluent cells in 6-well plates were serum-starved for 12 hours before treatment with Rho activator for 2 hours. Cells were washed with ice-cold PBS once and harvested in 60 µl lysis buffer. Protein concentration was measured, and samples were adjusted to the same protein concentration as described in “Protein analysis by western blot”. The enzyme reactions were assembled as indicated in the table below.

Table 2. 11 Reaction setup for ROCK activity assay

	Type of reaction:		
Component:	**positive control**	**blank control**	**Exp. group**
ROCK-II (1 mU/µL)	10 µL	-	-
5X ATP Solution	10 µL	10 µL	10 µL
5X $MgCl_2$ Solution	10 µL	10 µL	10 µL
Assay Dilution Buffer I	10 µL	10 µL	10 µL
Cell lysate	-	-	20 µL
Distilled water	10 µL	20 µL	-

The assembled reaction mix was added into wells pre-coated with recombinant MYPT1, which contains a Thr696 residue that may be phosphorylated upon the addition of ROCK-I, ROCK-II, or DMPK. Wells were incubated at 30°C for 30 minutes on an orbital shaker at 200 rpm. Wells were washed with 200 µl washing buffer 3 times. After washing, 100 µl of diluted anti-phosphor-MYPT1 (Thr696) antibody was added into each well and incubated on an orbital shaker at 200 rpm at room temperature for 1 hour. Wells were washed with 200 µl washing buffer 3 times. 100 µl goat anti-rabbit IgG HRP secondary antibody was added and incubated on an orbital shaker at 200 rpm at room temperature for 1 hour. Wells were washed with 200 µl washing buffer 3 times, then washed with 200 µl TBS buffer twice. Wells were incubated with 100 µl TMB/E substrate in the dark for 10 minutes to develop a blue clour. The reaction was stopped by adding 100 µl of stop solution to each well. Absorbance at 450 nm was read by a microplate spectrophotometer.

2.2.4.3 Co-Immunoprecipitation (Co-IP)

Confluent cells in T-175 flasks were washed with ice-cold PBS once. PBS was removed completely by aspirating. If Co-IP was not carried out immediately, flasks with cells were stored at -80°C. 1.5 mL of Pierce ™ IP Lysis buffer (1% NP-40) containing protease cocktail inhibitor (Roche) was added into each T-175 flask on ice. Cells were collected in the lysis buffer by a cell scraper. Cell lysates were transferred into a 2 ml tube, pipetted up and down several times, incubated on ice for 15 minutes. Cell lysates were centrifuged at 15,000 rpm at 2°C to precipitate cell debris. The supernatant was transferred to a fresh tube. Protein concentration was measured by the Quick Start Bradford assay (Bio-Rad): 1 part of Bradford reagent was diluted by 4 parts of ddH_2O. 1 µl of cell lysate was added into 200 µl of diluted Bradford reagent in 96-well plates. BSA solution ranged from 0.5 µg/µl to 5 µg/µl were used to establish the standard curve. The absorbance at 595 nm was measured by a microplate reader. The protein concentrations of each sample were calculated and equalized by adding the proper amount of IP lysis buffer to samples with higher protein concentrations. 100 µl cell lysate was transferred to a fresh tube to be used as input, and 6x SDS loading buffer was added. Samples were boiled at 95°C, then stored at -20 °C. 1 mL cell lysate was precleared by incubation with 40 µl of pre-washed magnetic Dynabeads (Thermo Fisher) at 4 °C on a rotor for 3 hours. Dynabeads were removed from cell lysate. The pre-cleared cell lysate was incubated with 5 µg antibody at 4 °C on a rotor overnight. On the next day, 40 µl of pre-washed magnetic Dynabeads was added into each sample and incubated at 4 °C on a roto for 1 hour. Dynabeads were washed with IP buffer three times on a rotor, 10 minutes each time. After washing, 30 µl 1xSDS loading buffer was added to Dynabeads. Samples were boiled at 95 °C for 3 minutes. Input samples and immunoprecipitant samples were submitted to western bolt to detect target proteins.

2.2.4.4 Protein analysis by western blot

Step 1. Sample preparation

Adherent cells were washed with ice-cold PBS once. If cell lysis was not carried out immediately, flasks or plates with cells were stored at -80°C. A proper amount of RIPA buffer containing protease inhibitors and phosphatase inhibitors (Roche) was added to cells. Cells were scraped off the plates by cell scrapers (Greiner), and RIPA buffer containing cells were transferred to 1.5 ml Eppendorf tubes. Cells were incubated in PIPA buffer for 20 minutes on ice with occasional agitation. Lysates were centrifuged at 15,000×g for 15 min at 4℃ and supernatants were transferred into fresh tubes. For fresh or frozen mouse tissues, a proper amount of RIPA buffer was added according to the weight of the tissue. Tissues in RIPA buffer were broken and homogenized by a tissue homogenizer. Samples were placed on ice for 15 minutes, then centrifuged at 15,000×g for 15 min at 4℃. Supernatants were transferred into fresh tubes.

Protein concentration was measured by the Quick Start Bradford assay (Bio-Rad): 1 part of Bradford reagent was diluted by 4 parts of ddH_2O. 1 µl of cell lysate was added into 200 µl of diluted Bradford reagent in a well of the 96-well plates. BSA solution ranged from 0.5 µg/µl to 5 µg/µl were used to establish the standard curve. The absorbance at 595 nm was measured by a microplate reader. The protein concentrations of each sample were calculated and equalized by adding the proper amount of RIPA buffer to samples with higher protein concentrations. The cell lysate was mixed with an appropriate volume of 6× SDS loading buffer. Samples were boiled for 5 min at 95℃ and were then ready for gel electrophoresis. If samples were not used immediately, they were stored at -80 ℃.

Step 2. Preparation of SDS-PAGE gels

SDS-PAGE gels were prepared with the Mini-PROTEAN® Tetra Cell system (Bio-Rad). The appropriate concentration of the resolving gel was chosen based on the molecular weights of target proteins. Resolving gel solution and stacking gel solution were prepared according to the following table:

Table 2. 12 Recipes for stacking and resolving gels

	Stacking Gel	Resolving Gel		
	4%	7.5%	12%	X%
30% Acrylamide/bis	1.98 ml	3.75 ml	6.0 ml	0.5 × X ml
0.5M Tris-HCl, pH 6.8	3.78 ml	—	—	—
1.5M Tris-HCl, pH 8.8	—	3.75 ml	3.75 ml	3.75 ml
10% SDS	150 µl	150 µl	150 µl	150 µl
diH_2O	9 ml	7.28 ml	5.03 ml	11.03–(0.5 × X) ml
TEMED	15 µl	7.5 µl	7.5 µl	7.5 µl
10% APS	75 µl	75 µl	75 µl	75 µl
Total Volume	15 ml	15 ml	15 ml	15 ml

Resolving gel solution was poured into the assembled glass plates. 1 mL of isopropanol was added to the resolving gel solution layer. Once the resolving gel polymerized, isopropanol was removed, and the stacking gel solution was added, then a 15-well comb was inserted immediately. Gels were allowed to polymerize at room temperature. For experiments in which proteins of low molecular weight and high molecular weight need to be nicely separated, pre-cast Protein TGX Gels (Bio-Rad) were used.

Step 3. SDS-PAGE electrophoresis and western blot

SDS-PAGE gels were installed in the gel tank filled with 1× SDS-PAGE running buffer. Prepared samples with equalized protein concentration and pre-stained protein marker

(New England Biolabs) were loaded into SDS-PAGE gels. When home-made gels were used, protein samples underwent electrophoresis at a constant voltage of 80 V for 20 minutes followed by electrophoresis at a constant voltage of 120 V for 90 minutes. When pre-cast gels were used, protein samples underwent electrophoresis at a constant voltage of 150 V for 45 minutes. When electrophoresis was finished, proteins in gels were transferred onto a PVDF membrane (Whatman) by wet transfer. The transfer was performed at a constant current of 280mA at 4℃ for 2 hours. When the transfer was completed, the PVDF membrane was stained with Ponceau S solution for 30 seconds to check for transfer efficacy. The membrane was then blocked with 5% (w/v) skimmed milk in TBST buffer for 1 hour at room temperature. After a brief wash with TBST buffer, the membrane was incubated with primary antibody diluted in 5% (w/v) BSA overnight at 4℃. On the next day, the membrane was washed with TBST buffer 3 times, 5 minutes each time then incubated with HRP-conjugated secondary antibodies for 1 hour at room temperature. After washed with TBST buffer for 3x10 minutes, enhanced chemiluminescence (ECL) solution was applied onto the membrane for 1 minute. Protein bands were visualized by X-ray film (Fujifilm) using a film developer in the dark or by ChemiDoc Imaging System (Bio-Rad). If the membrane needed to be probed by another antibody, the membrane was incubated with western blot stripping buffer (Santa Cruz) for 20 min at room temperature and blocked again before incubation with the new primary antibody.

2.2.5 Statistical analysis

Statistical analysis was performed using GraphPad. For experiments containing only two groups without any treatment, a two-tailed, unpaired *t*-test was used to determine the statistical significance of the difference between the two groups. For two experimental

groups receiving different treatments, two-way ANOVA was used to test if there was a significant effect of the treatments (eg. Rho activator), the difference between groups (eg. loss of ASPP2), or their interaction. If the p-value from ANOVA analysis was less than 0.05, Tukey's method was used as a post hoc test to compare all possible group pairings. Differences were considered significant at $p<0.05$.

Chapter 3: ASPP2 deficiency impairs chain migration of neuroblasts leading to diminished olfactory bulbs.

As mentioned in Chapter 1, *TP53BP2* (encoding human ASPP2) has been reported to be responsible for central nervous system defects, including hydrocephalus, hypoplasia, agenesis of the corpus callosum, neural tube defects (NTDs) and cerebellar hypoplasia in 1q41q42 microdeletion syndrome in human (Zak et al., 2016). *Aspp2-KO* mice showed neural tube defects at embryonic day 14.5 (E14.5) in a genetic background dependent manner: NTDs were detected in 46% (n=13) of embryos with C57BL/6 background, 15% (n=127) of embryos with mixed C57BL/6-129/Sv background, and 8% (n=12) of embryos with Balb/c background (Zak et al., 2016). ASPP2 mice also developed hydrocephalus across all genetic backgrounds. These data suggest that ASPP2 plays an essential role in the development of the central nervous system (CNS) in both humans and mice.

Under the mixed C57BL/6-129/Sv background, loss of ASPP2 disrupted neuroepithelial cell polarity through regulating Par3 function and resulted in increased proliferation of neural progenitor cells in embryonic brains (Sottocornola et al., 2010a). Whether the enhanced proliferation is a direct result of the disruption of neuroepithelium or caused by other factors remains unclear. Apart from regulating neuroepithelial cell polarity and proliferation of neural progenitor cells, the function of ASPP2 in other important cellular processes such as neuronal migration was unknown. Also, whether the loss of ASPP2 would lead to any brain malformation at postnatal stages in mice has never been systematically examined. Therefore, I started my study by examining brains from WT and

Aspp2-KO adult mice with Balb/c background. I choose Balb/c mice because *Aspp2-KO* in C57BL/6J background mice led to 100% neonatal lethality, and only 30% of the *Aspp2-KO* mice with mixed C57BL/6J-129/Sv background survived birth, but all died before weaning. The majority of *Aspp2-KO* mice with Balb/c background survived after weaning.

In this chapter, I will present the finding that *Aspp2-KO* mice have diminished olfactory bulbs, followed by the results of *in vivo* and *in vitro* neuroblast migration assays, which support that this phenotype is caused by disrupted chain migration in the RMS.

3.1 *Aspp2-KO* mice have smaller olfactory bulbs.

To understand whether *Aspp2-KO* mice develop brain malformations at postnatal stages, I examined brains from WT and *Aspp2-KO* Balb/c mice at postnatal day 30 (P30) and P60. I found that *Aspp2-KO* mice had enlarged brains, particularly dramatically oversized superior colliculus and inferior colliculus (**Figure 3.1**). These observations are consistent with the increased proliferation of neural progenitor cells in *Aspp2-KO* embryonic developing brains (Sottocornola et al., 2010a). Interestingly, *Aspp2-KO* mice exhibited smaller rather than bigger olfactory bulbs (**Figure 3.1**). This phenotype was consistently observed across all the *Aspp2-KO* mice examined.

Development of the olfactory bulbs relies on neurogenesis and subsequent neuronal migration: interneurons in the olfactory bulb are born in the embryonic lateral ganglionic eminences (LGE), which give rise to most of the postnatal anterior subventricular zone (SVZ) in the lateral ventricles. Neural stem cells in the LGE and SVZ produce postmitotic undifferentiated neuronal precursors called neuroblasts. Neuroblasts then migrate

tangentially to the olfactory bulb through the rostral migratory stream (RMS), a migratory path of SVZ neuroblasts which starts in the SVZ and reaches the olfactory bulb. The formation of the RMS starts from the embryonic day 15-17 (E15-17) in mouse (Pencea & Luskin, 2003). Upon reaching the olfactory bulb, neuroblasts migrate into the granule cell layer and the glomerular layer and differentiate into neurons. Hypoplasia of the olfactory bulbs can be caused by impaired neurogenesis or disrupted neuronal migration or both.

It is known that ASPP2 deletion leads to increased proliferation in the ganglionic eminences during embryonic development (Sottocornola et al., 2010a). Therefore, it is highly likely that other cellular process rather than neurogenesis, such as neuronal migration, contributes to the phenotype of smaller olfactory bulbs found in *Aspp2-KO* mice.

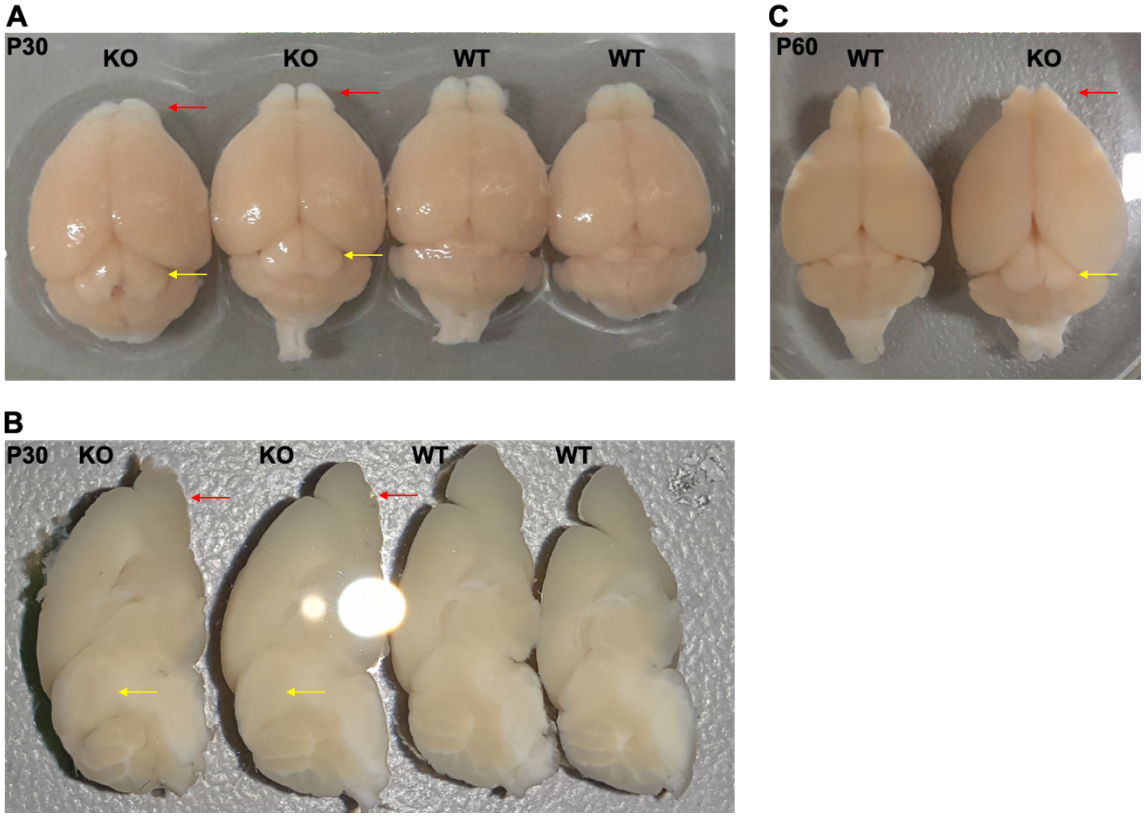


Figure 3. 1 *Aspp2-KO* mice showed diminished olfactory bulbs.

(A) Brains from WT and *Aspp2-KO* mice at P30. (B) The midline sagittal surfaces of the brains in (A). (C) Brian from WT and *Aspp2-KO* mice at P60. Red arrows indicate diminished olfactory bulbs. Yellow arrows indicate enlarged superior and inferior colliculus.

3.2 ASPP2 deficiency impairs the migration of neuroblasts from the SVZ to the olfactory bulb.

To determine the effect of ASPP2 deficiency on SVZ- olfactory bulb neurogenesis, DCX immunofluorescence staining was carried out on brain sections from WT and *Aspp2-KO* mice at P30. Doublecortin (DCX) is a widely used marker of the neuroblast. It is expressed in newly generated neuroblasts and continues to be expressed during the migration phase until neuroblasts become mature neurons at their destinations in the olfactory bulb, at which stage DCX expression diminishes below the level of detection.

I found that there were more DCX^+ neuroblasts in the lateral SVZ in *Aspp2-KO* mice (**Figure 3.2A**). However, *Aspp2-KO* olfactory bulb displayed fewer DCX^+ neuroblasts (**Figure 3.2B**), which suggested that neuroblasts produced in the SVZ failed to reach the olfactory bulb. On on hand, the increased number of DCX+ neuroblasts in *Aspp2-KO* SVZ can indicate increased neurogenesis, which is consistent with the function of ASPP2 in embryonic ganglionic eminence: increasing proliferation of neural stem cells/ neural progenitor cells (Sottocornola, R. 2010). On the other hand, the increased number of DCX+ neuroblasts in the SVZ could have accumulated there due to deficient migration into the OBs.

To distinguish the above scenarios, I carried out BrdU labelling experiments. *Aspp2-KO* and their WT littermates received single intraperitoneal injections of BrdU at P30 to label proliferating cells, including neural stem cells in the SVZ and neuroblasts produced by them, which remain mitotic while they migrate towards the olfactory bulb. Four days after injection, brains were harvested and $BrdU^+$ cells in SVZ and olfactory bulb were analyzed.

As shown in **figure 3.3A**, many $BrdU^+$ cells had reached the olfactory bulb in WT mice while many BrdU+ cells were found accumulating in the RMS and fewer $BrdU^+$ cells were located in the olfactory bulb in *Aspp2-KO* mice. Consistently, quantification results showed that there were fewer $BrdU^+$ cells in the OB (**Figure 3.3 B-C**), but more BrdU+ cells in the SVZ (**Figure 3.3 D-E**) in *Aspp2-KO* mice. These results suggest that ASPP2 deficient neuroblasts are not able to migrate effectively through the RMS.

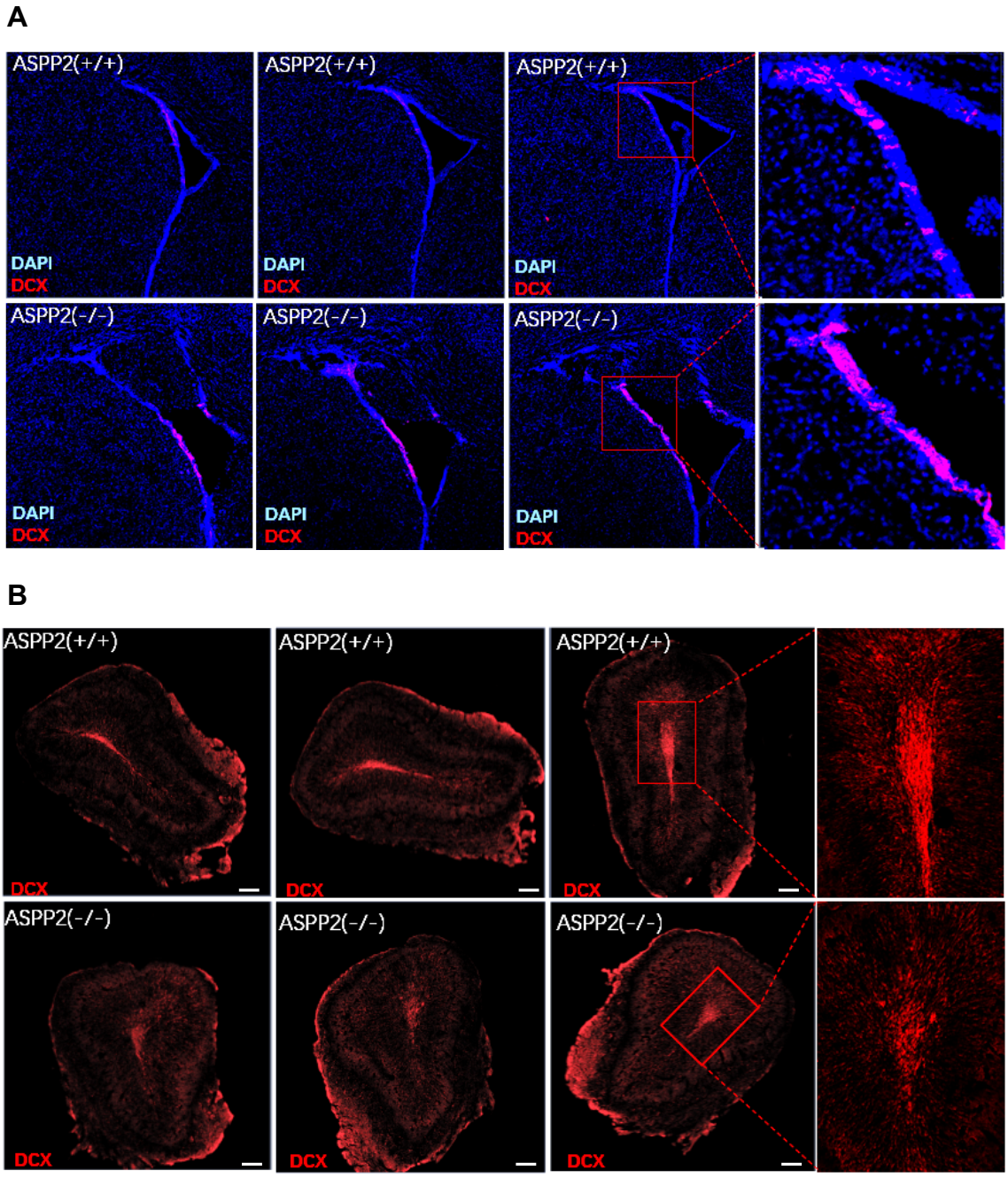


Figure 3. 2 *Aspp2-KO* mice showed more DCX+ cells in the SVZ but fewer in the OB.

(A) Immunofluorescence staining of DCX in the coronel sections of the SVZ. Representative images from 3 WT and 3 *Aspp2-KO* mice. (B) Immunofluorescence staining of DCX in the coronal sections of the olfactory bulb. Representative images from 3 WT and 3 *Aspp2-KO* mice. Scale bar = 200μm.

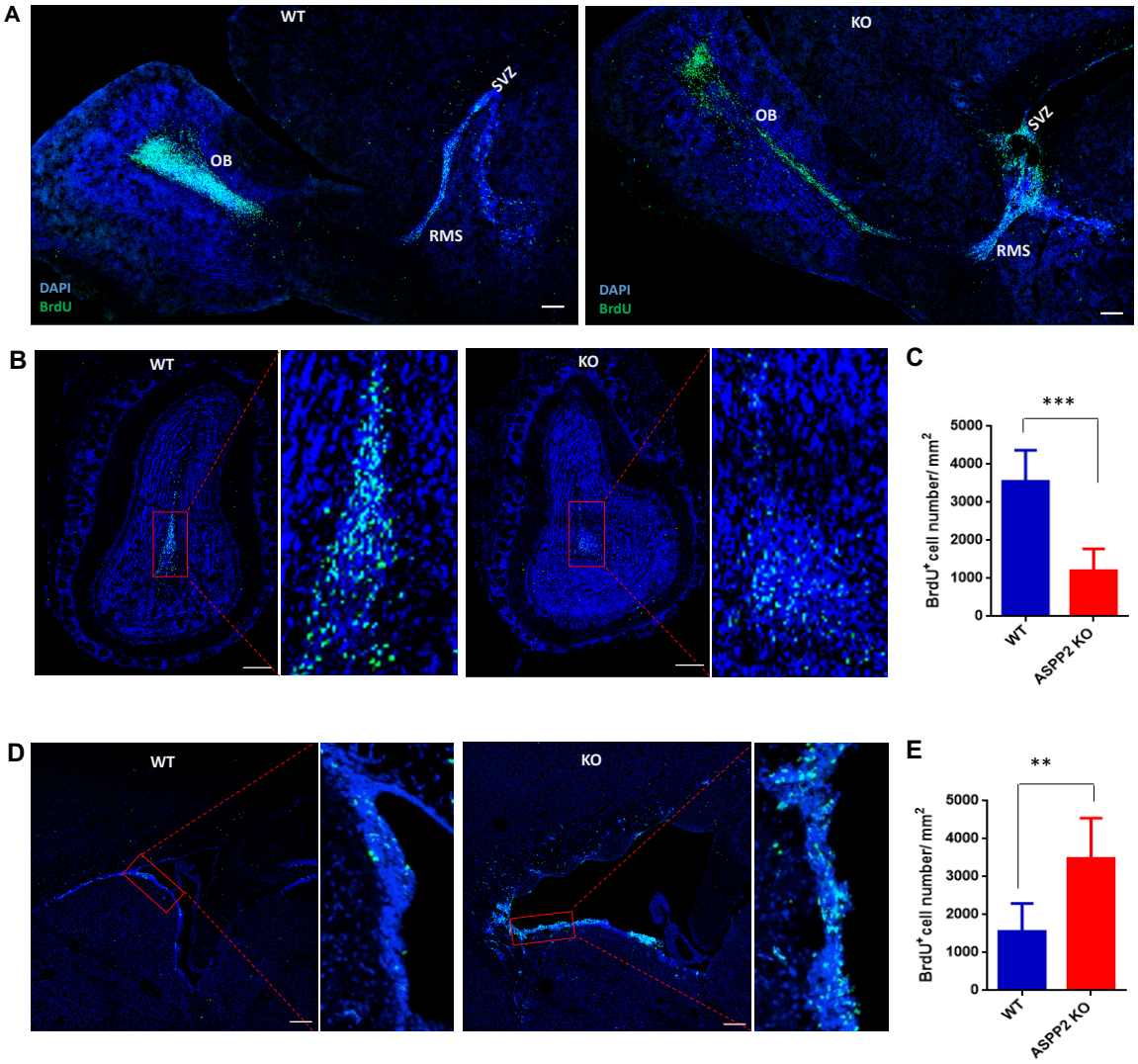


Figure 3. 3 Newborn neuroblasts failed to reach the olfactory bulb effectively in *Aspp2-KO* mice.

(A) Panoramic view of BrdU$^+$ cells in sagittal sections showing the SVZ, RMS, and the olfactory bulb. Representative images of 3 WT and 3 *Aspp2-KO* mice. Scale bar = 200μm. (B) Immunofluorescence staining of BrdU in coronal sections of the olfactory bulb. Representative images of 3 WT and 3 *Aspp2-KO* mice. Scale bar = 200μm. (C) Quantification of the surface density of BrdU+ cells in the olfactory bulb. (D) Immunofluorescence staining of BrdU in coronel sections of the SVZ. Representative images of 3 WT and 3 *Aspp2-KO* mice. Scale bar = 200μm. (E) Quantification of the surface density of BrdU+ cells in the SVZ. For quantification in (D) and (F), each group had 3 mice. Each mouse had six sections containing the RMS or the SVZ with an interval of 90 μm in between from comparable anatomic positions. The surface area of the RMS or

the SVZ and the number of BrdU positive cells within the ROI were measured by using ImageJ. The intensity of BrdU positive cells was presented as the number of BrdU positive cells per mm^2. Data were presented as mean ± SD. **p<0.01. ***p<0.001.

3.3 ASPP2 is necessary for neuroblasts to form chains in the SVZ and the RMS.

In the SVZ, neural stem cells (type B cells) proliferate and produce type C transit-amplifying cells, which then produce migrating neuroblasts. Right after their birth, neuroblasts start to express polysialylated neural cell adhesion molecule (PSA-NCAM), which is a homophilic binding cell adhesion molecule. Through PSA-NCAM-dependent homophilic aggregation, neuroblasts associate with each other to form chain-like clusters in the SVZ and the RMS. The formation of a chain-like structure enables neuroblasts to use each other as a migration scaffold and migrate along with each other (Sang et al., 2007). Disruption of NCAM-dependent chain formation leads to diminished olfactory bulbs and accumulation of neuroblasts in the caudal pole of the RMS (Cremer et al., 1994; Hu et al., 1996).

I revealed the accumulation of neuroblasts in the RMS in *Aspp2-KO* mice, which might be a result of disrupted chain migration. In order to test whether ASPP2 can influence chain formation, DCX staining was carried out on sagittal brain sections to show the morphology of neuroblasts. As shown in **figure 3.4A**, in WT mice, DCX^+ neuroblasts formed chain-like clusters in the lateral wall and the dorsolateral horn of the SVZ. However, DCX^+ neuroblasts in the *Aspp2-KO* mice were disorganized and failed to form chains. Similarly, DCX^+ neuroblasts show elongated migratory morphology and form chain-like structures in

the RMS of WT mice. In *Aspp2-KO* mice, DCX^+ neuroblasts did not associate with each other to form the chain-like structure in the RMS (**Figure 3.4B**).

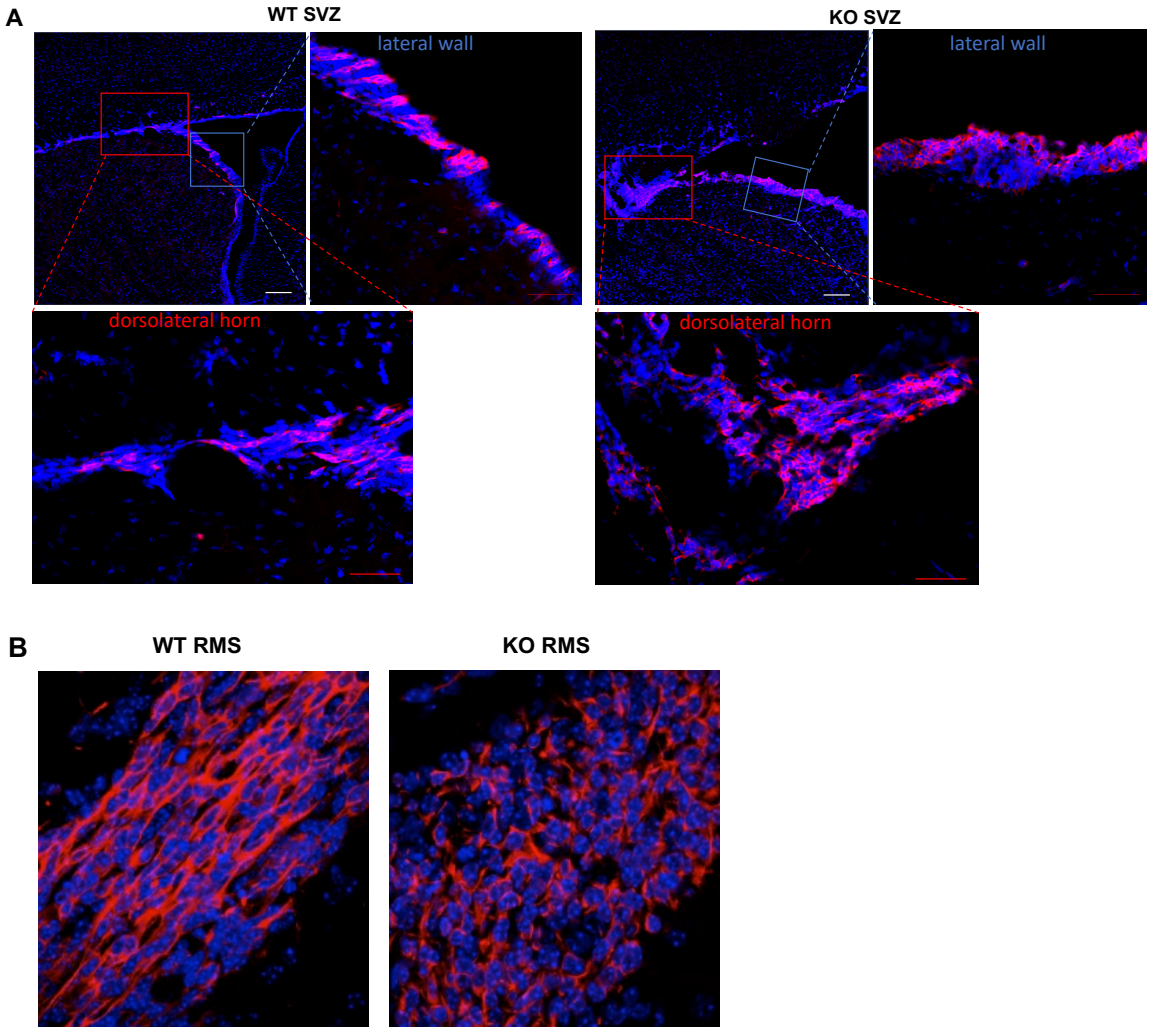


Figure 3. 4 ASPP2 deficiency leads to the failure of neuroblasts chain formation in the SVZ and the RMS.

(A) Immunofluorescence staining of DCX on sagittal sections of the SVZ. Representative images of 3 WT and 3 *Aspp2-KO* mice. The dorsolateral horn and the lateral wall of the SVZ were indicated by red and blue box respectively. White scale bar = 200μm. Red scale bar= 50μm. (B) Immunofluorescence staining of DCX in the RMS. Representative images of 3 WT and 3 *Aspp2-KO* mice. Scale bar = 200μm.

3.4 ASPP2 deficiency impairs chain formation and migration of neuroblasts *in vitro*.

Besides defects of neuroblasts themselves, migration of neuroblasts from the SVZ to the olfactory bulb is affected by various non-cell-autonomous mechanisms. For example, the initiation of migration in the SVZ may be regulated by the flow of cerebrospinal fluid (CSF) (Sawamoto, 2006). In the RMS, migrating neuroblasts are surrounded by astrocytes forming glial tubes and they are important for proper RMS migration (W. R. Kim et al., 2007; Soria et al., 2004). It has also been proposed that the blood vasculature within the RMS, which is arranged in parallel with the RMS, provides additional scaffolds for chain (Snapyan et al., 2009; Whitman et al., 2009). Neuroblast migration in the RMS is also regulated by chemoattractive signals such as Netrin expressed by mitral cells in the olfactory bulb and chemorepulsive signals such as Slit proteins secreted from the posterior brain structures (Murase & Horwitz, 2002; Nguyen-Ba-Charvet et al., 2004).

Defects of neuroblast migration observed in *Aspp2-KO* mice could be a combined result from both cell-autonomous and non-cell-autonomous factors. In order to test whether defects in neuroblasts themselves are the major cause of the phenotype, *in vitro* neuroblast migration assays using RMS explants were performed, in which the non-cell-autonomous effects, such as supports from the glial tube and blood vasculature, and chemoattractive signals from the olfactory bulb, are minimized.

The RMS was dissected out from WT and *Aspp2-KO* pups and cultured as previously described (Dixon et al., 2017). As shown in **figure 3.5A**, brains were dissected out from P2 pups, embedded in low-melting-point agarose, and then cut into 200 μm-thick coronal

sections by using a vibratome. Only the two sections containing the largest RMS area were used. The RMS was dissected out and cut into small blocks. Each RMS block was subsequently embedded in Matrigel in a well of 96-well plates and cultured for 48 hours. RMS explants from WT mice showed typical chain migration of neuroblasts while significantly fewer neuroblasts were found migrating out from *Aspp2-KO* RMS explants (**Figure 3.5B**). I quantified the migration capacity which is represented by the ratio of migration area/RMS explant area (**Figure 3.5C**). The results showed that *Aspp2-KO* RMS explants exhibited significantly lower migration capacity (**Figure 3.5D**). These results suggest that cell-autonomous defects in *Aspp2-KO* neuroblasts play an essential role in causing the phenotype of diminished olfactory bulbs. However, the non-cell-autonomous effect such as scaffold provided by the surrounding cells can not be ruled out because all the cells in the RMS explants are homogeneous WT cells or *Aspp2-KO* cells. If we can create a situation where *Aspp2-KO* cells are surrounded by WT cells, this issue can be solved. A possible way to achieve this goal is treating E18.5 pregnant mice carrying $Aspp2^{f/f}$ -NestinCre-Rosa26-GFP and $Aspp2^{+/+}$-NestinCre-Rosa26-GFP litters with tamoxifen then dissecting out the RMS from P0 pups for the RMS explants migration assay. In this way, the RMS would contain a few GFP+ *Aspp2-KO* neuroblasts or GFP+ WT neuroblasts while the rest of the cells are WT cells. If GFP+ *Aspp2-KO* neuroblasts show impaired migration compared to GFP+ WT neuroblasts, the migration defect is caused by the cell-autonomous effect.

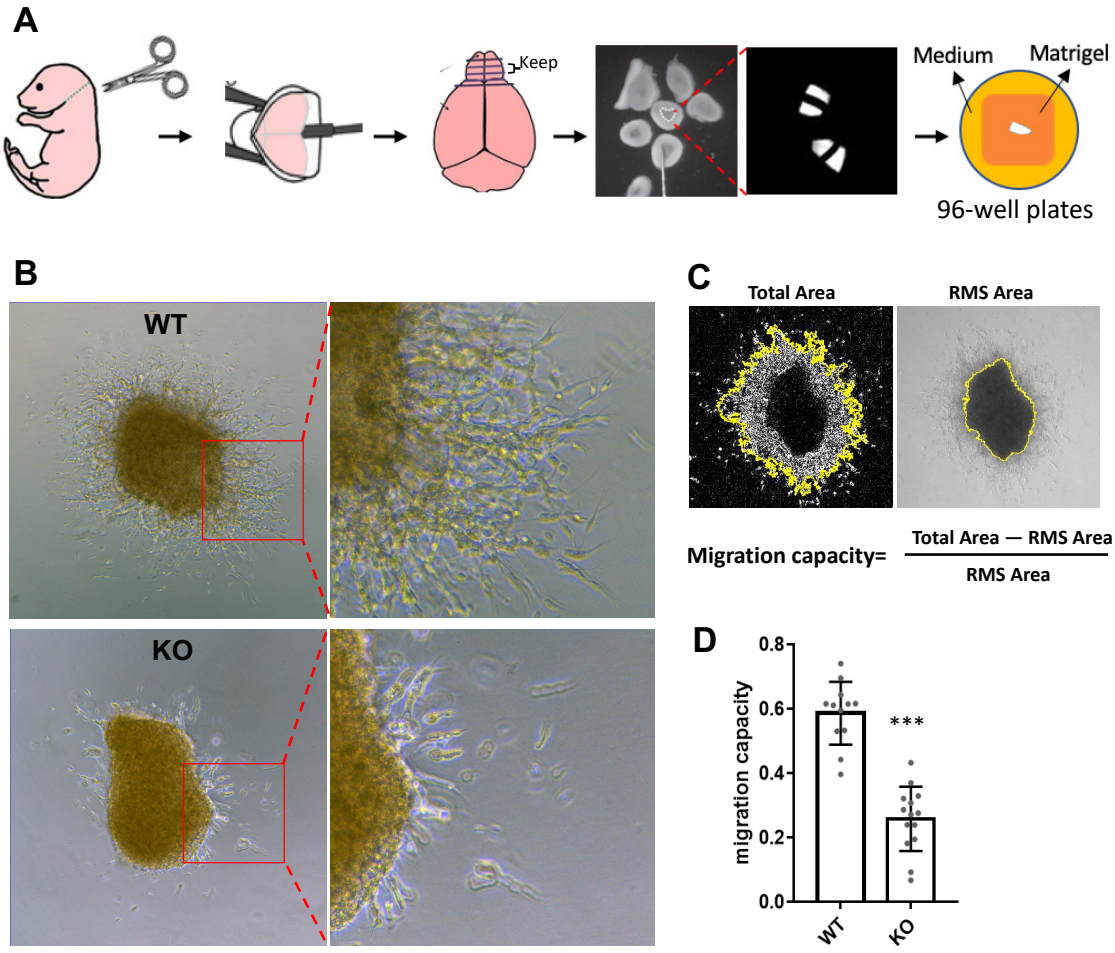


Figure 3. 5 ASPP2 deficiency impairs chain formation and migration of neuroblasts in vitro.

(A) Experimental workflow of culturing RMS explants. (B) Brightfield images of RMS explants dissected out from P1-P2 WT and *Aspp2-KO* pups after cultured in Matrigel for 2 days. (C) Methods used for calculating migration capacity. The total area and the RMS area are determined by using ImageJ. (D) Quantification of the migration capacity of WT and *Aspp2-KO* RMS explants. WT group has 12 RMS explants from 2 WT mice. KO group has 14 RMS explants from 3 *Aspp2-KO* mice. Data were presented as mean ± SD. ***p<0.001.

3.5 Summary

This chapter began with the examination of postnatal brains from *Aspp2-KO* mice on a Balb/c background where I found that loss of ASPP2 resulted in the slightly thicker cerebral

cortex, dramatically enlarged superior colliculus and inferior colliculus, and diminished olfactory bulbs. It was not surprising to find that *Aspp2-KO* mice have larger brains since a previous study from our lab revealed that ASPP2 deficiency increased proliferation and expanded the progenitor pool in the developing brain (Sottocornola R, 2010). The observation of diminished olfactory bulbs suggested that ASPP2 was involved in other cellular processes than proliferation. Indeed, I found that *Aspp2-KO* mice possess more DCX^+ neuroblasts in the lateral SVZ but fewer DCX^+ neuroblasts in the olfactory bulb. Similarly, results of BrdU labelling experiments also showed that there were more BrdU+ cells in the SVZ but fewer BrdU+ cells in the olfactory bulb. The increased number of DCX+ and BrdU+ cells in the SVZ could either be a result of increased proliferation of neural stem cells in the SVZ or accumulation of neuroblasts due to deficient migration or a combination of both. However, these results indicate that the phenotype of diminished olfactory bulbs is not caused by reduced neurogenesis in the SVZ, but could be a result of impaired chain migration of neuroblasts in the rostral migratory stream (RMS). In agreement with this idea, I found neuroblasts were not able to form the chain-like structure in the SVZ and RMS in *Aspp2-KO* mice. Furthermore, *Aspp2-KO* RMS explants showed impaired chain formation and migration when cultured in Matrigel *in vitro*, suggesting that failed neuroblast migration *in vivo* was, at least partly, caused by cell-autonomous effects of ASPP2 deletion on neuroblasts.

Chapter 4: ASPP2 deficiency impairs radial migration leading to periventricular nodular heterotopia (PNH).

Besides tangential chain migration, there is another type of migration called radial migration: In the developing neocortex, excitatory projection neurons born in the ventricular zone (VZ) and subventricular zone (SVZ) migrate radially into the neocortex wall and form the six cortical layers in an inside-out order. Instead of forming chain-like structures and migrating along with each other in the RMS, new-born neurons in the VZ/SVZ migrate as multipolar cells through the SVZ and the lower intermediate zone (IZ) (Tabata & Nakajima, 2003). They become bipolar as they leave the IZ and switch their migration mode to saltatory locomotion along with the radial processes of radial glial cells (RGCs) into the cortical plate (Nadarajah et al., 2001). Despite the different migration directions and modes, radial migration and tangential chain migration share basic machinery: neurons need to coordinate the extension and branching of their leading processes, nuclear and soma movement, and retraction of the tailing process over space and time, which is achieved by switching between actin and microtubule motors, and by assembling and disassembling attachments and recycling of diverse adhesion proteins (Cooper, 2013). In chapter 3, I revealed the importance of ASPP2 in the chain migration of neuroblasts in the RMS. Whether ASPP2 can also influence radial migration in the neocortex remains unclear.

As described in the introduction in chapter 1, periventricular nodular heterotopia (PNH) is composed of nodules of grey matter along the lateral ventricle wall and is believed to be a result of impaired radial migration. When I analyzed the SVZ sections from *Aspp2-KO* mice, I consistently found abnormal nodules at the dorsal wall of the lateral ventricle (**Figure 3.2A**), which may represent a model of periventricular nodular heterotopia (PNH). This observation indicates that ASPP2 is involved in radial migration and developing PNH.

In this chapter, I will show that *Aspp2-KO* mice developed PNH comprised of mature neurons. It has been reported that many cellular processes including the proliferation of neural stem cells, the integrity of the ventricular zone lining and radial glial cell processes, and most importantly neuronal migration are involved in developing PNH (Watrin et al., 2015). Therefore, I investigated the influence of ASPP2 deficiency on these cellular processes.

4.1 *Aspp2-KO* mice developed periventricular nodular heterotopia (PNH).

I consistently found abnormal nodules at the dorsal wall of the lateral ventricle in *Aspp2-KO* mice (**Figure 4.1A-B**), which resembled periventricular nodular heterotopia. To further characterize the abnormal nodules, hematoxylin and eosin (H&E) staining was carried out on sagittal sections from WT and *Aspp2-KO* mice at P5. As shown by **Figure 4.1C**, *Aspp2-KO* mice displayed nodular grey matter tissue along the ventricular surface. This phenotype constantly exists in all examined *Aspp2-KO* mice. To validate that the abnormal nodules are composed of neurons that failed to migrate into the cerebral cortex, brain sections were

stained with neuronal nuclei (NeuN), a marker of mature neurons. I found that the majority of the cells within the nodules in *Aspp2-KO* mice were positive for NeuN while $NeuN^+$ cells were rarely found in the VZ in WT brains (**Figure 4.1D**). Remarkably, the cortical plate overlying PNHs showed relatively normal lamination (**Figure 4.1B**), although I periodically observed several regions containing fewer $NeuN^+$ cells in the cortex of *Aspp2-KO* mice (**Figure 4.1D**), which suggests that neurons did not migrate to these areas properly.

To exam whether *Aspp2-KO* embryos show any sign of PNH at embryonic stages, I examined High-Resolution Episcopic Microscopy (HREM) data of the *Aspp2-KO* embryos at E14.5 in both C57/BL6 and Balb/c background. HREM imaging uses samples that have been embedded in a rigid matrix and sectioned with a microtome. By sequentially imaging the block face during the sectioning process, a comprehensive stack of accurately aligned images is acquired, documenting the 3D structure of the sample. Jerry Zak, a former lab member, did the experiment and collected the data. I examined the HREM images of the embryo heads. Among six *Aspp2-KO* embryos with C57/BL6 background examined, four embryos showed abnormal nodules at the ventricular surface of the neocortex (**Figure 4.2B**), which indicates disruption of the neuroepithelium and may represent an early sign of PNH. One embryo showed severely disrupted brain structures among which the neocortex could not be identified, another embryo showed a normal neocortex with a smooth ventricular surface. However, this type of abnormality was not detected in the three Balb/c *Aspp2-KO* embryos examined (**Figure 4.2C**). This observation is similar to our previous finding that the severity of neural tube defects (NTDs) caused by ASPP2 deletion was dependent on the mouse genetic background.

Even though HREM images of the E14.5 Balb/c *Aspp2-KO* embryos didn't show any obvious structural defect, it is possible that there were some subtle defects that can not be detected by the HREM technique because of its low spatial resolution. Therefore, in the future, other approaches should be adopted to precisely evaluate the brain structures in the E14.5 Balb/c *Aspp2-KO* embryos. First, Magnetic resonance imaging (MRI) is can be used. The spatial resolution of MRI for fixed brain samples range from 20-60 μm, which allows detailed anatomical comparisons(Benveniste et al., 2000; Johnson et al., 2002). In addition, MRI allows the three-dimensional morphology of anatomical structures to be examined in a non-destructive way, which means that if some structure defects are revealed by the MRI, the fixed brain samples can be used for histology analysis to further characterize the defects at cellular resolution. The anatomical positions of the defects can be easily located by using the 3D structure acquired by MRI as a reference. Second, tissue clearing combined with light-sheet microscopy can be performed to visualize the 3D structure of the brain at cellular resolution(H. R. Ueda et al., 2020). More importantly, whole-brain antibody labelling allows analysis of the amount and distribution of cells of interest. For instance, whole-brain staining with Pax6, Tbr2, NeuN can provide detailed information regarding whether loss of ASPP2 can affect the production and migration of aRGCs, IPCs, and neurons, respectively.

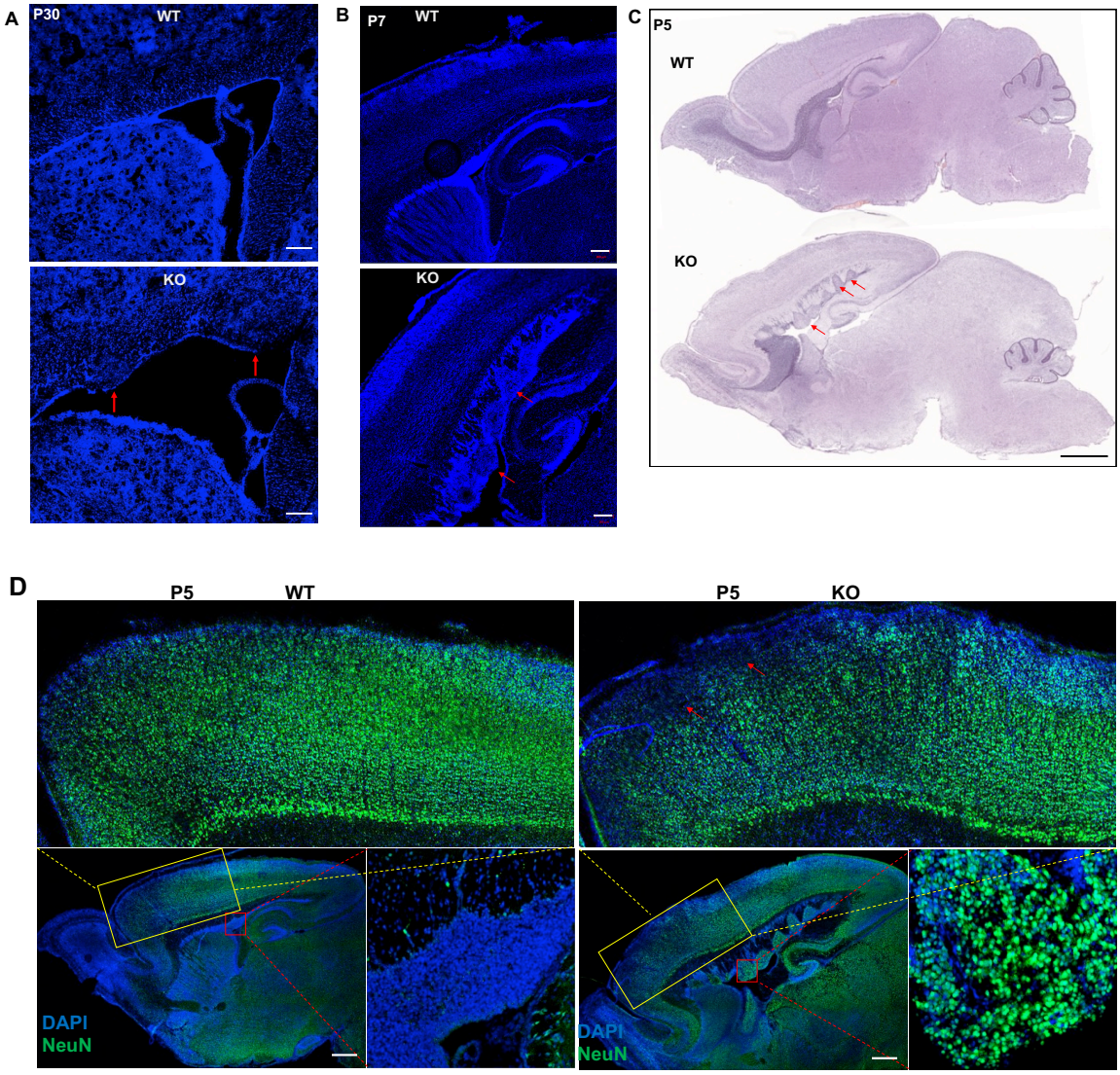


Figure 4. 1 *Aspp2-KO* mice develop PNH largely comprised of mature neurons.

(A) DAPI staining coronal brain sections of WT and KO mice at P30. Abnormal nodules at the surface of the ventricle in *Aspp2-KO* mice were indicated by red arrows. Scale bar = 200μm; Representative images from 5 KO mice and their WT littermates. (B) DAPI staining on sagittal brain sections from WT and KO mice at P7. PNH in KO mice is indicated by red arrows. Scale bar = 200μm; Representative images from 2 KO mice and their WT littermates. (C) HE staining on sagittal brain sections from WT and KO mice at P5. PNH in KO mice is indicated by red arrows. Scale bar = 500 μm. Representative images from 3 KO mice and their WT littermates. (D) NeuN staining on sagittal brain sections from WT and KO mice at P5. Red arrows indicate areas with a lower density of $NeuN^+$ cells in the cortex. Scale bar = 400 μm.

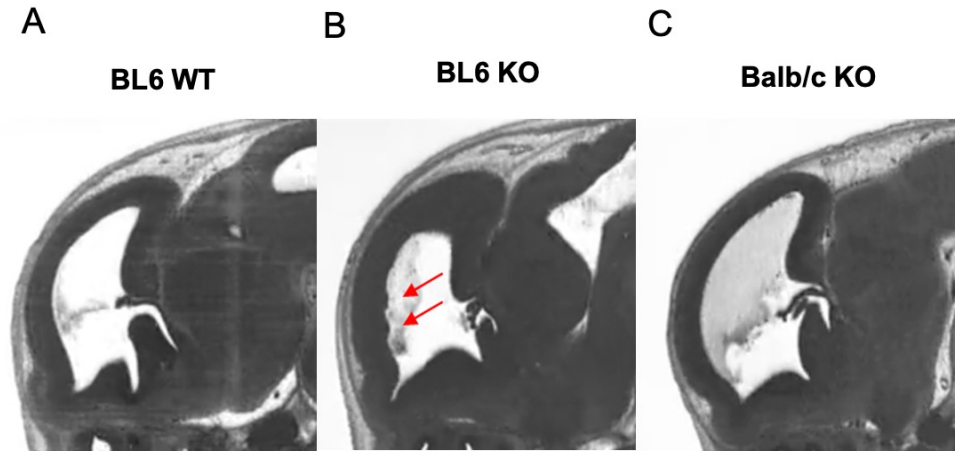


Figure 4. 2 *Aspp2-KO* embryos at E14.5 show abnormalities representing PNH.

(A) HREM images of embryo heads from E14.5 WT embryos with C57/BL6 background. (B) HREM images of embryo heads from E14.5 KO embryos with C57/BL6 background. Abnormalities along the apical surface of the neocortex are indicated by red arrows. (C) HREM images of embryo heads from E14.5 KO embryos with Balb/c background. **(Acknowledgements: Jerry Zak, a former Lu lab member, did the HREM experiment and collected the data.)**

4.2 ASPP2 deficiency leads to impaired radial migration.

To determine whether ASPP2 is directly involved in regulating the migratory capacity of neurons, I decided to investigate the effect of ASPP2 deletion on radial migration in cultured embryonic brain slices by doing *ex utero* electroporation and brain slice culture as previously described (Anda, 2013; Nelson, 2013). First, I tested whether pCAG-CRE-GFP plasmids can successfully induce CRE recombination and delete ASPP2 in NSCs in *Trp53bp2* $^{loxP/loxP}$ mice. *Trp53bp2* $^{loxP/loxP}$ pups at P0 were electroporated with pCAG-CRE-GFP plasmids or control pCAG-GFP plasmids into the dorsolateral SVZ of the lateral ventricle. Two days after electroporation, brains were cut into 200 μm-thick brain slices by a vibratome. GFP positive SVZ tissues were dissected out and collected under fluorescence microscopy. Example images of brain slices containing GFP^+ SVZ tissue electroporated with pCAG-GFP and pCAG-CRE-GFP plasmids were shown in **figure 4.3A**. It was notable that there were many GFP^+ cells with control GFP plasmids located in the RMS while rare GFP^+ cells with CRE-GFP plasmids were found in the RMS. This observation is in line with the results in Figure 3.3 showing that BrdU labelled neuroblasts failed to migrate through the RMS effectively. Collected SVZ tissues were submitted to RT-PCR by using primers targeting exon3 of *Trp53bp2*, which is flanked by two loxP sites. As shown by **figure 4.3B**, the mRNA level of *Trp53bp2* (exon3) decreased by approximately 87% in the SVZ tissue electroporated with CRE plasmids. There was still a notable amount of *Trp53bp2* (exon3) that can be detected in the CRE electroporated SVZ tissue, which is likely caused by GFP negative cells in the GFP positive SVZ tissues. This result supported that pCAG-CRE-GFP plasmids can successfully knockout ASPP2 in NSCs in *Trp53bp2* $^{loxP/loxP}$ mice.

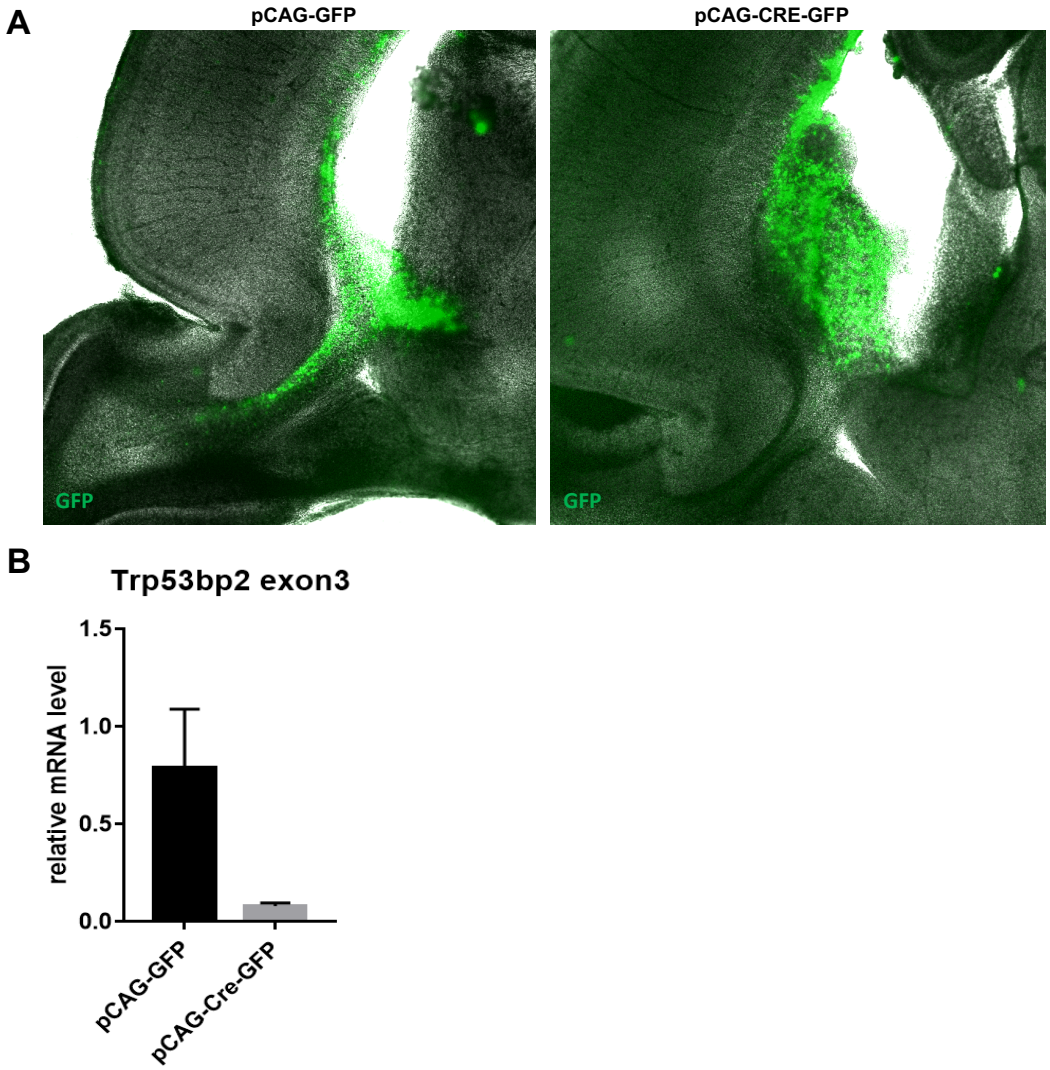


Figure 4. 3 pCAG-CRE-GFP plasmids successfully knockout ASPP2 in NSCs in *Trp53bp2* $^{loxP/loxP}$ mice.

(A) Example images of brain slices containing GFP positive SVZ tissue electroporated with pCAG-GFP and pCAG-CRE-GFP plasmids. Transmitted-light DIC channel and green channel were merged. (B) The relative expression level of *Trp53bp2*-exon3 evaluated by RT-PCR. Each group had two mice.

Next, I did *ex utero* electroporation and brain slice culture. The experiment workflow is depicted in **figure 4.4A**, *Trp53bp2* $^{f/f}$ embryos at E14.5 were dissected out and the neocortex was electroporated with pCAG-CRE-GFP plasmids to delete ASPP2 or with control pCAG-GFP plasmids. Then brains were cut into 300 μm-thick brain slices by a vibratome. Brain slices were cultured on membranes with 0.4 μm pore size in the brain slice culture medium for 48 hours. Then brain slices were fixed and cut into 30 μm-thick sections by frozen sectioning. The distribution of GFP positive cells was visualized by immunofluorescence staining. As shown in **figure 4.4B**, cells electroporated with control pCAG-GFP plasmids distributed across the entire thickness of the neocortex, with many neurons showing migratory morphology in the cortical plate (CP). However, fewer pCAG-CRE-GFP electroporated cells were found in the CP. Quantification of the proportion of GFP^+ cells in different layers of the neocortex confirmed that the pCAG-CRE-GFP group had a significantly lower proportion of GFP+ cells located in the CP but a higher proportion in the intermediate zone (IZ) comparing to the control group (**Figure 4.4C**). Brain slices electroporated with pCAG-CRE-GFP plasmids also showed slightly more GFP+ cells in VZ/SVZ (**Figure 4.4C**). These results suggest that ASPP2 deletion leads to inefficient radial migration.

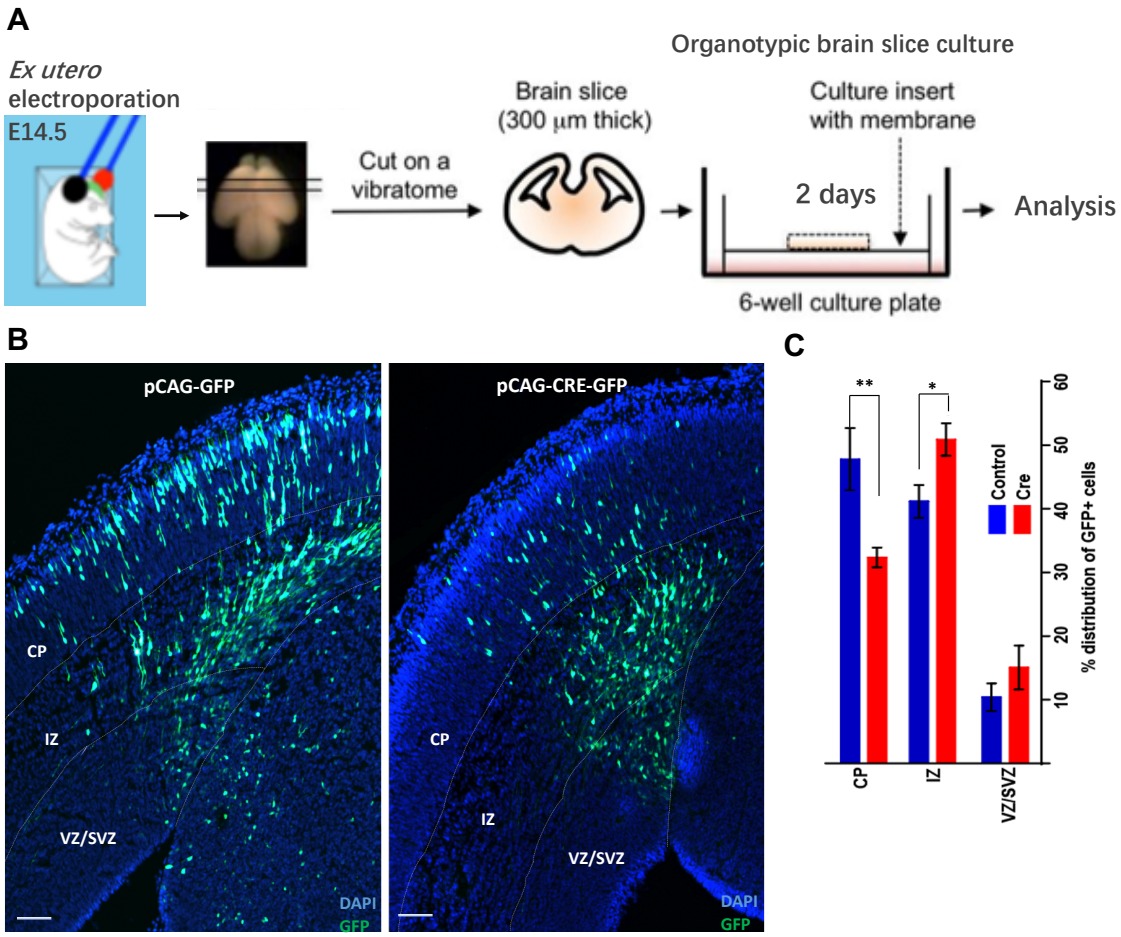


Figure 4. 4 ASPP2 deficiency leads to impaired radial migration.

(A) Experiment workflow of ex utero electroporation and brain slice culture. Trp53bp2 $^{f/f}$ embryos at E14.5 were dissected out and the neocortex was electroporated with pCAG-CRE-GFP plasmids or with control pCAG-GFP plasmids. Brains were cut into brain slices and cultured for 2 days before analysis. (B) Immunofluorescence staining of GFP on brains sliced electroporated with pCAG-CRE-GFP plasmids or with control pCAG-GFP plasmids. The cortex was divided into different layers. CP: cortical plate. SP: subplate. IZ: intermediate zone. VZ/SVZ: ventricular/subventricular zone. (C) Quantification of the percentage of GFP^+ cells in different layers. Each group contains 6 brain slices from 3 embryos. Data were presented as mean ± SEM. *p<0.05. **p<0.01.

4.3 ASPP2 does not affect the VZ lining and RGC scaffold.

Genetic animal models of PNH revealed that besides the migration capacity of newborn neurons, other cellular processes such as disruption of the integrity of ventricular zone (VZ) lining and the radial glial cell scaffold, as well as the proliferation of neural stem cells are also involved in developing PNH (Watrin et al., 2015).

It has been reported that *Aspp2-KO* disrupted the neuroepithelium at the ganglionic eminence as early as E13.5 in mixed C57/BL6-129/Sv genetic background (Sottocornola et al., 2010a). However, the ventricular zone lining of the neocortex was not disrupted in *Aspp2-KO* Balb/c embryos at E15.5, as indicated by β-catenin staining (**Figure 4.5A**). These results are consistent with *Aspp2-KO* C57/BL6 embryos exhibiting abnormal nodules at the apical surface of the neocortex while *Aspp2-KO* Balb/c embryos showed normal neocortex with a smooth ventricular surface, as shown in **figure 4.2**.

During the development of the cerebral cortex, newborn neurons in the VZ/SVZ migrate along the elongated apical process of radial glia cells (RGCs) into different layers of the neocortex. Disruption of the integrity of the radial processes of RGCs can also prevent neurons from migrating properly. To know whether ASPP2 can disrupt the scaffold provided by RGCs, I examined the effect of ASPP2 deletion on the integrity of the RGC scaffold. *Trp53bp2* $^{f/f}$ pups at P0 received electroporation of pCAG-CRE-GFP plasmids into the dorsal wall of the lateral ventricle to delete ASPP2 in the remaining RGCs. Pups in the control group were electroporated with control pCAG-GFP plasmids. Brains were harvested at P2. GFP staining revealed that both wild-type and ASPP2 deficient RGCs have radial processes properly spanning the entire thickness of the cerebral wall (**Figure 4.5B**),

which suggested that ASPP2 deficiency does not influence the maintenance of the RGC scaffolds in these conditions.

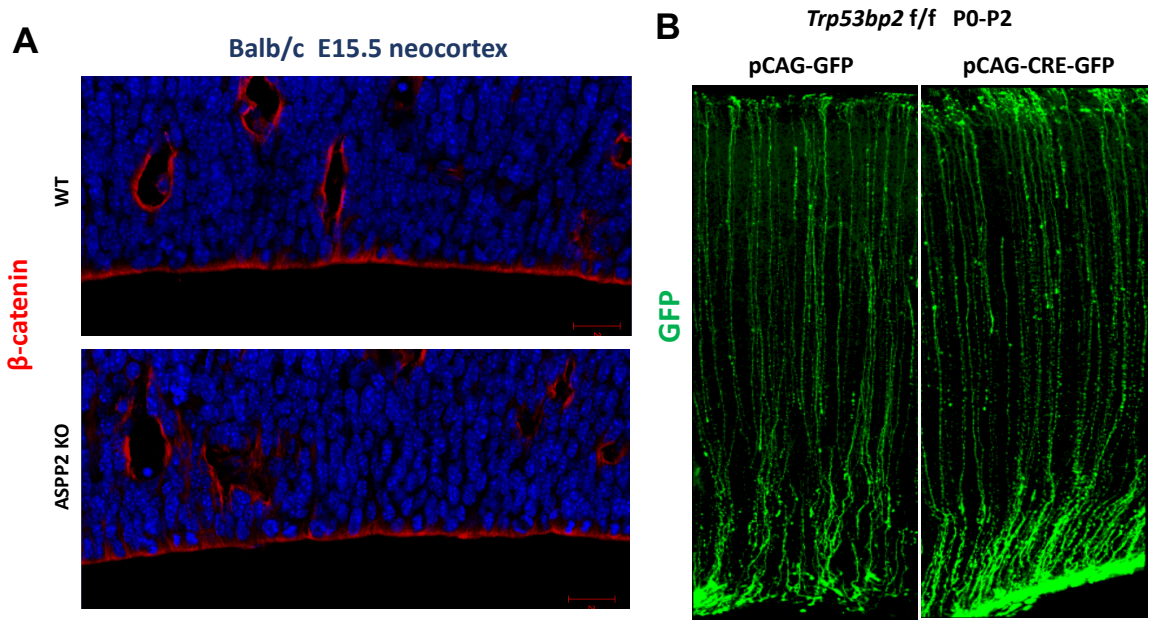


Figure 4. 5 ASPP2 doesn't affect VZ lining and RGC scaffold.

(A) β-catenin staining on neocortex form WT and KO embryos at E15.5 Scale bar = 20 μm; (B) Trp53bp2$^{f/f}$ pups at P0 received electroporation of CRE-GFP or control GFP plasmids into the dorsal wall of the lateral ventricle. Brains were harvested at P2. GFP staining revealed that both WT and *Aspp2-KO* RGCs have radial processes properly spanning the entire thickness of the neocortex.

4.4 The influence of ASPP2 on the proliferation of neural stem cells.

Our previous study has demonstrated that *Aspp2-KO* embryos showed increased proliferation and expanded neural progenitor pools in the embryonic developing brains (Sottocornola et al., 2010a). However, the underlying mechanism remained unclear.

Notch signalling is well known for its function in inhibiting differentiation, maintaining stemness, and promoting the proliferation of neural stem cells (Androutsellis-Theotokis et al., 2006; Hitoshi et al., 2002; Mizutani et al., 2007). Upon binding to Notch ligands such as Delta 1, the Notch intracellular domain (NICD) is released from the cell membrane through γ-secretase-mediated cleavage. NICD translocates into the nucleus and forms a transcriptional complex with Notch effectors such as RBPJ to induce transcription of target genes. The best-characterized Notch targets are the basic helix-loop-helix (bHLH) transcriptional repressors such as Hes1 and Hes5, which inhibit the expression of proneuronal genes (Iso et al., 2003). Preliminary unpublished data from our lab showed that ASPP2 selectively influences the transcription of Notch target gene Hey2 but not other gargets including *hes1* and *hey1* in mouse embryonic fibroblasts (MEFs). Also, ASPP2 was found to physically interact with RBPJ in MCF7 cells. Based on these data, I proposed the hypothesis that ASPP2 and RBPJ form heterodimers and alter the transcriptional activity of the NICD/RBPJ complex, thus regulates the proliferation of neural progenitors.

4.4.1 ASPP2 does not influence Notch signalling in neural stem cells *in vitro*.

To test this hypothesis, I first examined whether ASPP2 can influence Notch signalling in neural progenitor cells *in vitro*. Neural stem cells isolated from neurogenic regions can form free-floating spheres containing neural stem cells, neural progenitors, and differentiated neurons and glial cells in an environment lacking adherent substrates. The neurosphere culture system has been widely used for studying the proliferation of neural progenitor cells (Jensen & Parmar, 2006). In my experiment, Dll4, a ligand for Notch receptor, was used to induce Notch signaling. The expression of Notch target genes was measured by RT-PCR including canonical *hes1*, *hes5*, *hey1* and *hey2,* and noncanonical *nrarp, gli2, pax6,* and *otx2.* I found adding Dll4 in the culture medium was not able to induce activation of Notch signalling. Therefore, primary neurospheres derived from the neocortex of WT and *Aspp2-KO* embryos at E12.5 were disassociated into single cells and seeded into 6 well plates pre-coated with BSA or Dll4. mRNA levels of Notch target genes were detected 24 hours after seeding which allows cells to fully attach to the plate surface. As depicted in **Figure 4.6**, Dll4 treatment failed to significantly increase transcriptional levels of *hey1*, *hes1*, *pax6,* and *otx2.* Relative mRNA levels of *hes5*, *hey2*, *nrarp*, and *gli2* were increased by Dll4 treatment both in WT and *Aspp2-KO* cells. However, there was no significant difference between WT and *Aspp2-KO* cells. These results suggest that ASPP2 is not able to alter Notch signalling in neural stem cells/progenitor cells *in vitro*.

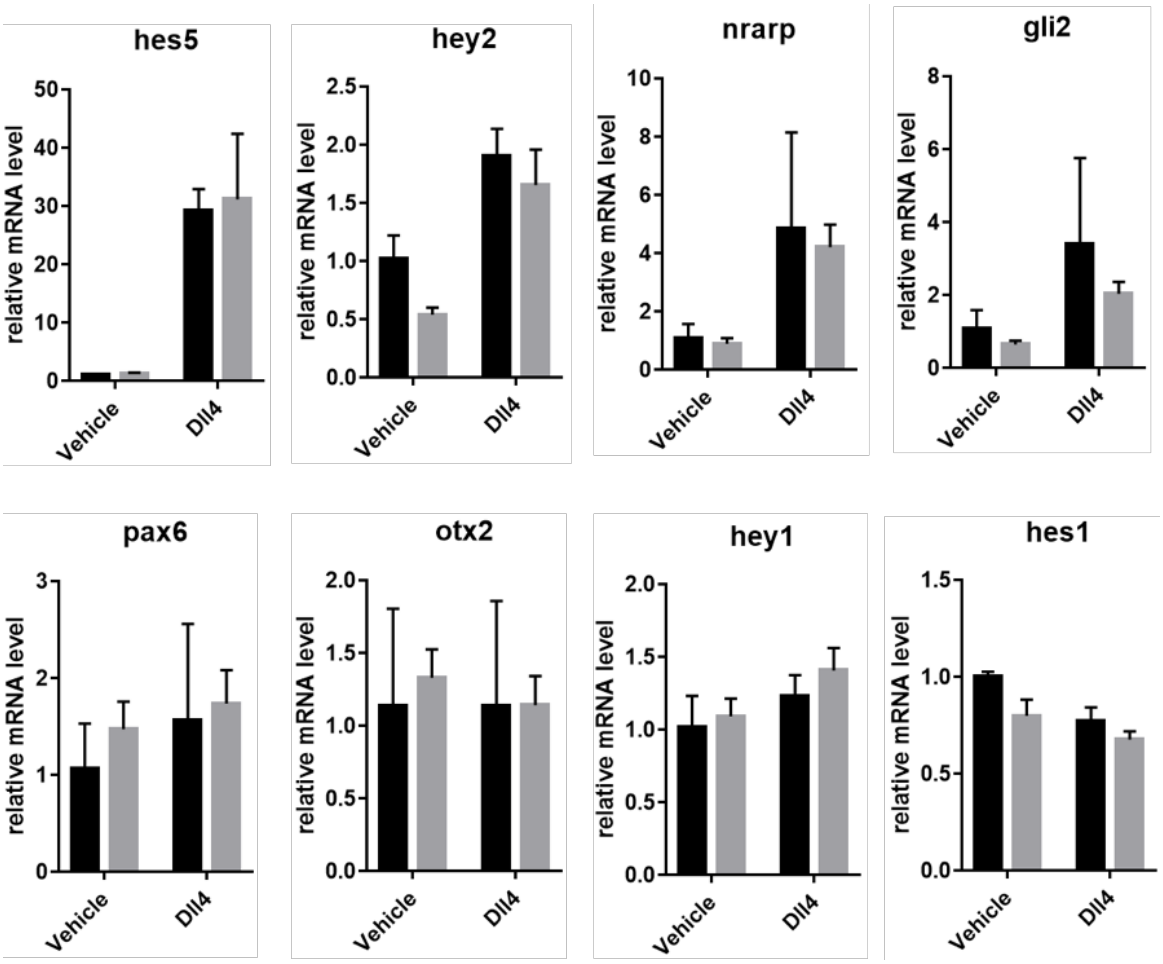


Figure 4. 6 mRNA levels of Notch target genes in WT and *Aspp2-KO* NSCs/NPCs with or without Dll4 treatment.

Relative expression levels of the indicated genes were evaluated by RT-qPCR. Each group has 3 cell lines derived from 3 WT embryos or 3 KO embryos. Data were presented as mean ± SEM.

4.4.2 ASPP2 does not influence NSC proliferation and neurosphere growth *in vitro*.

During the process of culturing WT and *Aspp2-KO* neurospheres, I noticed that *Aspp2-KO* neurospheres have similar sizes compared to WT neurospheres, suggesting that ASPP2 deficiency didn't result in increased proliferation of NSCs. This is unexpected because *Aspp2-KO* dramatically increased NSC proliferation and expanded the NSCs pool in vivo (Sottocornola et al., 2010a). Therefore, I carried out BrdU pulse-labelling and neurosphere growth assay to test whether ASPP2 can affect NSCs proliferation *in vitro*.

The experiment workflow is depicted in **figure 4.7A.** For the BrdU pulse experiment, WT and *Aspp2-KO* primary neurospheres were disassociated into single cells and seeded on coverslips. 48 hours after seeding, cells were pulsed with BrdU for 2 hours. Cells were fixed and stained for BrdU and DAPI (**Figure 4.7B**). The percentage of BrdU positive cells was quantified and it was comparable between WT cells and *Aspp2-KO* cells (**Figure 4.7C**). For neurosphere growth assay, secondary or tertiary neurospheres were disassociated into single cells and seeded into 6-well plates at a density of 300,000 cells per well. Three days later, bright field images were taken to analyze the sizes of neurospheres (**Figure 4.7D, F**). There was no significant difference between WT and *Aspp2-KO* secondary neurospheres (**Figure 4.7E**). *Aspp2-KO* tertiary neurospheres had a slightly smaller average size compared to that of WT tertiary neurospheres (**Figure 4.7G**). These results suggest that ASPP2 deficiency is not able to enhance the proliferation of NSCs *in vitro*.

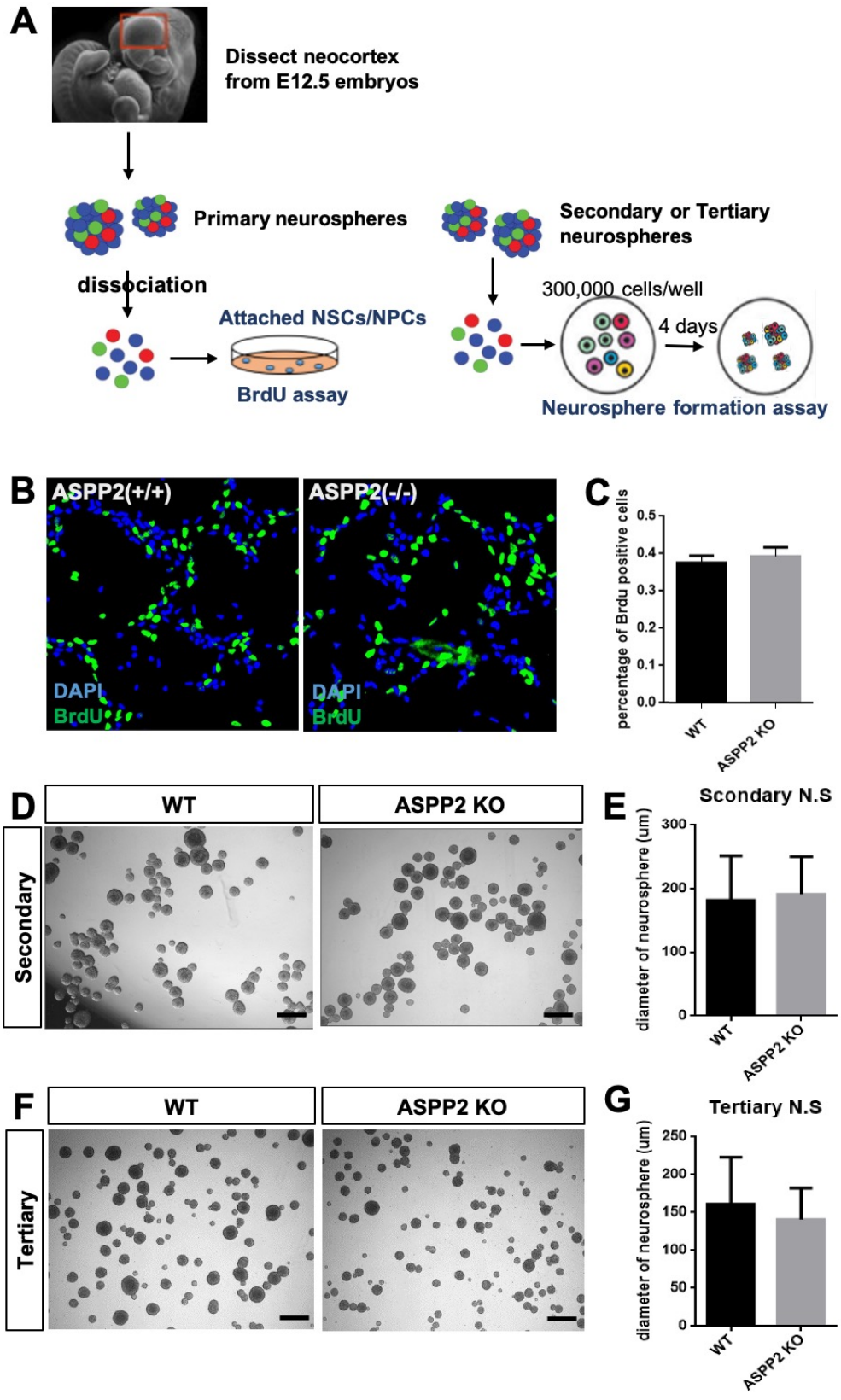


Figure 4. 7 ASPP2 does not influence NSCs proliferation and neurospheres growth in vitro.

(A) Experiment workflow of the BrdU pulse experiment and the neurospheres growth assay. (B) Immunofluorescence staining of BrdU in primary NSCs derived from E12.5 WT and *Aspp2-KO* neocortex. Nuclei were counterstained with DAPI. (C) Quantification of the percentage of BrdU positive cells. Each group has 3 cell lines derived from 3 WT embryos or 3 KO embryos. For each cell line, 6 images were used for quantification. (WT: n=18; KO: n=18.) (D) Brightfield images of secondary WT and KO neurospheres. Scale bar=500um. (E) Quantification of the diameter of secondary neurospheres. Each group has 3 cell lines derived from 3 embryos. 496 neurospheres and 525 neurospheres were quantified in the WT group and *Aspp2-KO* group, respectively. Data were presented as mean ± SD. (F) Brightfield images of tertiary WT and KO neurospheres. Scale bar=500um. (G) Quantification of the diameter of tertiary neurospheres. Each group has 3 cell lines derived from 3 embryos. 478 neurospheres and 451 neurospheres were quantified in the WT and *Aspp2-KO* group, respectively. Data were presented as mean ± SD.

4.4.3 ASPP2 deficiency leads to the randomization of the spindle orientation of RGCs *in vivo*.

The inconsistency between the *in vivo* and *in vitro* phenotypes caused by ASPP2 deficiency suggests that the *in vivo* microenvironment such as the cytoarchitecture of the neuroepithelium plays an essential role in the excessive proliferation of NSCs/NPCs in *Aspp2-KO* developing brains.

As mentioned in the introduction, the dynamic switch between asymmetric and symmetric cell division modes of radial glial cells (RGCs) is critical for maintaining the NSCs pool while generating the proper number of neurons. Spindle orientation seems to be a critical initial factor in determining the division mode of RGCs. The symmetric planar division is achieved by the localization of the LGN complex at the two lateral sides of the dividing cell where the LGN complex associates with both spindle poles (Peyre et al., 2011). The Par complex is responsible for the correct localization of the LGN complex by the exclusion of the LGN complex from the apical domain (Hao et al., 2010). Without a functional exclusion mechanism, astral microtubules would associate with the LGN complex over the entire cell cortex, which leads to the randomization of spindle pole orientation. Both Par3 knockdown and ectopic Par3 expression impair the asymmetric division of RGCs (Bultje et al., 2009). Interestingly, their effects on the outcome of symmetric division are different. Par3 knockdown promotes the production of neurons while ectopic expression of Par3 increases the generation of RGCs. ASPP2 can interact with PAR3 at primordial cell-cell contacts before the recruitment of aPKC-PAR-6 therefore is required for the development of the apical domain (Cong et al., 2010; Sottocornola et al., 2010a). A recent study has demonstrated that ASPP2 can recruit protein phosphatase1 (PP1) to dephosphorylate PAR3

thus facilitating rapid junctional localization of PAR3 (Yamashita et al., 2020). Therefore, it is possible that ASPP2 can also regulate Par3 localization and spindle orientation during the RGC division, thus influence neurogenesis.

To understand whether ASPP2 influences the spindle orientation of RGCs, the cleavage plane orientations of dividing RGCs in the neocortex of E14.5 WT and *Aspp2-KO* embryos were measured. As shown in **figure 4.8A**, all the RGCs in anaphase located at the ventricular surface of the neocortex were imaged, then the angle of the cleavage plane relative to the ventricular surface was calculated. **Figure 4.8B** shows some examples of RGCs that have different angles of the cleavage plane. By examining data from three pairs of WT and *Aspp2-KO* embryos, I found ASPP2 deficiency significantly altered the distribution pattern of cleavage plane angles (**Figure 4.8C).** In the WT neocortex, the majority of anaphase RGCs displayed perpendicular cleavage planes with an average angle of 72.9^{o} ±22.6^{o}, which is consistent with previously reported data: 70.15^{o} ±18.3^{o} (Yingling et al., 2008). However, in *Aspp2-KO* embryos, cleavage planes were more randomized, and more RGCs displayed horizontal cleavage planes (average angle: 55.1^{o} ±27.7^{o}). I classified cells with the angle of cleavage plane lower than 60^{o} into asymmetric division and the rest of the cells into symmetric division. The percentage of asymmetric division in the WT group is 18.7%±9.2% while that in the *Aspp2-KO* group increased to 46.9%±6.5% (**Figure 4.8D**). These results suggest that ASPP2 is necessary for proper regulation of the spindle orientation during RGC divisions and ASPP2 deficiency leads to increased asymmetric division of RGCs.

The outcome of the RGC asymmetric division is dependent on the phase of neurogenesis. At the beginning of neurogenesis, an RGC undergoes self-renewal symmetric division or undergoes asymmetric division to produce one RGC and one neuron. At the peak of neurogenesis (E14.5), an RGC can either undergo symmetric division to generate two RGCs or divides asymmetrically to produce one RGC and one intermediate progenitor cell (IPC). IPCs are transiently amplifying progenitors with high expression of the transcription factor Tbr2. Should ASPP2 deficiency leads to increased asymmetric division of RGCs, the number of IPCs would be increased with the cost of consuming RGCs. Indeed, E14.5 *Aspp2-KO* neocortex exhibited fewer Pax^+ RGCs and more $Tbr2^+$ IPCs (**Figure 4.9**). **[Figure 4.8A is adapted from a previously published paper (Sottocornola et al., 2010) from our lab. The experiment was carried out and data was collected by Roberta Sottocornola.]**

In conclusion, these results suggest that ASPP2 is necessary for maintaining proper spindle orientation in dividing RGCs, and randomization of spindle orientation caused by ASPP2 deficiency may be responsible for the expanded neural progenitor cells in *Aspp2-KO* developing brains.

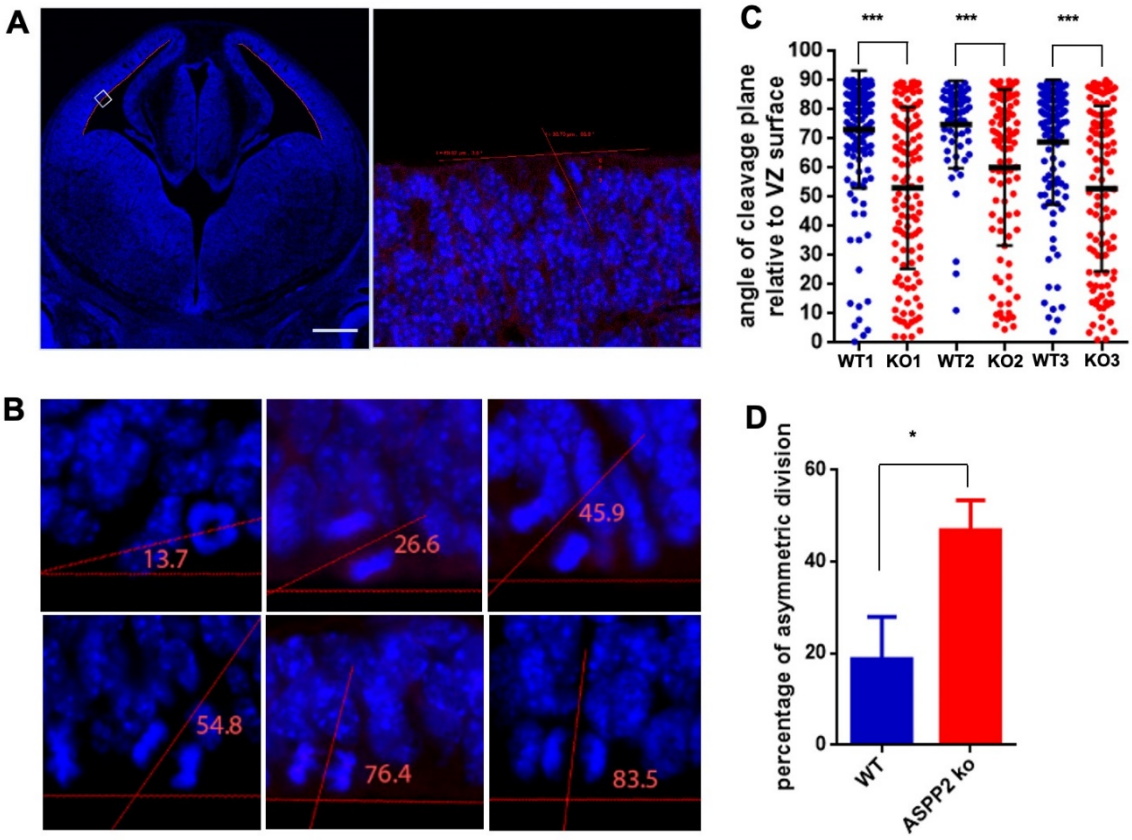
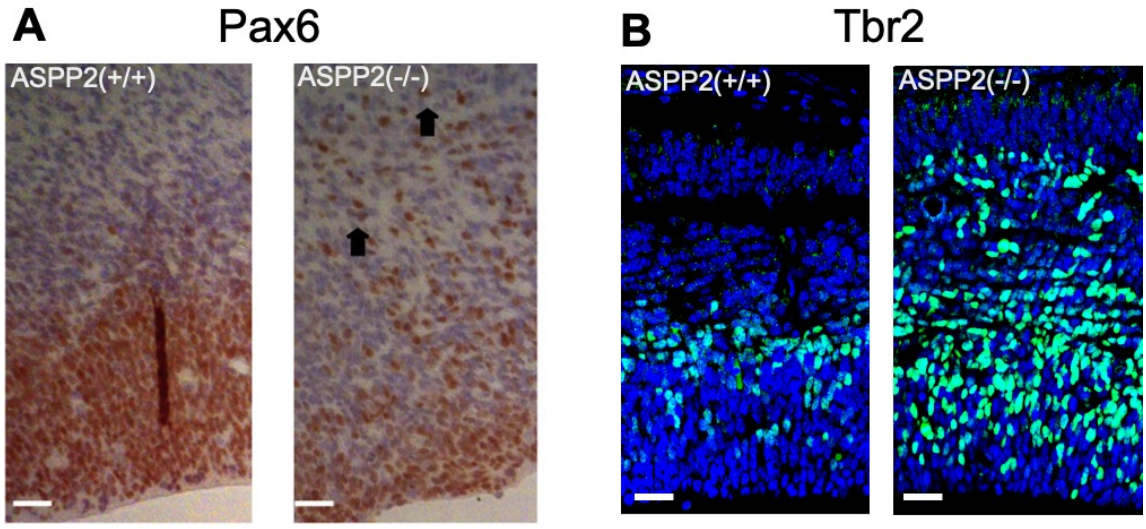


Figure 4. 8 ASPP2 deficiency leads to the randomization of spindle orientation in dividing RGCs in E14.5 neocortex.

(A) DAPI staining of coronal brain sections from E14.5 embryos. Red lines indicate the apical surface of the neocortex. The red box indicates an anaphase RGC. The enlarged view of the red box shows how the angle of the cleavage plane relative to the ventricular surface is calculated. (B) Some examples of RGCs having different angles of the cleavage plane. (C) Distribution of angels of cleavage planes of RGCs in each embryo. 3 pairs of WT and *Aspp2-KO* embryos were quantified. Approximately, 100-150 anaphase RGCs were analyzed in each embryo. Data are presented as mean ± SD. ***p<0.001. (D) Quantification of the percentage of asymmetric division. Each group has 3 embryos (n=3). Data are presented as mean ± SD. *p<0.05.



Figrue 4. 9 *Aspp2-KO* neocortex exhibited fewer Pax^{+} RGCs and more Tbr2^{+} IPCs.

(A) IHC staining of radial glial cell marker Pax6 on neocortex of WT and *Aspp2-KO* embryos at E14.5. **Data adapted from our previous published paper** (Sottocornola et al., 2010a)**.** (B) IF staining of intermediate progenitor cells marker Tbr2 on neocortex of WT and *Aspp2-KO* embryos at E14.5. Scale bar= 10μm.

4.5 Summary

In this chapter, I found that *Aspp2-KO* mice developed abnormal nodules composed of mature neurons at the dorsal wall of the lateral ventricle, which resembled periventricular nodular heterotopia (PNH). By doing *ex utero* electroporation of pCAG-CRE-GFP plasmids into the dorsolateral SVZ of *Trp53bp2* $^{loxP/loxP}$ mice and subsequent brain slice culture, I examined the effect of *Aspp2-KO* on radial migration in the neocortex. I found that *Aspp2-KO* led to a decreased number of GFP^{+} cells in the cortical plate and accumulation of GFP^{+} cells in the intermediate zone, suggesting ASPP2 is important for proper radial migration. In addition to neuronal migration, other cellular processes including the proliferation of neural stem cells, the integrity of the ventricular zone lining and the radial glial cell (RGC) processes are also involved in developing PNH (Watrin et

al., 2015). Preliminary data showed that loss of ASPP2 did not significantly disrupt the neuroepithelium lining of the neocortex at E15.5. However, whether the loss of ASPP2 could disrupt the neuroepithelium lining at later developmental stages needs further investigation. Deletion of ASPP2 at the dorsal wall of the lateral ventricle by *in vivo* electroporation failed to disrupt the RGC scaffold at the stage of P0-P2. Again, whether the loss of ASPP2 could disrupt the RGC scaffold at embryonic developmental stages remains to be examined in the future. *Aspp2-KO* embryonic brains showed increased proliferation and an expanded pool of neural progenitor cells (Sottocornola et al., 2010a). However, the underlying mechanism remained unclear. Preliminary unpublished data suggested that ASPP2 may influence NSC proliferation through regulating Notch signalling. I found that *Aspp2-KO* was not able to affect gene expressions of Notch targets in cultured NSCs. Surprisingly, I found ASPP2 deficiency failed to influence NSC proliferation *in vitro* according to the results of BrdU pulse experiments in cultured NSCs and neurosphere formation assay. However, ASPP2 deficiency resulted in randomization of the spindle orientation in dividing NSCs in the ventricular zone (VZ) of the neocortex, which is known to cause unregulated proliferation of NSCs. In conclusion, the PNH phenotype caused by ASPP2 deficiency could be a combined result of increased NSC proliferation and impaired neuronal migration.

Chapter 5: ASPP2 regulates actin cytoskeleton and cell migration through Rho-ROCK signalling.

In chapter 3 and chapter 4, I demonstrated that ASPP2 deficiency impairs tangential chain migration of neuroblasts in the rostral migratory stream (RMS) and radial migration in the neocortex leading to diminished olfactory bulbs and periventricular nodular heterotopia, respectively. However, it remains unknown how ASPP2 regulates neuronal migration.

As mentioned in the introduction, genetic analysis of the patients with periventricular heterotopia highlighted the essential roles of the actin cytoskeleton in developing neuronal migration disorders. Indeed, dynamic reorganization of the actin cytoskeleton is important for all three steps during neuronal migration including the extension of the leading process, nuclear movement and soma translocation, and retraction of the trailing process. The growth cone-like structure at the tip of the leading process actively extends lamellipodia and filopodia, which is driven by Rac1 and CDC42 mediated actin reorganization (Guan et al., 2007; Ono et al., 1997; Polleux et al., 2002). Actomyosin stress fibre is enriched in the leading process (Rivas & Hatten, 1995; Solecki et al., 2009; Trivedi et al., 2017). The dynamic of the growth cone-like structure and the F-actin flow along the leading process driven by actomyosin activity are necessary for generating traction force for nucleus movement and soma translocation (He et al., 2010; J. Jiang et al., 2015; Solecki et al., 2009; Trivedi et al., 2017; Umeshima et al., 2019). Actomyosin contractility also functions at the rear of the nucleus to push the cell body forward during retraction of the trailing tail (Bellion, 2005; Martini & Valdeolmillos, 2010; Schaar & McConnell, 2005).

Apart from the well-known function of binding p53 and selectively enhancing its DNA binding and transcriptional activity on proapoptotic genes in the nucleus, ASPP2 also has many important functions at the cell membrane and in the cytoplasm. 1). At the cell membrane, ASPP2 interacts with cell polarity protein PAR3 at primordial cell-cell contacts before the recruitment of aPKC-PAR-6, therefore, is required for the development of the apical domain (Cong et al., 2010; Sottocornola et al., 2010a). The PAR complex has been reported to reciprocally interact with RhoA-ROCK, which is one of the major signalling pathways regulating actin organization. PAR6/aPKC can activate p190A RhoGAP thus downregulate RhoA activity (H. Zhang & Macara, 2008). PAR3/aPKC can phosphorylate Rho-associated kinase (ROCK) thus suppress its junctional localization (Ishiuchi & Takeichi, 2011). In return, RhoA-ROCK mediated Thr833 phosphorylation of PAR3 leads to disassociation of the PAR complex (Nakayama et al., 2008). It remains unknown whether ASPP2 is involved in such reciprocal interaction. Besides, ASPP2 can also bind to Ras-GTP at the plasma membrane and stimulate Raf/MEK/ERK signalling cascade (Posada et al., 2016; Y Wang et al., 2013). It is possible that ASPP2 can bind to and regulate RhoA-GTP in a similar way. Therefore, ASPP2 is a potential regulator of RhoA-ROCK signalling. 2). In the cytoplasm, ASPP2 functions as an adaptor for protein phosphatase1 (PP1) and facilitates the dephosphorylation of ASPP2/PP1 targets (Bertran et al., 2019; C.-Y. Liu et al., 2011; Royer et al., 2014). PP1 has been shown to be enriched in the actin-rich cytoskeletal structure known as postsynaptic density in neurons (Terry-Lorenzo et al., 2000). Neurabin I, a neuronal actin-binding protein, targets PP1 activity to actin-rich structures to control the rearrangement of filopodia and the stress fibre network (Oliver et al., 2002). It is possible that ASPP2 can regulate actin network through PP1.

As a regulator of the PAR complex at the cell membrane and an adaptor of PP1 in the cytoplasm, ASPP2 may be a potential regulator of the actin cytoskeleton, which is a hypothesis that has never been addressed before. In this chapter, I will show results supporting that ASPP2 promotes cell migration through regulating RhoA-ROCK mediated reorganization of the actin cytoskeleton. Results of phosphoproteomic analysis using WT and *ASPP2-KO U2OS* cells will be presented at first, followed by studies of examining the effect of ASPP2 on actomyosin stress fibre formation, cell migration, and RhoA-ROCK signalling in U2OS cells.

5.1 Phosphoproteomic analysis reveals ASPP2 may regulate cytoskeleton through Rho-ROCK signalling.

To obtain a global picture of signalling pathways influenced by ASPP2/PP1, Dr Kundan Sharma, a former postdoc in our group, and James Hokfung Chan, a PhD student in our lab, carried out a deep-scale label-free phosphoproteomic mass spectrometry using WT and *ASPP2-KO U2OS* cells, which are human bone osteosarcoma epithelial cells. *ASPP2-KO U2OS* cell line was generated by James using the CRISPR-Cas9 system targeting exon 6 of *Tp53bp2* to cause frameshift and nonsense-mediated mRNA decay (NMD). The complete remove of ASPP2 protein was validated by Western Blot using two ASPP2 antibodies recognizing the N-terminal and the C-terminal, respectively.

U2OS cells were chosen for studying the potential effects of ASPP2 on actin cytoskeleton for the following reasons: (1) In U2OS cells, ASPP2 nicely locates at the inner plasma membrane where the initiation of Rho-ROCK signalling and actin reorganization takes

place. (2) U2OS cells show robust actin stress fibre formation in response to stimuli. (3) U2OS cells can easily undergo genetic manipulation.

As depicted in the experimental workflow (**Figure 5.1A**), proteins were extracted from WT and *ASPP2-KO U2OS* cells and digested by Trypsin. 95% of the digested peptides were submitted to TiO_2 affinity enrichment to enrich phosphopeptides. The 5% non-phosphoenriched fraction was used to determine expression levels of proteins in WT and *Aspp2-KO* cells. Only those with relatively constant expression across two conditions were included for subsequent analysis. Three stringent criteria were used to determine phosphosites that showed significant differences between WT and *Aspp2-KO* conditions, which were termed as binary phosphosites or ASPP2-sensitive phosphosites. First, such a phosphosite should be detected in only one but not the other condition; second, at least one phosphopeptide covering the said phosphosite should be observed in the same condition; third, at least one phosphosite should be observed in both conditions on the same protein. As shown in **Figure 5.1B**, 3,477 proteins were found to have relatively constant expression levels across two conditions. Among these proteins, 23,362 and 21,121 phosphopeptides were found in in the WT and *Aspp2-KO* phosphoenriched fractions, respectively. Using Andromeda score > 40 and localization probability > 0.75 as thresholds, 11,962 and 12,134 high-confidence phosphosites were identified in WT and *Aspp2-KO* conditions respectively. After screening with the three stringent criteria, 132 binary phosphosites, corresponding to 103 proteins, were identified in WT condition while 145 binary phosphosites, corresponding to 107 proteins, were observed in *Aspp2-KO* condition (**Figure 5.1B**).

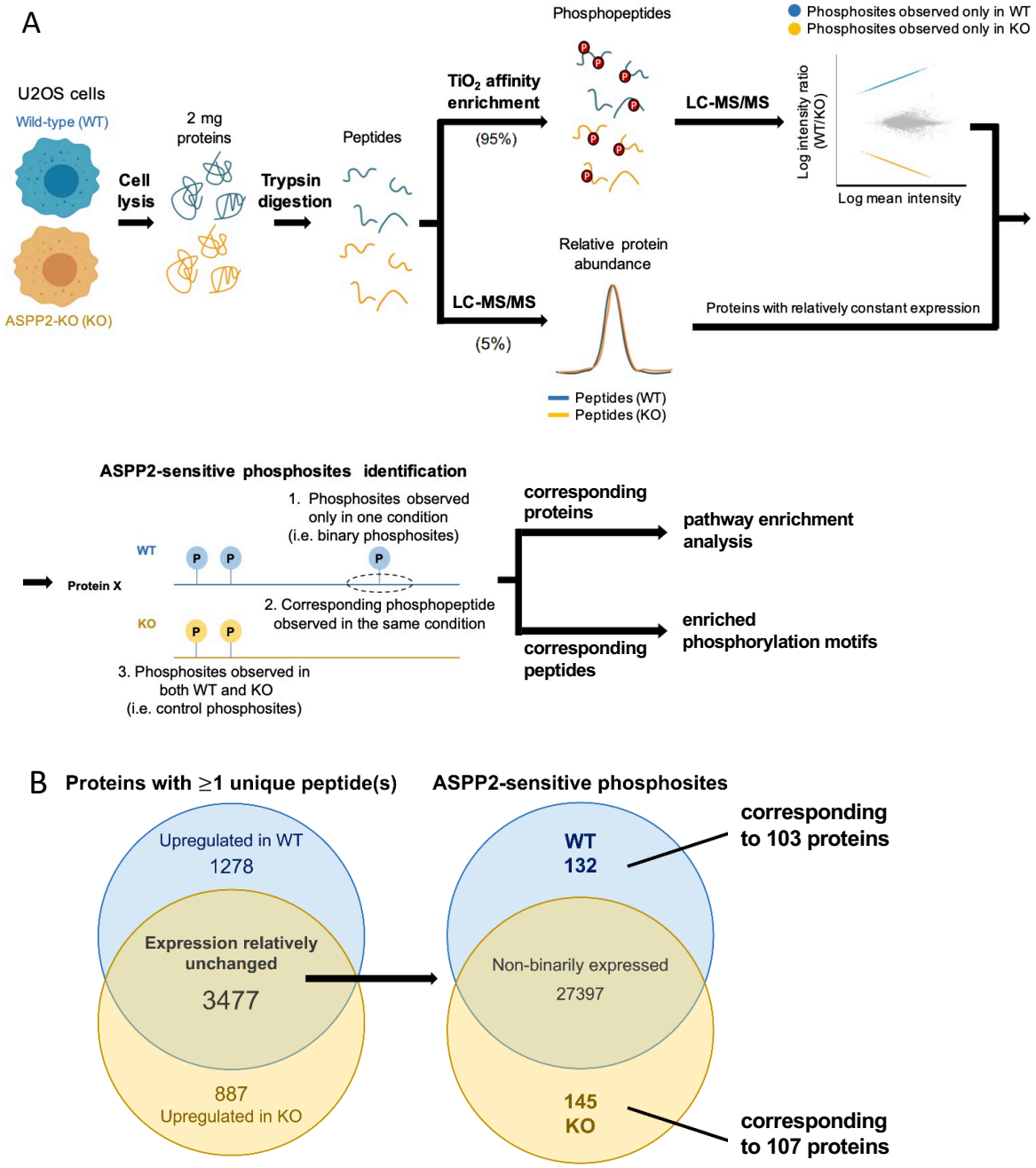
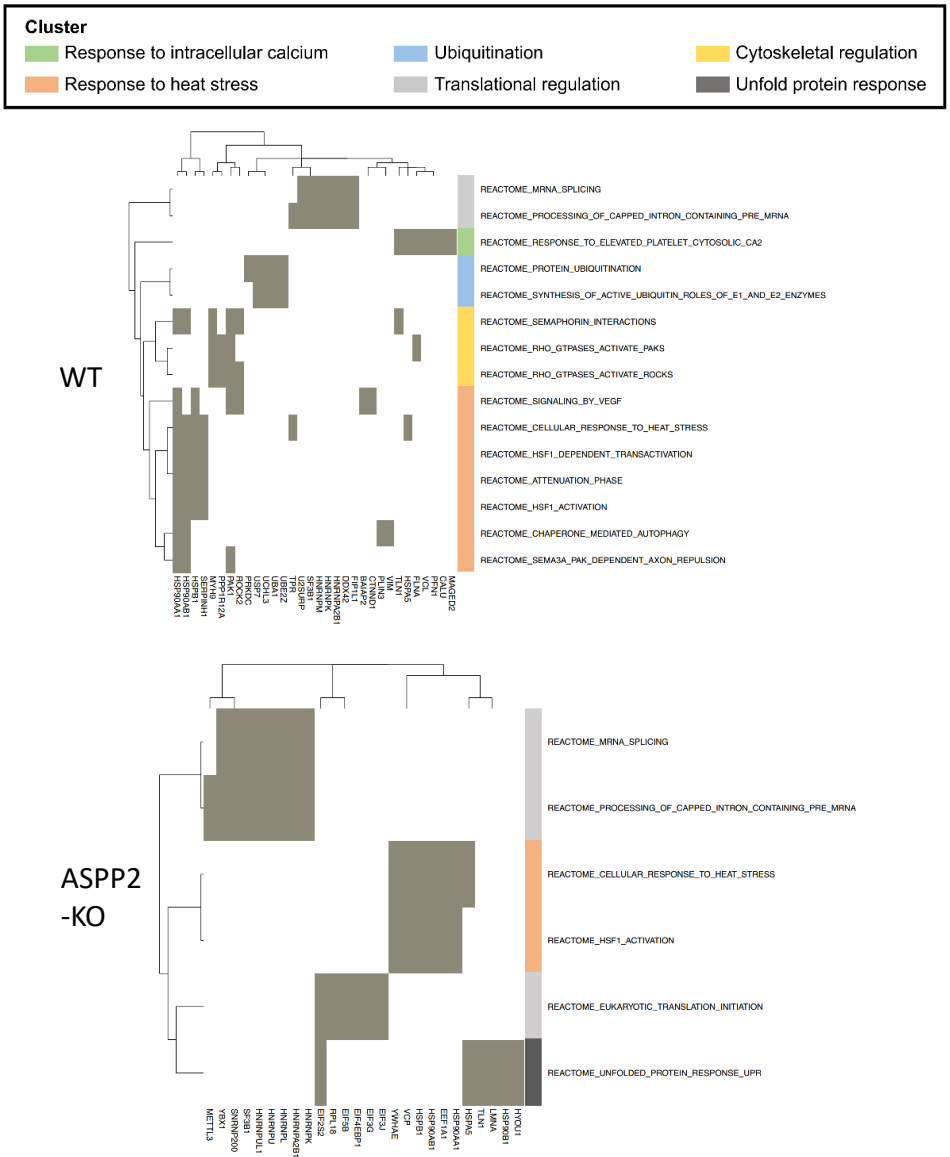


Figure 5. 1 Overview of the mass spectrometry-based phosphoproteomic analysis using WT and *ASPP2-KO U2OS* cells.

(A) Schematic illustrating the workflow of mass spectrometry-based phosphoproteomic analysis. (B) Overview of the proteome, phosphoproteome, and ASPP2-sensitive candidates identified in WT and *ASPP2-KO U2OS* cells.

The binary phosphosites containing proteins were used for pathway enrichment analysis. Pathway enrichment analysis on those proteins with ASPP2-sensitive phosphosites found 15 pathways and 6 pathways from the REACTOME Pathway Database enriched in WT and *Aspp2-KO* conditions, respectively (**Figure 5.2A)**. Enriched pathways were further clustered based on their biological functions. Interestingly, clusters related to cytoskeletal regulation, which containing Rho pathways such as Rho-ROCKs and Rho-PKAs, were exclusively observed in WT condition but not in *Aspp2-KO* condition (**Figure 5.2A)**, which suggests that ASPP2 may be involved in the phosphorylation of these proteins. Upon closer inspection of the ASPP2-sensitive phosphoproteins in cytoskeletal regulation-related clusters, I found many important regulators of actomyosin activity (**Figure 5.2B**): Myosin Phosphatase Target Subunit 1 (MYPT1) encoded by *PPP1R12A* recruits protein phosphatase 1 (PP1) to dephosphorylate myosin light chain 2 (MLC2) (Go Totsukawa et al., 2004); ROCK2, one of the major Rho effectors, activates myosin activity directly by phosphorylating the regulatory Ser19 on myosin light chain 2 (MLC2) and indirectly by the phosphorylation and inactivation of the myosin-associated phosphatase PP1δ–MYPT1 complex (M. A. Conti & Adelstein, 2008; Vicente-Manzanares et al., 2009); PAK1 is a serine/threonine kinase downstream of Rho GTPases Rac and Cdc42 and can activate or inhibit myosin activity in a context-dependent manner (Chu et al., 2013); MYH9 represents the heavy chain of non-muscle myosin IIa, which generates muscle contraction (Pecci et al., 2018); Filamin A encoded by *FLNA* is a major crosslinking protein responsible for actin filament bundling, thus is important for effective actomyosin contractility (Stossel et al., 2001).

A



B **List of proteins with ASPP2-sensitive phosphosites involved in cytoskeletal regulation.**

Gene Name	Protein Name	Phosphosite	Phosphorylation status	
			WT	KO
Filamin A	FLNA	S2026	✓	×
Heat Shock Protein HSP 90-alpha	HSP90AA1	S453, S468, S470, T645	✓	×
Heat Shock Protein HSP 90-beta	HSP90AB1	S470	✓	×
Myosin-9	MYH9	S1111	✓	×
Serine/threonine-protein kinase PAK1	PAK1	S220, T230	✓	×
Myosin Phosphatase-Targeting Subunit 1	PPP1R12A	T853	✓	×
Rho-associated protein kinase 2	ROCK2	S1137	✓	×
Talin 1	TLN1	S1898	✓	×

Figure 5. 2 Pathway enrichment analysis reveals ASPP2 is involved in Rho signalling- mediated cytoskeleton regulation.

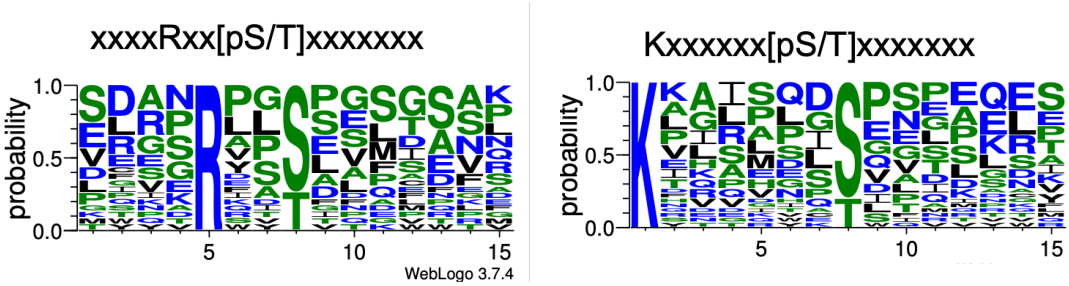
(A) Clustered heatmaps of REACTOME pathways enriched in proteins containing ASPP2-sensitive phosphosites observed in WT and *Aspp2-KO* cells, respectively. (B) List of proteins with ASPP2-sensitive phosphosites involved in cytoskeletal regulation.

The phosphopeptides with binary phosphosites were used for identifying enriched phosphorylation motifs. A search for enriched phosphorylation motifs in those 277 ASPP2-sensitive phosphopeptides using a window of 15 amino acids surrounding the phosphosites found two overrepresented phosphorylation motifs: xxxxRxx[pS/T]xxxxxxx and Kxxxxxx[pS/T]xxxxxxx (**Figure 5.3A**). While there is no report about the biological function of the Kxxxxxx[pS/T]xxxxxxx motif, the RXXS_T motif represents a consensus motif identified in ROCK substrate proteins (Bradley & Beltrao, 2019; Yoshizaki & Okuda, 2014, 2015). A list of proteins with ASPP2-sensitive phosphosites containing the RXXS_T motif can be found in **Figure 5.3B**. Although for most of these phosphosites their biological functions remain unknown, it is well-known that phosphorylation of threonine-853 of MYPT1 inhibits the phosphatase activity of the myosin light chain phosphatase (Khromov et al., 2009; Murányi et al., 2005; Velasco et al., 2002).

In conclusion, these results suggest that ASPP2 may regulate actin cytoskeleton through Rho-ROCK signalling.

(**Acknowledgement: *ASPP2-KO U2OS* cells were generated by James Hokfung Chan; Kundan Sharma and James Hokfung Chan did the phosphoproteomic mass spectrometry experiments.**)

A **Enriched phosphorylation motifs**



B **List of ASPP2-sensitive phosphoproteins containing the RXXS_T motif**

Protein Name	Gene Symbol	Phosphosite	Phosphorylation status	
			WT	KO
Activity Dependent Neuroprotector Homeobox	ADNP	S289	✓	×
Heterogeneous Nuclear Ribonucleoprotein M	HNRNPM	S204	✓	×
HECT, UBA And WWE Domain Containing E3 Ubiquitin Protein Ligase 1	HUWE1	S2887	✓	×
Lamin B2	LMNB2	S419	✓	×
Nucleosome Assembly Protein 1 Like 1	NAP1L1	T39	✓	×
Myosin Phosphatase-Targeting Subunit 1	PPP1R12A	T853	✓	×
Splicing Factor 3b Subunit 1	SF3B1	S400	✓	×
Talin 1	TLN1	S1898	✓	×
Adenylosuccinate Lyase	ADSL	S23	×	✓
Cytoplasmic Linker Associated Protein 1	CLASP1	S23, S254	×	✓
COPI Coat Complex Subunit Alpha	COPA	T591	×	✓
Family With Sequence Similarity 91 Member A1	FAM91A1	S828	×	✓
Filamin C	FLNC	S2200	×	✓
HECT And RLD Domain Containing E3 Ubiquitin Protein Ligase	HERC1	S1328	×	✓
Heterogeneous Nuclear Ribonucleoprotein L	HNRNPL	T487	×	✓
Nuclear Autoantigenic Sperm Protein	NASP	T700	×	✓
Reticulocalbin 1	RCN1	S43	×	✓
RuvB Like AAA ATPase 2	RUVBL2	S431	×	✓
Thymopoietin	TMPO	T74	×	✓
Tankyrase 1 Binding Protein 1	TNKS1BP1	S882, S983	×	✓

Figure 5. 3 Phosphorylation motif analysis identifies prominent ASPP2 regulating phosphoproteins as ROCK substrates.

(A) 277 candidate ASPP2-sensitive phosphosites were identified and used as an input for the in-silico motif analyses tool motif-X (Chou MF, 2011) to assess enriched motif patterns. Two candidate consensus motifs, identified as significantly enriched, are represented in individual motif logos. (B) List of proteins with ASPP2-sensitive phosphosites enriched in the RXXS/T motif.

5.2 ASPP2 deficiency impairs actomyosin stress fibre formation.

To test the hypothesis that ASPP2 is a potential regulator of the actin cytoskeleton, I examined the influence of ASPP2 deletion on actomyosin stress fibre formation by using WT and *ASPP2-KO U2OS* cells. Since RhoA is the major regulator of actomyosin formation, a specific Rho activator was used to induce robust stress fibre formation. This Rho activator is based on the catalytic domain of the bacterial cytotoxic necrotizing factor (CNF) toxin, which is covalently attached to a proprietary cell-penetrating moiety. It enters the cell and activates Rho GTPase isoforms, including RhoA, B, and C, by deamidating glutamine-63, which blocks GTPase activity resulting in constitutively active Rho (Schmidt et al., 1997). In order to make sure that WT and *Aspp2-KO* cells were under the exact same conditions, WT and *Aspp2-KO* cells were mixed and seeded in the same well. Cells were serum-starved for 12 hours then treated with Rho activator for 3 hours. Actomyosin stress fibre formation was indicated by immunofluorescence staining of phalloidin, which is a bicyclic peptide binding to actin filaments. As shown by **Figure 5.4A**, WT and *Aspp2-KO* cells can be distinguished by ASPP2 staining. Rho activator induced robust formation of thick actomyosin stress fibre in ASPP positive cells while ASPP2 negative cells showed less stress fibre in the cytoplasm. To quantify the degree of stress fibre formation, fluorescent intensities of phalloidin staining in the cytoplasm beneath the nucleus area were measured by ImageJ. Comparing to WT cells, *Aspp2-KO* cells had weaker fluorescent intensities of phalloidin both at the resting status and upon Rho stimulation (**Figure 5.4B**). These results suggest that ASPP2 is a positive regulator of Rho mediated actomyosin stress fibre assembly.

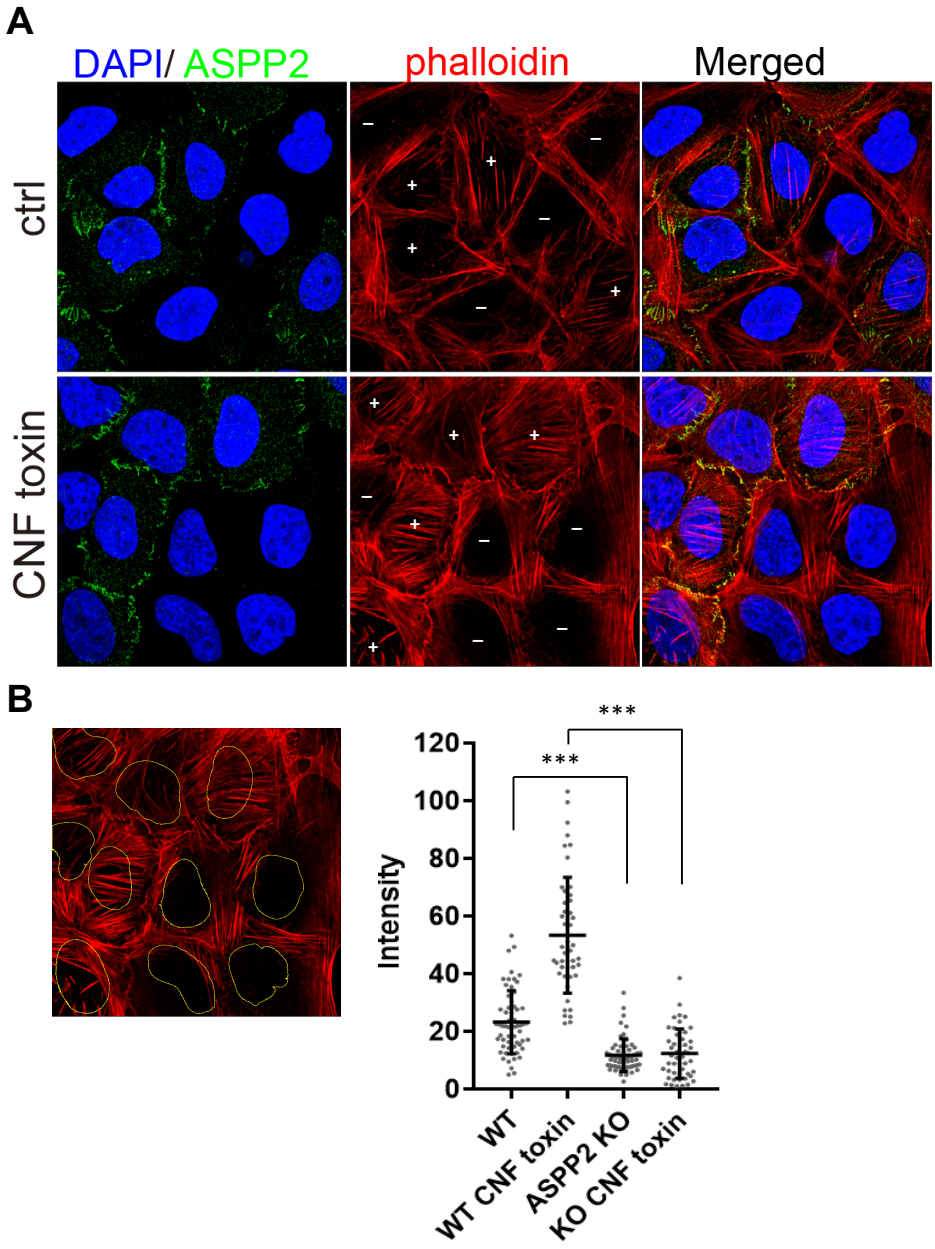


Figure 5. 4 ASPP2 deficiency impaired Rho activator induced actomyosin stress fibre formation.

(A) Mixed WT and *ASPP2-KO U2OS* cells were treated with vehicle or Rho activator (1ug/ml) for 3 hours before submitted to IF staining. WT and KO cells distinguished by ASPP2 staining were labelled with + and -, respectively. F-actin was showed by phalloidin staining; (B) Quantification of the intensity of phalloidin immunofluorescent signal beneath the nucleus area. Each group has around 50 cells for quantification. Data were presented as mean ± SD. ***p<0.001.

5.3 ASPP2 deficiency impairs cell migration.

It is well-known that Rho mediated reorganization of the actin cytoskeleton is important for cell motility. Therefore, I examined the influence of ASPP2 on cell migration by real-time quantitative migration assay. Cell migration assay was carried out by using the xCELLigence Real-Time Cell Analyzer Dual Plate (RTCA-DP) instrument. Cells were serum-starved for 12 hours then planted into the CIM-plate at a density of 50,000 cells per well in serum-free DMEM medium. As illustrated in **figure 5.5A**, each well of the CIM-Plate has an upper chamber sealed at the bottom with a microporous PET membrane having integrated microelectronic sensors underneath, and one lower chamber, which was loaded with DMEM medium containing 10% FBS. Cells migrate through the membrane and then attach to the electronic sensors, leading to an increase in the impedance signals measured by the electronic sensors. These electrical impedance changes were monitored every 15 minutes for 25 hours. Therefore, cell migration activity can be monitored by using the impedance readouts: cell index values, which are directly proportional to the area covered by cells. ROCK inhibitor Y27632, which has been wildly reported to inhibit cell migration (Sadok et al., 2015; Somlyo et al., 2000; Z. M. Wang et al., 2016), was used as a positive control. As expected, Y27632 largely blocked the migration of both WT and *Aspp2-KO* cells (**Figure 5.5B**). The results also showed that ASPP2 deficiency significantly impaired cell migration (**Figure 5.5B**).

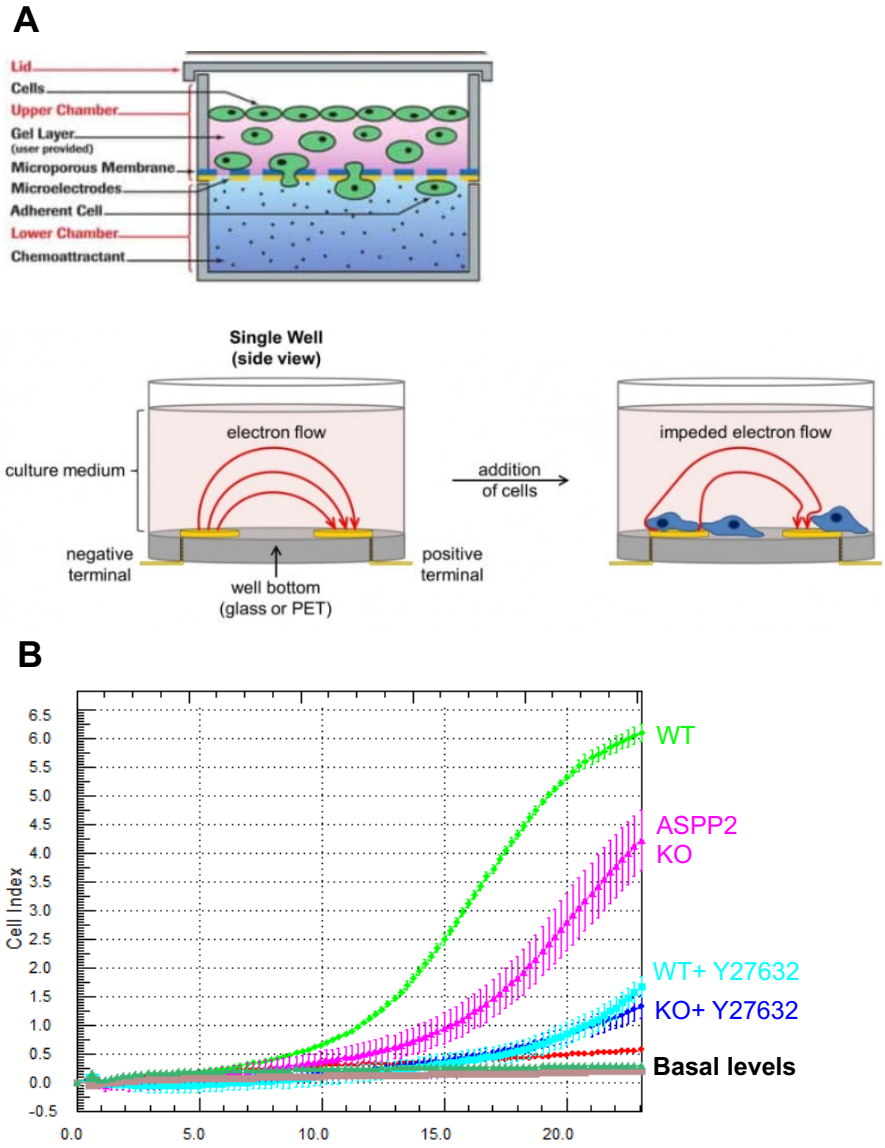


Figure 5. 5 ASPP2 deficiency impaired U2OS cell migration

(A) Schematic illustration of the principle of real-time cell migration assay using CIM-Plate. (B) The cell migration index was monitored every 15 minutes for 25 hours and plotted using the RTCA software of the xCELLigence system. WT and *ASPP2-KO U2OS* cells were treated with vehicle or ROCK inhibitor Y27632 during migration assay. Representative data of two independent experiments.

5.4 ASPP2 deficiency impaired phosphorylation of downstream effectors of Rho-ROCK signalling.

After finding out ASPP2 is a positive regulator of actomyosin stress fibre formation and cell migration, I would like to understand the underlying molecular mechanism. Stress fibre formation is mainly regulated by RhoA-ROCK signalling. RhoA shuttle between the inactive GDP-bound and the active GTP-bound states. RhoA-GTP activates ROCK to phosphorylate myosin regulatory light chain (MLC), promotes the assembly of actomyosin stress fibre. ROCK also phosphorylates MYPT1, which is a regulatory subunit of myosin-light-chain phosphatase (MLCP), to inactivate its phosphatase activity, thus maintains the phosphorylation of MLC. ROCK can also phosphorylate LIMK, which subsequently phosphorylate cofilin, thus inhibit actin depolymerization. RhoA-ROCK pathway mediated actomyosin stress fibre formation is illustrated in **figure 5.6A**.

The phosphoproteomic analysis suggests that ASPP2 may regulate Rho-ROCK signalling. More importantly, the phosphoproteomic data revealed that Thr853 of MYPT1 is phosphorylated in WT U2OS cells while it remains unphosphorylated in *Aspp2-KO* cells (**Figure 5.2B**). Since Thr853 of MYPT1 is a well-known residue phosphorylated by ROCK to inhibit the ability of myosin light chain phosphatase (MLCP), we speculated that ASPP2 is involved in ROCK-mediated phosphorylation of MYPT1 and MLC. To validate this idea, I examined the phosphorylation of MYPT1 and MLC2 upon Rho-ROCK activation by western blot. WT and *Aspp2-KO* cells were serum-starved for 12 hours then treated with Rho activator for 1 hour, 2 hours, and 3 hours. Phosphorylation of MYPT1 at Thr853 and MLC2 at Ser19 was detected by western blot. I found that Rho activator induced robust phosphorylation of MLC2 and MYPT1 in WT U2OS cells (**Figure 5.6B and D**). But such

phosphorylation was largely blocked in *Aspp2-KO* cells (**Figure 5.4B and D**). Quantification of Western Blot results from three independent experiments showed that the relative phosphorylation levels of Phosphor-MLC2-S19 and Phosphor-MYPT1-T853 were significantly lower in *ASPP2-KO U2OS* cells after Rho activator treatment for 2 hours (**Figure 5.4C and E**). Together with the finding that the formation of actomyosin stress fibres is impaired in *ASPP2-KO U2OS* cells, these results suggest that ASPP2 affects actomyosin activity through the MYPT1/MLC2 axis. Next, I tested whether ASPP2 could also influence the LIMK-Cofilin axis by examining the phosphorylation of LIMK1(Thr508)/LIMK2(Thr505) and Cofilin (Ser3) after treatment with Rho activator in WT and *ASPP2-KO U2OS* cells. Unfortunately, I failed to find a good antibody against phosphor-LIMK. However, I found that Rho activator induced robust phosphorylation of Cofilin (Ser3) in both WT and *Aspp2-KO* cells (**Figure 5.6F**), suggesting that the LIMK-Cofilin axis is not significantly affected by the loss of ASPP2.

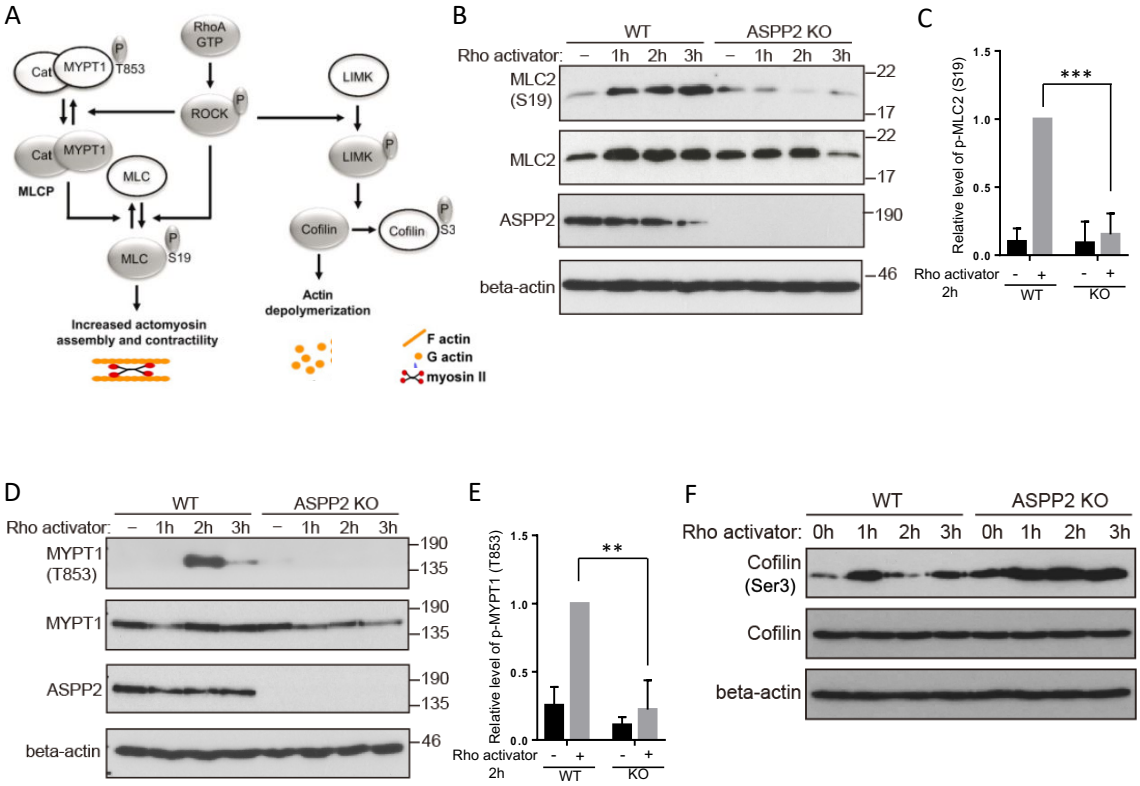


Figure 5. 6 ASPP2 deficiency impaired the phosphorylation of downstream effectors of Rho-ROCK signalling.

(A) Schematic illustration of RhoA-ROCK-mediated stress fibre formation; (B, D, F) WT and *Aspp2-KO* cells were treated with vehicle or Rho activator (1ug/ml) for indicated periods (1hour, 2 hours and 3 hours). MLC2, P-MLC2, MYPT1, P-MYPT1, Cofilin, and P-Cofilin were detected by WB. Beta-actin was used as the loading control. (C, E) Quantification of the protein level of P-MLC2 or P-MYPT1 relative to the protein level of MLC2 or MYPT1 after treatment of vehicle or Rho activator for 2 hours. n= 3 independent experiments.

5.5 ASPP2 does not regulate RhoA-ROCK signalling by interacting with RhoA.

After finding out ASPP2 is a positive regulator of RhoA-ROCK signalling, the next important question would be whether ASPP2 influence RhoA-ROCK signalling through RhoA or ROCK. ASPP2 has been found to bind to Ras-GTP and enhance its activity by promoting GTP loading (Posada et al., 2016; Y Wang et al., 2013). It is possible that ASPP2 can bind to RhoA and regulate its activity in a similar way. Therefore, I first test the effect of ASPP2 deficiency on RhoA activity and whether ASPP2 can physically interact with RhoA. WT and *Aspp2-KO* cells were serum-starved for 12 hours then treated with Rho activator for 2 hours. The total RhoA level was determined by western blot. RhoA activity is determined by the level of RhoA -GTP in cell lysate, which was measured by Rhotekin-RBD based ELISA (**Figure 5.7A**). Rhotekin-RBD, which contains the Rho binding domain of the Rhotekin protein that binds specifically to GTP-bound, and not GDP-bound RhoA, was used as the capture antibody. Then antibody against RhoA was used as the detective antibody. Active RhoA-GTP protein was used as the positive control. I found *Aspp2-KO* didn't affect the total RhoA level (**Figure 5.7B**), and the Rho activator increased RhoA-GTP level to a similar extent in *Aspp2-KO* cells compared to that in WT cells (**Figure 5.7C**). To test whether ASPP2 physically interacts with RhoA, cells were treated with Rho activator to induce a high level of RhoA-GTP, and cell lysates were immunoprecipitated with the anti-ASPP2 antibody. *Aspp2-KO* cells were included to rule out the possibility that the positive interaction was an artefact caused by antibody non-specificity. PP1, a well-known binding partner of ASPP2, was included as a positive control. As shown in **Figure 5.7D**, PP1 was detected in the immunoprecipitants but RhoA and MLC2 were not,

suggesting ASPP2 does not physically interact with RhoA and MLC2. These results indicate that ASPP2 does not regulate RhoA-ROCK signalling through RhoA.

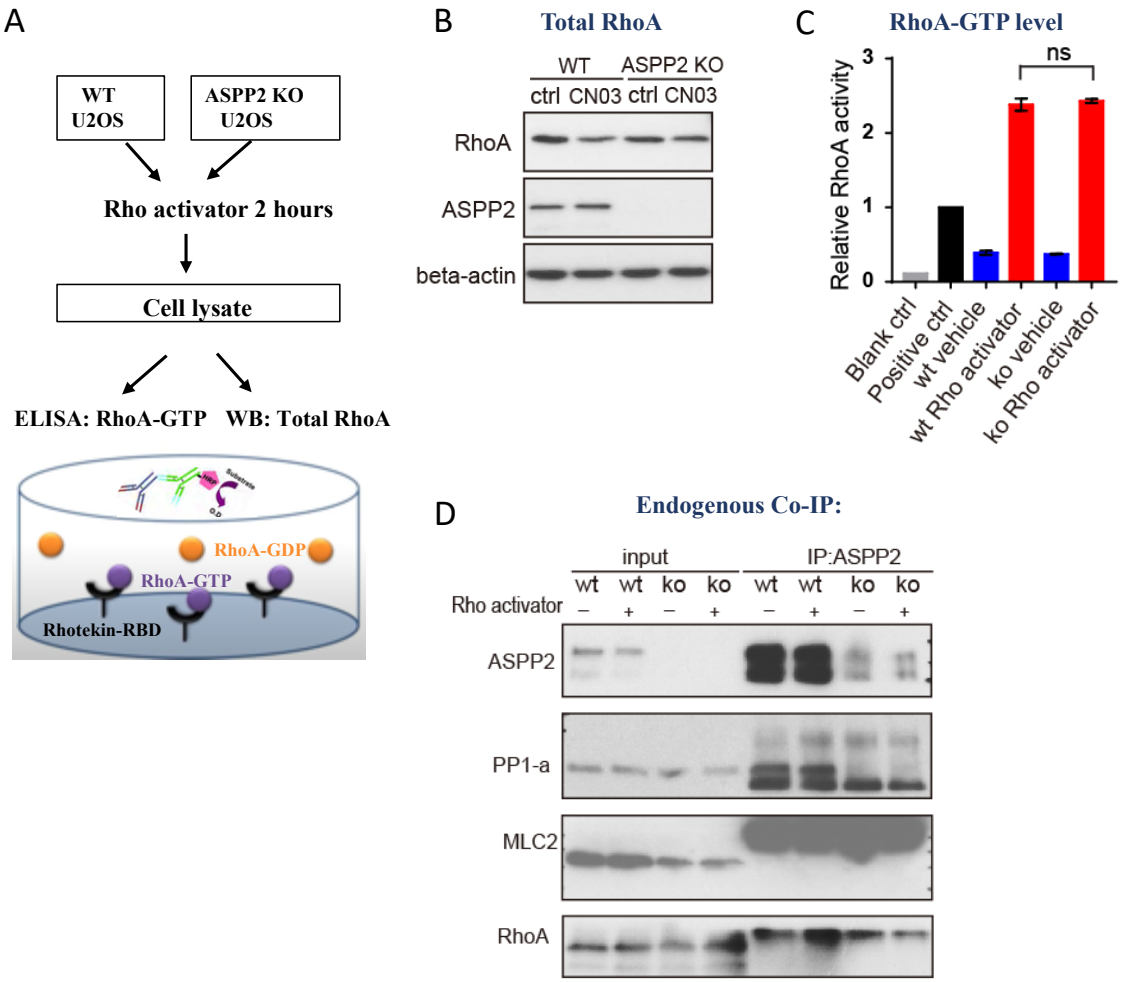


Figure 5. 7 ASPP2 does not regulate RhoA-ROCK signalling through RhoA.

(A) Schematic illustration of the RhoA activity assay; (B-C) WT and *Aspp2-KO* cells were treated with vehicle or Rho activator (1ug/ml) for 2 hours. The total RhoA level was determined by western blot (B). The RhoA-GTP level was measured by the RhoA G-LISA kit (C). Active RhoA-GTP protein was used as the positive control. n= 3 biological repeats from 1 experiment. (D) WT and *Aspp2-KO* cells were treated with vehicle or Rho activator (1ug/ml) for 2 hours. Endogenous ASPP2 was immunoprecipitated by the anti-ASPP2 antibody. PP1a (a known ASPP2 binding protein) was detected in the immunoprecipitants while RhoA and MLC2 were not. Representative data of three independent experiments.

5.6 ASPP2 interacts with ROCK2 and enhance its activity.

Next, I examined the effect of ASPP2 deficiency on ROCK activity. WT and *Aspp2-KO* cells were serum-starved for 12 hours then treated with Rho activator for 2 hours. ROCK activity was determined by enzyme immunoassay (**Figure 5.8A**): plates were pre-coated with recombinant MYPT1, which contains a Thr696 residue that can be phosphorylated upon addition of cell lysates containing active ROCK. Then antibody that specifically detects only MYPT1 phosphorylated at Thr696 was used as the detective antibody. Active ROCK2 protein was used as the positive control. I found Rho activator increased ROCK activity to a significantly higher level in WT cells compared to that in *Aspp2-KO* cells (**Figure 5.8B**). To test whether ASPP2 regulates ROCK activity by physically interacting with ROCK, I did Co-Immunoprecipitation experiments. Both ROCK1 and ROCK2 were detected in the immunoprecipitants pulled down by the anti-ASPP2 antibody. However, only the interaction between ROCK2 and ASPP2 was increased by Rho activator treatment (**Figure 5.8C-D**), suggesting that ASPP2 prefers ROCK2 to ROCK1 upon Rho stimulation. In conclusion, ASPP2 regulates RhoA-ROCK signalling by interacting with ROCK2 and enhancing its activity.

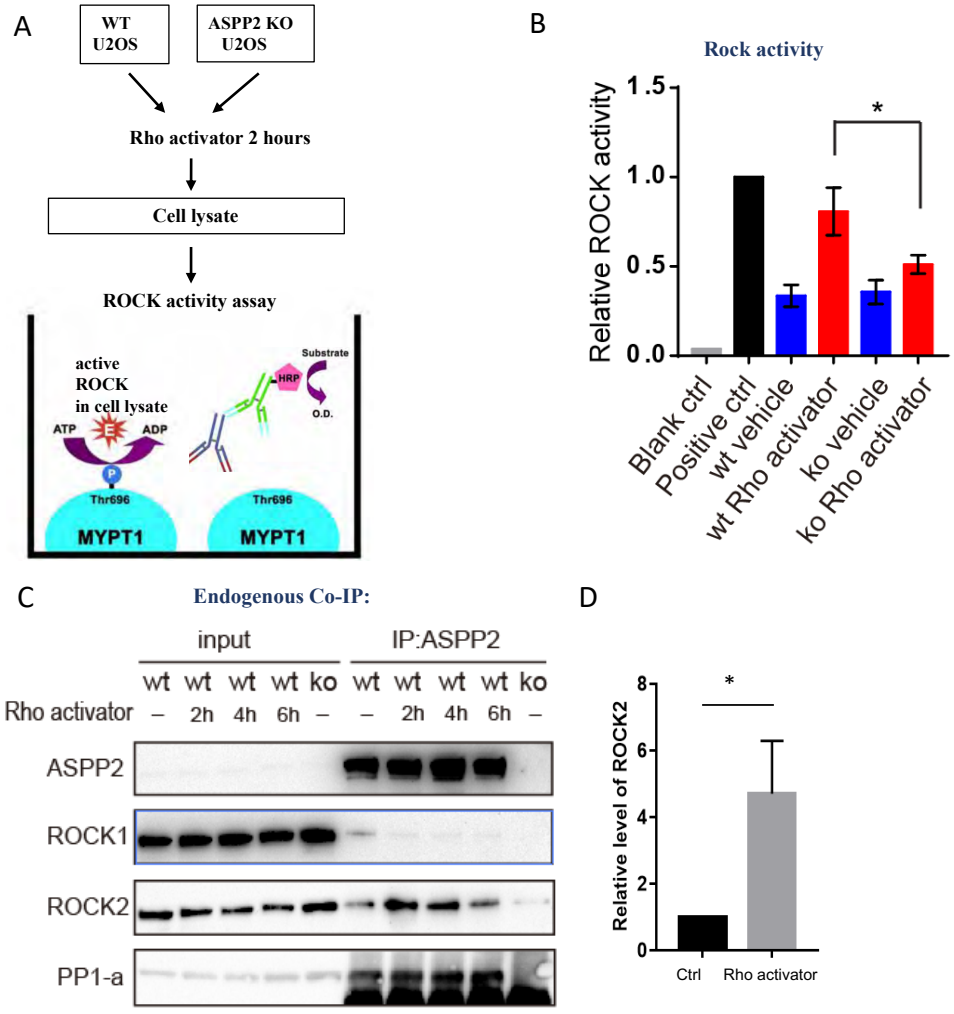


Figure 5. 8 ASPP2 interacts with ROCK2 and enhances its activity.

(A) Schematic illustration of the ROCK activity assay. (B) WT and *ASPP2-KO U2OS* cells were treated with vehicle or Rho activator (1ug/ml) for 2 hours. ROCK activity in the cell lysate was measured. Active ROCK2 protein was used as the positive control. n= 3 independent experiments. *P<0.05; (C) WT and *Aspp2-KO* cells were treated with vehicle or Rho activator (1ug/ml) for indicated periods. Endogenous ASPP2 was immunoprecipitated by the anti-ASPP2 antibody. Interaction between ASPP2 and ROCK1/2 was examed. (D) Quantification of the protein level of ROCK2 co-immunoprecipitated by ASPP2 upon treatment of vehicle or Rho activator for 2 hours. n= 3 independent experiments.

5.7 ASPP2 may influence ROCK activity in a PP1-dependent manner.

Next, I decided to look into how ASPP2-ROCK2 interaction relates to the enzyme activity of ROCK2. ROCK2 is enzymatically inactive in its native form because the ROCK kinase domain is inhibited by the C-terminal region of ROCK (Jacobs et al., 2006). The most characterized regulatory mechanism of ROCK2 is through RhoA-GTP. Upon RhoA-GTP binds to the Rho binding domain of ROCK2, the kinase domain is transiently released from auto-inhibition because of conformational changes. Alternatively, during apoptosis, the C-terminal region can be cleaved and removed by granzyme-B, leading to constitutively active ROCK2 (Sebbagh et al., 2005). ROCK2 activity can also be regulated by its phosphorylation. For instance, phosphorylation of ROCK2 at Tyr-722 disturbs the binding between ROCK2 and RhoA-GTP, therefore, inhibits ROCK2 activity (H.-H. Lee et al., 2010) while dephosphorylation at this residue mediated by SHP2 increases ROCK2 activity (Hsiao-Hui Lee & Chang, 2008). Polo-like kinase-1 can phosphorylate Thr-967, Ser-1099, Ser-1133, and Ser-1374 of ROCK2 thereby working together with RhoA to maximumly activate ROCK2 (Lowery et al., 2007). The autophosphorylation of ROCK2 at Ser1366 was reported to reflect the activation status of ROCK2 (Chuang et al., 2012). Moreover, GTP-binding protein Rad1 interacts with the coiled-coil region of ROCK2 and inhibits its activity (Ward et al., 2002). Coronin1B can bind to the pleckstrin homology region of ROCK2 and attenuate its activity (Rana & Worthylake, 2012).

To understand how ASPP2 influences ROCK2 activity, I firstly examed whether the interaction between ROCK2 and its activator RhoA, as well as the interaction between ROCK2 and its substrate MYPT1 and MLC2, were affected by *Aspp2-KO* . Surprisingly, I found no evidence of ROCK2-RhoA or ROCK2-MYPT2 interaction (**Figure 5.9A**).

However, the interaction between ROCK2 and MLC2 was detected and this interaction was disturbed in *Aspp2-KO* cells (**Figure 5.9B**), suggesting ASPP2 is involved in mediating the binding between ROCK2 and MLC2. Considering ASPP2 is a well-known adaptor and regulator of protein phosphatase 1(PP1), I speculated that ASPP2 might regulate the phosphorylation of ROCK2 through PP1-mediated dephosphorylation, thus influences the binding ability of ROCK2 to its substrate. One of the ideal ways to test this hypothesis is to exam the phosphorylation of ROCK2 at those residues that have been reported to be important for ROCK2 activity such as Tyr-722, Thr-967, Ser-1099, Ser-1133, Ser-1374, and Ser1366. Unfortunately, only the antibody against phosphor-ROCK2-Ser1366 is commercially available. So, I examed the phosphorylation of ROCK2-Ser1366 in WT and *ASPP2-KO U2OS* cells. As shown by **Figure 5.9C**, Rho activator treatment increased the phosphorylation of ROCK2-Ser1366 in both WT and *Aspp2-KO* cells, suggesting the phosphorylation status of this residue is independent of ASPP2. Whether ASPP2 can influence other phosphosites of ROCK2 remains further investigation. I also tested the hypothesis indirectly by examing whether the function of ASPP2 in regulating the phosphorylation of ROCK2 targets including MLC2 and MYPT1 is dependent on PP1. ASPP2 possesses a PP1-binding RVXF motif at residues 916-927, preceding the ankyrin repeats. RVXF mutant ASPP2 (V922A, F924A) losses the ability to bind to PP1. Stable *ASPP2-KO U2OS* cells re-expressing doxycycline-inducible WT or RVXF mutant ASPP2 were generated by inserting pTet-On-Tp53bp2 (WT or RVXF mutant) and pCAG-rtTA (reverse tetracycline transactivator) using the PiggyBac transposon system. Either WT ASPP2 or ASPP2 RVXF mutant was reintroduced into *Aspp2-KO* cells by 30ng/ml doxycycline treatment. As shown in **figure 5.9D**, the Co-IP experiment confirmed that ASPP2 RVXF mutant can not bind to PP1a while the physical interaction between ASPP2

and ROCK2 was not influenced by RVXF mutation. Next, I examined the effect of reintroducing WT or RVXF mutant ASPP2 on the phosphorylation of MYPT1 and MLC2. Interestingly, I found that Rho activator was able to induce robust phosphorylation of MLC2 and MYPT1 after reintroducing WT ASPP2 but not RVXF mutant ASPP2 (**Figure 5.9E**), which suggests that ASPP2 may influence ROCK2-mediated phosphorylation of MLC2 and MYPT1 in a PP1-dependent manner.

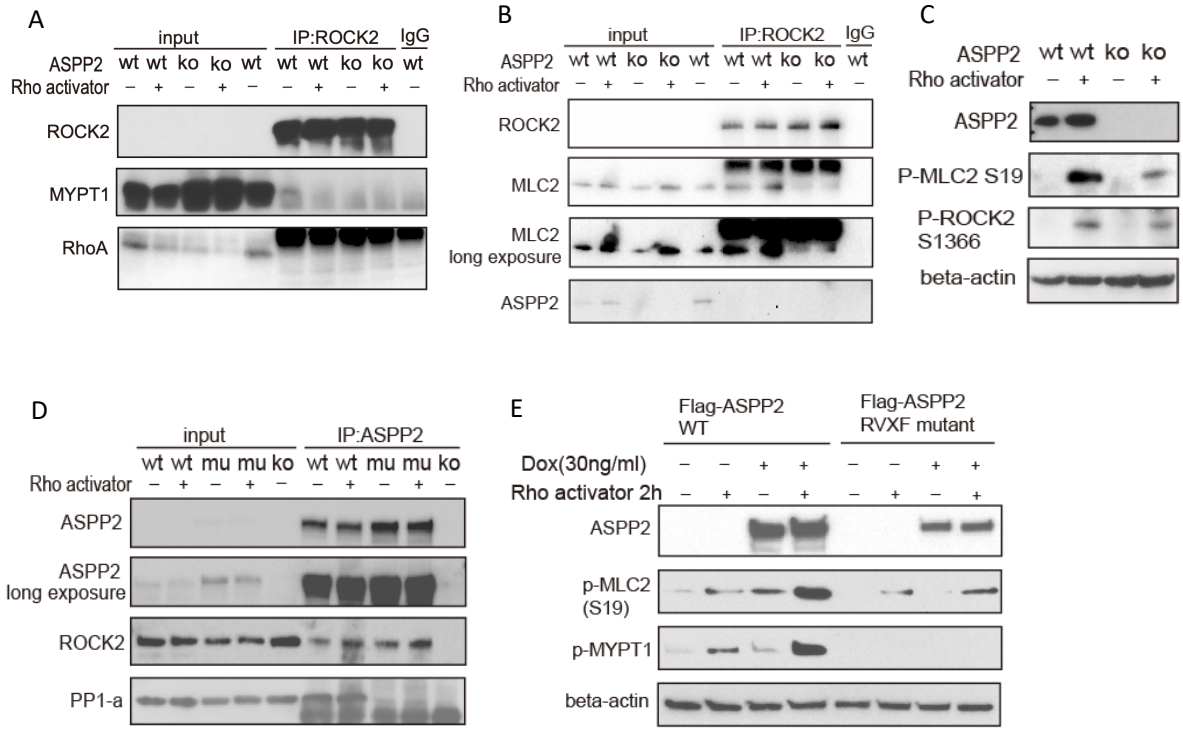


Figure 5. 9 ASPP2 may influence ROCK activity in a PP1-dependent manner.

(A-B) WT and *Aspp2-KO* cells were treated with vehicle or Rho activator (1ug/ml) for 2 hours. Endogenous ROCK2 was immunoprecipitated by the anti-ROCK2 antibody. Interactions between ROCK2 and MYPT1/RhoA were examed in (A), Interaction between ROCK2 and MLC2 was examed in (B); (C) WT and *ASPP2-KO U2OS* cells were treated with vehicle or Rho activator (1ug/ml) for 2 hours. Rho activator induced phosphorylation of MLC2-S19 was inhibited in *Aspp2-KO* cells while phosphorylation of ROCK2-S1366 was not affected; (D) Inducible WT or RVXF mutant ASPP2 expressing U2OS cells were treated with vehicle or 30ng/ml doxycycline for 24 hours to induce ASPP2 expression. Then cells were treated with the vehicle or Rho activator (1ug/ml) for 2 hours. ASPP2 was immunoprecipitated by the anti-ASPP2 antibody. RVXF mutant ASPP2 failed to interact with PP1a but can still interact with ROCK2; (E) Inducible WT or RVXF mutant ASPP2 expressing U2OS cells were treated with doxycycline and Rho activator as described in (D). Rho activator was able to induce robust phosphorylation of MLC2 and MYPT1 after reintroducing WT ASPP2 but not RVXF mutant ASPP2.

5.8 ASPP2 does not interact with Filamin A.

The phosphoproteomic data revealed that Ser2026 of Filamin A (encoded by *FLNA*) was phosphorylated in WT U2OS cells but unphosphorylated in *ASPP2-KO U2OS* cells (**Figure 5.2B**). *FLNA* is the most commonly mutated gene found in patients with periventricular heterotopia (PNH). FLNA mutations were found in 49% of PNH patients irrespective of familial or sporadic occurrence (Parrini et al., 2006). Filamin A is an actin-binding protein that crosslinks actin filaments into orthogonal networks (Nakamura et al., 2007) and regulates reorganization of the actin cytoskeleton leading to changes in cell shape and migration (Stossel et al., 2001). Interestingly, regulation of the phosphorylation of Filamin A has been reported to be involved in developing PNH in mice. It has been demonstrated that mice mutant for MEKK4, a MAP kinase that regulates the CSBP2 and JNK-MAPK pathways, developed PNH (Sarkisian et al., 2006). The expression of Filamin A was elevated near sites of failed neuronal migration and overexpression of Filamin A inhibits radial migration in the neocortex. MEKK4 suppression by RNAi led to increased Filamin A phosphorylation at Ser2152, which has been implicated in providing resistance to Filamin A cleavage (Sarkisian et al., 2006). Therefore, MEKK4 deficiency might cause PNH through increasing Ser2152 phosphorylation and protein level of Filamin A. The finding that phosphorylation status of Filamin A is altered in *ASPP2-KO U2OS* cells suggests Filamin A might be involved in the molecular mechanism underlying the PNH phenotype found in *Aspp2-KO* mice. Therefore, I decided to look into the link between ASPP2 and Filamin A phosphorylation.

ASPP2 may directly interact with Filamin A and mediate its dephosphorylation through PP1. Therefore, I checked the interaction between ASPP2 and Filamin A by Co-IP

experiment. I found no evidence of physical interaction between ASPP2 and Filamin A under both the endogenous condition (**Figure 5.10A**) and the condition of ASPP2 overexpression (**Figure 5.10B**). These results indicate that ASPP2 is not able to recruit PP1 to dephosphorylate Filamin A. Apart from directly affecting Filamin A through ASPP2/PP1 complex, ASPP2 may also indirectly influence Filamin A via ROCK2. I have demonstrated that ASPP2 is important for ROCK activity induced by Rho activator. It has been reported that the PH domain of ROCK2 directly binds to the 24th tandem repeat of Filamin-A (aa2554-aa2647) (K. Ueda et al., 2003). Interestingly, many PNH-associated missense mutations occur in the N-terminal actin-binding domain and the 24th tandem repeat of Filamin A (Cannaerts et al., 2018). These data suggest that FilaminA could be a potential ROCK2 substrate. Consistent with this idea, ROCK1/2 is among the predicted kinases of Ser-2026 according to the PhosphoNET Kinase Predictor. Therefore, ASPP2 may indirectly influence FilaminA phosphorylation through ROCK2. Unfortunately, the biological function of Ser-2026 of Filamin A remains unknown and there is no available antibody against this phosphosite. However, I examed the influence of ASPP2 deficiency on the phosphorylation of Filmin A at Ser-2152 under the condition of Rho activator treatment. The result showed that Rho activator increased the phosphorylation of Filamin A-Ser2152 to comparable levels in WT and *ASPP2-KO U2OS* cells (**Figure 5.10C**). Whether ASPP2 could influence the phosphorylation of Filamin A at Ser-2026 and the biological significance of this phosphosite needs further investigation in the future.

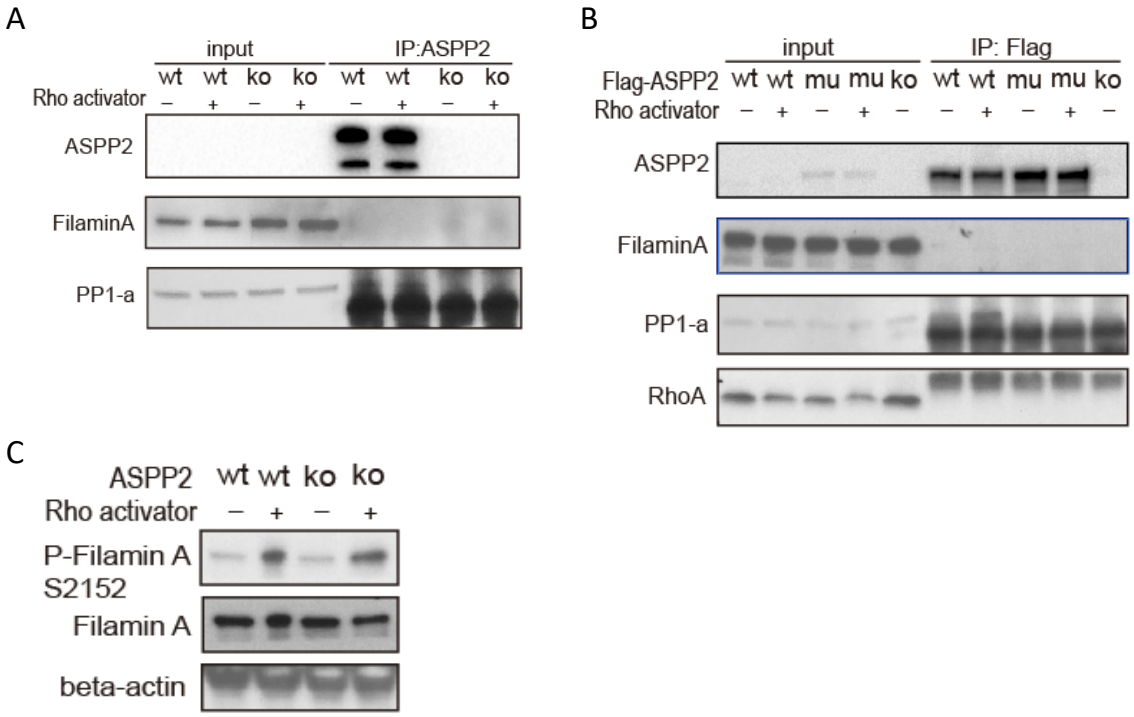


Figure 5. 10 ASPP2 does not interact with Filamin A.

(A) WT and *ASPP2-KO U2OS* cells were treated with vehicle or Rho activator (1ug/ml) for 2 hours. ASPP2 was immunoprecipitated by the anti-ASPP2 antibody. Filamin A was not detected in the immunoprecipitate. (B) Inducible WT or RVXF mutant ASPP2 expressing U2OS cells were treated with v 30ng/ml doxycycline for 24 hours to induce ASPP2 expression. Then cells were treated with the vehicle or Rho activator (1ug/ml) for 2 hours. ASPP2 was immunoprecipitated by the anti-ASPP2 antibody. Filamin A was not detected in the immunoprecipitate. (C) WT and *ASPP2-KO U2OS* cells were treated with vehicle or Rho activator (1ug/ml) for 2 hours. Rho activator increased the phosphorylation of Filamin A at S2152 in both WT and *Aspp2-KO* cells.

5.9 Summary

Dynamic regulation of the actin cytoskeleton is pivotal for neuronal migration. Impairment of this process serves as an important mechanism of developing periventricular heterotopia. As a regulator of the PAR complex at the cell membrane and an adaptor of PP1 in the cytoplasm, ASPP2 may be a potential regulator of the actin cytoskeleton. This hypothesis was tested in this chapter. Mass spectrometry-based phosphoproteomic analysis using WT and *ASPP2-KO U2OS* cells revealed that pathways related to cytoskeletal regulation, especially the Rho-PAK and Rho-ROCK pathway, were affected by the loss of ASPP2. One of the phosphorylation motifs enriched in ASPP2-sensitive phosphosites represented a consensus motif identified in ROCK substrates. These results suggested that ASPP2 may regulate cytoskeleton through Rho-ROCK signalling. Therefore, I investigated the influence of ASPP2 deficiency on the actin cytoskeleton in U2OS cells and I found *ASPP2-KO U2OS* cells displayed impaired actomyosin stress fibre formation upon Rho activator treatment as well as deficient cell migration. Mechanistically, ASPP2 deficiency largely abolished Rho activator-induced phosphorylation of ROCK substrates MYPT1 and MLC2, which are necessary for actomyosin stress fibre formation. To understand whether ASPP2 regulates Rho-ROCK signalling through RhoA or ROCK, I studied the influence of ASPP2 deficiency on RhoA activity and ROCK activity. The results showed that ASPP2 did not physically interact with RhoA, and ASPP2 did not influence the RhoA-GTP level either. Instead, ASPP2 physically interacted with ROCK2 and potentiated its phospho-kinase activity. More importantly, the interaction between ROCK2 and its substrate MLC2 was inhibited in ASPP2 deficient cells. Interestingly, reintroducing WT ASPP2 into *Aspp2-KO* cells can rescue the phosphorylation of MLC2 and MYPT1. while reintroducing ASPP2 RVXF mutant, which is not able to bind to PP1, failed to do so, indicating that ASPP2 may

regulate ROCK2 activity in a PP1 dependent manner. However, Rho activator-induced phosphorylation of ROCK2 at Ser1366, which has been shown to positively reflect the activation of ROCK2, was not affected by the loss of ASPP2. Whether ASPP2 could influence the phosphorylations of other phosphosites of ROCK2, for instance, Ser1377 which was identified as an ASPP2-sensitive phosphosite by mass spectrometry, needs further study in the future. The phosphoproteomic data also revealed that phosphorylation of Filamin A, encoded by *FLNA* which is the most commonly mutated gene in PNH patients, was affected by ASPP2 deficiency. I found no evidence of physical interaction between ASPP2 and Filamin A in U2OS cells, suggesting it is unlikely that ASPP2 can recruit PP1 to affect the phosphorylation status of Filamin A. Since Filamin A is a potential ROCK2 substrate, ASPP2 may indirectly regulate Filamin A phosphorylation via ROCK2. Even though I found that phosphorylation of Ser2152 of Filamin A, which has been shown to be involved in developing PNH in mice, was not affected by ASPP2 knockout, whether ASPP2 could influence the phosphorylations of other phosphosites of Filamin A, for instance, Ser2026 which was identified as an ASPP2-sensitive phosphosite by mass spectrometry, remains unclear.

Chapter 6: Discussion

6.1 ASPP2 in regulating Rho-ROCK signalling and the actin cytoskeleton.

Apart from its central role in regulating apoptosis through the P53 family and the Bcl-2 family proteins, ASPP2 has been found to be involved in many cellular processes through interacting with various proteins. Structural studies reveal that ASPP2 N-terminus contains a potential Ras-association domain (RAD), which specifically binds to the GTP-bound G protein (Tidow et al., 2007). It has been reported that the N-terminal of ASPP2 binds to Ras-GTP and promotes GTP loading, thus stimulates Ras-induced ERK signalling (Posada et al., 2016; Y Wang et al., 2013). As a member of the Ras superfamily, can RhoA be regulated by ASPP2 in a similar way? The result of the Co-IP experiment in this study suggests that ASPP2 is not able to interact with RhoA in the presence of a high RhoA-GTP level induced by Rho activator. This could be explained by the structural difference between the Ras family and the Rho family. Although the core G-domains of Ras, Rho, and Rab family members share sequence and structural similarity, the C-terminal hypervariable region of Ras, Rho, and Rab family members exhibits significant sequence differences (Chenette & Der, 2011).

Instead of interacting with RhoA, this study reveals that ASPP2 physically interacts with ROCK1 and ROCK2. However, only the interaction between ASPP2 and ROCK2 interaction is enhanced while the ASPP2-ROCK1 interaction is impaired under the condition of RhoA activation. This result suggests that ASPP2 prefer ROCK2 upon RhoA stimulation. How does ASPP2 discriminate ROCK1 and ROCK2 upon Rho activation?

ROCK1 and ROCK2 both contain an N-terminal kinase domain, a coiled-coiled region followed by a Rho-binding domain (RBD), and a C-terminal PH-domain, which plays an autoinhibitory role by sequestering the kinase domain. Their kinase domains have the highest amino acid similarity (92% homology) while their coiled-coil domains and PH domains have 55% and 65% identity, respectively. Upon binding to RhoA-GTP through the Rho-binding domain, ROCK1 and ROCK2 undergo conformational changes that release the kinase domain from the PH-domain. Although ROCK I and ROCK II have closely similar rho-binding domains, crystal structures of ROCK I and ROCK II with active RhoA showed slightly different spatial arrangements (Dvorsky et al., 2004). It is possible that conformational changes induced by RhoA-GTP binding are involved in ASPP2's preference in ROCK2 versus ROCK1 upon Rho activation. Also, it has been proposed that difference in the PH domains of ROCK1 and ROCK2 may confer specificity of protein interaction, for instance, the PH domain of ROCK2 binds to phosphatidylinositol trisphosphate (PIP3) and phosphatidylinositol bisphosphate (PIP2), whereas the PH domain of ROCK1 does not (Yoneda et al., 2005). It is possible that the binding affinity between ASPP2 and ROCK2 is higher than that between ASPP2 and ROCK1 because of the difference in the PH domains. In this study, ROCK2 was co-immunoprecipitated by anti-ASPP2 antibody while ASPP2 was not co-immunoprecipitated by anti-ROCK2 antibody, which is produced by immunizing rabbits with a synthetic peptide corresponding to residues around the PH domain of human ROCK2 protein. A possible explanation is that both ASPP2 and anti-ROCK2 antibody bind to the PH domain of ROCK2 therefore ASPP2 can not be detected in the immunoprecipitates pulled down by this specific antibody. However, this study did not check which domain of ROCK2 mediates the interaction

between ASPP2 and ROCK2. It is worthy to identify the binding regions between ASPP2 and ROCK2 by using various ROCK2 and ASPP2 truncations.

This study reveals that the loss of ASPP2 largely blocked the phosphorylation of MYPT1 and MLC2. ROCKs are believed to be able to directly phosphorylate MLC2 at Ser-19 and Thr-18 (Amano et al., 1996; G Totsukawa et al., 2000), although some studies suggest that phosphorylation of MLC2 is mainly caused by MLC kinase (MLCK) and ROCK may largely contribute to elevating MLC phosphorylation indirectly by inhibiting dephosphorylation of MLC2 through phosphorylating MYPT1 (Iizuka et al., 1999; Swärd et al., 2000). In this study, I found that the phosphorylations of both MYPT1-T853 and MLC2-S19 were inhibited by ASPP2 deficiency. This could be explained by two possibilities: first, ASPP2 only affect the phosphorylation of MYPT1 through ROCK2 but is not involved in the regulation of ROCK2 on MLC2. The change of MLC2 phosphorylation is totally a result of inhibition of MYPT1. Second, ASPP2 has a direct influence on both MYPT1 and MLC2. It has been shown that ROCK2 can directly bind MYPT1 through its coiled-coil domain (Yuepeng Wang et al., 2009) and binds to myosin heavy chain IIA and IIB via its PH domain (Kawabata et al., 2004). Surprisingly, I failed to find any evidence showing that ROCK2 directly binds MLC2 among published literature. The result of endogenous Co-IP experiments in this study showed that ROCK2 physically interacts with MLC2 and this interaction was dramatically disrupted by the loss of ASPP2. This result further supports that ROCK2 can directly phosphorylate MLC2, and the ROCK2-MLCs axis contributes a lot to the impairment of MLC2 phosphorylation and actomyosin stress fiber formation caused by ASPP2 deficiency.

How does ASPP2 deficiency lead to impaired ROCK activity and ROCK2-MLC2 interaction? Apart from the most characterized regulatory mechanism through RhoA-GTP binding, ROCK2 activity can also be regulated by phosphorylation. Structure analyses showed that the ROCK kinase domain had a catalytically competent conformation without phosphorylation, indicating that the ROCK kinase domains do not require phosphorylation for activity (Jacobs et al., 2006). However, ROCK activity can be regulated by phosphorylating other regions. For instance, binding between ROCK2 and RhoA-GTP is interfered with by phosphorylation of ROCK2 on Tyr-722 and thereby inhibits ROCK2 activity (H.-H. Lee et al., 2010) while dephosphorylation on this residue mediated by SHP2 increases ROCK2 activity (Hsiao-Hui Lee & Chang, 2008). Polo-like kinase-1 can phosphorylate Thr-967, Ser-1099, Ser-1133, and Ser-1374 of ROCK2 thereby working together with RhoA to maximumly activate ROCK2 (Lowery et al., 2007). The autophosphorylation of ROCK2 at Ser1366 was reported to reflect the activation status of ROCK2 (Chuang et al., 2012). Moreover, GTP-binding protein Rad1 interacts with the coiled-coil region of ROCK2 and inhibits its activity (Ward et al., 2002). Coronin1B can bind to the PH domain of ROCK2 and attenuate its activity through phosphatase Slingshot IL (SSH1L)- mediated dephosphorylation (Rana & Worthylake, 2012). As a targeting subunit of protein phosphatase 1(PP1) and binding partner of ROCK2, ASPP2 might regulate ROCK2 activity through PP1-mediated dephosphorylation. This hypothesis is supported by the finding that Rho activator can induce robust phosphorylation of MLC2 and MYPT1 after reintroducing WT ASPP2 but not ASPP2 RVXF mutant into *Aspp2-KO* cells. Large scale phosphoproteomics studies have identified 45 phosphosites on human ROCK2 (www.phosphosite.org). However, the biological function of the majority of them

remains unknown. In the future, it is worthy to investigate the biological significance of the frequently detected phosphorylations of ROCK2 such as S1379, S1374, S1137, and S289.

Very recently, it has been reported that overexpression of N-terminal truncated ASPP2 (766aa-1134aa) containing RVXF motif, Ank repeat and SH3 domain in E-cadherin–deficient mammary myoepithelial cells (MMECs) resulted in reduced MLC2 phosphorylation, actomyosin relaxation, and promoted cell adhesion and survival (Schipper et al., 2020). The authors also found that the inhibition effect of truncated ASPP2 on MLC2 phosphorylation is dependent on its PP1 binding RVXF motif. Although the authors did not investigate the mechanism of how truncated ASPP2 in E-cadherin–deficient MMECs inhibits MLC2 phosphorylation, in the discussion section of that paper they proposed that truncated ASPP2 might directly dephosphorylate myosin through recruiting PP1, which is different from the model proposed by this study which is that ASPP2 regulates MLC2 phosphorylation through ROCK2. However, a peptide derived from ASPP2 838aa-1128aa containing the RVXF motif, Ank repeats, and the SH3 domain, which is required for ASPP2/PP1 substrate dephosphorylation (Bertran et al., 2019), showed no influence on PP1c activity towards MLC2 *in vitro* (Helps et al., 1995). Besides, this study showed that ASPP2 is not able to physically interact with MLC2. These results suggest that MLC2 is unlikely to be an ASPP2/PP1 target.

Interestingly, both overexpression of N-terminal truncated ASPP2 (766aa-1134aa) in E-cadherin–deficient MMECs and knocking out ASPP2 in U2OS cells inhibited the phosphorylation of MLC2, which indicates that full-length ASPP2 and N-terminal truncated ASPP2 (766aa-1134aa) have opposite functions in terms of regulating MLC2

phosphorylation. The previous study revealed that short peptides from ASPP2 903aa–934aa containing only the RVXF motif disrupted the interaction between MYPT and PP1 thus inhibited the dephosphorylation rate of MLC2 (Egloff, 1997). This result can be explained by that RVXF motif-containing short peptides compete with MYPT1 for PP1 binding. Can N-terminal truncated ASPP2 (766aa-1134aa) also disturb the interaction between MYPT1 and PP1? ASPP2 SH3 domain can discriminate between PP1 isoforms using an acidic specificity pocket in the n-Src domain resulting that ASPP2 shows a strong preference for PP1α with an affinity which is 13- and 14-fold higher than that for PP1β and PP1γ, respectively (Bertran et al., 2019). MYPT1 interacts with PP1β to form the myosin phosphatase holoenzyme (Pinheiro et al., 2011). The N-terminal truncated ASPP2 (766aa-1134aa) contains the SH3 domain, which makes it unlikely to compete with MYPT1 for binding PP1β because of its low affinity to PP1β. Then how does overexpression of N-terminal truncated ASPP2 (766aa-1134aa) inhibited MLC2 phosphorylation? This study revealed that ASPP2 physically interacted with ROCK2 and potentiated ROCK2 activity as well as ROCK2-MLC2 interaction. It is possible that the interaction between ASPP2 and ROCK2 is mediated by the UBL domain (1aa-83aa) or the proline-rich domain (674aa-902aa) which are not included in the truncated ASPP2 (766aa-1134aa). Therefore, the truncated ASPP2 (766aa-1134aa) losses the function of regulating ROCK2 activity or even adversely affect the function of normal ASPP2 through binding to the Ankyrin repeats normal ASPP2. Because the truncated ASPP2 lacks the proline-rich domain which is reported to inhibit protein–protein interactions of ASPP2 by masking the C-terminal ankyrin and SH3 domains (Rotem et al., 2008).

Apart from regulating rearrangement of the actin cytoskeleton, RhoA-ROCK signalling is important downstream effectors of polarity proteins and they can also regulate the PAR complex in return. PAR6/aPKC can activate p190A RhoGAP thus downregulate RhoA activity (H. Zhang & Macara, 2008) and PAR3/aPKC phosphorylate Rho-associated kinase (ROCK) thus suppress its junctional localization (Ishiuchi & Takeichi, 2011). RhoA-ROCK mediated Thr833 phosphorylation of PAR3 leads to disassociation of the PAR complex (Nakayama et al., 2008). The feedback loop between RhoA-ROCK and the PAR complex is essential for finetuning the actomyosin contractility needed for cell migration. RhoA-ROCK signalling provides an ideal link between polarity proteins and the actin cytoskeleton. As a regulator of the PAR complex and ROCK mediated actomyosin stress fibre formation, ASPP2 provides another important link between polarity proteins and the actin cytoskeleton. Interestingly, high-content screening of 367 kinase inhibitors and 1600 bioactive compounds carried out by a former Lu lab member Jerry Zak revealed that reduced ROCK activity as a hallmark of top hits that alter the junctional localization pattern of ASPP2, suggesting mutual regulation between ASPP2 and ROCK.

6.2 ASPP2 in neuronal migration.

This study revealed that ASPP2 deficiency resulted in impaired radial migration in the neocortex and chain migration in the RMS, leading to periventricular nodular heterotopia and diminished olfactory bulbs, respectively. These phenotypes observed in *Aspp2-KO* mice are in line with the function of ASPP2 revealed by the mechanism study in U2OS cells which is potentiating ROCK activity and actomyosin formation. Even though the molecular mechanism has not been directly validated in migrating neuroblasts, it is reasonable to speculate that ASPP2 may regulate neuronal migration in a similar way.

The functions of RhoA and its downstream targets in neuronal migration have been extensively studied in the past. Active RhoA has been reported in the leading process of migrating neurons (Guan et al., 2007). Expression of constitutively active RhoA in the VZ inhibits radial migration while dominant negative-RhoA increases radial migration (Nguyen, 2006; Tang et al., 2014). Similarly, the expression of constitutively active RhoA or dominant-negative RhoA in the SVZ explants decreases or increases migration, respectively (Wong et al., 2001). These results suggest that RhoA signalling is necessary for neuronal migration *in vivo* and *in vitro*. Controversially, RhoA KO mice did not show any impairment in chain migration through the RMS (Cappello et al., 2012). RhoA KO mice showed impaired radial neuronal migration in the neocortex and developed subcortical band heterotopia. However, impaired radial migration was mainly caused by the disrupted radial scaffold of radial glial cells since RhoA knockout neurons transplanted into WT neocortex can migrate normally (Cappello et al., 2012). These results suggest that RhoA activity is not necessary for both radial migration in the neocortex and tangential chain migration in the RMS, which is not in line with previous findings. This may be

partially explained by that the function of RhoA can be compensated by other Rho family proteins such as RhoB and RhoC, which share many effectors with RhoA including ROCK, suggesting potentially overlapping functions. Supporting this hypothesis, RhoA conditional knockout in the developing brain resulted in significantly increased expression of RhoB and RhoC (Mulherkar et al., 2013). Furthermore, mounting evidence suggests the existence of compensation mechanisms: RhoA and RhoC can compensate each other's function in regulating MLC phosphorylation and stress fibre formation (Simpson et al., 2004); RhoA and RhoB may mutually compensate each other's function in regulating cell shape and motility (Königs et al., 2014); Loss of RhoA causes increased Rho signalling via overcompensation by RhoB (García-Mariscal et al., 2017).

While the function of RhoA in neuronal migration is controversial, the downstream effectors of Rho signalling are important for proper neuronal migration. Two major downstream effectors of RhoA that mediate cytoskeleton regulation are ROCKs and the Diaphanous formin subfamily (Dia). mDia1/mDia3 double knockout mice showed smaller olfactory bulbs as a result of the disrupted chain migration of SVZ-derived neuroblasts. But the radial migration remains unaffected (Shinohara et al., 2012). ROCK knockdown by siRNA or ROCK inhibitor Y-27632 inhibited chain formation of neuroblast derived from SVZ explants, ROCK inhibitor reduced migration in the RMS in vivo (Leong et al., 2011; Shinohara et al., 2012). As a final downstream target of Rho signalling, myosin is also essential for neuronal migration. Myosin IIb KO mice display severe brain development abnormalities with related neuronal migration defects (Ma et al., 2007; Tullio et al., 2001). A single point mutation in the motor domain of myosin IIb inhibits the migration of multiple subtypes of neurons (Ma et al., 2004). Besides, blebbistatin, a selective inhibitor

of myosin II (Limouze et al., 2004), significantly inhibits neuronal migration in vitro (Schaar & McConnell, 2005). It is reasonable to speculate that impaired regulation of the actin cytoskeleton is the common mechanism behind these phenotypes.

In this study, I found that ASPP2 deletion resulted in the impaired formation of chain-like structure and migration of neuroblast in the RMS in vivo and in cultured RMS explants, which is similar to the phenotypes caused by mDia1/mDia3 deletion, ROCK deficiency and ROCK inhibitor, as described above. Dia collaborates with ROCK to induce actomyosin stress fibre formation. mDia1/ mDia3 knockout neuroblasts failed to form a cup-shaped actomyosin structure at the rear during nuclear translocation (Shinohara et al., 2012), which indicates that actomyosin formation is responsible for the deficient chain migration in the RMS caused by mDia1/ mDia3 deletion. Since ASPP2 deletion and mDia1/ mDia3 deletion cause similar cellular phenotypes, ASPP2 might also regulate the chain migration of neuroblasts through regulating actomyosin activity.

ASPP2 deficiency also impaired radial migration in the neocortex while mDia1/mDia3 deletion had no effect on radial migration. This suggests that ASPP2 influences radial migration by utilizing extra Dia independent mechanisms. mDia1/ mDia3 knockout neuroblasts did not show apparent abnormality in cage-like microtubule structure around the nucleus, suggesting mDia have no significant effect on microtubule regulation during neuronal migration. However, ROCK has been shown to control microtubule dynamics via the phosphorylation of Tubulin Polymerization Promoting Protein 1 (TPPP1) to promote cell migration (Breuzard et al., 2019; Schofield et al., 2012). Therefore, ASPP2 might

regulate radial migration through ROCK-mediated microtubule dynamics apart from regulating actomyosin.

Besides, the Par complex-mediated regulation of microtubule might also be involved in impaired neuronal migration caused by loss of ASPP2. Par3 has been shown to interact with the microtubule minus-end motor dynein and Par3 knockdown disrupted the position of the centrosome at the cell centre during migration (Schmoranzer et al., 2009), which is critical for nuclear translocation because the centrosome serves as a microtubule-organizing centre between microtubule in the leading edge and the perinuclear microtubule cage. Loss of Par3 disturbed neural crest migration by reducing microtubule catastrophe (Moore et al., 2013). Silencing Par3 in the developing cerebral cortex by *in utero* electroporation resulted in the accumulation of multipolar neurons in the intermediate zone (IZ), suggesting that impaired migration was most probably caused by defects in the multipolar to bipolar transition (Funahashi et al., 2013).

6.3 ASPP2 in developing periventricular nodular heterotopia (PNH).

Based on the localization of ectopic neurons, grey matter heterotopia can be classified into periventricular nodular heterotopia (PNH) and subcortical band heterotopia (SBH). As indicated by the names, PNH is characterized by nodular clusters of neurons that locate at the surface of ventricular walls and protrude into the lumen while SBH is characterized by a packaged band of neurons beneath the cerebral cortex. Although the causes of grey matter heterotopia are not yet fully elucidated, it may result from a diversity of alterations of cellular processes such as neuronal migration, radial glial scaffold, the proliferation of progenitors, although the final phenotype can be read as a migration defect.

Growing evidence supports that SBH may mainly result from an alteration of neural progenitors. Four rodent model including spontaneous HeCo mice (Eml1 mutant), spontaneous tish rat, RhoA$^{-/-}$ cKO (Emx1:Cre-RhoA$^{fl/fl}$) mice, and Par3$^{-/-}$ cKO (Emx1:Cre-Par3$^{fl/fl}$) mice shared a similar progenitor related phenotype: ectopic progenitors in the intermediate zone (IZ) and the cortical plate (CP) displaying increased proliferation (Cappello et al., 2012； Croquelois et al., 2008； W. A. Liu et al., 2018； Fitzgerald et al., 2011). A model of the formation of SBH has been proposed: excessively proliferating progenitor cells may form a broad band in the middle of the cortical wall, from which the neurons separate into two bands either toward the cortical plate or the ventricular zone. The latter gives rise to SBH. However, the causes of ectopic progenitor cells outside of VZ/SVZ are different: In RhoA cKO mice, ectopic progenitors may be a result of radial glial cells (RGCs) losing their apical anchoring. Disorganized radial fibres of RGCs were also observed (Cappello et al., 2012). In HeCo mice, mislocalized progenitors were not associated with adherens junction breakdown or loss of RGCs polarity in the VZ. Abnormal spindle orientations in dividing RGCs, which indicates abnormal division mode of RGCs, might be the cause (Croquelois et al., 2008). In Par3 cKO mice, although junction defects were observed at the late neurogenic stage, there was no drastic global disorganization of the VZ and radial fibres of RGCs were normal (W. A. Liu et al., 2018). The authors proposed that the over-proliferation of RGCs caused by increased symmetric division in the early neurogenic phase was responsible for the ectopic progenitors (W. A. Liu et al., 2018). In spontaneous tish rat, adherens junction of RGCs and the integrity of VZ were maintained. Increased proliferation of ectopic progenitors has been proposed to be a consequence of their mislocalization rather than a cell-autonomous defect. The cause of

ectopic progenitors remains unclear (Fitzgerald et al., 2011). These results showed that ectopic progenitors can be caused by loss of apical anchoring of RGCs or simply as a consequence of overproduction caused by abnormal switches in division mode.

The mechanism involved in the genesis of PNH remains elusive although it is widely accepted that it results from a defective migration of neurons which remain blocked in the ventricular (VZ)–subventricular zone (SVZ). Defective migration of neurons could be caused by several mechanisms including disruption of the neuroepithelium, abnormal differentiation of new-born neurons in the VZ/SVZ, and cell-autonomous impairment of cell movement machinery.

Interestingly, the deletion of RhoA and Par3, whose functions are likely to be influenced by ASPP2, resulted in SBH in mice. Whereas *Aspp2-KO* mice developed PNH. Similar to *Rhoa* and *Par3* KO mice, *Aspp2-KO* mice showed ectopic localization of progenitors in the IZ and the CP. However, the underlying mechanisms are different. Unlike *Rhoa* KO mice, the integrity of VZ was maintained at E15.5 in *Aspp2-KO* Balb/c embryos, suggesting that ectopic localization of progenitors maybe not caused by loss of apical anchoring of RGCs, even though ASPP2 deletion has been shown to cause loss of the planer cell polarity at the ganglionic eminence as early as E13.5 under the C57/BL6-J129 mixed background (Sottocornola et al., 2010a). Interestingly, ASPP2 deficiency resulted in the randomization of spindle orientation in dividing RGCs and increased asymmetric division at the peak of neurogenesis, during which an RGC can either undergo symmetric division to generate two RGCs or undergo asymmetric division to produce one RGC and one intermediate progenitor. This division mode switch resulted in increased production of intermediate

progenitors with the cost of symmetric self-renewal of RGCs. This effect caused by ASPP2 deletion is different from that caused by Par3 removal. Par3 removal led to a switch in RGCs division mode from asymmetric neurogenic division to symmetric proliferative division at the early neurogenetic phase, during which an RGC can either undergo symmetric division to generate two RGCs or undergo asymmetric division to produce one RGC and one neuron. This division mode switch resulted in progressive overproduction of RGCs at the early phase of cortical neurogenesis and the concomitant loss of early-born deep-layer neurons (W. A. Liu et al., 2018). Can ASPP2 affect the division mode of RGCs at the early phase of neurogenesis? It has been reported that a comparable amount of $Foxp2^+$ early-born deep layer neurons was detected in the correct layer in the *Aspp2-KO* cortex while $SMI32^+$ late-born neurons were mislocalized (Sottocornola et al., 2010a), suggesting neurogenesis at the early phase was not affected by ASPP2.

Why did the ectopic progenitors in *Aspp2-KO* neocortex eventually fail to form SBH? Firstly, the increased intermediate progenitors in *Aspp2-KO* neocortex were at the cost of consuming the RGC pool, which might be not able to generate enough progenitors for late-stage neurogenesis. However, the RGC pool was expanded at the early phase already in the Par3 knockout neocortex. Secondly, the increased number of NPCs may be cancelled out by increased apoptosis in *Aspp2-KO* embryos as discussed before. Thirdly, the ectopic progenitors underwent excessive proliferation in the Par3 knockout neocortex. Simultaneous deletion of YAP and TAZ in Par3 knockout mice fully suppressed the overproduction of progenitors and the formation of SBH, suggesting the excessive proliferation of progenitors outside of VZ/SVZ was highly dependent on YAP and TAZ, which are well-known transcriptional cofactors downstream the Hippo pathway promoting

cell proliferation. ASPP2 is known to recruit PP1 to dephosphorylate YAP and TAZ, which is necessary for their nuclear translocation. YAP/TAZ activity may be inhibited in ASPP2-deficient progenitors therefore they cannot undergo excessive proliferation before they differentiated into postmitotic neurons.

How does ASPP2 deficiency lead to the formation of PVH? By summarizing the revealed roles of ASPP2 in regulating cell polarity, the proliferation of NSCs, neuronal migration, and actomyosin activity, I propose the following model:

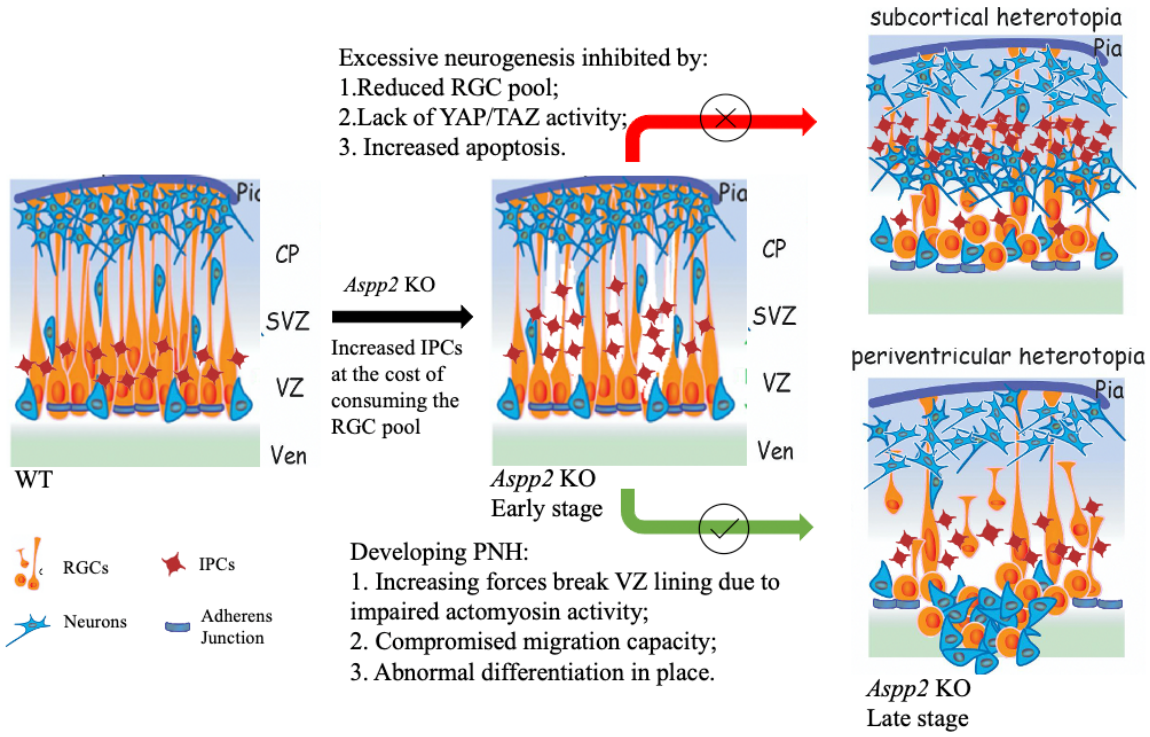


Figure 6. 1 Proposed model of how *Aspp2-KO* mice develop PNH.

The biological significance of ASPP2-Par3 interaction may be more predominant in regulating the proliferation of NSCs than in maintaining the integrity of the VZ. While Par3 was deleted in RGCs, no obvious defects in junction organization and centrosome

localization at the VZ surface were observed until E15.5. Even though, Par3 KO neocortex showed no drastic global disorganization of the VZ, which is quite different from severe disruption of the junction and VZ caused by loss of adherens junction proteins such as cadherin and catenin (Gil-Sanz et al., 2014; Schmid et al., 2014). *Aspp2-KO* neocortex showed no obvious disruption of the VZ at E15.5 in Balb/c mice. This may be partially explained by that RGCs only contain adherens junctions but not tight junctions to maintain the attachment between their endfeet at the VZ surface. ASPP2 and Par3 colocalize with ZO-1 to promote the formation of tight junctions in epithelial cells. This function might be less important in RGCs. However, ASPP2 might play an essential role in reinforcing junctional adhesive strength at the VZ surface through regulating actomyosin activity at later developmental stages. As brain development precedes, the neuroepithelium needs to be more and more resistant to rising tensile forces from increasing cerebrospinal fluid (CSF) volume and mechanical force associated with the expansion of the cortex. Actomyosin activity dynamically responds to tension at the junction through regulating actin remodelling (Priya & Yap, 2015; Yap et al., 2018), thereby is essential for ensuring the stability of adherens junctions. *Aspp2-KO* RGCs may exhibit compromised adherens junctions due to impaired actomyosin activity, which makes it challenging for them to buffer the increasing forces, especially with the presence of hydrocephalus in *Aspp2-KO* embryos. ASPP2 deficiency leads to increased production of progenitor cells caused by randomization of spindle orientation of dividing RGCs, and subsequent overproduction of neurons. Importantly, the migration capacity of these neurons is also impaired by ASPP2 removal, probably due to impaired actomyosin activity as well. Actomyosin contractility has been shown to play central roles in various steps of neuronal migration such as initiating radial migration by promoting the abscission of new-born neurons from the VZ (Das &

Storey, 2014), generating traction force for nucleus movement and soma translocation (He et al., 2010; Solecki et al., 2009; Trivedi et al., 2017; Umeshima et al., 2019), and pushing the cell body forward during retraction of the trailing tail (Bellion, 2005; Martini & Valdeolmillos, 2010; Schaar & McConnell, 2005). Furthermore, the migration defect may be a result of abnormal differentiation of new-born neurons in the VZ/SVZ. It has been reported that there were Tuj-1 positive cells in the VZ/SVZ in *Aspp2-KO* embryos at E14.5 (Sottocornola et al., 2010a) suggesting premature differentiation. In conclusion, a weakened ventricular lining at later neurodevelopmental stages could allow differentiated neurons or/and neurons with compromised migration capacity to form clumps around the ventricles, which eventually develop into PNH.

Human ASPP2 has been reported to be responsible for the central nervous system defects in 1q41q42 microdeletion syndrome which including neural tube defects (NTDs), agenesis of the corpus callosum, microcephaly, and hydrocephalus. However, no patient developed heterotopia. This may be partially due to heterozygous deletions of ASPP2 in these patients. Also, although rodents and humans share most of the mechanisms of brain development, the development of a gyrated human cortex involves far more complex processes. During human cortex development, a unique group of progenitor cells (oRGs) located at the outer SVZ undergo both symmetric and self-renewing asymmetric divisions to generate additional neurons for the outer cortical layers (Hansen et al., 2010; Lui et al., 2011). Neurons also have to migrate a much longer way. Taking these differences into account, it is not shocking to see that some animal models created by deleting causative genes found in human heterotopia patients such as DCX and LIS1 fail to reproduce heterotopia

phonotype. Also, genes being proved to cause heterotopia in rodents such as RhoA, Par3, and Rapgef2 are not identified in human patients.

Grey matter heterotopia is often associated with epilepsy in human patients. Seizures were found to start from heterotopic nodules or the surrounding anatomically unaltered cortical regions (Dubeau et al., 1995; Stefan et al., 2007). Spontaneous seizures have been occasionally found in *Aspp2-KO* adult mice, suggesting *Aspp2-KO* mice could be PNH models for studying the origin and propagation of epileptiform activity.

6.4 Drawbacks and Future directions

6.4.1 The CNS phenotypes caused by loss of ASPP2 were not comprehensively characterized.

Besides the PNH and the diminished olfactory bulb, Balb/C *Aspp2-KO* mice also showed other structural abnormalities of the CNS including enlarged cortexes, enlarged inferior and superior colliculus, and possible diminished cerebellar and altered foliation pattern in the vermis.

In theory, brain enlargement can be caused by many mechanisms such as increased production of neurons and/or astrocytes, the increased cell size of astrocytes, and decreased cell death. ASPP2 has been shown to inhibit the proliferation of NSCs/NPCs as indicated by increased mitotic index in the E11.5 neural tube and the E13.5 ganglionic eminence in *Aspp2-KO* embryos (Sottocornola et al., 2010b). This result suggests that increased neurogenesis may contribute to brain enlargement. However, quantification of the βIII

tubulin-positive cells in the cortex showed an overall reduction in the number of differentiated neurons in E14.5 *Aspp2-KO* embryos (Sottocornola et al., 2010b), which suggests that enlargement of the neocortex is not directly caused by the increased number of neurons. Why did not increased proliferation of NSCs/NPCs results in the increased number of neurons in the cortex? The answer might be increased apoptosis. Apoptosis of developing neural precursor cells, differentiated postmitotic neurons and glial cells occur extensively during the normal development of CNS and this mechanism of cell death is important for establishing neuronal and glial populations of the correct size (Fricker et al., 2018). ASPP2 is widely known to enhance p53-mediated apoptosis. Interestingly, the number of apoptotic cells detected in the *Aspp2-KO* ganglionic eminence was higher than that detected in the wild-type counterpart (Sottocornola et al., 2010b). This phenomenon may be explained by compensatory enhanced apoptosis triggered by the accumulation of excessive NPCs. Besides increased apoptosis, impaired neuronal migration revealed by this thesis can also provide another explanation that neurons generated in the VZ/SVZ, especially late-born neurons, failed to migrate into the neocortex in *Aspp2-KO* mice. Similarly, the diminished olfactory bulbs in *Aspp2-KO* mice could be caused by impaired neuronal migration or/and increased cell death in the olfactory bulb. Whether increased cell death is involved in this phenotype remains unknown. This question can be easily addressed by quantifying the apoptotic neuroblasts (DCX+ Caspase3+) in the RMS and the olfactory bulbs in wild-type and *Aspp2-KO* mice. In addition to neurons, I also investigated the influence of ASPP2 deficiency on astrocytes. I quantified the number of astrocytes and compared the sizes of astrocytes in the cortex of wild-type and *Aspp2-KO* mice at P10. The results suggested that ASPP2 deficiency did not change the number and size of astrocytes.

The phenotype of enlarged inferior and superior colliculus was consistent across all the *Aspp2-KO* mice examined. However, the mechanism behind remains unknown and it needs to be addressed in the future. Regarding the phenotype of diminished cerebellar and altered foliation pattern in the vermis, I did not systemically evaluate the size of the cerebellar and the foliation pattern, so this phenotype needs to be validated in the future.

6.4.2 The role of ASPP2 in regulating migratory behaviors of neurons needs further investigation.

During brain development, there are mainly three modes of migration: radial migration of excitatory projection neurons from the VZ/SVZ to the cerebral cortex, tangential migration of inhibitory interneurons from the medial ganglionic eminence (MGE) to the cerebral cortex, and chain migration of neuroblasts in the RMS. This study revealed that ASPP2 deficiency resulted in the impaired radial migration to the cerebral cortex and chain migration in the RMS. However, whether ASPP2 is involved in tangential migration remains to be investigated. I did try to address this question by doing IHC staining of GAD67, which is a marker of the interneuron, on brain sections from E15.5 WT and *Aspp2-KO* embryos. Unfortunately, I failed to get any conclusive data because of the poor signal of GAD67 staining. Indeed, there are better ways to visualize tangential migration such as electroporating GFP-expression plasmids into the MGE to label newborn interneurons. I did *Ex Utero* electroporation on E14.5 embryos and I found it difficult to deliver plasmids into the MGE by precisely placing the electrodes tweezer. Most of my experiments ended up with no GFP signal in the MGE. In the future, focal electroporation on brain slices can be adapted to precisely deliver plasmids to the MGE. pCAG-CRE-GFP or pCAG-GFP

plasmids can be injected into the MGE in cultured brains slices from *Aspp2* $^{f/f}$ embryos at E14.5. Then, plasmids can be electroplated into the cells by placing the MGE in the middle of the electrodes. The migration of GFP-labelled neurons can be visualized by live imaging.

Similarly, live imaging can be used to further study the function of ASPP2 in regulating radial migration and chain migration. For example, focal electroporation of plasmids into the neocortex in cultured brain slices from E14.5 embryos and live imaging can visualize *ex vivo* radial migration. *In vivo* electroporation of plasmids into the lateral SVZ in P0 pups can label neuroblasts in the RMS. Those brains can be submitted to brain slice culturing for *ex vivo* live imaging or even *in vivo* live imaging by using state-of-art 3-photon microscopy.

One of the drawbacks of this study is that which steps of neuronal migration are affected by ASPP2 deletion is not addressed. Does ASPP2 mainly affect the soma translocation which relies heavily on actomyosin activity or the leading process extension that requires dynamic actin organization or it can also affect centrosome migration? Those important questions can be answered through live imaging (*in vivo, ex vivo,* or *in vitro*) and motion analysis which allows monitoring the migration pattern and cellular behaviours such as leading process extension and trailing process retraction.

6.4.3 There is a gap between molecular mechanism identified in U2OS cells and the mouse phenotypes.

I found ASPP2 deficiency resulted in the impaired migration of neuroblasts in the RMS, which resulted in the diminished olfactory bulb. ASPP2 deficiency also impaired radial neuronal migration in the neocortex leading to periventricular nodular heterotopia (PNH). Then I revealed that ASPP2 physically interacted with ROCK2 and potentiated its phospho-kinase activity towards MYPT1 and MLC2, thus positively regulating RhoA-mediated actomyosin stress fibre formation and cell migration in U2OS cells. However, this mechanism has not been validated neither in cultured neuronal cells nor in mouse brain. In the future, this gap needs to be filled.

First, it is worthy to test whether ASPP2 can also interact with ROCK and potentiate the phosphorylation of MYPT1 and MLC2 in neuronal cell lines such as Neuro2A or SH-SY5Y. Since it would be difficult to generate stable *Aspp2-KO* neuronal cell lines, those experiments can be performed using *Aspp2* siRNA. Besides, primary neuroblasts can be cultured from mouse RMS tissue. The phosphorylation of MLC2 in cultured WT and *Aspp2-KO* neuroblasts or brain tissues can be evaluated by IF staining or Western Blot, respectively.

Second, it is critical to validate that Aspp2 can influence actin organization both in neuroblasts and in mouse brain tissue. The dynamic of the actin cytoskeleton in cultured WT and *Aspp2-KO* neuroblasts can be monitored by live imaging. This can be achieved by using commercially available biosensors binding cytoskeleton such as SiR-actin, which are cell-permeable small silicon rhodamine-based fluorogenic molecules that increase their

fluorescence up to 100x fold when bound to F-actin (Lukinavičius et al., 2014). To study whether ASPP2 can influence actin organization in vivo, the F-actin / G-actin ratio in WT and *Aspp2-KO* brain tissues can be measured by busing G-Actin/F-Actin separation kit followed by Western Blot.

Another drawback of this study is that how ASPP2 regulates ROCK2 activity are not fully understood. I found ASPP2 regulate ROCK activity in a PP1 dependent manner, which suggests that the phosphorylation of ROCK can be can altered by ASPP2. I found that phosphorylation of ROCK2 at Ser1366, which has been shown to positively reflect the activation of ROCK2, was not affected by the loss of ASPP2. Ser1377 of ROCK2 was identified as an ASPP2-sensitive phosphosite by mass spectrometry. However, the biological function of this phosphosite remains unknown. Mutant ROCK2, such as S1377A which can not be phosphorylated or S1377E which is constitutively active, can be used to test whether phosphorylation at this residue is involved in regulating ROCK2 activity.

Reference

Agirre, X., Román-Gómez, J., Jiménez-Velasco, A., Garate, L., Montiel-Duarte, C., Navarro, G., Vázquez, I., Zalacain, M., Calasanz, M. J., Heiniger, A., Torres, A., Minna, J. D., & Prósper, F. (2006). ASPP1, a common activator of TP53, is inactivated by aberrant methylation of its promoter in acute lymphoblastic leukemia. *Oncogene*. https://doi.org/10.1038/sj.onc.1209236

Amano, M., Ito, M., Kimura, K., Fukata, Y., Chihara, K., Nakano, T., Matsuura, Y., & Kaibuchi, K. (1996). Phosphorylation and Activation of Myosin by Rho-associated Kinase (Rho-kinase). *Journal of Biological Chemistry*, *271*(34), 20246–20249. https://doi.org/10.1074/jbc.271.34.20246

Anda, F. (2013). Organotypic Slice Culture of Embryonic Brain Sections. *BIO-PROTOCOL*, *3*(3). https://doi.org/10.21769/bioprotoc.327

Anderson, S. A. (1997). Interneuron Migration from Basal Forebrain to Neocortex: Dependence on Dlx Genes. *Science*, *278*(5337), 474–476. https://doi.org/10.1126/science.278.5337.474

Androutsellis-Theotokis, A., Leker, R. R., Soldner, F., Hoeppner, D. J., Ravin, R., Poser, S. W., Rueger, M. A., Bae, S.-K., Kittappa, R., & McKay, R. D. G. (2006). Notch signalling regulates stem cell numbers in vitro and in vivo. *Nature*, *442*(7104), 823–826. https://doi.org/10.1038/nature04940

Ang, E. S. B. C., Haydar, T. F., Gluncic, V., & Rakic, P. (2003). Four-Dimensional Migratory Coordinates of GABAergic Interneurons in the Developing Mouse Cortex. *The Journal of Neuroscience*, *23*(13), 5805–5815. https://doi.org/10.1523/jneurosci.23-13-05805.2003

Bai, J., Ramos, R. L., Ackman, J. B., Thomas, A. M., Lee, R. V, & LoTurco, J. J. (2003). RNAi reveals doublecortin is required for radial migration in rat neocortex. *Nature Neuroscience*, *6*(12), 1277–1283. https://doi.org/10.1038/nn1153

Barkovich, A. J., Guerrini, R., Kuzniecky, R. I., Jackson, G. D., & Dobyns, W. B. (2012). A developmental and genetic classification for malformations of cortical development: update 2012. *Brain : A Journal of Neurology*, *135*(Pt 5), 1348–1369. https://doi.org/10.1093/brain/aws019

Bellion, A. (2005). Nucleokinesis in Tangentially Migrating Neurons Comprises Two

Alternating Phases: Forward Migration of the Golgi/Centrosome Associated with Centrosome Splitting and Myosin Contraction at the Rear. *Journal of Neuroscience*, *25*(24), 5691–5699. https://doi.org/10.1523/jneurosci.1030-05.2005

Benton, R., & Johnston, D. S. (2003). Drosophila PAR-1 and 14-3-3 Inhibit Bazooka/PAR-3 to Establish Complementary Cortical Domains in Polarized Cells. *Cell*, *115*(6), 691–704. https://doi.org/10.1016/s0092-8674(03)00938-3

Benveniste, H., Kim, K., Zhang, L., & Johnson, G. A. (2000). Magnetic resonance microscopy of the C57BL mouse brain. *NeuroImage*. https://doi.org/10.1006/nimg.2000.0567

Berg, A. T., Tarquinio, D., & Koh, S. (2017). Early Life Epilepsies are a Comorbidity of Developmental Brain Disorders. *Seminars in Pediatric Neurology*. https://doi.org/10.1016/j.spen.2017.10.008

Bergamaschi, D., Samuels, Y., Jin, B., Duraisingham, S., Crook, T., & Lu, X. (2004). ASPP1 and ASPP2: common activators of p53 family members. *Molecular and Cellular Biology*, *24*(3), 1341–1350. https://doi.org/10.1128/mcb.24.3.1341-1350.2004

Bertran, M. T., Mouilleron, S., Zhou, Y., Bajaj, R., Uliana, F., Kumar, G. S., van Drogen, A., Lee, R., Banerjee, J. J., Hauri, S., O'Reilly, N., Gstaiger, M., Page, R., Peti, W., & Tapon, N. (2019). ASPP proteins discriminate between PP1 catalytic subunits through their SH3 domain and the PP1 C-tail. *Nature Communications*. https://doi.org/10.1038/s41467-019-08686-0

Betizeau, M., Cortay, V., Patti, D., Pfister, S., Gautier, E., Bellemin-Ménard, A., Afanassieff, M., Huissoud, C., Douglas, R. J., Kennedy, H., & Dehay, C. (2013). Precursor Diversity and Complexity of Lineage Relationships in the Outer Subventricular Zone of the Primate. *Neuron*. https://doi.org/10.1016/j.neuron.2013.09.032

Betschinger, J., Mechtler, K., & Knoblich, J. A. (2003). The Par complex directs asymmetric cell division by phosphorylating the cytoskeletal protein Lgl. *Nature*, *422*(6929), 326–330. https://doi.org/10.1038/nature01486

Bradley, D., & Beltrao, P. (2019). Evolution of protein kinase substrate recognition at the active site. *PLoS Biology*. https://doi.org/10.1371/journal.pbio.3000341

Breuzard, G., Pagano, A., Bastonero, S., Malesinski, S., Parat, F., Barbier, P., Peyrot, V.,

& Kovacic, H. (2019). Tau regulates the microtubule-dependent migration of glioblastoma cells via the Rho-ROCK signaling pathway. *Journal of Cell Science*, *132*(3), jcs222851. https://doi.org/10.1242/jcs.222851

Brown, J. P., Couillard-Després, S., Cooper-Kuhn, C. M., Winkler, J., Aigner, L., & Kuhn, H. G. (2003). Transient expression of doublecortin during adult neurogenesis. *Journal of Comparative Neurology*, *467*(1), 1–10. https://doi.org/10.1002/cne.10874

Bultje, R. S., Castaneda-Castellanos, D. R., Jan, L. Y., Jan, Y.-N., Kriegstein, A. R., & Shi, S.-H. (2009). Mammalian Par3 regulates progenitor cell asymmetric division via notch signaling in the developing neocortex. *Neuron*, *63*(2), 189–202. https://doi.org/10.1016/j.neuron.2009.07.004

Buti, L., Ruiz-Puig, C., Sangberg, D., Leissing, T. M., Brewer, R. C., Owen, R. P., Sgromo, B., Royer, C., Ebner, D., & Lu, X. (2020). CagA–ASPP2 complex mediates loss of cell polarity and favors H. pylori colonization of human gastric organoids. *Proceedings of the National Academy of Sciences*, *117*(5), 2645–2655. https://doi.org/10.1073/pnas.1908787117

Cannaerts, E., Shukla, A., Hasanhodzic, M., Alaerts, M., Schepers, D., Van Laer, L., Girisha, K. M., Hojsak, I., Loeys, B., & Verstraeten, A. (2018). FLNA mutations in surviving males presenting with connective tissue findings: two new case reports and review of the literature. *BMC Medical Genetics*, *19*(1), 140. https://doi.org/10.1186/s12881-018-0655-0

Canning, P., von Delft, F., & Bullock, A. N. (2012). Structural basis for ASPP2 recognition by the tumor suppressor p73. *Journal of Molecular Biology*, *423*(4), 515–527. https://doi.org/10.1016/j.jmb.2012.08.005

Cappello, S., Böhringer, C. R. J., Bergami, M., Conzelmann, K.-K., Ghanem, A., Tomassy, G. S., Arlotta, P., Mainardi, M., Allegra, M., Caleo, M., van Hengel, J., Brakebusch, C., & Götz, M. (2012). A Radial Glia-Specific Role of RhoA in Double Cortex Formation. *Neuron*, *73*(5), 911–924. https://doi.org/10.1016/j.neuron.2011.12.030

Cappello, S., Gray, M. J., Badouel, C., Lange, S., Einsiedler, M., Srour, M., Chitayat, D., Hamdan, F. F., Jenkins, Z. A., Morgan, T., Preitner, N., Uster, T., Thomas, J., Shannon, P., Morrison, V., Di Donato, N., Van Maldergem, L., Neuhann, T., Newbury-Ecob, R., … Robertson, S. P. (2013). Mutations in genes encoding the

cadherin receptor-ligand pair DCHS1 and FAT4 disrupt cerebral cortical development. *Nature Genetics*. https://doi.org/10.1038/ng.2765

Carabalona, A., Beguin, S., Pallesi-pocachard, E., Buhler, E., Pellegrino, C., Arnaud, K., Hubert, P., Oualha, M., Siffroi, J. P., Khantane, S., Coupry, I., Goizet, C., Gelot, A. B., Represa, A., & Cardoso, C. (2012). A glial origin for periventricular nodular heterotopia caused by impaired expression of Filamin-A. *Human Molecular Genetics*. https://doi.org/10.1093/hmg/ddr531

Cardoso, C., Boys, A., Parrini, E., Mignon-Ravix, C., McMahon, J. M., Khantane, S., Bertini, E., Pallesi, E., Missirian, C., Zuffardi, O., Novara, F., Villard, L., Giglio, S., Chabrol, B., Slater, H. R., Moncla, A., Scheffer, I. E., & Guerrini, R. (2008). Periventricular heterotopia, mental retardation, and epilepsy associated with 5q14.3-q15 deletion. *Neurology*, *72*(9), 784–792. https://doi.org/10.1212/01.wnl.0000336339.08878.2d

Caspi, M., Atlas, R., Kantor, A., Sapir, T., & Reiner, O. (2000). Interaction between LIS1 and doublecortin, two lissencephaly gene products. *Human Molecular Genetics*, *9*(15), 2205–2213. https://doi.org/10.1093/oxfordjournals.hmg.a018911

Cellini, E., Disciglio, V., Novara, F., Barkovich, J. A., Mencarelli, M. A., Hayek, J., Renieri, A., Zuffardi, O., & Guerrini, R. (2012). Periventricular heterotopia with white matter abnormalities associated with 6p25 deletion. *American Journal of Medical Genetics Part A*, *158A*(7), 1793–1797. https://doi.org/10.1002/ajmg.a.35416

Chenette, E. J., & Der, C. J. (2011). Lipid Modification of Ras Superfamily GTPases. In *Protein Prenylation PART A* (pp. 59–95). Elsevier. https://doi.org/10.1016/b978-0-12-381339-8.00005-6

Chu, J., Pham, N. T., Olate, N., Kislitsyna, K., Day, M.-C., LeTourneau, P. A., Kots, A., Stewart, R. H., Laine, G. A., Cox Jr, C. S., & Uray, K. (2013). Biphasic regulation of myosin light chain phosphorylation by p21-activated kinase modulates intestinal smooth muscle contractility. *The Journal of Biological Chemistry*, *288*(2), 1200–1213. https://doi.org/10.1074/jbc.M112.370718

Chuang, H. H., Yang, C. H., Tsay, Y. G., Hsu, C. Y., Tseng, L. M., Chang, Z. F., & Lee, H. H. (2012). ROCKII Ser 1366 phosphorylation reflects the activation status. *Biochemical Journal*. https://doi.org/10.1042/BJ20111839

Cobleigh, M. A., Tabesh, B., Bitterman, P., Baker, J., Cronin, M., Liu, M.-L., Borchik,

R., Mosquera, J.-M., Walker, M. G., & Shak, S. (2005). Tumor Gene Expression and Prognosis in Breast Cancer Patients with 10 or More Positive Lymph Nodes. *Clinical Cancer Research*, *11*(24), 8623–8631. https://doi.org/10.1158/1078-0432.ccr-05-0735

Cong, W., Hirose, T., Harita, Y., Yamashita, A., Mizuno, K., Hirano, H., & Ohno, S. (2010). ASPP2 Regulates Epithelial Cell Polarity through the PAR Complex. *Current Biology*, *20*(15), 1408–1414. https://doi.org/10.1016/j.cub.2010.06.024

Conti, M. A., & Adelstein, R. S. (2008). Nonmuscle myosin II moves in new directions. *Journal of Cell Science*, *121*(1), 11–18. https://doi.org/10.1242/jcs.007112

Conti, V., Carabalona, A., Pallesi-Pocachard, E., Parrini, E., Leventer, R. J., Buhler, E., McGillivray, G., Michel, F. J., Striano, P., Mei, D., Watrin, F., Lise, S., Pagnamenta, A. T., Taylor, J. C., Kini, U., Clayton-Smith, J., Novara, F., Zuffardi, O., Dobyns, W. B., … Guerrini, R. (2013). Periventricular heterotopia in 6q terminal deletion syndrome: role of the C6orf70 gene. *Brain*, *136*(11), 3378–3394. https://doi.org/10.1093/brain/awt249

Cooper, J. A. (2013). Cell biology in neuroscience: mechanisms of cell migration in the nervous system. *The Journal of Cell Biology*, *202*(5), 725–734. https://doi.org/10.1083/jcb.201305021

Corbo, J. C., Deuel, T. A., Long, J. M., LaPorte, P., Tsai, E., Wynshaw-Boris, A., & Walsh, C. A. (2002). Doublecortin is required in mice for lamination of the hippocampus but not the neocortex. *The Journal of Neuroscience : The Official Journal of the Society for Neuroscience*, *22*(17), 7548–7557. https://doi.org/10.1523/JNEUROSCI.22-17-07548.2002

Cremer, H., Lange, R., Christoph, A., Plomann, M., Vopper, G., Roes, J., Brown, R., Baldwin, S., Kraemer, P., Scheff, S., Barthels, D., Rajewsky, K., & Wille, W. (1994). Inactivation of the N-CAM gene in mice results in size reduction of the olfactory bulb and deficits in spatial learning. *Nature*, *367*(6462), 455–459. https://doi.org/10.1038/367455a0

Croquelois, A., Giuliani, F., Savary, C., Kielar, M., Amiot, C., Schenk, F., & Welker, E. (2008). Characterization of the HeCo Mutant Mouse: A New Model of Subcortical Band Heterotopia Associated with Seizures and Behavioral Deficits. *Cerebral Cortex*, *19*(3), 563–575. https://doi.org/10.1093/cercor/bhn106

D'Agostino, M. D. (2002). Subcortical band heterotopia (SBH) in males: clinical, imaging and genetic findings in comparison with females. *Brain*, *125*(11), 2507–2522. https://doi.org/10.1093/brain/awf248

Das, R. M., & Storey, K. G. (2014). Apical abscission alters cell polarity and dismantles the primary cilium during neurogenesis. *Science (New York, N.Y.)*, *343*(6167), 200–204. https://doi.org/10.1126/science.1247521

Dehay, C., Kennedy, H., & Kosik, K. S. (2015). The Outer Subventricular Zone and Primate-Specific Cortical Complexification. In *Neuron*. https://doi.org/10.1016/j.neuron.2014.12.060

Dixon, K., Turbic, A., Turnley, A., & Liebl, D. (2017). Explant Methodology for Analyzing Neuroblast Migration. *BIO-PROTOCOL*. https://doi.org/10.21769/bioprotoc.2249

Dobyns, W. B. (2010). The clinical patterns and molecular genetics of lissencephaly and subcortical band heterotopia. *Epilepsia*, *51*, 5–9. https://doi.org/10.1111/j.1528-1167.2009.02433.x

Dubeau, F., Tampieri, D., Lee, N., Andermann, E., Carpenter, S., Leblanc, R., Olivier, A., Radtke, R., Villemure, J. G., & Andermann, F. (1995). Periventricular and subcortical nodular heterotopia. A study of 33 patients. *Brain*. https://doi.org/10.1093/brain/118.5.1273

Dvorsky, R., Blumenstein, L., Vetter, I. R., & Ahmadian, M. R. (2004). Structural Insights into the Interaction of ROCKI with the Switch Regions of RhoA. *Journal of Biological Chemistry*, *279*(8), 7098–7104. https://doi.org/10.1074/jbc.m311911200

Egloff, M.-P. (1997). Structural basis for the recognition of regulatory subunits by the catalytic subunit of protein phosphatase 1. *The EMBO Journal*, *16*(8), 1876–1887. https://doi.org/10.1093/emboj/16.8.1876

El-Hashash, A. H., & Warburton, D. (2011). Cell polarity and spindle orientation in the distal epithelium of embryonic lung. *Developmental Dynamics : An Official Publication of the American Association of Anatomists*, *240*(2), 441–445. https://doi.org/10.1002/dvdy.22551

Feng, Y., Chen, M. H., Moskowitz, I. P., Mendonza, A. M., Vidali, L., Nakamura, F., Kwiatkowski, D. J., & Walsh, C. A. (2006). Filamin a (FLNA) is required for cell-cell contact in vascular development and cardiac morphogenesis. *Proceedings of the*

National Academy of Sciences of the United States of America. https://doi.org/10.1073/pnas.0609628104

Ferland, R. J., Gaitanis, J. N., Apse, K., Tantravahi, U., Walsh, C. A., & Sheen, V. L. (2006). Periventricular nodular heterotopia and Williams syndrome. *American Journal of Medical Genetics Part A*, *140A*(12), 1305–1311. https://doi.org/10.1002/ajmg.a.31259

Fietz, S. A., Lachmann, R., Brandl, H., Kircher, M., Samusik, N., Schroder, R., Lakshmanaperumal, N., Henry, I., Vogt, J., Riehn, A., Distler, W., Nitsch, R., Enard, W., Paäbo, S., & Huttner, W. B. (2012). Transcriptomes of germinal zones of human and mouse fetal neocortex suggest a role of extracellular matrix in progenitor self-renewal. *Proceedings of the National Academy of Sciences of the United States of America*. https://doi.org/10.1073/pnas.1209647109

Fitzgerald, M. P., Covio, M., & Lee, K. S. (2011). Disturbances in the positioning, proliferation and apoptosis of neural progenitors contribute to subcortical band heterotopia formation. *Neuroscience*, *176*, 455–471. https://doi.org/10.1016/j.neuroscience.2010.12.003

Fogal, V., Kartasheva, N. N., Trigiante, G., Llanos, S., Yap, D., Vousden, K. H., & Lu, X. (2005). ASPP1 and ASPP2 are new transcriptional targets of E2F. *Cell Death & Differentiation*, *12*(4), 369–376. https://doi.org/10.1038/sj.cdd.4401562

Fox, J. W., Lamperti, E. D., Ekşioğlu, Y. Z., Hong, S. E., Feng, Y., Graham, D. A., Scheffer, I. E., Dobyns, W. B., Hirsch, B. A., Radtke, R. A., Berkovic, S. F., Huttenlocher, P. R., & Walsh, C. A. (1998). Mutations in filamin 1 prevent migration of cerebral cortical neurons in human Periventricular heterotopia. *Neuron*. https://doi.org/10.1016/S0896-6273(00)80651-0

Fricker, M., Tolkovsky, A. M., Borutaite, V., Coleman, M., & Brown, G. C. (2018). Neuronal cell death. In *Physiological Reviews*. https://doi.org/10.1152/physrev.00011.2017

Funahashi, Y., Namba, T., Fujisue, S., Itoh, N., Nakamuta, S., Kato, K., Shimada, A., Xu, C., Shan, W., Nishioka, T., & Kaibuchi, K. (2013). ERK2-mediated phosphorylation of Par3 regulates neuronal polarization. *The Journal of Neuroscience : The Official Journal of the Society for Neuroscience*, *33*(33), 13270–13285. https://doi.org/10.1523/JNEUROSCI.4210-12.2013

Gambello, M. J., Darling, D. L., Yingling, J., Tanaka, T., Gleeson, J. G., & Wynshaw-Boris, A. (2003). Multiple dose-dependent effects of Lis1 on cerebral cortical development. *The Journal of Neuroscience : The Official Journal of the Society for Neuroscience*, *23*(5), 1719–1729. https://doi.org/10.1523/JNEUROSCI.23-05-01719.2003

Gao, P., Postiglione, M. P., Krieger, T. G., Hernandez, L., Wang, C., Han, Z., Streicher, C., Papusheva, E., Insolera, R., Chugh, K., Kodish, O., Huang, K., Simons, B. D., Luo, L., Hippenmeyer, S., & Shi, S. H. (2014). Deterministic progenitor behavior and unitary production of neurons in the neocortex. *Cell*. https://doi.org/10.1016/j.cell.2014.10.027

García-Mariscal, A., Li, H., Pedersen, E., Peyrollier, K., Ryan, K. M., Stanley, A., Quondamatteo, F., & Brakebusch, C. (2017). Loss of RhoA promotes skin tumor formation and invasion by upregulation of RhoB. *Oncogene*, *37*(7), 847–860. https://doi.org/10.1038/onc.2017.333

Gil-Sanz, C., Landeira, B., Ramos, C., Costa, M. R., & Müller, U. (2014). Proliferative defects and formation of a double cortex in mice lacking Mltt4 and Cdh2 in the dorsal telencephalon. *The Journal of Neuroscience : The Official Journal of the Society for Neuroscience*, *34*(32), 10475–10487. https://doi.org/10.1523/JNEUROSCI.1793-14.2014

Gorina, S., & Pavletich, N. P. (1996). Structure of the p53 Tumor Suppressor Bound to the Ankyrin and SH3 Domains of 53BP2. *Science*, *274*(5289), 1001–1005. https://doi.org/10.1126/science.274.5289.1001

Guan, C., Xu, H., Jin, M., Yuan, X., & Poo, M. (2007). Long-Range Ca2+ Signaling from Growth Cone to Soma Mediates Reversal of Neuronal Migration Induced by Slit-2. *Cell*, *129*(2), 385–395. https://doi.org/10.1016/j.cell.2007.01.051

Guerrini, R., & Dobyns, W. B. (2014). Malformations of cortical development: clinical features and genetic causes. *The Lancet. Neurology*, *13*(7), 710–726. https://doi.org/10.1016/S1474-4422(14)70040-7

Hansen, D. V., Lui, J. H., Parker, P. R. L., & Kriegstein, A. R. (2010). Neurogenic radial glia in the outer subventricular zone of human neocortex. *Nature*. https://doi.org/10.1038/nature08845

Hao, Y., Du, Q., Chen, X., Zheng, Z., Balsbaugh, J. L., Maitra, S., Shabanowitz, J., Hunt,

D. F., & Macara, I. G. (2010). Par3 controls epithelial spindle orientation by aPKC-mediated phosphorylation of apical Pins. *Current Biology : CB*, *20*(20), 1809–1818. https://doi.org/10.1016/j.cub.2010.09.032

Hartfuss, E., Galli, R., Heins, N., & Götz, M. (2001). Characterization of CNS precursor subtypes and radial glia. *Developmental Biology*. https://doi.org/10.1006/dbio.2000.9962

He, M., Zhang, Z. -h., Guan, C. -b., Xia, D., & Yuan, X. -b. (2010). Leading Tip Drives Soma Translocation via Forward F-Actin Flow during Neuronal Migration. *Journal of Neuroscience*, *30*(32), 10885–10898. https://doi.org/10.1523/jneurosci.0240-10.2010

Hedenfalk, I., Duggan, D., Chen, Y., Radmacher, M., Bittner, M., Simon, R., Meltzer, P., Gusterson, B., Esteller, M., Raffeld, M., Yakhini, Z., Ben-Dor, A., Dougherty, E., Kononen, J., Bubendorf, L., Fehrle, W., Pittaluga, S., Gruvberger, S., Loman, N., … Trent, J. (2001). Gene-Expression Profiles in Hereditary Breast Cancer. *New England Journal of Medicine*. https://doi.org/10.1056/nejm200102223440801

Helps, N. R., Barker, H. M., Elledge, S. J., & Cohen, P. T. W. (1995). Protein phosphatase 1 interacts with p53BP2, a protein which binds to the tumour suppressor p53. *FEBS Letters*. https://doi.org/10.1016/0014-5793(95)01347-4

Hirota, Y., Ohshima, T., Kaneko, N., Ikeda, M., Iwasato, T., Kulkarni, A. B., Mikoshiba, K., Okano, H., & Sawamoto, K. (2007). Cyclin-dependent kinase 5 is required for control of neuroblast migration in the postnatal subventricular zone. *The Journal of Neuroscience : The Official Journal of the Society for Neuroscience*, *27*(47), 12829–12838. https://doi.org/10.1523/JNEUROSCI.1014-07.2007

Hirotsune, S., Fleck, M. W., Gambello, M. J., Bix, G. J., Chen, A., Clark, G. D., Ledbetter, D. H., McBain, C. J., & Wynshaw-Boris, A. (1998). Graded reduction of Pafah1b1 (Lis1) activity results in neuronal migration defects and early embryonic lethality. *Nature Genetics*, *19*(4), 333–339. https://doi.org/10.1038/1221

Hisata, S., Sakisaka, T., Baba, T., Yamada, T., Aoki, K., Matsuda, M., & Takai, Y. (2007). Rap1-PDZ-GEF1 interacts with a neurotrophin receptor at late endosomes, leading to sustained activation of Rap1 and ERK and neurite outgrowth. *The Journal of Cell Biology*, *178*(5), 843–860. https://doi.org/10.1083/jcb.200610073

Hitoshi, S., Alexson, T., Tropepe, V., Donoviel, D., Elia, A. J., Nye, J. S., Conlon, R. A.,

Mak, T. W., Bernstein, A., & van der Kooy, D. (2002). Notch pathway molecules are essential for the maintenance, but not the generation, of mammalian neural stem cells. *Genes & Development*, *16*(7), 846–858. https://doi.org/10.1101/gad.975202

Homma, N., Takei, Y., Tanaka, Y., Nakata, T., Terada, S., Kikkawa, M., Noda, Y., & Hirokawa, N. (2003). Kinesin Superfamily Protein 2A (KIF2A) Functions in Suppression of Collateral Branch Extension. *Cell*, *114*(2), 229–239. https://doi.org/10.1016/s0092-8674(03)00522-1

Horesh, D., Sapir, T., Francis, F., Grayer Wolf, S., Caspi, M., Elbaum, M., Chelly, J., & Reiner, O. (1999). Doublecortin, a Stabilizer of Microtubules. *Human Molecular Genetics*, *8*(9), 1599–1610. https://doi.org/10.1093/hmg/8.9.1599

Hu, H., Tomasiewicz, H., Magnuson, T., & Rutishauser, U. (1996). The Role of Polysialic Acid in Migration of Olfactory Bulb Interneuron Precursors in the Subventricular Zone. *Neuron*, *16*(4), 735–743. https://doi.org/10.1016/s0896-6273(00)80094-x

Iizuka, K., Yoshii, A., Samizo, K., Tsukagoshi, H., Ishizuka, T., Dobashi, K., Nakazawa, T., & Mori, M. (1999). A major role for the rho-associated coiled coil forming protein kinase in G-protein-mediated Ca2+ sensitization through inhibition of myosin phosphatase in rabbit trachea. *British Journal of Pharmacology*, *128*(4), 925–933. https://doi.org/10.1038/sj.bjp.0702864

Ishiuchi, T., Misaki, K., Yonemura, S., Takeichi, M., & Tanoue, T. (2009). Mammalian Fat and Dachsous cadherins regulate apical membrane organization in the embryonic cerebral cortex. *The Journal of Cell Biology*, *185*(6), 959–967. https://doi.org/10.1083/jcb.200811030

Ishiuchi, T., & Takeichi, M. (2011). Willin and Par3 cooperatively regulate epithelial apical constriction through aPKC-mediated ROCK phosphorylation. *Nature Cell Biology*, *13*(7), 860–866. https://doi.org/10.1038/ncb2274

Iso, T., Kedes, L., & Hamamori, Y. (2003). HES and HERP families: Multiple effectors of the notch signaling pathway. *Journal of Cellular Physiology*, *194*(3), 237–255. https://doi.org/10.1002/jcp.10208

Jacobs, M., Hayakawa, K., Swenson, L., Bellon, S., Fleming, M., Taslimi, P., & Doran, J. (2006). The Structure of Dimeric ROCK I Reveals the Mechanism for Ligand Selectivity. *Journal of Biological Chemistry*, *281*(1), 260–268.

https://doi.org/10.1074/jbc.m508847200

Janke, K., Brockmeier, U., Kuhlmann, K., Eisenacher, M., Nolde, J., Meyer, H. E., Mairbaurl, H., & Metzen, E. (2013). Factor inhibiting HIF-1 (FIH-1) modulates protein interactions of apoptosis-stimulating p53 binding protein 2 (ASPP2). *Journal of Cell Science*, *126*(12), 2629–2640. https://doi.org/10.1242/jcs.117564

Jensen, J. B., & Parmar, M. (2006). Strengths and Limitations of the Neurosphere Culture System. *Molecular Neurobiology*, *34*(3), 153–162. https://doi.org/10.1385/mn:34:3:153

Jiang, J., Zhang, Z., Yuan, X., & Poo, M. (2015). Spatiotemporal dynamics of traction forces show three contraction centers in migratory neurons. *Journal of Cell Biology*, *209*(5), 759–774. https://doi.org/10.1083/jcb.201410068

Jiang, X., & Nardelli, J. (2016). Cellular and molecular introduction to brain development. In *Neurobiology of Disease*. https://doi.org/10.1016/j.nbd.2015.07.007

Johnson, G. A., Cofer, G. P., Fubara, B., Gewalt, S. L., Hedlund, L. W., & Maronpot, R. R. (2002). Magnetic resonance histology for morphologic phenotyping. In *Journal of Magnetic Resonance Imaging*. https://doi.org/10.1002/jmri.10175

Ju, H., Lee, K.-A., Yang, M., Kim, H.-J., Kang, C. P., Sohn, T.-S., Rhee, J.-C., Kang, C., & Kim, J.-W. (2005). TP53BP2 locus is associated with gastric cancer susceptibility. *International Journal of Cancer*, *117*(6), 957–960. https://doi.org/10.1002/ijc.21281

Kampa, K. M., Acoba, J. D., Chen, D., Gay, J., Lee, H., Beemer, K., Padiernos, E., Boonmark, N., Zhu, Z., Fan, A. C., Bailey, A. S., Fleming, W. H., Corless, C., Felsher, D. W., Naumovski, L., & Lopez, C. D. (2009). Apoptosis-stimulating protein of p53 (ASPP2) heterozygous mice are tumor-prone and have attenuated cellular damage-response thresholds. *Proceedings of the National Academy of Sciences of the United States of America*, *106*(11), 4390–4395. https://doi.org/10.1073/pnas.0809080106

Kaneko, N., Sawada, M., & Sawamoto, K. (2017). Mechanisms of neuronal migration in the adult brain. *Journal of Neurochemistry*, *141*(6), 835–847. https://doi.org/10.1111/jnc.14002

Katz, C., Benyamini, H., Rotem, S., Lebendiker, M., Danieli, T., Iosub, A., Refaely, H., Dines, M., Bronner, V., Bravman, T., Shalev, D. E., Rüdiger, S., & Friedler, A. (2008). Molecular basis of the interaction between the antiapoptotic Bcl-2 family

proteins and the proapoptotic protein ASPP2. *Proceedings of the National Academy of Sciences of the United States of America*, *105*(34), 12277–12282. https://doi.org/10.1073/pnas.0711269105

Kawabata, S., Usukura, J., Morone, N., Ito, M., Iwamatsu, A., Kaibuchi, K., & Amano, M. (2004). Interaction of Rho-kinase with myosin II at stress fibres. *Genes to Cells*. https://doi.org/10.1111/j.1356-9597.2004.00749.x

Keays, D. A., Tian, G., Poirier, K., Huang, G.-J., Siebold, C., Cleak, J., Oliver, P. L., Fray, M., Harvey, R. J., Molnár, Z., Piñon, M. C., Dear, N., Valdar, W., Brown, S. D. M., Davies, K. E., Rawlins, J. N. P., Cowan, N. J., Nolan, P., Chelly, J., & Flint, J. (2007). Mutations in alpha-tubulin cause abnormal neuronal migration in mice and lissencephaly in humans. *Cell*, *128*(1), 45–57. https://doi.org/10.1016/j.cell.2006.12.017

Khodosevich, K., Seeburg, P. H., & Monyer, H. (2009). Major signaling pathways in migrating neuroblasts. *Frontiers in Molecular Neuroscience*, *2*, 7. https://doi.org/10.3389/neuro.02.007.2009

Khromov, A., Choudhury, N., Stevenson, A. S., Somiyo, A. V., & Eto, M. (2009). Phosphorylation-dependent autoinhibition of myosin light chain phosphatase accounts for Ca2+ sensitization force of smooth muscle contraction. *Journal of Biological Chemistry*. https://doi.org/10.1074/jbc.M109.019729

Kielar, M., Tuy, F. P. D., Bizzotto, S., Lebrand, C., de Juan Romero, C., Poirier, K., Oegema, R., Mancini, G. M., Bahi-Buisson, N., Olaso, R., Le Moing, A.-G., Boutourlinsky, K., Boucher, D., Carpentier, W., Berquin, P., Deleuze, J.-F., Belvindrah, R., Borrell, V., Welker, E., … Francis, F. (2014). Mutations in Eml1 lead to ectopic progenitors and neuronal heterotopia in mouse and human. *Nature Neuroscience*, *17*(7), 923–933. https://doi.org/10.1038/nn.3729

Kim, H., Claps, G., Möller, A., Bowtell, D., Lu, X., & Ronai, Z. A. (2014). Siah2 regulates tight junction integrity and cell polarity through control of ASPP2 stability. *Oncogene*, *33*(15), 2004–2010. https://doi.org/10.1038/onc.2013.149

Kim, W. R., Kim, Y., Eun, B., Park, O., Kim, H., Kim, K., Park, C.-H., Vinsant, S., Oppenheim, R. W., & Sun, W. (2007). Impaired migration in the rostral migratory stream but spared olfactory function after the elimination of programmed cell death in Bax knock-out mice. *The Journal of Neuroscience : The Official Journal of the*

Society for Neuroscience, *27*(52), 14392–14403. https://doi.org/10.1523/JNEUROSCI.3903-07.2007

Kobayashi, S., Kajino, S., Takahashi, N., Kanazawa, S., Imai, K., Hibi, Y., Ohara, H., Itoh, M., & Okamoto, T. (2005). 53BP2 induces apoptosis through the mitochondrial death pathway. *Genes to Cells*, *10*(3), 253–260. https://doi.org/10.1111/j.1365-2443.2005.00835.x

Koizumi, H., Higginbotham, H., Poon, T., Tanaka, T., Brinkman, B. C., & Gleeson, J. G. (2006). Doublecortin maintains bipolar shape and nuclear translocation during migration in the adult forebrain. *Nature Neuroscience*, *9*(6), 779–786. https://doi.org/10.1038/nn1704

Koizumi, H., Tanaka, T., & Gleeson, J. G. (2006). doublecortin-like kinase Functions with doublecortin to Mediate Fiber Tract Decussation and Neuronal Migration. *Neuron*, *49*(1), 55–66. https://doi.org/10.1016/j.neuron.2005.10.040

Königs, V., Jennings, R., Vogl, T., Horsthemke, M., Bachg, A. C., Xu, Y., Grobe, K., Brakebusch, C., Schwab, A., Bähler, M., Knaus, U. G., & Hanley, P. J. (2014). Mouse Macrophages completely lacking Rho subfamily GTPases (RhoA, RhoB, and RhoC) have severe lamellipodial retraction defects, but robust chemotactic navigation and altered motility. *Journal of Biological Chemistry*. https://doi.org/10.1074/jbc.M114.563270

Kosodo, Y., Suetsugu, T., Suda, M., Mimori-Kiyosue, Y., Toida, K., Baba, S. A., Kimura, A., & Matsuzaki, F. (2011). Regulation of interkinetic nuclear migration by cell cycle-coupled active and passive mechanisms in the developing brain. *The EMBO Journal*, *30*(9), 1690–1704. https://doi.org/10.1038/emboj.2011.81

Kusek, G., Campbell, M., Doyle, F., Tenenbaum, S. A., Kiebler, M., & Temple, S. (2012). Asymmetric segregation of the double-stranded RNA binding protein Staufen2 during mammalian neural stem cell divisions promotes lineage progression. *Cell Stem Cell*, *11*(4), 505–516. https://doi.org/10.1016/j.stem.2012.06.006

Lamonica, B. E., Lui, J. H., Hansen, D. V., & Kriegstein, A. R. (2013). Mitotic spindle orientation predicts outer radial glial cell generation in human neocortex. *Nature Communications*. https://doi.org/10.1038/ncomms2647

Lancaster, M. A., & Knoblich, J. A. (2012). Spindle orientation in mammalian cerebral cortical development. *Current Opinion in Neurobiology*, *22*(5), 737–746.

https://doi.org/10.1016/j.conb.2012.04.003

Lee, H.-H., Tien, S.-C., Jou, T.-S., Chang, Y.-C., Jhong, J.-G., & Chang, Z.-F. (2010). Src-dependent phosphorylation of ROCK participates in regulation of focal adhesion dynamics. *Journal of Cell Science*, *123*(19), 3368–3377. https://doi.org/10.1242/jcs.071555

Lee, Hsiao-Hui, & Chang, Z.-F. (2008). Regulation of RhoA-dependent ROCKII activation by Shp2. *Journal of Cell Biology*, *181*(6), 999–1012. https://doi.org/10.1083/jcb.200710187

Leong, S. Y., Faux, C. H., Turbic, A., Dixon, K. J., & Turnley, A. M. (2011). The Rho Kinase Pathway Regulates Mouse Adult Neural Precursor Cell Migration. *STEM CELLS*, *29*(2), 332–343. https://doi.org/10.1002/stem.577

Leventer, R. J., Phelan, E. M., Coleman, L. T., Kean, M. J., Jackson, G. D., & Harvey, A. S. (1999). Clinical and imaging features of cortical malformations in childhood. *Neurology*, *53*(4), 715. https://doi.org/10.1212/wnl.53.4.715

Limouze, J., Straight, A. F., Mitchison, T., & Sellers, J. R. (2004). Specificity of blebbistatin, an inhibitor of myosin II. *Journal of Muscle Research and Cell Motility*, *25*(4–5), 337–341. https://doi.org/10.1007/s10974-004-6060-7

Liu, C.-Y., Lv, X., Li, T., Xu, Y., Zhou, X., Zhao, S., Xiong, Y., Lei, Q.-Y., & Guan, K.-L. (2011). PP1 cooperates with ASPP2 to dephosphorylate and activate TAZ. *The Journal of Biological Chemistry*, *286*(7), 5558–5566. https://doi.org/10.1074/jbc.M110.194019

Liu, W. A., Chen, S., Li, Z., Lee, C. H., Mirzaa, G., Dobyns, W. B., Ross, M. E., Zhang, J., & Shi, S. H. (2018). PARD3 dysfunction in conjunction with dynamic HIPPO signaling drives cortical enlargement with massive heterotopia. *Genes and Development*. https://doi.org/10.1101/gad.313171.118

Liu, Z.-J., Lu, X., Zhang, Y., Zhong, S., Gu, S.-Z., Zhang, X.-B., Yang, X., & Xin, H.-M. (2005). Downregulated mRNA expression of ASPP and the hypermethylation of the 5′-untranslated region in cancer cell lines retaining wild-type p53. *FEBS Letters*, *579*(7), 1587–1590. https://doi.org/10.1016/j.febslet.2005.01.069

Lois, C., & Alvarez-Buylla, A. (1994). Long-distance neuronal migration in the adult mammalian brain. *Science*, *264*(5162), 1145–1148. https://doi.org/10.1126/science.8178174

Lois, C., Garc a-Verdugo, J.-M., & Alvarez-Buylla, A. (1996). Chain Migration of Neuronal Precursors. *Science*, *271*(5251), 978–981. https://doi.org/10.1126/science.271.5251.978

Lossos, I. S., Natkunam, Y., Levy, R., & Lopez, C. D. (2002). Apoptosis Stimulating Protein of p53 (ASPP2) Expression Differs in Diffuse Large B-cell and Follicular Center Lymphoma: Correlation with Clinical Outcome. *Leukemia & Lymphoma*, *43*(12), 2309–2317. https://doi.org/10.1080/1042819021000040017

Lowery, D. M., Clauser, K. R., Hjerrild, M., Lim, D., Alexander, J., Kishi, K., Ong, S.-E., Gammeltoft, S., Carr, S. A., & Yaffe, M. B. (2007). Proteomic screen defines the Polo-box domain interactome and identifies Rock2 as a Plk1 substrate. *The EMBO Journal*, *26*(9), 2262–2273. https://doi.org/10.1038/sj.emboj.7601683

Lui, J. H., Hansen, D. V., & Kriegstein, A. R. (2011). Development and Evolution of the Human Neocortex. *Cell*, *146*(1), 18–36. https://doi.org/10.1016/j.cell.2011.06.030

Lukinavičius, G., Reymond, L., D'Este, E., Masharina, A., Göttfert, F., Ta, H., Güther, A., Fournier, M., Rizzo, S., Waldmann, H., Blaukopf, C., Sommer, C., Gerlich, D. W., Arndt, H.-D., Hell, S. W., & Johnsson, K. (2014). Fluorogenic probes for live-cell imaging of the cytoskeleton. *Nature Methods*, *11*(7), 731–733. https://doi.org/10.1038/nmeth.2972

Ma, X., Bao, J., & Adelstein, R. S. (2007). Loss of Cell Adhesion Causes Hydrocephalus in Nonmuscle Myosin II-B–ablated and Mutated Mice. *Molecular Biology of the Cell*, *18*(6), 2305–2312. https://doi.org/10.1091/mbc.e07-01-0073

Ma, X., Kawamoto, S., Hara, Y., & Adelstein, R. S. (2004). A Point Mutation in the Motor Domain of Nonmuscle Myosin II-B Impairs Migration of Distinct Groups of Neurons. *Molecular Biology of the Cell*, *15*(6), 2568–2579. https://doi.org/10.1091/mbc.e03-11-0836

Martínez-Cerdeño, V., Cunningham, C. L., Camacho, J., Antczak, J. L., Prakash, A. N., Cziep, M. E., Walker, A. I., & Noctor, S. C. (2012). Comparative analysis of the subventricular zone in rat, ferret and macaque: Evidence for an outer subventricular zone in rodents. *PLoS ONE*. https://doi.org/10.1371/journal.pone.0030178

Martini, F. J., & Valdeolmillos, M. (2010). Actomyosin Contraction at the Cell Rear Drives Nuclear Translocation in Migrating Cortical Interneurons. *Journal of Neuroscience*, *30*(25), 8660–8670. https://doi.org/10.1523/jneurosci.1962-10.2010

Mineyko, A., Doja, A., Hurteau, J., Dobyns, W. B., Das, S., & Boycott, K. M. (2009). A Novel Missense Mutation in LIS1 in a Child With Subcortical Band Heterotopia and Pachygyria Inherited From His Mildly Affected Mother With Somatic Mosaicism. *Journal of Child Neurology*, *25*(6), 738–741. https://doi.org/10.1177/0883073809343312

Mizutani, K., Yoon, K., Dang, L., Tokunaga, A., & Gaiano, N. (2007). Differential Notch signalling distinguishes neural stem cells from intermediate progenitors. *Nature*, *449*(7160), 351–355. https://doi.org/10.1038/nature06090

Moffat, J. J., Ka, M., Jung, E. M., & Kim, W. Y. (2015). Genes and brain malformations associated with abnormal neuron positioning. In *Molecular Brain*. https://doi.org/10.1186/s13041-015-0164-4

Moore, R., Theveneau, E., Pozzi, S., Alexandre, P., Richardson, J., Merks, A., Parsons, M., Kashef, J., Linker, C., & Mayor, R. (2013). Par3 controls neural crest migration by promoting microtubule catastrophe during contact inhibition of locomotion. *Development (Cambridge, England)*, *140*(23), 4763–4775. https://doi.org/10.1242/dev.098509

Moores, C. A., Perderiset, M., Francis, F., Chelly, J., Houdusse, A., & Milligan, R. A. (2004). Mechanism of Microtubule Stabilization by Doublecortin. *Molecular Cell*, *14*(6), 833–839. https://doi.org/10.1016/j.molcel.2004.06.009

Mulherkar, S., Liu, F., Chen, Q., Narayanan, A., Couvillon, A. D., Shine, H. D., & Tolias, K. F. (2013). The Small GTPase RhoA Is Required for Proper Locomotor Circuit Assembly. *PLoS ONE*. https://doi.org/10.1371/journal.pone.0067015

Murányi, A., Derkach, D., Erdődi, F., Kiss, A., Ito, M., & Hartshorne, D. J. (2005). Phosphorylation of Thr695 and Thr850 on the myosin phosphatase target subunit: Inhibitory effects and occurrence in A7r5 cells. *FEBS Letters*, *579*(29), 6611–6615. https://doi.org/10.1016/j.febslet.2005.10.055

Murase, S., & Horwitz, A. F. (2002). Deleted in colorectal carcinoma and differentially expressed integrins mediate the directional migration of neural precursors in the rostral migratory stream. *The Journal of Neuroscience : The Official Journal of the Society for Neuroscience*, *22*(9), 3568–3579. https://doi.org/10.1523/JNEUROSCI.22-09-03568.2002

Nadarajah, B., Brunstrom, J. E., Grutzendler, J., Wong, R. O. L., & Pearlman, A. L.

(2001). Two modes of radial migration in early development of the cerebral cortex. *Nature Neuroscience*, *4*(2), 143–150. https://doi.org/10.1038/83967

Nagano, T., Morikubo, S., & Sato, M. (2004). Filamin A and FILIP (Filamin A-interacting protein) regulate cell polarity and motility in neocortical subventricular and intermediate zones during radial migration. *Journal of Neuroscience*. https://doi.org/10.1523/JNEUROSCI.2363-04.2004

Nakamura, F., Osborn, T. M., Hartemink, C. A., Hartwig, J. H., & Stossel, T. P. (2007). Structural basis of filamin A functions. *Journal of Cell Biology*, *179*(5), 1011–1025. https://doi.org/10.1083/jcb.200707073

Nakayama, M., Goto, T. M., Sugimoto, M., Nishimura, T., Shinagawa, T., Ohno, S., Amano, M., & Kaibuchi, K. (2008). Rho-Kinase Phosphorylates PAR-3 and Disrupts PAR Complex Formation. *Developmental Cell*, *14*(2), 205–215. https://doi.org/10.1016/j.devcel.2007.11.021

Nelson, B. (2013). Ex utero Electroporation into Mouse Embryonic Neocortex. *BIO-PROTOCOL*, *3*(24). https://doi.org/10.21769/bioprotoc.998

Nguyen-Ba-Charvet, K. T., Picard-Riera, N., Tessier-Lavigne, M., Baron-Van Evercooren, A., Sotelo, C., & Chédotal, A. (2004). Multiple roles for slits in the control of cell migration in the rostral migratory stream. *The Journal of Neuroscience : The Official Journal of the Society for Neuroscience*, *24*(6), 1497–1506. https://doi.org/10.1523/JNEUROSCI.4729-03.2004

Nguyen, L. (2006). p27kip1 independently promotes neuronal differentiation and migration in the cerebral cortex. *Genes & Development*, *20*(11), 1511–1524. https://doi.org/10.1101/gad.377106

Noctor, S. C., Martínez-Cerdeño, V., Ivic, L., & Kriegstein, A. R. (2004). Cortical neurons arise in symmetric and asymmetric division zones and migrate through specific phases. *Nature Neuroscience*, *7*(2), 136–144. https://doi.org/10.1038/nn1172

Oliver, C. J., Terry-Lorenzo, R. T., Elliott, E., Bloomer, W. A. C., Li, S., Brautigan, D. L., Colbran, R. J., & Shenolikar, S. (2002). Targeting Protein Phosphatase 1 (PP1) to the Actin Cytoskeleton: the Neurabin I/PP1 Complex Regulates Cell Morphology. *Molecular and Cellular Biology*, *22*(13), 4690–4701. https://doi.org/10.1128/mcb.22.13.4690-4701.2002

Ono, K., Shokunbi, T., Nagata, I., Tokunaga, A., Yasui, Y., & Nakatsuji, N. (1997).

Filopodia and growth cones in the vertically migrating granule cells of the postnatal mouse cerebellum. *Experimental Brain Research*, *117*(1), 17–29. https://doi.org/10.1007/pl00005787

Ota, H., Hikita, T., Sawada, M., Nishioka, T., Matsumoto, M., Komura, M., Ohno, A., Kamiya, Y., Miyamoto, T., Asai, N., Enomoto, A., Takahashi, M., Kaibuchi, K., Sobue, K., & Sawamoto, K. (2014). Speed control for neuronal migration in the postnatal brain by Gmip-mediated local inactivation of RhoA. *Nature Communications*, *5*(1). https://doi.org/10.1038/ncomms5532

Paridaen, J. T. M. L., & Huttner, W. B. (2014). Neurogenesis during development of the vertebrate central nervous system. *EMBO Reports*, *15*(4), 351–364. https://doi.org/10.1002/embr.201438447

Parrini, E., Ramazzotti, A., Dobyns, W. B., Mei, D., Moro, F., Veggiotti, P., Marini, C., Brilstra, E. H., Bernardina, B. D., Goodwin, L., Bodell, A., Jones, M. C., Nangeroni, M., Palmeri, S., Said, E., Sander, J. W., Striano, P., Takahashi, Y., Van Maldergem, L., … Guerrini, R. (2006). Periventricular heterotopia: Phenotypic heterogeneity and correlation with Filamin a mutations. *Brain*. https://doi.org/10.1093/brain/awl125

Pecci, A., Ma, X., Savoia, A., & Adelstein, R. S. (2018). MYH9: Structure, functions and role of non-muscle myosin IIA in human disease. *Gene*, *664*, 152–167. https://doi.org/10.1016/j.gene.2018.04.048

Pencea, V., & Luskin, M. B. (2003). Prenatal development of the rodent rostral migratory stream. *The Journal of Comparative Neurology*, *463*(4), 402–418. https://doi.org/10.1002/cne.10746

Peyre, E., Jaouen, F., Saadaoui, M., Haren, L., Merdes, A., Durbec, P., & Morin, X. (2011). A lateral belt of cortical LGN and NuMA guides mitotic spindle movements and planar division in neuroepithelial cells. *The Journal of Cell Biology*, *193*(1), 141–154. https://doi.org/10.1083/jcb.201101039

Pham, N., Cheglakov, I., Koch, C. A., de Hoog, C. L., Moran, M. F., & Rotin, D. (2000). The guanine nucleotide exchange factor CNrasGEF activates Ras in response to cAMP and cGMP. *Current Biology*, *10*(9), 555–558. https://doi.org/10.1016/s0960-9822(00)00473-5

Pinheiro, A. S., Marsh, J. A., Forman-Kay, J. D., & Peti, W. (2011). Structural signature of the MYPT1-PP1 interaction. *Journal of the American Chemical Society*.

https://doi.org/10.1021/ja107810r

Poirier, K., Keays, D. A., Francis, F., Saillour, Y., Bahi, N., Manouvrier, S., Fallet-Bianco, C., Pasquier, L., Toutain, A., Tuy, F. P. D., Bienvenu, T., Joriot, S., Odent, S., Ville, D., Desguerre, I., Goldenberg, A., Moutard, M.-L., Fryns, J.-P., van Esch, H., … Chelly, J. (2007). Large spectrum of lissencephaly and pachygyria phenotypes resulting from de novo missense mutations in tubulin alpha 1A (TUBA1A). *Human Mutation*, *28*(11), 1055–1064. https://doi.org/10.1002/humu.20572

Poirier, K., Lebrun, N., Broix, L., Tian, G., Saillour, Y., Boscheron, C., Parrini, E., Valence, S., Pierre, B. Saint, Oger, M., Lacombe, D., Geneviève, D., Fontana, E., Darra, F., Cances, C., Barth, M., Bonneau, D., Bernadina, B. D., N'Guyen, S., … Chelly, J. (2013). Mutations in TUBG1, DYNC1H1, KIF5C and KIF2A cause malformations of cortical development and microcephaly. *Nature Genetics*. https://doi.org/10.1038/ng.2613

Polleux, F., Whitford, K. L., Dijkhuizen, P. A., Vitalis, T., & Ghosh, A. (2002). Control of cortical interneuron migration by neurotrophins and PI3-kinase signaling. In *Development*.

Posada, I. M. D., Serulla, M., Zhou, Y., Oetken-Lindholm, C., Abankwa, D., & Lectez, B. (2016). ASPP2 Is a Novel Pan-Ras Nanocluster Scaffold. *PLOS ONE*, *11*(7), e0159677. https://doi.org/10.1371/journal.pone.0159677

Postiglione, M. P., Jüschke, C., Xie, Y., Haas, G. A., Charalambous, C., & Knoblich, J. A. (2011). Mouse inscuteable induces apical-basal spindle orientation to facilitate intermediate progenitor generation in the developing neocortex. *Neuron*, *72*(2), 269–284. https://doi.org/10.1016/j.neuron.2011.09.022

Pramparo, T., Youn, Y. H., Yingling, J., Hirotsune, S., & Wynshaw-Boris, A. (2010). Novel embryonic neuronal migration and proliferation defects in Dcx mutant mice are exacerbated by Lis1 reduction. *The Journal of Neuroscience : The Official Journal of the Society for Neuroscience*, *30*(8), 3002–3012. https://doi.org/10.1523/JNEUROSCI.4851-09.2010

Priya, R., & Yap, A. S. (2015). Active Tension. In *Current Topics in Developmental Biology* (pp. 65–102). Elsevier. https://doi.org/10.1016/bs.ctdb.2014.11.016

Quélin, C., Saillour, Y., Souville, I., Poirier, K., N'Guyen-Morel, M. A., Vercueil, L., Millisher-Bellaiche, A. E., Boddaert, N., Dubois, F., Chelly, J., Beldjord, C., &

Bahi-Buisson, N. (2012). Mosaic DCX deletion causes subcortical band heterotopia in males. *Neurogenetics*, *13*(4), 367–373. https://doi.org/10.1007/s10048-012-0339-4

Rakic, P. (1995). A small step for the cell, a giant leap for mankind: a hypothesis of neocortical expansion during evolution. *Trends in Neurosciences*, *18*(9), 383–388. https://doi.org/10.1016/0166-2236(95)93934-p

Ramos, R. L., Bai, J., & LoTurco, J. J. (2005). Heterotopia Formation in Rat but Not Mouse Neocortex after RNA Interference Knockdown of DCX. *Cerebral Cortex*, *16*(9), 1323–1331. https://doi.org/10.1093/cercor/bhj074

Rana, M. K., & Worthylake, R. A. (2012). Novel mechanism for negatively regulating Rho-kinase (ROCK) signaling through Coronin1B protein in neuregulin 1 (NRG-1)-induced tumor cell motility. *The Journal of Biological Chemistry*, *287*(26), 21836–21845. https://doi.org/10.1074/jbc.M112.346114

Ridley, A. J. (2003). Cell Migration: Integrating Signals from Front to Back. *Science*, *302*(5651), 1704–1709. https://doi.org/10.1126/science.1092053

Rivas, R. J., & Hatten, M. E. (1995). Motility and cytoskeletal organization of migrating cerebellar granule neurons. *The Journal of Neuroscience*, *15*(2), 981–989. https://doi.org/10.1523/jneurosci.15-02-00981.1995

Rotem, S., Katz, C., Benyamini, H., Lebendiker, M., Veprintsev, D., Rüdiger, S., Danieli, T., & Friedler, A. (2008). The Structure and Interactions of the Proline-rich Domain of ASPP2. *Journal of Biological Chemistry*, *283*(27), 18990–18999. https://doi.org/10.1074/jbc.m708717200

Royer, C., Koch, S., Qin, X., Zak, J., Buti, L., Dudziec, E., Zhong, S., Ratnayaka, I., Srinivas, S., & Lu, X. (2014). ASPP2 links the apical lateral polarity complex to the regulation of YAP activity in epithelial cells. *PLoS ONE*. https://doi.org/10.1371/journal.pone.0111384

Sadok, A., McCarthy, A., Caldwell, J., Collins, I., Garrett, M. D., Yeo, M., Hooper, S., Sahai, E., Kuemper, S., Mardakheh, F. K., & Marshall, C. J. (2015). Rho Kinase Inhibitors Block Melanoma Cell Migration and Inhibit Metastasis. *Cancer Research*, *75*(11), 2272–2284. https://doi.org/10.1158/0008-5472.can-14-2156

Samuels-Lev, Y., O'Connor, D. J., Bergamaschi, D., Trigiante, G., Hsieh, J.-K., Zhong, S., Campargue, I., Naumovski, L., Crook, T., & Lu, X. (2001). ASPP Proteins

Specifically Stimulate the Apoptotic Function of p53. *Molecular Cell*, *8*(4), 781–794. https://doi.org/10.1016/s1097-2765(01)00367-7

Sang, C. N., Kim, Y., Dryanovski, D., Walker, A., Goings, G., Woolfrey, K., Seong, S. K., Chu, C., Chenn, A., Erdelyi, F., Szabo, G., Hockberger, P., & Szele, F. G. (2007). Dynamic features of postnatal subventricular zone cell motility: A two-photon time-lapse study. *Journal of Comparative Neurology*. https://doi.org/10.1002/cne.21473

Sapir, T. (2000). Doublecortin mutations cluster in evolutionarily conserved functional domains. *Human Molecular Genetics*, *9*(5), 703–712. https://doi.org/10.1093/hmg/9.5.703

Sarkisian, M. R., Bartley, C. M., Chi, H., Nakamura, F., Hashimoto-Torii, K., Torii, M., Flavell, R. A., & Rakic, P. (2006). MEKK4 signaling regulates filamin expression and neuronal migration. *Neuron*, *52*(5), 789–801. https://doi.org/10.1016/j.neuron.2006.10.024

Sawamoto, K. (2006). New Neurons Follow the Flow of Cerebrospinal Fluid in the Adult Brain. *Science*, *311*(5761), 629–632. https://doi.org/10.1126/science.1119133

Schaar, B. T., & McConnell, S. K. (2005). Cytoskeletal coordination during neuronal migration. *Proceedings of the National Academy of Sciences of the United States of America*. https://doi.org/10.1073/pnas.0506008102

Schipper, K., Drenth, A. P., van der Burg, E., Cornelissen, S., Klarenbeek, S., Nethe, M., & Jonkers, J. (2020). Truncated ASPP2 Drives Initiation and Progression of Invasive Lobular Carcinoma via Distinct Mechanisms. *Cancer Research*, *80*(7), 1486–1497. https://doi.org/10.1158/0008-5472.can-19-3607

Schmid, M.-T., Weinandy, F., Wilsch-Bräuninger, M., Huttner, W. B., Cappello, S., & Götz, M. (2014). The role of α-E-catenin in cerebral cortex development: radial glia specific effect on neuronal migration. *Frontiers in Cellular Neuroscience*, *8*, 215. https://doi.org/10.3389/fncel.2014.00215

Schmidt, G., Sehr, P., Wilm, M., Selzer, J., Mann, M., & Aktories, K. (1997). Gln 63 of Rho is deamidated by Escherichia coli cytotoxic necrotizing factor-1. *Nature*, *387*(6634), 725–729. https://doi.org/10.1038/42735

Schmoranzer, J., Fawcett, J. P., Segura, M., Tan, S., Vallee, R. B., Pawson, T., & Gundersen, G. G. (2009). Par3 and dynein associate to regulate local microtubule

dynamics and centrosome orientation during migration. *Current Biology : CB*, *19*(13), 1065–1074. https://doi.org/10.1016/j.cub.2009.05.065

Schofield, A. V, Steel, R., & Bernard, O. (2012). Rho-associated Coiled-coil Kinase (ROCK) Protein Controls Microtubule Dynamics in a Novel Signaling Pathway That Regulates Cell Migration. *Journal of Biological Chemistry*, *287*(52), 43620–43629. https://doi.org/10.1074/jbc.m112.394965

Schwamborn, J. C., & Püschel, A. W. (2004). The sequential activity of the GTPases Rap1B and Cdc42 determines neuronal polarity. *Nature Neuroscience*, *7*(9), 923–929. https://doi.org/10.1038/nn1295

Sebbagh, M., Hamelin, J., Bertoglio, J., Solary, E., & Bréard, J. (2005). Direct cleavage of ROCK II by granzyme B induces target cell membrane blebbing in a caspase-independent manner. *The Journal of Experimental Medicine*, *201*(3), 465–471. https://doi.org/10.1084/jem.20031877

Sheen, V L. (2001). Mutations in the X-linked filamin 1 gene cause periventricular nodular heterotopia in males as well as in females. *Human Molecular Genetics*, *10*(17), 1775–1783. https://doi.org/10.1093/hmg/10.17.1775

Sheen, V L, Wheless, J. W., Bodell, A., Braverman, E., Cotter, P. D., Rauen, K. A., Glenn, O., Weisiger, K., Packman, S., Walsh, C. A., & Sherr, E. H. (2003). Periventricular heterotopia associated with chromosome 5p anomalies. *Neurology*, *60*(6), 1033–1036. https://doi.org/10.1212/01.wnl.0000052689.03214.61

Sheen, Volney L., Ganesh, V. S., Topcu, M., Sebire, G., Bodell, A., Hill, R. S., Grant, P. E., Shugart, Y. Y., Imitola, J., Khoury, S. J., Guerrini, R., & Walsh, C. A. (2004). Mutations in ARFGEF2 implicate vesicle trafficking in neural progenitor proliferation and migration in the human cerebral cortex. *Nature Genetics*. https://doi.org/10.1038/ng1276

Shin, H., Shinotsuka, C., & Nakayama, K. (2005). Expression of BIG2 and Analysis of Its Function in Mammalian Cells. In *Methods in Enzymology* (pp. 206–215). Elsevier. https://doi.org/10.1016/s0076-6879(05)04020-6

Shinohara, R., Thumkeo, D., Kamijo, H., Kaneko, N., Sawamoto, K., Watanabe, K., Takebayashi, H., Kiyonari, H., Ishizaki, T., Furuyashiki, T., & Narumiya, S. (2012). A role for mDia, a Rho-regulated actin nucleator, in tangential migration of interneuron precursors. *Nature Neuroscience*. https://doi.org/10.1038/nn.3020

Shitamukai, A., & Matsuzaki, F. (2012). Control of asymmetric cell division of mammalian neural progenitors. In *Development Growth and Differentiation*. https://doi.org/10.1111/j.1440-169X.2012.01345.x

Sicca, F., Kelemen, A., Genton, P., Das, S., Mei, D., Moro, F., Dobyns, W. B., & Guerrini, R. (2003). Mosaic mutations of the LIS1 gene cause subcortical band heterotopia. *Neurology*, *61*(8), 1042–1046. https://doi.org/10.1212/wnl.61.8.1042

Simpson, K. J., Dugan, A. S., & Mercurio, A. M. (2004). Functional Analysis of the Contribution of RhoA and RhoC GTPases to Invasive Breast Carcinoma. *Cancer Research*, *64*(23), 8694–8701. https://doi.org/10.1158/0008-5472.can-04-2247

Snapyan, M., Lemasson, M., Brill, M. S., Blais, M., Massouh, M., Ninkovic, J., Gravel, C., Berthod, F., Götz, M., Barker, P. A., Parent, A., & Saghatelyan, A. (2009). Vasculature guides migrating neuronal precursors in the adult mammalian forebrain via brain-derived neurotrophic factor signaling. *The Journal of Neuroscience : The Official Journal of the Society for Neuroscience*, *29*(13), 4172–4188. https://doi.org/10.1523/JNEUROSCI.4956-08.2009

Solecki, D. J., Trivedi, N., Govek, E.-E., Kerekes, R. A., Gleason, S. S., & Hatten, M. E. (2009). Myosin II Motors and F-Actin Dynamics Drive the Coordinated Movement of the Centrosome and Soma during CNS Glial-Guided Neuronal Migration. *Neuron*, *63*(1), 63–80. https://doi.org/10.1016/j.neuron.2009.05.028

Somlyo, A. V, Bradshaw, D., Ramos, S., Murphy, C., Myers, C. E., & Somlyo, A. P. (2000). Rho-Kinase Inhibitor Retards Migration and in Vivo Dissemination of Human Prostate Cancer Cells. *Biochemical and Biophysical Research Communications*, *269*(3), 652–659. https://doi.org/10.1006/bbrc.2000.2343

Sonego, M., Gajendra, S., Parsons, M., Ma, Y., Hobbs, C., Zentar, M. P., Williams, G., Machesky, L. M., Doherty, P., & Lalli, G. (2013). Fascin regulates the migration of subventricular zone-derived neuroblasts in the postnatal brain. *The Journal of Neuroscience : The Official Journal of the Society for Neuroscience*, *33*(30), 12171–12185. https://doi.org/10.1523/JNEUROSCI.0653-13.2013

Sonego, M., Oberoi, M., Stoddart, J., Gajendra, S., Hendricusdottir, R., Oozeer, F., Worth, D. C., Hobbs, C., Eickholt, B. J., Gordon-Weeks, P. R., Doherty, P., & Lalli, G. (2015). Drebrin regulates neuroblast migration in the postnatal mammalian brain. *PloS One*, *10*(5), e0126478–e0126478. https://doi.org/10.1371/journal.pone.0126478

Soria, J. M., Taglialatela, P., Gil-Perotin, S., Galli, R., Gritti, A., Verdugo, J. M. G., & Bertuzzi, S. (2004). Defective postnatal neurogenesis and disorganization of the rostral migratory stream in absence of the Vax1 homeobox gene. *The Journal of Neuroscience : The Official Journal of the Society for Neuroscience*, *24*(49), 11171–11181. https://doi.org/10.1523/JNEUROSCI.3248-04.2004

Sottocornola, R., Royer, C., Vives, V., Tordella, L., Zhong, S., Wang, Y., Ratnayaka, I., Shipman, M., Cheung, A., Gaston-Massuet, C., Ferretti, P., Molnár, Z., & Lu, X. (2010a). ASPP2 Binds Par-3 and Controls the Polarity and Proliferation of Neural Progenitors during CNS Development. *Developmental Cell*. https://doi.org/10.1016/j.devcel.2010.06.003

Sottocornola, R., Royer, C., Vives, V., Tordella, L., Zhong, S., Wang, Y., Ratnayaka, I., Shipman, M., Cheung, A., Gaston-Massuet, C., Ferretti, P., Molnár, Z., & Lu, X. (2010b). ASPP2 Binds Par-3 and Controls the Polarity and Proliferation of Neural Progenitors during CNS Development. *Developmental Cell*, *19*(1), 126–137. https://doi.org/10.1016/j.devcel.2010.06.003

Stefan, H., Nimsky, C., Scheler, G., Rampp, S., Hopfengärtner, R., Hammen, T., Dörfler, A., Blümcke, I., & Romstöck, J. (2007). Periventricular nodular heterotopia: A challenge for epilepsy surgery. *Seizure*, *16*(1), 81–86. https://doi.org/10.1016/j.seizure.2006.10.004

Stossel, T. P., Condeelis, J., Cooley, L., Hartwig, J. H., Noegel, A., Schleicher, M., & Shapiro, S. S. (2001). Filamins as integrators of cell mechanics and signalling. In *Nature Reviews Molecular Cell Biology*. https://doi.org/10.1038/35052082

Sui, Y., Horne, M. K., & Stanić, D. (2012). Reduced proliferation in the adult mouse subventricular zone increases survival of olfactory bulb interneurons. *PLoS ONE*. https://doi.org/10.1371/journal.pone.0031549

Sun, T., & Hevner, R. F. (2014). Growth and folding of the mammalian cerebral cortex: from molecules to malformations. In *Nature Reviews Neuroscience*. https://doi.org/10.1038/nrn3707

Suzuki, A. (2002). aPKC kinase activity is required for the asymmetric differentiation of the premature junctional complex during epithelial cell polarization. *Journal of Cell Science*, *115*(18), 3565–3573. https://doi.org/10.1242/jcs.00032

Suzuki, Atsushi, Hirata, M., Kamimura, K., Maniwa, R., Yamanaka, T., Mizuno, K.,

Kishikawa, M., Hirose, H., Amano, Y., Izumi, N., Miwa, Y., & Ohno, S. (2004). aPKC Acts Upstream of PAR-1b in Both the Establishment and Maintenance of Mammalian Epithelial Polarity. *Current Biology*, *14*(16), 1425–1435. https://doi.org/10.1016/j.cub.2004.08.021

Swärd, K., Dreja, K., Susnjar, M., Hellstrand, P., Hartshorne, D. J., & Walsh, M. P. (2000). Inhibition of Rho-associated kinase blocks agonist-induced Ca2+ sensitization of myosin phosphorylation and force in guinea-pig ileum. *The Journal of Physiology*, *522 Pt 1*(Pt 1), 33–49. https://doi.org/10.1111/j.1469-7793.2000.0033m.x

Tabata, H., & Nakajima, K. (2003). Multipolar migration: the third mode of radial neuronal migration in the developing cerebral cortex. *The Journal of Neuroscience : The Official Journal of the Society for Neuroscience*, *23*(31), 9996–10001. https://doi.org/10.1523/JNEUROSCI.23-31-09996.2003

Takahashi, N., Kobayashi, S., Kajino, S., Imai, K., Tomoda, K., Shimizu, S., & Okamoto, T. (2005). Inhibition of the 53BP2S-mediated apoptosis by nuclear factor kappaB and Bcl-2 family proteins. *Genes to Cells*, *10*(8), 803–811. https://doi.org/10.1111/j.1365-2443.2005.00878.x

Tanaka, T., Serneo, F. F., Higgins, C., Gambello, M. J., Wynshaw-Boris, A., & Gleeson, J. G. (2004). Lis1 and doublecortin function with dynein to mediate coupling of the nucleus to the centrosome in neuronal migration. *The Journal of Cell Biology*, *165*(5), 709–721. https://doi.org/10.1083/jcb.200309025

Tang, J., Ip, J. P. K., Ye, T., Ng, Y.-P., Yung, W.-H., Wu, Z., Fang, W., Fu, A. K. Y., & Ip, N. Y. (2014). Cdk5-Dependent Mst3 Phosphorylation and Activity Regulate Neuronal Migration through RhoA Inhibition. *Journal of Neuroscience*, *34*(22), 7425–7436. https://doi.org/10.1523/jneurosci.5449-13.2014

Tassi, L., Colombo, N., Cossu, M., Mai, R., Francione, S., Lo Russo, G., Galli, C., Bramerio, M., Battaglia, G., Garbelli, R., Meroni, A., & Spreafico, R. (2005). Electroclinical, MRI and neuropathological study of 10 patients with nodular heterotopia, with surgical outcomes. *Brain*. https://doi.org/10.1093/brain/awh357

Taverna, E., & Huttner, W. B. (2010). Neural Progenitor Nuclei IN Motion. *Neuron*, *67*(6), 906–914. https://doi.org/10.1016/j.neuron.2010.08.027

Terashima, T., Bilasy, S. E., Satoh, T., Ueda, S., Wei, P., Kanemura, H., Aiba, A., &

Kataoka, T. (2009). Dorsal telencephalon-specific RA-GEF-1 knockout mice develop heterotopic cortical mass and commissural fiber defect. *Neuroscience Research*, *65*, S97. https://doi.org/10.1016/j.neures.2009.09.418

Terry-Lorenzo, R. T., Inoue, M., Connor, J. H., Haystead, T. A. J., Armbruster, B. N., Gupta, R. P., Oliver, C. J., & Shenolikar, S. (2000). Neurofilament-L Is a Protein Phosphatase-1-binding Protein Associated with Neuronal Plasma Membrane and Post-synaptic Density. *Journal of Biological Chemistry*, *275*(4), 2439–2446. https://doi.org/10.1074/jbc.275.4.2439

Tidow, H., Andreeva, A., Rutherford, T. J., & Fersht, A. R. (2007). Solution Structure of ASPP2 N-terminal Domain (N-ASPP2) Reveals a Ubiquitin-like Fold. *Journal of Molecular Biology*, *371*(4), 948–958. https://doi.org/10.1016/j.jmb.2007.05.024

Totsukawa, G, Yamakita, Y., Yamashiro, S., Hartshorne, D. J., Sasaki, Y., & Matsumura, F. (2000). Distinct roles of ROCK (Rho-kinase) and MLCK in spatial regulation of MLC phosphorylation for assembly of stress fibers and focal adhesions in 3T3 fibroblasts. *The Journal of Cell Biology*, *150*(4), 797–806. https://doi.org/10.1083/jcb.150.4.797

Totsukawa, Go, Wu, Y., Sasaki, Y., Hartshorne, D. J., Yamakita, Y., Yamashiro, S., & Matsumura, F. (2004). Distinct roles of MLCK and ROCK in the regulation of membrane protrusions and focal adhesion dynamics during cell migration of fibroblasts. *The Journal of Cell Biology*, *164*(3), 427–439. https://doi.org/10.1083/jcb.200306172

Traweger, A., Wiggin, G., Taylor, L., Tate, S. A., Metalnikov, P., & Pawson, T. (2008). Protein phosphatase 1 regulates the phosphorylation state of the polarity scaffold Par-3. *Proceedings of the National Academy of Sciences of the United States of America*. https://doi.org/10.1073/pnas.0804102105

Trivedi, N., Stabley, D. R., Cain, B., Howell, D., Laumonnerie, C., Ramahi, J. S., Temirov, J., Kerekes, R. A., Gordon-Weeks, P. R., & Solecki, D. J. (2017). Drebrin-mediated microtubule–actomyosin coupling steers cerebellar granule neuron nucleokinesis and migration pathway selection. *Nature Communications*, *8*(1). https://doi.org/10.1038/ncomms14484

Tsai, J.-W., Bremner, K. H., & Vallee, R. B. (2007). Dual subcellular roles for LIS1 and dynein in radial neuronal migration in live brain tissue. *Nature Neuroscience*, *10*(8),

970–979. https://doi.org/10.1038/nn1934

Tsai, J.-W., Chen, Y., Kriegstein, A. R., & Vallee, R. B. (2005). LIS1 RNA interference blocks neural stem cell division, morphogenesis, and motility at multiple stages. *The Journal of Cell Biology*, *170*(6), 935–945. https://doi.org/10.1083/jcb.200505166

Tullio, A. N., Bridgman, P. C., Tresser, N. J., Chan, C.-C., Conti, M. A., Adelstein, R. S., & Hara, Y. (2001). Structural abnormalities develop in the brain after ablation of the gene encoding nonmuscle myosin II-B heavy chain. *The Journal of Comparative Neurology*, *433*(1), 62–74. https://doi.org/10.1002/cne.1125

Ueda, H. R., Ertürk, A., Chung, K., Gradinaru, V., Chédotal, A., Tomancak, P., & Keller, P. J. (2020). Tissue clearing and its applications in neuroscience. In *Nature Reviews Neuroscience*. https://doi.org/10.1038/s41583-019-0250-1

Ueda, K., Ohta, Y., & Hosoya, H. (2003). The carboxy-terminal pleckstrin homology domain of ROCK interacts with filamin-A. *Biochemical and Biophysical Research Communications*, *301*(4), 886–890. https://doi.org/10.1016/s0006-291x(03)00048-2

Umeshima, H., Nomura, K., Yoshikawa, S., Hörning, M., Tanaka, M., Sakuma, S., Arai, F., Kaneko, M., & Kengaku, M. (2019). Local traction force in the proximal leading process triggers nuclear translocation during neuronal migration. *Neuroscience Research*, *142*, 38–48. https://doi.org/10.1016/j.neures.2018.04.001

Valiente, M., & Martini, F. J. (2009). Migration of cortical interneurons relies on branched leading process dynamics. *Cell Adhesion & Migration*, *3*(3), 278–280. https://doi.org/10.4161/cam.3.3.8832

Velasco, G., Armstrong, C., Morrice, N., Frame, S., & Cohen, P. (2002). Phosphorylation of the regulatory subunit of smooth muscle protein phosphatase 1M at Thr850 induces its dissociation from myosin. *FEBS Letters*. https://doi.org/10.1016/S0014-5793(02)03175-7

Vessey, J. P., Amadei, G., Burns, S. E., Kiebler, M. A., Kaplan, D. R., & Miller, F. D. (2012). An Asymmetrically Localized Staufen2-Dependent RNA Complex Regulates Maintenance of Mammalian Neural Stem Cells. *Cell Stem Cell*, *11*(4), 517–528. https://doi.org/10.1016/j.stem.2012.06.010

Vicente-Manzanares, M., Ma, X., Adelstein, R. S., & Horwitz, A. R. (2009). Non-muscle myosin II takes centre stage in cell adhesion and migration. *Nature Reviews. Molecular Cell Biology*, *10*(11), 778–790. https://doi.org/10.1038/nrm2786

Virshup, D. M., & Shenolikar, S. (2009). From Promiscuity to Precision: Protein Phosphatases Get a Makeover. *Molecular Cell*, *33*(5), 537–545. https://doi.org/10.1016/j.molcel.2009.02.015

Vives, V. (2006). ASPP2 is a haploinsufficient tumor suppressor that cooperates with p53 to suppress tumor growth. *Genes & Development*, *20*(10), 1262–1267. https://doi.org/10.1101/gad.374006

Wakula, P., Beullens, M., Ceulemans, H., Stalmans, W., & Bollen, M. (2003). Degeneracy and Function of the Ubiquitous RVXF Motif That Mediates Binding to Protein Phosphatase-1. *Journal of Biological Chemistry*, *278*(21), 18817–18823. https://doi.org/10.1074/jbc.m300175200

Walsh, C. (2000). Potential mechanisms of mutations that affect neuronal migration in man and mouse. *Current Opinion in Genetics & Development*, *10*(3), 270–274. https://doi.org/10.1016/s0959-437x(00)00076-9

Wang, X., Tsai, J.-W., LaMonica, B., & Kriegstein, A. R. (2011). A new subtype of progenitor cell in the mouse embryonic neocortex. *Nature Neuroscience*, *14*(5), 555–561. https://doi.org/10.1038/nn.2807

Wang, Y, Godin-Heymann, N., Dan Wang, X., Bergamaschi, D., Llanos, S., & Lu, X. (2013). ASPP1 and ASPP2 bind active RAS, potentiate RAS signalling and enhance p53 activity in cancer cells. *Cell Death & Differentiation*, *20*(4), 525–534. https://doi.org/10.1038/cdd.2013.3

Wang, Yuepeng, Zheng, X. R., Riddick, N., Bryden, M., Baur, W., Zhang, X., & Surks, H. K. (2009). ROCK isoform regulation of myosin phosphatase and contractility in vascular smooth muscle cells. *Circulation Research*, *104*(4), 531–540. https://doi.org/10.1161/CIRCRESAHA.108.188524

Wang, Z. M., Yang, D. S., Liu, J., Liu, H. B., Ye, M., & Zhang, Y. F. (2016). ROCK inhibitor Y-27632 inhibits the growth, migration, and invasion of Tca8113 and CAL-27 cells in tongue squamous cell carcinoma. *Tumor Biology*. https://doi.org/10.1007/s13277-015-4115-6

Ward, Y., Yap, S.-F., Ravichandran, V., Matsumura, F., Ito, M., Spinelli, B., & Kelly, K. (2002). The GTP binding proteins Gem and Rad are negative regulators of the Rho-Rho kinase pathway. *The Journal of Cell Biology*, *157*(2), 291–302. https://doi.org/10.1083/jcb.200111026

Watrin, F., Manent, J.-B., Cardoso, C., & Represa, A. (2015). Causes and consequences of gray matter heterotopia. *CNS Neuroscience & Therapeutics*, *21*(2), 112–122. https://doi.org/10.1111/cns.12322

Wei, R., Ngo, B., Wu, G., & Lee, W.-H. (2011). Phosphorylation of the Ndc80 complex protein, HEC1, by Nek2 kinase modulates chromosome alignment and signaling of the spindle assembly checkpoint. *Molecular Biology of the Cell*, *22*(19), 3584–3594. https://doi.org/10.1091/mbc.E11-01-0012

Whitford, K. L., Dijkhuizen, P., Polleux, F., & Ghosh, A. (2002). Molecular Control of Cortical Dendrite Development. *Annual Review of Neuroscience*, *25*(1), 127–149. https://doi.org/10.1146/annurev.neuro.25.112701.142932

Whitman, M. C., Fan, W., Rela, L., Rodriguez-Gil, D. J., & Greer, C. A. (2009). Blood vessels form a migratory scaffold in the rostral migratory stream. *The Journal of Comparative Neurology*, *516*(2), 94–104. https://doi.org/10.1002/cne.22093

Wonders, C. P., & Anderson, S. A. (2006). The origin and specification of cortical interneurons. *Nature Reviews Neuroscience*, *7*(9), 687–696. https://doi.org/10.1038/nrn1954

Wong, K., Ren, X. R., Huang, Y. Z., Xie, Y., Liu, G., Saito, H., Tang, H., Wen, L., Brady-Kalnay, S. M., Mei, L., Wu, J. Y., Xiong, W. C., & Rao, Y. (2001). Signal transduction in neuronal migration: Roles of GTPase activating proteins and the small GTPase Cdc42 in the Slit-Robo pathway. *Cell*. https://doi.org/10.1016/S0092-8674(01)00530-X

Yamanaka, T., Horikoshi, Y., Sugiyama, Y., Ishiyama, C., Suzuki, A., Hirose, T., Iwamatsu, A., Shinohara, A., & Ohno, S. (2003). Mammalian Lgl Forms a Protein Complex with PAR-6 and aPKC Independently of PAR-3 to Regulate Epithelial Cell Polarity. *Current Biology*, *13*(9), 734–743. https://doi.org/10.1016/s0960-9822(03)00244-6

Yamashita, K., Mizuno, K., Furukawa, K., Hirose, H., Sakurai, N., Masuda-Hirata, M., Amano, Y., Hirose, T., Suzuki, A., & Ohno, S. (2020). Phosphorylation and dephosphorylation of Ser852 and Ser889 control the clustering, localization and function of PAR3. *Journal of Cell Science*. https://doi.org/10.1242/jcs.244830

Yap, A. S., Duszyc, K., & Viasnoff, V. (2018). Mechanosensing and mechanotransduction at cell –cell junctions. *Cold Spring Harbor Perspectives in*

Biology. https://doi.org/10.1101/cshperspect.a028761

Yingling, J., Youn, Y. H., Darling, D., Toyo-Oka, K., Pramparo, T., Hirotsune, S., & Wynshaw-Boris, A. (2008). Neuroepithelial stem cell proliferation requires LIS1 for precise spindle orientation and symmetric division. *Cell*, *132*(3), 474–486. https://doi.org/10.1016/j.cell.2008.01.026

Yoneda, A., Multhaupt, H. A. B., & Couchman, J. R. (2005). The Rho kinases I and II regulate different aspects of myosin II activity. *The Journal of Cell Biology*, *170*(3), 443–453. https://doi.org/10.1083/jcb.200412043

Yoshizaki, H., & Okuda, S. (2014). Elucidation of the evolutionary expansion of phosphorylation signaling networks using comparative phosphomotif analysis. *BMC Genomics*. https://doi.org/10.1186/1471-2164-15-546

Yoshizaki, H., & Okuda, S. (2015). Large-scale analysis of the evolutionary histories of phosphorylation motifs in the human genome. *GigaScience*. https://doi.org/10.1186/s13742-015-0057-6

Zak, J., Vives, V., Szumska, D., Vernet, A., Schneider, J. E., Miller, P., Slee, E. A., Joss, S., Lacassie, Y., Chen, E., Escobar, L. F., Tucker, M., Aylsworth, A. S., Dubbs, H. A., Collins, A. T., Andrieux, J., Dieux-Coeslier, A., Haberlandt, E., Kotzot, D., … Lu, X. (2016). ASPP2 deficiency causes features of 1q41q42 microdeletion syndrome. *Cell Death and Differentiation*. https://doi.org/10.1038/cdd.2016.76

Zhang, H., & Macara, I. G. (2008). The PAR-6 Polarity Protein Regulates Dendritic Spine Morphogenesis through p190 RhoGAP and the Rho GTPase. *Developmental Cell*, *14*(2), 216–226. https://doi.org/10.1016/j.devcel.2007.11.020

Zhang, P., Zhang, Y., Gao, K., Wang, Y., Jin, X., Wei, Y., Saiyin, H., Wang, D., Peng, J., Ma, J., Tang, Y., Wumaier, R., Yu, H., Dong, Y., Huang, H., Yu, L., & Wang, C. (2015). ASPP1/2-PP1 complexes are required for chromosome segregation and kinetochore-microtubule attachments. *Oncotarget*. https://doi.org/10.18632/oncotarget.6355

Zhao, J., Wu, G., Bu, F., Lu, B., Liang, A., Cao, L., Tong, X., Lu, X., Wu, M., & Guo, Y. (2009). Epigenetic silence of ankyrin-repeat-containing, SH3-domain-containing, and proline-rich-region- containing protein 1 (ASPP1) and ASPP2 genes promotes tumor growth in hepatitis B virus-positive hepatocellular carcinoma. *Hepatology*, *51*(1), 142–153. https://doi.org/10.1002/hep.23247

Žigman, M., Cayouette, M., Charalambous, C., Schleiffer, A., Hoeller, O., Dunican, D., McCudden, C. R., Firnberg, N., Barres, B. A., Siderovski, D. P., & Knoblich, J. A. (2005). Mammalian Inscuteable Regulates Spindle Orientation and Cell Fate in the Developing Retina. *Neuron*, *48*(4), 539–545. https://doi.org/10.1016/j.neuron.2005.09.030